# INVESTIGATIONS TOWARD THE APPLICATION OF ORGANIC PHOTOREDOX CATALYSIS TO THE SYNTHESIS OF NATURAL PRODUCTS

Hudson Gordon Roth

A dissertation submitted to the faculty at the University of North Carolina at Chapel Hill in partial fulfillment of the requirements for the degree of Doctor of Philosophy in the Department of Chemistry.

Chapel Hill
2019

Approved by:

David A. Nicewicz

Sidney M. Wilkerson-Hill

Abigail S. Knight

Frank A. Leibfarth

Wei You

## ABSTRACT

Hudson Gordon Roth: Investigations Toward the Application of Organic Photoredox Catalysis to the Synthesis of Natural Products
(Under the direction of David A. Nicewicz)

While chemistry proceeding through radical intermediates has been known and studied for centuries, photoredox catalysis as a means of generating these species has only entered the forefront of synthetic organic chemistry within the past few decades. This approach has gained traction due to the use of visible light and generally mild conditions, making it compatible with a range of functional groups and late-stage functionalization.

Chapters 1 and 2 of this work focus on photoredox catalysis in general. The first chapter covers the basic principles of photoredox catalysis, giving special attention to acridinium ion dyes as photoredox catalysts; in addition, select applications of acridinium ion photoredox catalysis to the synthesis of natural products are discussed. The second chapter details the importance of electrochemical potentials in planning and conducting photoredox transformations. Our work on compiling a database of experimental and computational potentials, and a collaboration with Merck on the advantages of organic photoredox catalysis are presented.

Chapters 3 and 4 focus on our endeavors to apply acridinium ion photoredox catalysis to the synthesis of the natural products rubriflordilactone B and stemocurtisine. This work has culminated in a diastereoselective route to the left side of rubriflordilactone B and preliminary results for an approach to stemocurtisine.

## ACKNOWLEDGMENTS

I am truly gratefully for the time I have had to study at UNC-Chapel Hill. This chemistry department holds many fond memories I will remember for years to come. First and foremost, I would like to thank Dave for letting me join his lab. Dave's patience, understanding, and guidance have helped me develop into the scientist I am today. In addition, I would like to thank the other UNC chemistry faculty members I have had the privilege to interact with, particularly my committee members for their time.

I want to thank all my coworkers in the Nicewicz lab throughout the years. Working with you helped make graduate school an enjoyable experience. I would specifically like to thank Jean-Marc Grandjean and Nathan Gesmundo, both of whom guided and trained me during my earliest days in the lab. In addition, I want to thank all of those I had the chance to work with on various projects during my time here: Nathan Gesmundo, Susanna Liang, Peter Morse, Hunter Ripberger, and Nathan Romero.

To all the friends I made within the chemistry department, I want to thank you all for being a fantastic support system throughout the years. As we went through this process together, it was always comforting to know I could talk to people who understood the challenges I was facing in graduate school.

I also want to thank my dad, Charity, Abigail, and Steven for their support during these five years. While you may not always understand the chemistry, you have always taken an interest in my work and life throughout graduate school.

Last, but not least, I would like to thank Randy. You are the person who has experienced my long work hours, frustrations, and successes with me on a daily basis. Knowing you would always be there for me as a source of love and support has been an invaluable asset on this journey.

## PREFACE

The second chapter of this work is adapted, with permission, from Roth, H. G.; Romero, N. A.; Nicewicz, D. A. "Experimental and Calculated Electrochemical Potentials of Common Organic Molecules for Applications to Single Electron Redox Chemistry." *Synlett*, **2016**, *27*, 714-713 Copyright 2016 Georg Thieme Verlag KG and Joshi-Pangu, A.; Lévesque, F.; Roth, H. G.; Oliver, S. F.; Campeau, L.-C.; Nicewicz, D. A.; DiRocco, D. A. "Acridinium-Based Photocatalysts: A Sustainable Option in Photoredox Catalysis." *J. Org. Chem.*, **2016**, *81*, 7244-7249 Copyright 2016 American Chemical Society.

The content of chapters three and four are unpublished. A portion of chapter three detailing a diastereoselective route to the left side of rubriflordilactone B is intended for submission in the near future. Chapter four is included to serve as a compilation of the work we have conducted on stemocurtisine so far, and will hopefully serve as a useful source of information to guide future endeavors on this project.

*In memory of my mother,*
*Marianne Roth.*

## TABLE OF CONTENTS

LIST OF FIGURES ..... xii

LIST OF SCHEMES ..... xviii

LIST OF TABLES ..... xxiv

LIST OF ABBREVIATIONS ..... xxv

CHAPTER 1: INTRODUCTION TO ACRIDINIUM ION PHOTOREDOX CATALYSIS ..... 1

1.1 Introduction ..... 1

1.2 Fundamentals of Organic Photoredox Catalysis ..... 2

1.2.1 Photophysical Properties ..... 2

1.2.2 Thermodynamics of Photoinduced Electron Transfer ..... 4

1.2.3 Acridinium Cations as Photoredox Catalysts ..... 7

1.3 Acridinium Ion Photoredox Catalysis in Total Synthesis ..... 10

1.3.1 Polar Radical Crossover Cycloaddition ..... 10

1.3.2 Formal [3+2] Cycloaddition ..... 13

1.3.3 α-Amino Alkyation ..... 14

1.3.4 Conclusions and Outlook ..... 15

CHAPTER 2: EXPERIMENTAL AND CALCULATED ELECTROCHEMICAL POTENTIALS OF COMMON ORGANIC MOLECULES ..... 17

2.1 Introduction ..... 17

2.2 Experimental Electrochemical Potentials ..... 20

2.3 Calculated Electrochemical Potentials ..... 29

2.4 Acridinium Ions as Sustainable Photoredox Catalysts ..... 32

2.5 Conclusion ..... 35

2.6 Associated Data ..... 35

2.7 Acknowledgements ..... 35

CHAPTER 3: SYNTHETIC STUDIES TOWARD THE SYNTHESIS OF RUBRIFLORDILACTONE B ..... 36

3.1 Introduction ..... 36

3.1.1 Schisandraceae Natural Products ..... 36

3.1.2 Reported Efforts Toward Rubriflordilactone B ..... 37

3.1.3 Stereochemistry of Rubriflordilactone B ..... 43

3.2 Synthetic Strategy for Rubriflordilactone B ..... 47

3.2.1 Initial Retrosynthetic Analysis ..... 48

3.3 Synthesis of the Western Half of Rubriflordilactone B ..... 50

3.3.1 Conjugate Addition and Olefination ..... 51

3.3.2 Seven-Membered Ring Formation ..... 54

3.3.3 Synthesis of the Terminal Lactone ..... 60

3.3.4 Diastereoselective Route to the Left Half of Rubriflordilactone B ..... 65

3.4 Progress Toward the Synthesis of the Eastern Half of Rubriflordilactone B ..... 66

3.4.1 Propargyl Alcohol Synthesis ..... 68

3.4.2 Polar Radical Crossover Cycloaddition ..... 72

3.4.3 Substituted Indene Synthesis ..... 78

3.5 Investigating a Decarboxylative Diels-Alder Reaction ..... 82

3.5.1 Pyrone Synthesis ..... 84

3.5.2 Cyclopentene Synthesis ..... 86

3.5.3 Attempts at a Decarboxylative Diels-Alder ..... 89

3.6 Conclusion ..... 91

3.7 Associated Data ..... 92

3.8 Acknowledgements ..... 92

CHAPTER 4: SYNTHETIC STUDIES TOWARD THE SYNTHESIS OF STEMOCURTISINE AND RELATED NATURAL PRODUCTS ..... 93

4.1 Introduction ..... 93

4.1.1 Stemonaceae Natural Products ..... 93

4.1.2 Reported Efforts Toward Stemocurtisine ..... 95

4.2 Synthetic Approach to Stemocurtisine ..... 97

4.2.1 Attempting the Organic Photoredox Cascade ..... 99

4.3 Synthetic Approach to seco-Stemocurtisine ..... 100

4.3.1 Attempt at a PRCC ..... 101

4.3.2 Application of α-Amino Alkylation ..... 103

4.4 Conclusion ..... 104

4.5 Associated Data ..... 104

4.6 Acknowledgements ..... 104

APPENDIX A: EXPERIMENTAL DETAILS AND ELECTROCHEMICAL AND PHOTOCHEMICAL DATA ..... 105

A.1 Electrochemical Measurements ..... 105

A.1.1 General Information ..... 105

A.1.2 Cyclic Voltammetry ..... 105

A.2 Photophysical Measurements ..... 117

A.2.1 General Information ..... 117

A.2.2 Experimental Procedures and Data ..... 117

APPENDIX B: EXPERIMENTAL DETAILS AND CHARACTERIZATION DATA OF KEY INTERMEDIATES ..... 124

B.1 General Information ..... 124

B.2 Experimental Details ..... 125

B.2.1 Synthesis of the Western Half of Rubriflordilactone B ..... 125

B.2.2 Progress Toward the Synthesis of the Eastern Half of Rubriflordilactone B ..... 144

B.2.3 Investigating a Decarboxylative Diels-Alder Reaction ..... 157

B.3 Characterization Data ..... 169

B.3.1 NMR Spectra ..... 169

B.3.2 Crystallographic Information ..... 194

APPENDIX C: EXPERIMENTAL DETAILS AND CHARACTERIZATION OF KEY INTERMEDIATES ..... 197

C.1 General Information ..... 197

C.2 Experimental Details ..... 197

C.2.1 Attempting the Organic Photoredox Cascade ..... 197

C.2.2 Attempt at a PRCC ..... 201

C.2.3 Application of α-Amino Alkylation ..... 204

REFERENCES ..... 206

## LIST OF FIGURES

**Figure 1.1** Electrochemical Series of Photoredox Catalysts and Simple Organic Molecules (V vs SCE) – Oxidations ..... 6

**Figure 1.2** Electrochemical Series of Photoredox Catalysts and Simple Organic Molecules (V vs SCE) – Reductions ..... 7

**Figure 2.1** Examples of a Reversible and Irreversible CV with the Relevant Electrochemical Potentials Labeled ..... 18

**Figure 2.2** Electrochemical Series of Functional Groups Common in Organic Molecules (V vs SCE) ..... 20

**Figure 2.3** Electrochemical Series of Aromatic Hydrocarbons and Aryl Alkynes (V vs SCE) ..... 21

**Figure 2.4** Electrochemical Series of Alkenes between +1.00 to +1.75 V (V vs SCE) ..... 22

**Figure 2.5** Electrochemical Series of Alkenes between +1.75 and +2.50 V (V vs SCE) ..... 22

**Figure 2.6** Electrochemical Series of Phenols (V vs SCE) ..... 23

**Figure 2.7** Electrochemical Series of Ethers (V vs SCE) ..... 23

**Figure 2.8** Electrochemical Series of Amines (V vs SCE) ..... 24

**Figure 2.9** Electrochemical Series of Thiophenols and Aryl Disulfides (V vs SCE) ..... 24

**Figure 2.10** Electrochemical Series of Aromatic Heterocycles (V vs SCE) ..... 25

**Figure 2.11** Electrochemical Series of Alkyl and Aryl Halides (V vs SCE) ..... 25

**Figure 2.12** Electrochemical Series of Aldehydes (V vs SCE) ..... 26

**Figure 2.13** Electrochemical Series of Imines and Related Compounds (V vs SCE) ..... 26

**Figure 2.14** Electrochemical Series of Ketones (V vs SCE) ..... 27

**Figure 2.15** Electrochemical Series of Amides and TBA Carboxylates (V vs SCE) ..... 27

**Figure 2.16** Electrochemical Series of Carboxylic Acids and Derivatives (V vs SCE) ..... 28

**Figure 2.17** Electrochemical Series of Acyl and Sulfonyl Chlorides and Anhydrides (V vs SCE) ..... 28

**Figure 2.18** Electrochemical Series of Inorganic Compounds, Aryl Silanes, and TBA Salts (V vs SCE) ..... 29

**Figure 2.19** Electrochemical Series of Hypervalent Iodine Compounds, Nitrobenzene, and NCS (V vs SCE) ..... 29

**Figure 2.20** Plot of Experimental vs. Calculated Redox Potentials ..... 31

**Figure 3.1** Cycloartane ..... 37

**Figure 3.2** Bisnortriterpenoids Isolated by Sun ..... 37

**Figure 3.3** Rubriflordilactone B ..... 38

**Figure 3.4** 23-*epi*-Rubriflodilactone B ..... 43

**Figure 3.5** Stereocenters in pseudo-Rubriflordilactone B ..... 44

**Figure 3.6** Remaining Stereocenters to Resolve in pseudo-Rubriflordilactone B ..... 44

**Figure 3.7** Remaining Stereocenters to Resolve in pseudo-Rubriflordilactone B ..... 45

**Figure 3.8** Four Remaining Diastereomeric Possibilities ..... 45

**Figure 3.9** Computational Models Reported by Kaufman and Sarotti ..... 46

**Figure 3.10** Comparison of Rubriflordilactone B (**6**) and pseudo-Rubriflordilactone B (**11**) ..... 46

**Figure 3.11** Crystal Structures of α-Hydroxylactone Diastereomers ..... 60

**Figure 3.12** $^{1}$H NMR (pyridine-*d*5) of Product Formed in Both Routes ..... 64

**Figure 3.13** $^{1}$H NMR (pyridine-*d*5) of Product at 60 $^{o}$C ..... 65

**Figure 3.14** Crystal Structure of Left Half of Rubriflordilactone B ..... 65

**Figure 3.15** [2+2] Homodimer of Indene ..... 76

**Figure 3.16** $E_{p/2}$ Values Obtained for α-Silylalcohols ..... 77

**Figure 4.1** The Pyrrolo[1,2-*a*]azepine Nucleus of Stemona Alkaloids ..... 93

**Figure 4.2** Five Parent Compounds of Stemona Alkaloids Subclasses ..... 94

**Figure 4.3** Novel Pyrido[1,2-*a*]azapine Core ..... 94

**Figure 4.4** Structure of Stemocurtisine ..... 94

**Figure 4.5** Structure of 6-Hydroxy-5,6-seco-stemocurtisine ..... 100

**Figure A.1** Cyclic Voltammogram of Mesitylene ..... 106

**Figure A.2** Cyclic Voltammogram of Phenylacetylene ..... 106

**Figure A.3** Cyclic Voltammogram of 2-Methyl-2-butene ..... 106

**Figure A.4** Cyclic Voltammogram of *trans*-β-methylstyrene ..... 107

**Figure A.5** Cyclic Voltammogram of Carbon tetrachloride ..... 107

**Figure A.6** Cyclic Voltammogram of Ethyl bromoacetate ..... 107

**Figure A.7** Cyclic Voltammogram of 1-Chloro-4-iodobenzene (oxidation) ..... 108

**Figure A.8** Cyclic Voltammogram of 1-Chloro-4-iodobenzene (reduction) ..... 108

**Figure A.9** Cyclic Voltammogram of Phenol ..... 108

**Figure A.10** Cyclic Voltammogram of *o*-Dimethylbenzene ..... 109

**Figure A.11** Cyclic Voltammogram of 1,4-Dioxane ..... 109

**Figure A.12** Cyclic Voltammogram of 3,4-Dihydro-2*H*-pyran ..... 109

**Figure A.13** Cyclic Voltammogram of 2-Naphthalenethiol ..... 110

**Figure A.14** Cyclic Voltammogram of *p*-Methoxyphenyldisulfide ..... 110

**Figure A.15** Cyclic Voltammogram of Aniline ..... 110

**Figure A.16** Cyclic Voltammogram of Triethylamine ..... 111

**Figure A.17** Cyclic Voltammogram of 1-Morpholinocyclohexene ..... 111

**Figure A.18** Cyclic Voltammogram of Furan ..... 111

**Figure A.19** Cyclic Voltammogram of 5-Methoxyindole ..... 112

**Figure A.20** Cyclic Voltammogram of Quinoline ..... 112

**Figure A.21** Cyclic Voltammogram of 4-Chlorobenzaldehyde ..... 112

**Figure A.22** Cyclic Voltammogram of (*E*)-*N*-Benzylidene-3-methoxyaniline (oxidation) ..... 113

**Figure A.23** Cyclic Voltammogram of (*E*)-*N*-benzylidene-3-methoxyaniline (reduction) ..... 113

**Figure A.24** Cyclic Voltammogram of Acetophenone ..... 113

**Figure A.25** Cyclic Voltammogram of Tetra-*n*-butylammonium acetate ..... 114

**Figure A.26** Cyclic Voltammogram of Methyl benzoate ..... 114

**Figure A.27** Cyclic Voltammogram of *N*,*N*-Dimethylformamide ..... 114

**Figure A.28** Cyclic Voltammogram of Phthalic anhydride ..... 115

**Figure A.29** Cyclic Voltammogram of Benzoyl chloride ..... 115

**Figure A.30** Cyclic Voltammogram of *p*-Dicyanobenzene ..... 115

**Figure A.31** Cyclic Voltammogram of *p*-Toluenesulfonyl chloride ..... 116

**Figure A.32** Cyclic Voltammogram of Tetra-*n*-butylammonium bromide ..... 116

**Figure A.33** Cyclic Voltammogram of Ferrocene ..... 116

**Figure A.34** Cyclic Voltammogram of Catalyst **5** ..... 118

**Figure A.35** Absorption and Emission Spectra of Catalyst **5** ..... 118

**Figure A.36** Fluorescence Decay Data of Catalyst **5** ..... 119

**Figure A.37** Cyclic Voltammogram of Catalyst **6** ..... 119

**Figure A.38** Absorption and Emission Spectra of Catalyst **6** ..... 120

**Figure A.39** Fluorescence Decay Data of Catalyst **6** ..... 120

**Figure A.40** Cyclic Voltammogram of Catalyst **7** ..... 121

**Figure A.41** Absorption and Emission Spectra of Catalyst **7** ..... 121

**Figure A.42** Fluorescence Decay Data of Catalyst **7** ..... 122

**Figure A.43** Cyclic Voltammogram of Catalyst **8** ..... 122

**Figure A.44** Absorption and Emission Spectra of Catalyst **8** ..... 123

**Figure A.45** Fluorescence Decay Data of Catalyst **8** ..... 123

**Figure B.1** $^{1}$H NMR Spectrum of **5** ..... 169

**Figure B.2** $^{1}$H NMR Spectrum of **6** ..... 170

**Figure B.3** $^{1}$H NMR Spectrum of **7** ..... 170

**Figure B.4** $^{1}$H NMR Spectrum of **8** ..... 171

**Figure B.5** $^{1}$H NMR Spectrum of **9** ..... 171

**Figure B.6** $^{1}$H NMR Spectrum of **10** ..... 172

**Figure B.7** $^{1}$H NMR Spectrum of **11** ..... 172

**Figure B.8** $^{1}$H NMR Spectrum of **12**..... 173

**Figure B.9** $^{13}$C NMR Spectrum of **12** ..... 173

**Figure B.10** $^{31}$P NMR Spectrum of **12**..... 174

**Figure B.11** $^{1}$H NMR Spectrum of **13**..... 174

**Figure B.12** $^{13}$C NMR Spectrum of **13** ..... 175

**Figure B.13** $^{31}$P NMR Spectrum of **13**..... 175

**Figure B.14** $^{1}$H NMR Spectrum of **14**..... 176

**Figure B.15** $^{13}$C NMR Spectrum of **14** ..... 176

**Figure B.16** $^{1}$H NMR Spectrum of **20**..... 177

**Figure B.17** $^{1}$H NMR Spectrum of **21**..... 177

**Figure B.18** $^{13}$C NMR Spectrum of **21** ..... 178

**Figure B.19** $^{1}$H NMR Spectrum of **22**..... 178

**Figure B.20** $^{1}$H NMR Spectrum of **23**..... 179

**Figure B.21** $^{1}$H NMR Spectrum of **24**..... 179

**Figure B.22** $^{1}$H NM Spectrum of **25** ..... 180

**Figure B.23** $^{13}$C NMR Spectrum of **25** ..... 180

**Figure B.24** $^{1}$H NMR Spectrum of **26**..... 181

**Figure B.25** $^{13}$C NMR Spectrum of **26** ..... 181

**Figure B.26** $^{1}$H NMR Spectrum of **27**..... 182

**Figure B.27** $^{13}$C NMR Spectrum of **27** ..... 182

**Figure B.28** $^{1}$H NMR Spectrum of **28**..... 183

**Figure B.29** $^{13}$C NMR Spectrum of **28** ..... 183

**Figure B.30** $^{1}$H NMR Spectrum of **29**..... 184

**Figure B.31** $^{13}$C NMR Spectrum of **29** ..... 184

**Figure B.32** $^{1}$H NMR Spectrum of **30**..... 185

**Figure B.33** $^{13}$C NMR Spectrum of **30** ..... 185

**Figure B.34** $^{1}$H NMR Spectrum of **31** ..... 186

**Figure B.35** $^{13}$C NMR Spectrum of **31** ..... 186

**Figure B.36** $^{1}$H NMR Spectrum of **32** ..... 187

**Figure B.37** $^{13}$C NMR Spectrum of **32** ..... 187

**Figure B.38** $^{1}$H NMR Spectrum of **33** ..... 188

**Figure B.39** $^{13}$C NMR Spectrum of **33** ..... 188

**Figure B.40** $^{1}$H NMR Spectrum of **34** ..... 189

**Figure B.41** $^{13}$C NMR Spectrum of **34** ..... 189

**Figure B.42** $^{1}$H NMR ($CDCl_3$) Spectrum of **35** ..... 190

**Figure B.43** $^{1}$H NMR Spectrum (pyridine-$d_5$) of **35** ..... 190

**Figure B.44** $^{1}$H NMR Spectrum (pyridine-$d_5$, 60 $^{o}$C) of **35** ..... 191

**Figure B.45** $^{13}$C NMR Spectrum (pyridine-$d_5$) of **35** ..... 191

**Figure B.46** $^{13}$C NMR Spectrum (pyridine-$d_5$, 60 $^{o}$C) of **35** ..... 192

**Figure B.47** $^{1}$H NMR Spectrum of **36** ..... 192

**Figure B.48** $^{13}$C NMR Spectrum of **36** ..... 193

## LIST OF SCHEMES

**Scheme 1.1** Molecular Orbital Depiction of PET ..... 3

**Scheme 1.2** Simplified Jablonski Diagram Showing Photophysical Processes of Organic Molecules ..... 4

**Scheme 1.3** Comparison of Nucleophilic Attack on Unsubstituted and 9-Mesitylacridinium Ions ..... 8

**Scheme 1.4** Select Examples of Acridinium Ion Photoredox Transformations ..... 8

**Scheme 1.5** Traditional and Novel Routes for Acridinium Ion Synthesis ..... 9

**Scheme 1.6** Mechanism for γ-Butyrolactone Synthesis via a PRCC ..... 11

**Scheme 1.7** Synthesize of α-Methylene-γ-butyrolactones ..... 12

**Scheme 1.8** Routes to (±)-Methylenolactocin and (±)-Protolichesterinic Acid ..... 12

**Scheme 1.9** Mechanism of the Formal [3+2] Cycloaddition ..... 13

**Scheme 1.10** Formal Synthesis of HMG-CoA Reductase Inhibitor ..... 14

**Scheme 1.11** Mechanism of α-Amino Alkylation ..... 15

**Scheme 1.12** Synthesis of Monomorine I ..... 15

**Scheme 2.1** Common Degradation Pathways for Organic Molecules that Prevent Back Electron Transfer in CV Experiments ..... 18

**Scheme 2.2** Half Reactions for Oxidation and Reduction ..... 30

**Scheme 2.3** Important Tautomers of 2-Mercaptobenzothiazole ..... 32

**Scheme 2.4** Decarboxylative Conjugate Addition ..... 33

**Scheme 2.5** Mechanism of Decarboxylative Conjugate Addition ..... 34

**Scheme 3.1** Peng's Synthesis of the Eastern Hemisphere of Rubriflordilactone B ..... 38

**Scheme 3.2** Xie's Synthesis of the Left Half of Rubriflordilactone B ..... 39

**Scheme 3.3** Ang Li's Synthesis of Rubriflordilactone B ..... 41

**Scheme 3.4** Mechanism for Tetrahydrofuran Synthesis via a PRCC ..... 47

**Scheme 3.5** PRCC Adduct of Indene and Allyl Alcohol and its Comparison to Rubriflordilactone B ..... 48

**Scheme 3.6** Reported Methods for *A* Ring Synthesis ..... 49

**Scheme 3.7** Retrosynthetic Analysis of Rubriflordilactone B ..... 50

**Scheme 3.8** Retrosynthesis of Left Side Model System ..... 50

**Scheme 3.9** Synthesis of Butenolide Starting Material ..... 52

**Scheme 3.10** Attempted Conjugate Additions ..... 53

**Scheme 3.11** Synthesis of the α-Phosphonate Butenolide ..... 54

**Scheme 3.12** Route to the α-Methylene-γ-butyrolactone ..... 54

**Scheme 3.13** Attempts at a Reductive Cyclization to form the Cycloheptene ..... 55

**Scheme 3.14** Nucleophilic Epoxidation ..... 55

**Scheme 3.15** Initial Plan for Diene Synthesis ..... 57

**Scheme 3.16** Difference in Diels-Alder Selectivity Impacts Enolate Alkylation ..... 58

**Scheme 3.17** Synthesis of the Diene for the Ring Closing Metathesis ..... 58

**Scheme 3.18** Two Routes to Tricyclic α-Hydroxylactone ..... 59

**Scheme 3.19** Mechanism of Dieneoate Formation ..... 61

**Scheme 3.20** Attempts at Enolate Oxidation with Different Oxidants ..... 62

**Scheme 3.21** Initial Cascade Attempt Result ..... 62

**Scheme 3.22** Cascade Attempts with Wittig Salt and Meldrum's Acid ..... 63

**Scheme 3.23** Initial Sequence for the Synthesis of Ring *A* ..... 63

**Scheme 3.24** Alternate Route to Ring *A* ..... 64

**Scheme 3.25** Diastereoselective Route to the Left Half of Rubrilfordilactone B ..... 66

**Scheme 3.26** Retrosynthesis for the Right Side of Rubriflordilactone B ..... 67

**Scheme 3.27** Initial PRCC Results ..... 67

**Scheme 3.28** Attempt to Alter PRCC Diastereoselectivity ..... 67

**Scheme 3.29** Retrosynthesis Employing a Propargyl Alcohol in the PRCC ..... 68

**Scheme 3.30** Synthesis of Propargyl Alcohol ..... 68

**Scheme 3.31** Rate Enhancement by Water Observed by Kabayashi ..... 71

**Scheme 3.32** Optimized Vinylogous Mukaiyama Aldol with Catalytic Water ..... 71

**Scheme 3.33** Deprotection of TIPS-Acetylene ..... 72

**Scheme 3.34** Proposed Route with α-Silylallyl Alcohols ..... 76

**Scheme 3.35** Results from PRCC with α-Silylallyl Alcohols ..... 76

**Scheme 3.36** Proposed Route with Diol Nucleophile ..... 77

**Scheme 3.37** Results from PRCC with Diol Nucleophile ..... 77

**Scheme 3.38** Results from PRCC with 1,5-Hexadiene-3-ol ..... 78

**Scheme 3.39** Results from PRCC with Propargyl Alcohol ..... 78

**Scheme 3.40** Altering the Retrosynthesis ..... 79

**Scheme 3.41** Attempt at an *ortho*-Directed Formylation ..... 80

**Scheme 3.42** Synthesis of Disubstituted Indene ..... 81

**Scheme 3.43** Attempted Lithiation-Formylation ..... 81

**Scheme 3.44** Orthogonal Reactivity of Aryl Bromides and Aryl Ethers ..... 81

**Scheme 3.45** Attempts at a Palladium-Catalyzed Formylation ..... 82

**Scheme 3.46** PRCC Attempted by Xie ..... 82

**Scheme 3.47** Electrocyclization Employed by Ang Li ..... 83

**Scheme 3.48** Retrosynthesis with Decarboxylative Diels-Alder ..... 83

**Scheme 3.49** Synthesis of Enone for RCM ..... 84

**Scheme 3.50** Conjugate Addition with Acrylic Acid Weinreb Amide ..... 85

**Scheme 3.51** Synthesis of Cycloheptenone ..... 85

**Scheme 3.52** Synthesis of Pyrone for Decarboxylative Diels-Alder Model System ..... 86

**Scheme 3.53** Conjugate Reduction and Desilylation Attempt with PRCC Product ..... 90

**Scheme 3.54** Cation-Radical Diels-Alder Attempts ..... 91

**Scheme 4.1** Synthesis of Substituted Lactam ..... 95

**Scheme 4.2** Constructing the Seven-Membered Ring ..... 96

**Scheme 4.3** Synthesizing the *C* Ring ..... 96

**Scheme 4.4** Attempts at a Photochemical Oxidative Cyclization ..... 97

**Scheme 4.5** Precedent for Dehydrogenation and Hydrofunctionalization ..... 98

**Scheme 4.6** Proposed Organic Photoredox Cascade ..... 98

**Scheme 4.7** Synthesis of Stemocurtisine from Cascade Product ..... 98

**Scheme 4.8** Attempts at Synthesizing the Photoredox Cascade Precursor ..... 99

**Scheme 4.9** Synthesis of the Photoredox Cascade Precursor ..... 99

**Scheme 4.10** Photoredox Cascade Results ..... 100

**Scheme 4.11** Proposed Synthesis of Stemocurtisine from seco-Stemocurtisine ..... 101

**Scheme 4.12** Proposed Synthesis of seco-Stemocurtisine via a PRCC ..... 101

**Scheme 4.13** Synthesis of Protected Enamine and γ-Hydroxybutenolide ..... 102

**Scheme 4.14** Proposed Synthesis of *seco*-Stemocurtisine via Intramolecular α-Amino Alkylation ..... 103

**Scheme 4.15** Synthesis of α-Amino Alkylation Model System ..... 104

**Scheme B.1** Synthesis of **1-4** ..... 125

**Scheme B.2** Synthesis of **5** ..... 126

**Scheme B.3** Synthesis of **6** and **5** ..... 127

**Scheme B.4** Synthesis of **7-9** ..... 127

**Scheme B.5** Synthesis of **10-11** ..... 129

**Scheme B.6** Synthesis of **12-14** ..... 130

**Scheme B.7** Synthesis of **15-18** ..... 132

**Scheme B.8** Synthesis of **19** ..... 133

**Scheme B.9** Synthesis of **20-21** ..... 134

**Scheme B.10** Synthesis of **22-24** ..... 134

**Scheme B.11** Synthesis of **25-27** ..... 136

**Scheme B.12** Synthesis of **28-29** ..... 138

**Scheme B.13** Synthesis of **31-32** ..... 139

**Scheme B.14** Synthesis of **32** ..... 140

**Scheme B.15** Synthesis of **33-35** ..... 141

**Scheme B.16** Synthesis of **36** and **35** ..... 142

**Scheme B.17** Synthesis of **37** ..... 144

**Scheme B.18** Synthesis of **38-41** ..... 144

**Scheme B.19** Synthesis of **42-45** ..... 146

**Scheme B.20** Synthesis of **46-48** ..... 148

**Scheme B.21** Synthesis of **49-50** ..... 149

**Scheme B.22** Synthesis of **51-53** ..... 150

**Scheme B.23** Synthesis of **54-56** ..... 151

**Scheme B.24** Synthesis of **57-58** ..... 152

**Scheme B.25** Synthesis of **59-62** ..... 153

**Scheme B.26** Synthesis of **63-65** ..... 155

**Scheme B.27** Synthesis of **66-69** ..... 156

**Scheme B.28** Synthesis of **70-71** ..... 157

**Scheme B.29** Synthesis of **72-75** ..... 158

**Scheme B.30** Synthesis of **76-77** ..... 160

**Scheme B.31** Synthesis of **78-79** ..... 161

**Scheme B.32** Synthesis of **80-83** ..... 162

**Scheme B.33** Synthesis of **84-87** ..... 164

**Scheme B.34** Synthesis of **88-89** ..... 165

**Scheme B.35** Synthesis of **90-91** ..... 167

**Scheme B.36** Synthesis of **92** ..... 168

**Scheme B.37** Synthesis of **93** ..... 168

**Scheme C.1** Synthesis of **1-3** ..... 197

**Scheme C.2** Synthesis of **4-5** ..... 199

**Scheme C.3** Synthesis of **6-8** ..... 199

**Scheme C.4** Synthesis of **9** ..... 201

**Scheme C.5** Synthesis of **10-11** ..... 201

**Scheme C.6** Synthesis of **12-15** ..... 202

**Scheme C.7** Synthesis of **16-17** ..... 204

## LIST OF TABLES

**Table 1.1** Impact of Substitution on Acridinium Ion Excited-State Reduction Potential and Lifetime ..... 9

**Table 2.1** Electrochemical and Photophysical Properties of Photoredox Catalysts ..... 33

**Table 2.2** Decarboxylative Conjugate Addition with Acridinium Ion Catalysts ..... 34

**Table 3.1** Attempts at an Acid-Mediated Epoxide Opening ..... 56

**Table 3.2** Impact of Enolate Oxidation Scale on Yield ..... 61

**Table 3.3** Impact of Silyl Group on Vinylogous Mukaiyama Aldol ..... 69

**Table 3.4** Impact of Solvent on Vinylogous Mukaiyama Aldol ..... 70

**Table 3.5** Summary of Deprotection Conditions with TBAF ..... 72

**Table 3.6** Hydrogen Atom Donor Screen for PRCC with 3-Butyn-1-ol ..... 73

**Table 3.7** PRCC Conditions Screened with Alcohol **37** ..... 74

**Table 3.8** PRCC Conditions Screened with Silylated Alkyne ..... 75

**Table 3.9** Optimization of the PRCC with 1,3-Cyclohexadiene – Solvent ..... 87

**Table 3.10** Optimization of the PRCC with 1,3-Cyclohexadiene – Loading ..... 87

**Table 3.11** Optimization of the PRCC with 1,3-Cyclohexadiene – Slow Addition ..... 88

**Table 3.12** Optimization of the PRCC with Cyclpentadiene ..... 89

**Table 3.13** Attempt at Decarboxylative Diels-Alder with Conventional Heating ..... 89

**Table 3.14** Attempted at Decarboxylative Diels-Alder with Microwave Heating ..... 90

**Table 3.15** Attempt at Decarboxylative Diels-Alder with Electron-Poor Pyrone ..... 91

**Table 4.1** Conditions Employed for PRCC Attempts ..... 102

**Table B.1** Crystal Data for **29** ..... 194

**Table B.2** Crystal Data for **31** ..... 195

**Table B.3** Crystal Data for **35** ..... 196

## LIST OF ABBREVIATIONS

| | |
|---|---|
| $^{o}$ | Degree |
| Å | Angstrom |
| Acr | Acridinium ion |
| Ag\|AgCl | Silver-silver chloride electrode |
| AIBN | Azobisisobutyronitrile |
| approx. | Approximately |
| aq | Aqueous |
| Ar | Arene |
| B | Generic base |
| BAIB | Bis(acetoxy)iodobenzene |
| BDMS | Benzyldimethylsilyl |
| BINAP | 2,2’-bis(diphenylphosphino)-1,1’-binaphthyl |
| Boc | *tert*-Butyoxycarbonyl |
| BPO | Benzoyl peroxide |
| bs | broad singlet |
| $^{o}$C | Degrees Celsius |
| Cbz | Carboxybenzyl |
| CDI | 1,1’-Carbonyldiimidazole |
| CFL | Compact fluorescent light |
| cod | Cyclooctadiene |
| conc. | Concentrated |
| CSA | Camphorsulfonic acid |

| | |
|---|---|
| CV | Cyclic voltammogram |
| δ | ppm |
| *d* | Deuterated |
| d | doublet |
| dd | doublet of doublets |
| ddd | doublet of doublets of doublets |
| dddd | doublet of doublets of doublet of doublets |
| ddt | doublet of doublet of triplets |
| dp | doublet of pentets |
| dq | doublet of quartets |
| dqd | doublet of quartets of doublets |
| dt | doublet of triplets |
| dtd | doublet of triplets of doublets |
| dba | Dibenzylideneacetone |
| DBU | 1,8-Diaza[5.4.0]undec-7ene |
| DDQ | 2,3-Dichloro-5,6-dicyano-1,4-benzoquinone |
| dq | doublet of quartets |
| dt | doublet of triplets |
| DCE | 1,2-Dichloroethane |
| DCM | Dichloromethane |
| DDQ | 2,3-Dichloro-5,6-dicyano-1,4-benzoquinone |
| DIBAL | Diisobutylaluminum hydride |
| DIPA | Diisopropylamine |

| | |
|---|---|
| DIPEA | *N*,*N*-diisopropylethylamine |
| DMAP | 4-Dimethylaminopyridine |
| DMF | *N*,*N*-Dimethylformamide |
| DMP | Dess-Martin periodinane |
| DMPS | Dimethylphenylsilyl |
| DMPU | 1,3-Dimethyl-3,4,5,6-tetrahydro-2(1*H*)-pyrimidinone |
| DMS | Dimethylsulfide |
| DMS | Dimethylsulfoxide |
| dppb | 1,4-bis(diphenylphosphino)butane |
| dppf | 1,1'-Bis(diphenylphosphino)ferrocene |
| d.r. | Diastereomeric ratio |
| $-e^-$ | Single-electron oxidation |
| $+e^-$ | Single-electron reduction |
| $\Delta E$ | Difference in electrochemical potential |
| ee | Enantiomeric excess |
| $E_{1/2}^{0,calc}$ | Calculated standard reduction potential |
| $E_{1/2}^{,ref}$ | Absolute potential for a standard electrode |
| $E_{0,0}$ | Excited-state energy |
| $E_{1/2}$ | Reduction potential |
| $E_{ex}$ | Experimental electrochemical potential |
| $E_{calc}$ | Calculated electrochemical potential |
| $E_{ox}$ | Oxidation potential |
| $E_p$ | Peak potential |

| | |
|---|---|
| $E_{p/2}$ | Half-peak potential |
| $E_{red}$ | Reduction potential |
| $^*E_{red}$ | Excited-state reduction potential |
| equiv | Equivalents |
| ET | Electron transfer |
| EWG | Electron-withdrawing group |
| $F$ | Faraday's constant |
| F(000) | Structure factor |
| Fmoc | Fluorenylmethyloxycarbonyl |
| $\Delta G_{1/2}^{0,calc}$ | Calculated standard free energy difference of a redox event |
| $\Delta G_{1/2}$ | Gibbs free energy of an electrochemical reduction |
| $\Delta G_{ET}$ | Gibbs free energy of electron transfer |
| $\Delta G_{PET}$ | Gibbs free energy of photoinduced electron transfer |
| GC | Gas chromatography |
| GC-MS | Gas chromatography-mass spectrometry |
| $-H^+$ | Deprotonation |
| $+H^+$ | Protonation |
| $-H_2$ | Dehydrogenation |
| hept | heptet |
| HOMO | Highest occupied molecular orbital |
| HMDSO | Hexamethyldisiloxane |
| HMPA | Hexamethylphosphoric triamide |
| hr | Hours |

| | |
|---|---|
| h$\nu$ | Photon |
| HWE | Horner-Wadsworth-Emmons |
| Hz | Hertz |
| IPr | 1,3-Bis(2,6-diisopropylphenyl)-1,3-dihydro-2*H*-imidazol-2-ylidene |
| *J* | Coupling constant |
| K | Kelvin |
| kcal | Kilocalorie |
| KHMDS | Potassium bis(trimethylsilyl)amide |
| λ | Wavelength |
| LAH | Lithium aluminum hydride |
| LDA | Lithium diisopropylamide |
| LED | Light-emitting diode |
| LiHMDS | Lithium bis(trimethylsilyl)amide |
| LTMP | Lithium tetramethylpiperidide |
| LUMO | Lowest unoccupied molecular orbital |
| μ | Absorption coefficient |
| μL | Microliters |
| μM | Micromolar |
| μmol | Micromoles |
| μs | Microseconds |
| μW | Microwave irradiation |
| M | Molar |
| m | Multiplet |

| | |
|---|---|
| *m* | *meta* |
| mm | Millimeter |
| *m*CPBA | *meta*-Chloroperbenzoic acid |
| MeCN | Acetonitrile |
| MHz | Megahertz |
| min | Minutes |
| mol | Moles |
| MoOPD | Oxodiperoxymolybdenum(pyridine)(DMPU) |
| MoOPH | Oxodiperoxymolybdenum(pyridine)(HMPA) |
| mL | Milliliters |
| mmol | Millimoles |
| ms | Milliseconds |
| N | Normal |
| n | Electrons |
| NA | Not applicable |
| NBS | *N*-Bromosuccinimide |
| NCS | *N*-Chlorosuccinimide |
| NIS | *N*-Iodosuccinimide |
| nm | Nanometer |
| NMR | Nuclear magnetic resonance |
| NOBIN | 2-Amino-2’-hydroxy-1,1’-binaphthyl |
| NOESY | Nuclear Overhauser effect spectroscopy |
| ns | Nanoseconds |

| | |
|---|---|
| Nu | Nucleophile |
| *o* | *ortho* |
| OAc | Acetate |
| OTf | Triflate |
| *p* | *para* |
| p | pentet |
| ppm | Parts per million |
| PCC | Pyridinium chlorochromate |
| PET | Photoinduced electron transfer |
| PG | Protecting group |
| PMB | *para*-Methoxybenzyl |
| PMHS | Polymethylhydrosiloxane |
| PMN | Phenylmalononitrile |
| PMP | *para*-Methoxyphenyl |
| PRCC | Polar radical crossover cycloaddition |
| ps | Picosecond |
| PTFE | Polytetrafluoroethylene |
| q | Quartet |
| *R* | Gas constant |
| *rac* | Racemic |
| RBF | Round-bottom flask |
| RCM | Ring-closing metathesis |
| RT | Room temperature |

| | |
|---|---|
| s | Singlet |
| sat | Saturated |
| SCE | Saturated calomel electrode |
| SET | Single electron transfer |
| SHE | Standard hydrogen electrode |
| SOMO | Singly occupied molecular orbital |
| τ | Excited-state lifetime |
| θ | Angle of reflection |
| T | Temperature |
| TBACl | Tetra-*n*-butylammonium chloride |
| TBAF | Tetra-*n*-butylammonium fluoride |
| TBDPS | *tert*-Butyldiphenylsilyl |
| TBHP | *tert*-Butyl hydroperoxide |
| TBS | *tert*-Butyldimethylsilyl |
| TCSPC | Time-correlated single photon counting |
| td | triplet of doublets |
| TEA | Triethylamine |
| TEMPO | 2,2,6,6-Tetramethyl-1-piperidinyloxy free radical |
| TES | Triethylsilyl |
| TFE | 3,3,3-Trifluoroethanol |
| THF | Tetrahydrofuran |
| TIPS | Triisopropylsilyl |
| TFA | Trifluoroacetic acid |

| | |
|---|---|
| TLC | Thin-layer chromatography |
| TMEDA | *N*,*N*,*N*',*N*,'-Tetramethylethylenediamine |
| TMS | Trimethylsilyl |
| TPS | Triphenylsilyl |
| tq | triplet of quartets |
| Tr | Trityl |
| UV | Ultraviolet |
| V | Volts |
| W | Watts |
| X | Halogen |

# CHAPTER 1: INTRODUCTION TO ACRIDINIUM ION PHOTOREDOX CATALYSIS

## 1.1 Introduction

Living organisms have relied on biochemical pathways involving electron transfers and radical intermediates for millennia. Two important examples of this are the electron transport chain and photosynthesis, both of which have enabled life as we know it to exist. Radical reactions are a powerful tool in synthesis, allowing one to access compounds that are difficult or impossible to form via polar mechanisms; however, these processes remain less studied than their polar counterparts. Open-shell intermediates can be generated a number of ways including heat, UV light, electrical currents, and strong oxidants/reductants. While such methods have allowed for a plethora of reactions to be developed, the safety, simplicity, and substrate compatibility of such systems can be problematic.[1]

Within the past forty years, there has been a growing interest in using visible light, as opposed to UV light, to generate radicals. Though all organic molecules absorb UV light, only those with extended conjugation absorb visible light. Therefore, by utilizing a photocatalyst that absorbs in the visible region, one can selectively generate open-shell intermediates via an electron transfer between an organic substrate and the photoexcited catalyst. The majority of studies to date employ ruthenium(II)- or iridium(III)-based complexes as the catalyst, and often involve reduction of the metal center after photoexcitation; the resulting ruthenium(I) and iridium(II) species are potent reductants, and have been used to facilitate numerous transformations which are discussed in several reviews.[2–6]

Despite the utility of these complexes, ruthenium and iridium remain expensive, and this often limits their use, especially on industrial scale. As a result, there is a growing interest in developing organic photoredox catalysts that are able to facilitate the same, or better, chemistry. These species would be much cheaper to make and therefore more readily available to the synthetic community at large.[7]

This chapter will provide an overview of photoredox catalysis by looking at photophysical properties, thermodynamics of electron transfer, and the use of acridinium ion dyes as photoredox catalysts. Finally, the use of acridinium ion-based photoredox reactions in natural product synthesis will be discussed.

## 1.2 Fundamentals of Organic Photoredox Catalysis

### 1.2.1 Photophysical Properties

Electron transfer (ET) involves movement of an electron from an electron donor to an electron acceptor. When this process is initiated by photoexcitation, it is termed photoinduced electron transfer (PET). Furthermore, when the photoexcited species is used catalytically, and the PET facilitates a productive reaction between organic molecules, the cumulative process is classified as photoredox catalysis.

In order for a photoredox reaction to be successful, an appropriate wavelength of light must be employed. Ideally, this would primarily be absorbed by the catalyst and not the other molecules present in the system in order to minimize undesired side reactions. When a photoredox catalyst absorbs a photon of light, an electron present in its HOMO is promoted to the LUMO, giving rise to two SOMOs of different energy (Scheme 1.1A). This state is referred to as the lowest-energy singlet excited state[i] ($S_1$). From here, PET can occur in one of two ways.

[i] While excitation to a molecular orbital higher in energy than the LUMO is possible, this situation will not be discussed here.

The first option is oxidation of the excited catalyst, in which the unpaired electron in the higher-energy SOMO can be transferred to the LUMO of an electron-acceptor (Scheme 1.1B). Alternatively, reduction can take place, which involves transfer of an electron from a donor molecule into the vacancy present in the lower-energy SOMO of the catalyst (Scheme 1.1C).

**Scheme 1.1** Molecular Orbital Depiction of PET

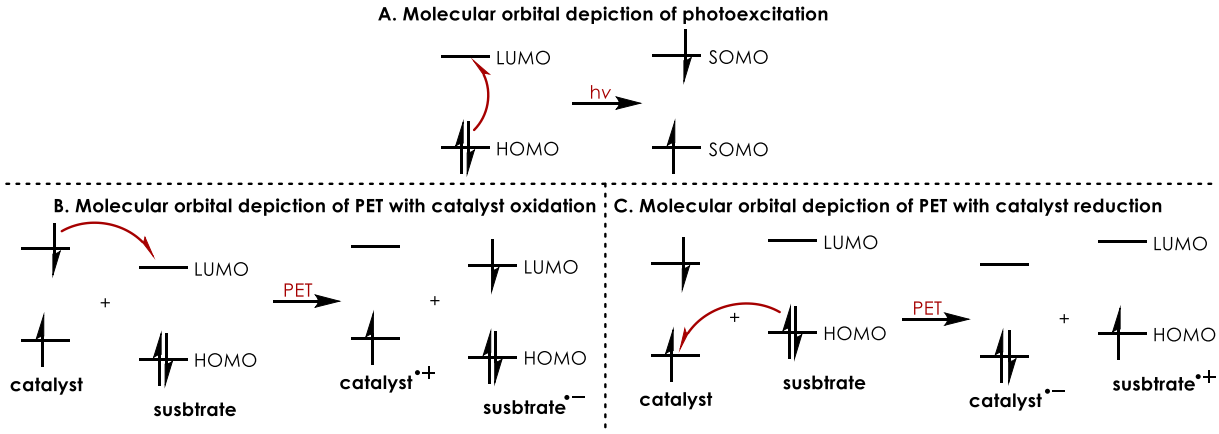


While a PET ultimately results in productive chemistry, several other non-productive pathways may also occur after photoexcitation (Scheme 1.2). After excitation to the $S_1$ state (a), vibrational relaxation (b) causes the lowest-energy vibrational state to be the most populated. From here, four processes may occur: PET, non-radiative decay (c), fluorescence (d) and intersystem crossing (e). Both fluorescence and non-radiative decay result in a ground state electronic configuration without an ET, but they differ in how the excited-state energy is dissipated. In fluorescence, the excited species releases the energy in the form a photon, often of a different wavelength than the one initially absorbed; in the case of non-radiative decay, the energy can be lost in several ways such as by collisions with solvent molecules. In the case of intersystem crossing, one of the unpaired electrons undergoes a spin-flip, this results in occupation of the lowest-energy triplet state ($T_1$). From here, a process known as

phosphorescence (f) can occur, which involves the molecule returning to the ground state with release of a photon *and* a spin-flip.

**Scheme 1.2** Jablonski Diagram Showing Photophysical Processes of Organic Molecules

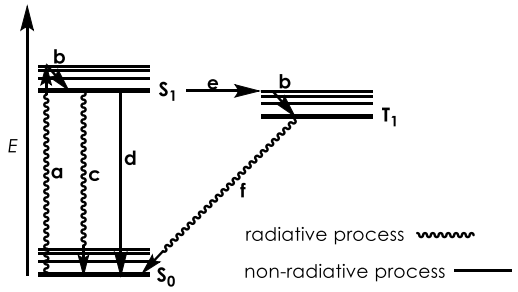


The length of time in which a molecule remains in the excited state is referred to as the excited-state lifetime (τ). In the case of species who primarily occupy the $S_1$ state, τ is typically on the scale of 2-20 ns, while those that undergo intersystem crossing have much longer τ-values due to the electron-flip required for phosphorescence, giving lifetimes on the scale of μs to ms.[7] While there is a difference in terms of energy and lifetime between the $S_1$ and $T_1$ states, the general rule of thumb is that catalysts with longer τ-values will be more efficient photoredox catalysts as they stand a better chance of encountering an electron donor/acceptor before returning to the ground state via a non-productive pathway.

### 1.2.2 Thermodynamics of Photoinduced Electron Transfer

The remainder of this chapter will focus on the use of acridinium ion dyes as photoredox catalysts, which behave as strong oxidants in the excited state. The thermodynamics of an ET event depends on the electrochemical redox potentials of the compounds involved. The free energy change for such a process can be calculated with a variation of the Nernst equation (Equation 1.1), where n is number of electrons transferred[ii], *F* is Faraday's constant (23.061 kcal

[ii] While more than one electron may be transferred during a single process, it will be assumed that n = 1 throughout this discussion

$V^{-1}$ $mol^{-1}$), $E_{red}$ is the reduction potential of an electron-acceptor, and $E_{ox}$ is the oxidation potential[iii] of an electron donor.[7]

**Equation 1.1**

$$\Delta G_{ET} = -nF\Delta E = -nF[E_{red}(A/A^{\cdot-}) - E_{ox}(D^{+\cdot}/D)]$$

In the case of acridinium ion photoredox catalysis, the electron-acceptor is the acridinium ion and the electron-donor is the substrate. Since ET occurs with an excited-state catalyst, a revised equation (Equation 1.2) is utilized, which replaces $E_{red}$ with $^*E_{red}$, the excited-state reduction potential of the catalyst.[8]

**Equation 1.2**

$$\Delta G_{PET} = -nF\Delta E = -nF[{}^*E_{red}(^*A/A^{\cdot-}) - E_{ox}(D^{+\cdot}/D)]$$

The excited-state reduction potential of an acridinium ion is estimated from its ground-state reduction potential and its excited state energy ($E_{0,0}$) (Equation 3), which is itself estimated from the wavelength at which the normalized excitation and emission spectra of the species intersect.

**Equation 1.3**

$$^*E_{red} = E_{red} - E_{0,0}$$

Therefore, in order for a PET to be thermodynamically favorable ($\Delta G_{PET} < 0$), the excited-state reduction potential of the acridinium ion must be *more positive* than the ground-state oxidation potential of the substrate. A small set of organic molecule oxidation potentials and excited-state reduction potentials of photoredox catalysts are compiled here (Figure 1.1).[8]

[iii] While all electrochemical potentials are formally written as reductions, many organic molecules only undergo oxidation under normal circumstances, and hence the term oxidation potential is often used

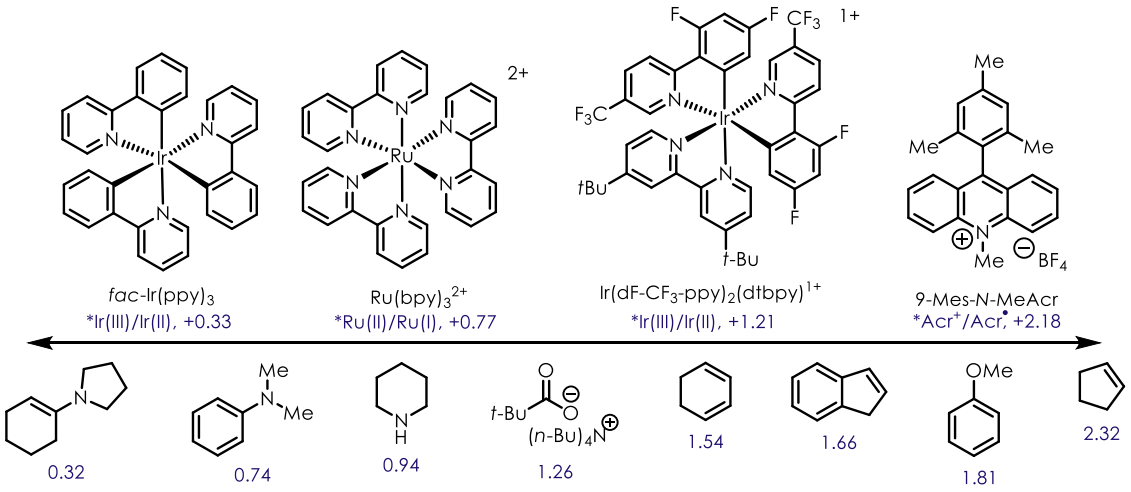


**Figure 1.1** Electrochemical Series of Photoredox Catalysts and Simple Organic Molecules (V vs SCE) – Oxidations

Based on this sampling of data, it is evident that the excited-state metal complexes are only capable of oxidizing very electron-rich species such as enamines and anilines. On the other hand, the acridinium ion catalyst shown can oxidize a variety of olefins and less electron-rich arenes in addition to the electron-rich substrates. Since the acridinium ion is such a potent excited-state oxidant, it is an attractive alternative for photoredox reactions where substrate oxidation is desired.

After reduction of the excited-state acridinium ion by an electron donor, the acridinium cation must be regenerated by a suitable reductant. Based on Equation 1.1, for this process to be exergonic ($\Delta G_{ET} < 0$), the reduction potential of the catalyst must be *more negative* than that of the reductant. Another set of redox potentials, this time detailing organic molecule reduction potentials and ground-state reduction potentials of photoredox catalysts are compiled here (Figure 1.2).[8]

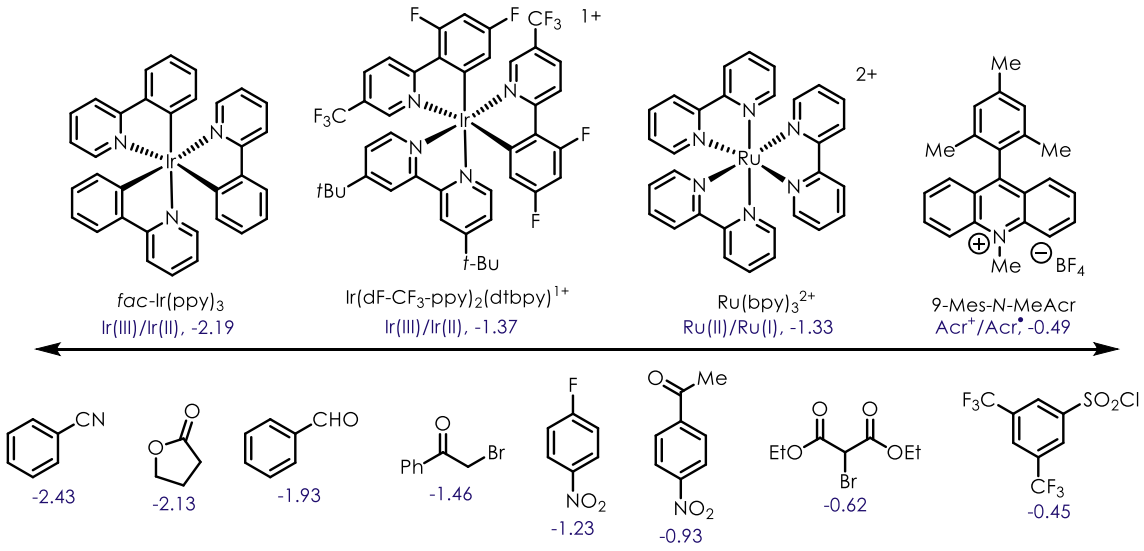


**Figure 1.2** Electrochemical Series of Photoredox Catalysts and Simple Organic Molecules (V vs SCE) – Reductions

In this electrochemical series, it is clear that the acridinium ion is the weakest ground-state reductant. Because of this, the acridinium ion catalyst is quite limited in terms of what reductants are capable of turning it over; as a result, radical species are often used to do this, but their reduction potentials cannot be measured directly with traditional methods, and therefore this data is not included here.

### 1.2.3 Acridinium Cations as Photoredox Catalysts

While acridinium ions have been known for years, their susceptibility to nucleophilic attack at the 9-position (Scheme 1.3A) limited their use as catalysts.[7] When Fukuzumi reported a 9-mesityl-substituted acridinium ion that was more resistant to nucleophilic deactivation (Scheme 1.3B), these species quickly gained popularity as photoredox catalysts due to their high excited-state reduction potentials, which are typically greater than 2 V vs SCE.[9]

**Scheme 1.3** Comparison of Nucleophilic Attack on Unsubstituted and 9-Mesitylacridinium Ions

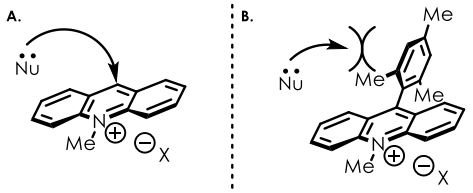


Within the past decade, acridinium ions have been used to catalyzed a variety of transformations including anti-Markovnikov alkene functionalization, arene functionalization, decarboxylations, cycloadditions, and alkylations to name a few examples (Scheme 1.4).[10–14] Each of these transformations demonstrate the ability of acridinium ions to oxidize a variety of functional groups including alkenes, arenes, carboxylates, and amines.

**Scheme 1.4** Select Examples of Acridinium Ion Photoredox Transformations

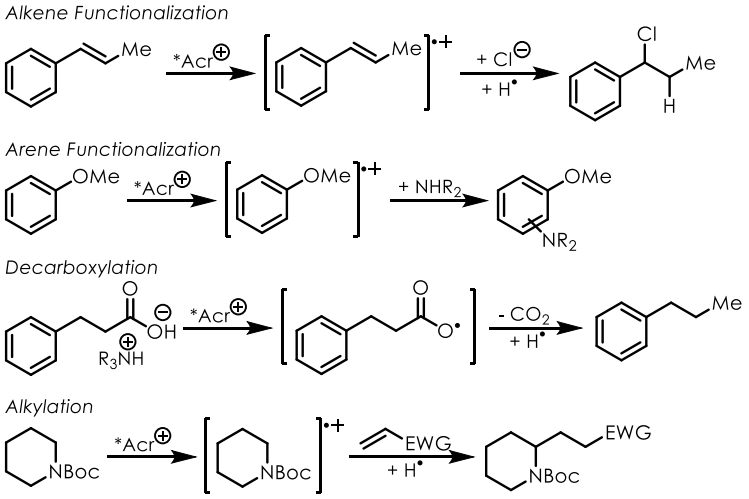


In addition to their compatibility with a broad range of functional groups, acridinium ions are attractive as photocatalysts due to their stability and tuneability. Introducing substituents on the acridinium ion core along with varying the substituents at the 9- and 10-positions can have profound impacts on their $^*E_{red}$ and τ-values (Table 1.1).[15,16]

**Table 1.1** Impact of Substitution on Acridinium Ion Excited-State Reduction Potential and Lifetime

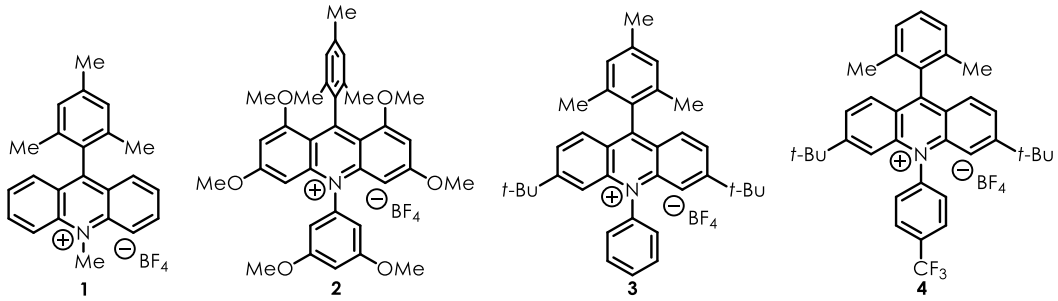


| Acridinium Ion | $^{*}E_{red}$ (V vs SCE) | τ (ns) |
|---|---|---|
| **1** | 2.18 | 6.40 |
| **2** | 1.62 | 1.3, 8.9[iv] |
| **3** | 2.15 | 14.4 |
| **4** | 2.14 | 20.7 |

Unfortunately, many of the more complicated acridinium cations require multistep sequences that can be costly, slow, and inconsistent in terms of yield (Scheme 1.5A), which has limited their use by industry and the synthetic community at large. Recently, a more stream-lined route was reported by our lab (Scheme 1.5 B).[16]

**Scheme 1.5** Traditional and Novel Routes for Acridinium Ion Synthesis

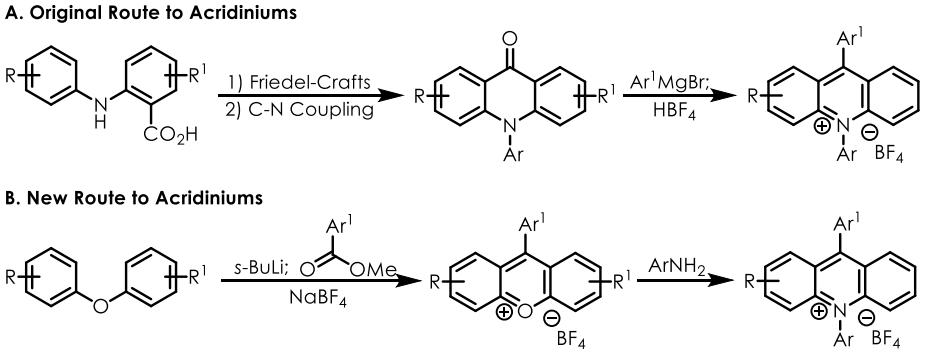


This work circumvented many of the issues with the previous method by replacing the Friedel-Crafts cyclization and the aryl-Grignard addition steps with a one-pot lithiation, 1,2-

[iv] Some catalysts exhibit a non-linear excited-state lifetime, which may indicate the presence of a charge-transfer complex

addition sequence. Furthermore, a range of diverse acridinium ions could be accessed not only by varying substituents on the biaryl ether, but also the identity of the arenes in the methyl ester and aniline reagents. We anticipate this report will help make the use of these powerful catalysts more widespread, particularly in industry, where many of the ruthenium- and iridium-complexes would be too costly to even consider.

### 1.3 Acridinium Ion Photoredox Catalysis in Total Synthesis

Heterocycles are important structural motifs in natural products and bioactive molecules; as a result, synthetic chemists are always interested in developing novel routes to make these motifs more efficiently. Providing a means to introduce a range of substituents at each position around the heterocycle is also greatly desired.

Acridinium cations have been utilized to access a wide range of heterocycles including cyclic ethers, cyclic amines, lactones, lactams, and aromatic heterocycles.[11,17–21] Despite this, the application of these transformations to the synthesis of complex natural products is not well explored. This section will highlight a few select transformations and how they were utilized to access bioactive molecules.

#### 1.3.1 Polar Radical Crossover Cycloaddition

Our lab has published a number of anti-Markovnikov hydrofunctionalization reactions of olefins mediated by acridinium ion photoredox catalysis. When an allylic or propargylic nucleophile is utilized, heterocycles are formed via a process referred to as a polar radical crossover cycloaddition (PRCC). We have used this approach to synthesize highly substituted cyclic ethers and amines, lactones, and lactams.[17,19–21]

In a 2014 we reported PRCC conditions to access a variety of substituted γ-hydroxybutyrolactones. This reaction involves oxidation of the alkene (**1**) by the excited-state

acridinium ion and trapping of the resultant radical cation (**2**) by the unsaturated acid (**3**) to provide the more stable radical (**4**); the product (**5**) is then formed after a 5-*exo*-trig radical cyclization and a hydrogen-atom abstraction. The radical cyclization is under kinetic control as opposed to thermodynamic, resulting in only 5-*exo*-trig cyclization and no evidence for a 6-*endo*-trig cyclization product. Lastly, the thiyl radical (**6**) formed from this abstraction is able to regenerate the catalyst (Scheme 1.6).[20]

**Scheme 1.6** Mechanism for γ-Butyrolactone Synthesis via a PRCC

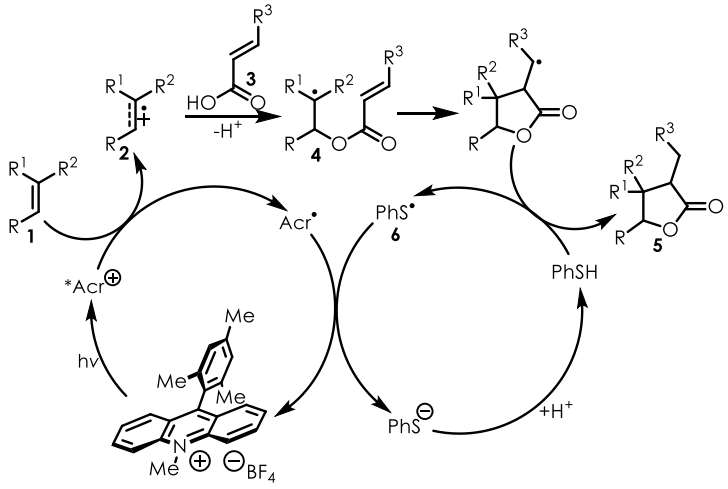


This work was found to be compatible with a variety of alkenes and both allylic and propargylic acids could be utilized. One challenge encountered by the lab during this work was how to synthesize α-methylene-γ-butyrolactones (**7**). Initial attempts with propiolic acid (**8**) proved ineffective, but switching to 3-trimethylsilylpropiolic acid (**9**) afforded products in good yields, likely by facilitating the radical cyclization step via stabilization of the resultant vinyl radical (Scheme 1.7A).[20] Unfortunately, deprotection of these species proved problematic as only the *Z*-isomer could be effectively desilylated. Ultimately, we moved to *Z*-3-chloroacrylic acid and *Z*-3-bromoacrylic acid nucleophiles as the resultant β-halo-γ-butyrolactones (**10**) could

undergo base-induced elimination to give the desired α-methylene-γ-butyrolactones (Scheme 1.7B).

**Scheme 1.7** Synthesis of α-Methylene-γ-butyrolactones

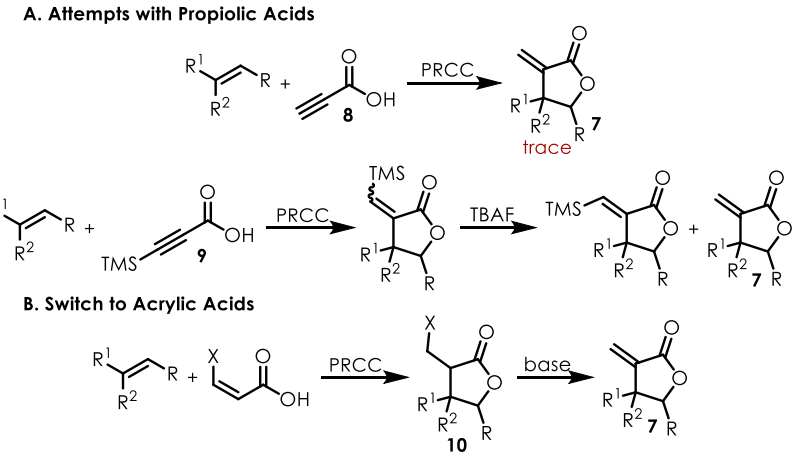


Two simple natural products (±)-methylenolactocin and (±)-protolichesterinic acid were made using this strategy in 3 steps (Scheme 1.8). After the initial PRCC reaction, oxidation of the arene to a carboxylic acid followed by base-induced elimination gave the desired compounds in 16% and 37% overall yield, respectively

**Scheme 1.8** Synthesis of (±)-Methylenolactocin and (±)-Protolichesterinic Acid

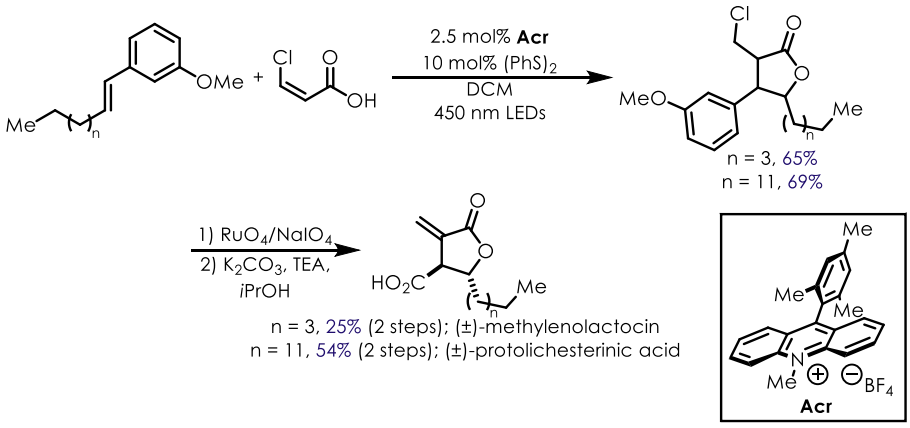

### 1.3.2 Formal [3+2] Cycloaddition

Another class of heterocycles that have been synthesized with acridinium ion photoredox catalysis is substituted pyrroles. Work by the Xiao lab demonstrates the ability of 2*H*-azirines and electron-poor alkynes to participate in a formal [3+2] cycloaddition to form such compounds. The proposed mechanism involves oxidation of the azirine (**11**) by the excited-state acridinium ion to give a nitrogen-centered radical cation (**12**). This species is able to undergo ring opening togive a 2-azaallenyl radical cation (**13**) which can add into the electron-deficient alkyne (**14**). The resulting distonic radical cation[v] (**15**) can regenerate the catalyst to give a zwitterion (**16**) that undergoes a cyclization/aromatization process to give the product (**17**) (Scheme 1.9).[22]

**Scheme 1.9** Mechanism of the Formal [3+2] Cycloaddition

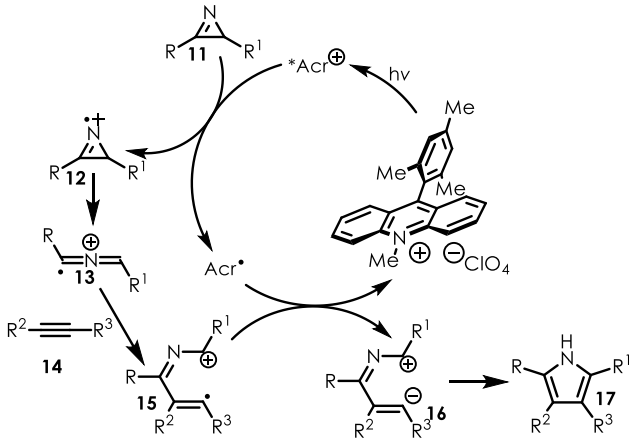


A variety of substituents were tolerated on the azirine ring and the alkyne partner could be terminal or disubstituted. In addition, decent regiomeric ratios were observed when unsymmetrical coupling partners were employed. To demonstrate the utility of this transformation, Xiao reported a formal synthesis of a HMG-CoA reductase inhibitor. The novel

[v] A distonic radical cation is one in which the positive charge and radical character are not on adjacent atoms

transformation enabled them to access a highly-substituted pyrrole precursor (**18**) to the inhibitor in just two steps, as opposed to the five originally reported in 1991 (Scheme 1.10).[22,23]

**Scheme 1.10** Formal Synthesis of HMG-CoA Reductase Inhibitor

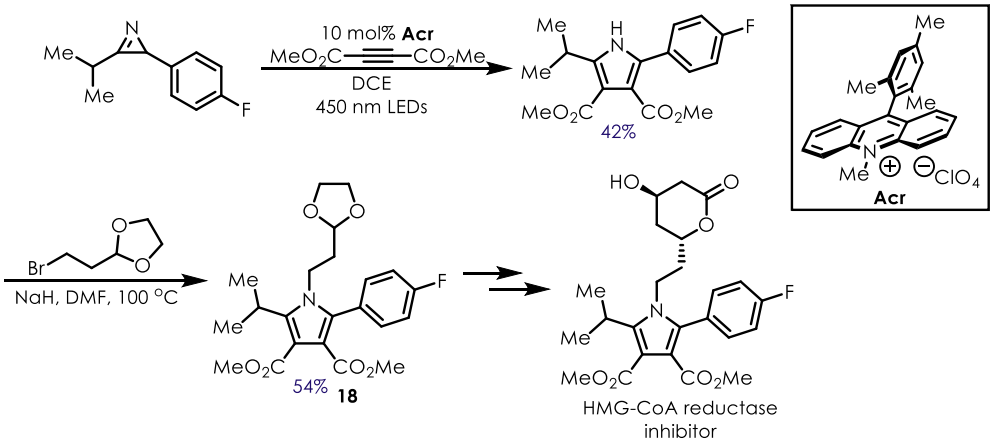


### 1.3.3 α-Amino Alkyation

In addition to constructing heterocycles, acridinium ion photoredox catalysis has been utilized to functionalize these compounds. A report by our lab from 2018 details the alkylation of cyclic amines adjacent to the nitrogen.[14] The mechanism for this process involves oxidation of the amine (**19**) by the excited-state acridinium ion; the resultant amine radical cation (**20**) undergoes deprotonation to give an α-amino radical (**21**) that can be trapped by a variety of Michael acceptors (**22**). Finally, the α-keto radical (**23**) formed in this sequence is capable of regenerating the catalyst (Scheme 1.11).

**Scheme 1.11** Mechanism of α-Amino Alkylation

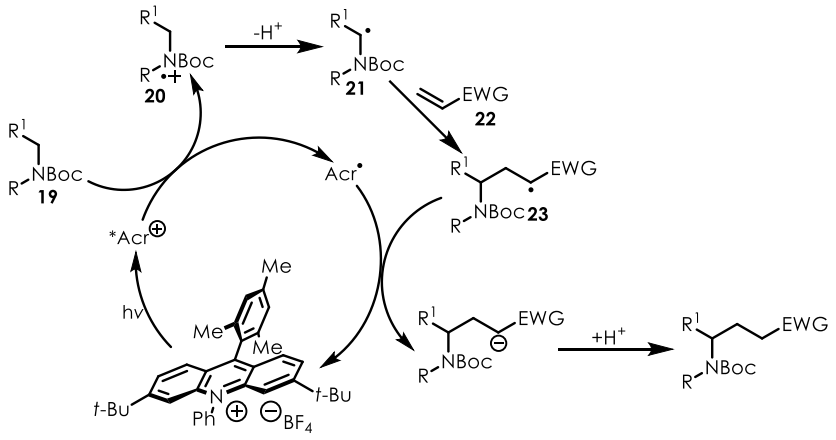


The reported conditions show that a variety of carbamate protecting groups and Michael acceptors were compatible. In addition, high diastereoselectivity favoring the *syn*-isomer was observed when enantiopure amines were employed. This allowed them to synthesize the natural product monomorine I in just three steps – α-aminoalkylation, Boc-deprotection, and reductive amination (Scheme 1.12).

**Scheme 1.12** Synthesis of Monomorine I

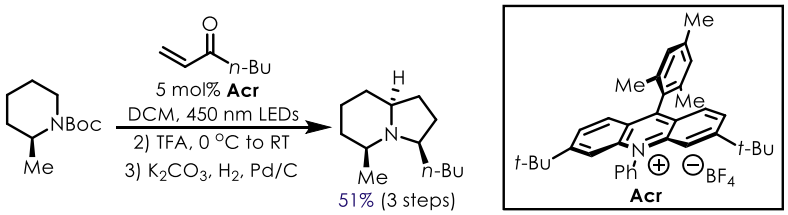


### 1.3.4 Conclusions and Outlook

While the natural products synthesized via acridinium ion photoredox catalysis are not very structurally complex, these organic dyes are promising total synthesis based on the variety of heterocycles to which they enable access.

One drawback of acridinium ion photoredox catalysis is the lack of enantioselective transformations in the literature; however, most reports demonstrate moderate to good diastereoselectivity, suggesting that these reactions could be used to access more complex

molecules if the absolute stereochemistry is set prior to the photoredox step. As a result, we believe acridinium ion photoredox catalysis will continue to grow as a powerful tool in the synthesis of natural products and bioactive molecules.

# CHAPTER 2: EXPERIMENTAL AND CALCULATED ELECTROCHEMICAL POTENTIALS OF COMMON ORGANIC MOLECULES

## 2.1 Introduction

As discussed in the previous chapter, the recent interest in photoredox catalysis has led to the development of many novel transformations.[6,7] The success of this chemistry hinges on the thermodynamics of the associated electron transfers, which can be calculated if the electrochemical potentials of the catalyst and substrate are known (Equation 2.1).

**Equation 2.1**

$$\Delta G_{ET} = -nF\Delta E = -nF[E_{red}(A/A^{\cdot-}) - E_{ox}(D^{+\cdot}/D)]$$

While electrochemical data for photoredox catalysis is present in the literature,[4,7,24] there is little information on the electrochemical potentials of organic molecules commonly employed as substrates. The reduction potential ($E_{1/2}$) of a molecule can be easily measured using cyclic voltammetry, which involves passing a current through an unstirred solution of the analyte. Because the solution is not stirred, only the analyte molecule present at or near the surface of the working electrode participate in ET; if this process is truly reversible, the oxidized and reduced forms of the substrate will exist in dynamic equilibrium at the electrode surface and the observed current will be directly related to the ET (Equation 2.2). Alternatively, a simplified, but reliable, way to calculated $E_{1/2}$ is to average the forward and reverse peak potentials present in the reversible cyclic voltammogram (CV) produced during the experiment.[25]

**Equation 2.2**

$$E_{1/2} = -\frac{RT\ln\left(\frac{[\text{reduced}]}{[\text{oxidized}]}\right)}{nF} = -\frac{\Delta G_{1/2}}{nF}$$

A reversible CV has an oxidation and a reduction wave of equal magnitude, but opposite sign (Figure 2.1A). This ideal scenario is commonly observed for photoredox catalysts and as such their $E_{1/2}$ values are readily obtained. One reason for the lack of electrochemical data for organic molecules is that these species often exhibit irreversible CVs, meaning that only an oxidation or a reduction wave is present (Figure 2.1B). The reason for this is due to the instability of the intermediate radical cations or anions, which decompose by a number of pathways faster than back-electron transfer with the electrode can occur (Scheme 2.1).

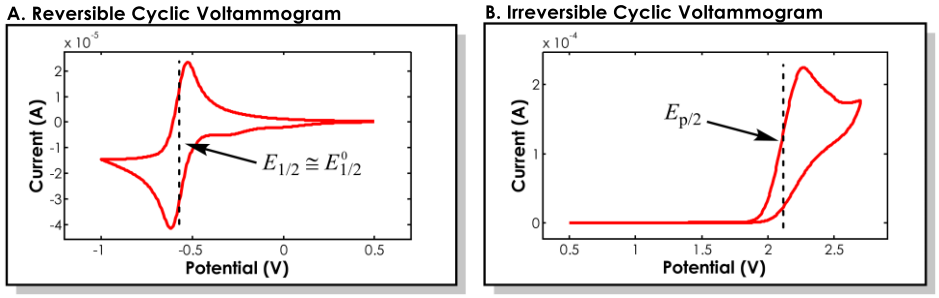


**Figure 2.1** Examples of a Reversible and Irreversible CV with the Relevant Electrochemical Potentials Labeled

**Scheme 2.1** Common Degradation Pathways for Organic Molecules that Prevent Back Electron Transfer in CV Experiments

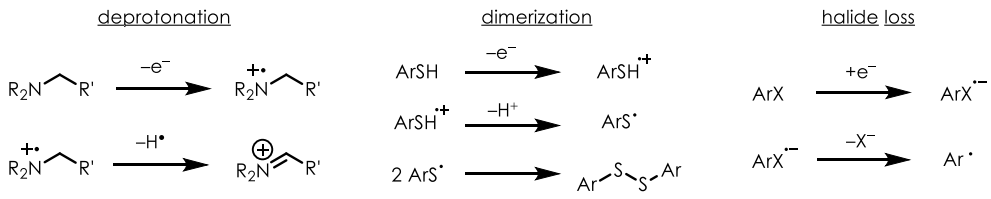


This decomposition causes the redox couple to not be in equilibrium at the electrode surface, and thus the current observed is *not* directly related to the rate of electron transfer. As a result, several mathematic corrections are required to determine the true $E_{1/2}$ value for the

substrate, but this requires knowledge of the competing degradation pathways and their corresponding rate constants; examples of these calculations have been published by Savéant for thiophenoxides.[26] While this would provide the most accurate understanding of an ET's thermodynamics, the experimental setup and time required to collect data on transient species can make collecting the necessary data impractical.

Therefore, organic chemists often estimate the $E_{1/2}$ value by measuring the half-peak potential ($E_{p/2}$) of the molecule, which is the voltage at half the peak maximum in the CV. This approach is somewhat debated in the literature, and the opponents of this tend to argue that peak potentials ($E_p$), the voltage at the peak maximum in the CV, should be used instead.[27] However, we have found that these values tend to over-estimate $E_{1/2}$ for simple organic molecules. As an example, for mesitylene we measured an $E_{p/2}$ of 2.07 V vs SCE and an $E_p$ of 2.30 V vs SCE. A study by Farid allowed him to calculate the $E_{1/2}$ of mesitylene as 2.05 V,[28] indicating the $E_{p/2}$ value we measured is much closer to the true electrochemical potential than the corresponding $E_p$ value. Based on this example and other arguments in the literature, we advocate the $E_{p/2}$ values are sufficient for the purpose of an organic chemist to estimate $\Delta G$ for a given PET.[29]

In an effort to make $E_{p/2}$ values more available and used by organic chemists, we reported redox potentials for over 180 organic molecules, which were organized by functional group (Figure 2.2).[8] Potentials that indicate an oxidation event have a positive value while those for a reduction are negative.

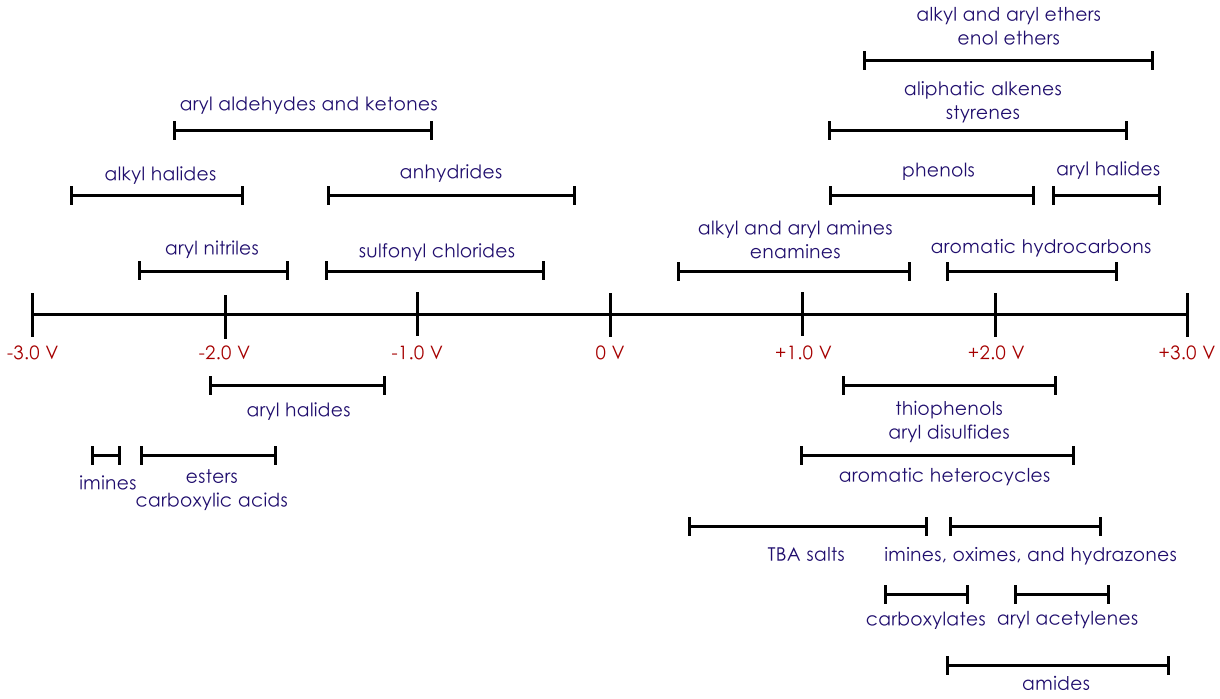


**Figure 2.2** Electrochemical Series of Functional Groups Common in Organic Molecules (V vs SCE)

Furthermore, the data was collected using a standard set of conditions to maintain internal consistency, and we sought to reduce the ambiguity of the potentials by reporting an experimental $E_{1/2}$ value for a standard redox couple and the means by which we converted the values measured against Ag|AgCl to those reported against SCE[vi].[30,31]

## 2.2 Experimental Electrochemical Potentials

This section will detail the $E_{p/2}$ values collected for a variety of organic molecules and provide a brief description of the general trends observed. This will entail ranking molecules based on how easily they are oxidized – a compound with a less positive $E_{p/2}$ is more easily oxidized than one with a more positive $E_{p/2}$ – or reduced – a compound with a less negative $E_{p/2}$ is more readily reduced than one with a more negative $E_{p/2}$.

[vi] The $Fc/Fc^+$ redox couple provided a $E_{1/2}$ = +0.45 V vs Ag|AgCl. Converting this to versus SCE involving subtraction of 0.03 V, providing a value of +0.42 V vs SCE.

Aromatic hydrocarbons become increasingly harder to oxidize the closer they resembled benzene, naphthalene < mesitylene < *o*-xylene. Aliphatic alkynes are very difficult to oxidize due to the instability of the resultant vinyl radical cation, and as a result their $E_{p/2}$ values could not be measured; however, a few aromatic alkynes did measurable give oxidation potentials (Figure 2.3).

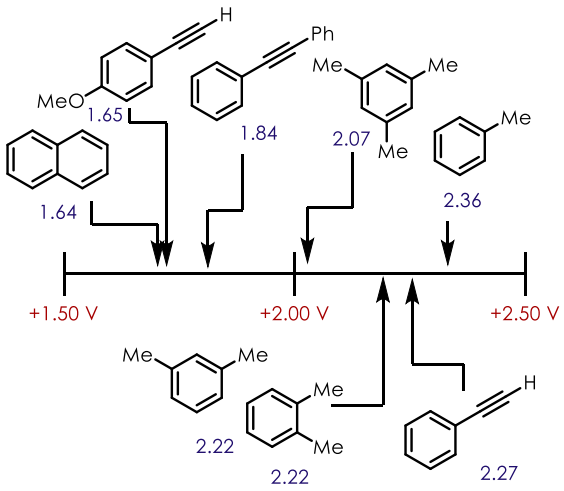


**Figure 2.3** Electrochemical Series of Aromatic Hydrocarbons and Aryl Alkynes (V vs SCE)

Olefins in less conjugated systems and with less substituents became increasingly harder to oxidize; terminal primary-substituted alkenes such as 1-octene exhibit $E_{p/2}$ values out of the measurable range[vii] (Figure 2.4 and 2.5).

[vii] For MeCN, the measurable range spans from -2.7 to +2.7 V vs Ag|AgCl

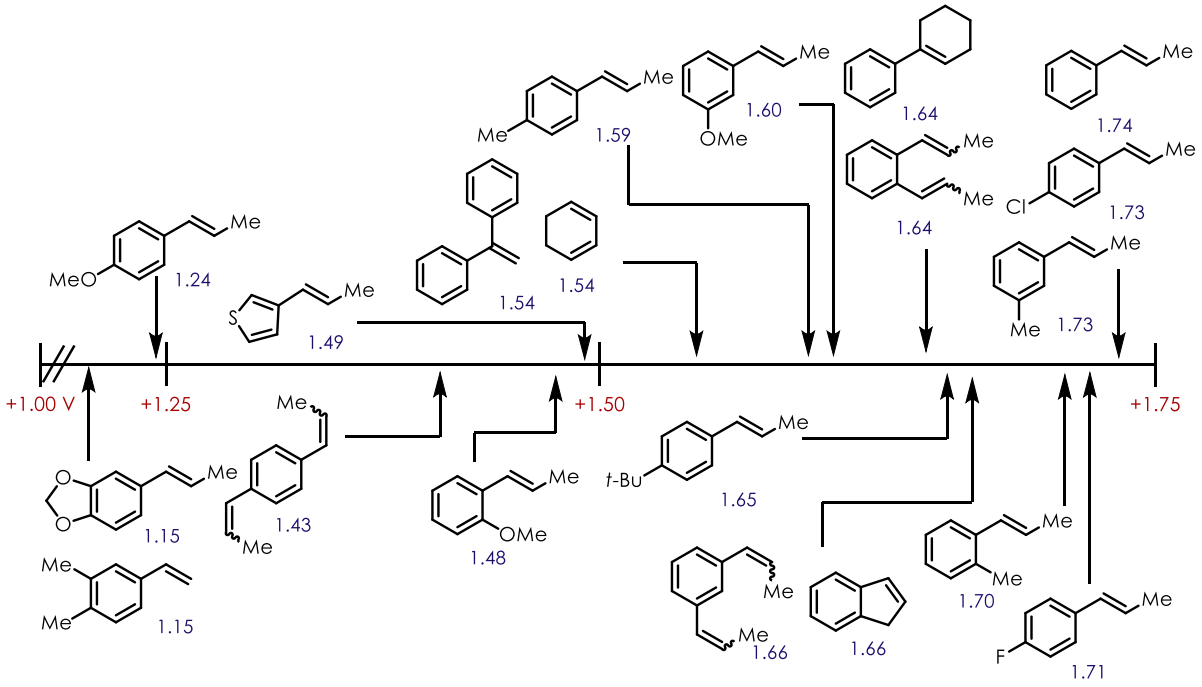


**Figure 2.4** Electrochemical Series of Alkenes between +1.00 to +1.75 V (V vs SCE)

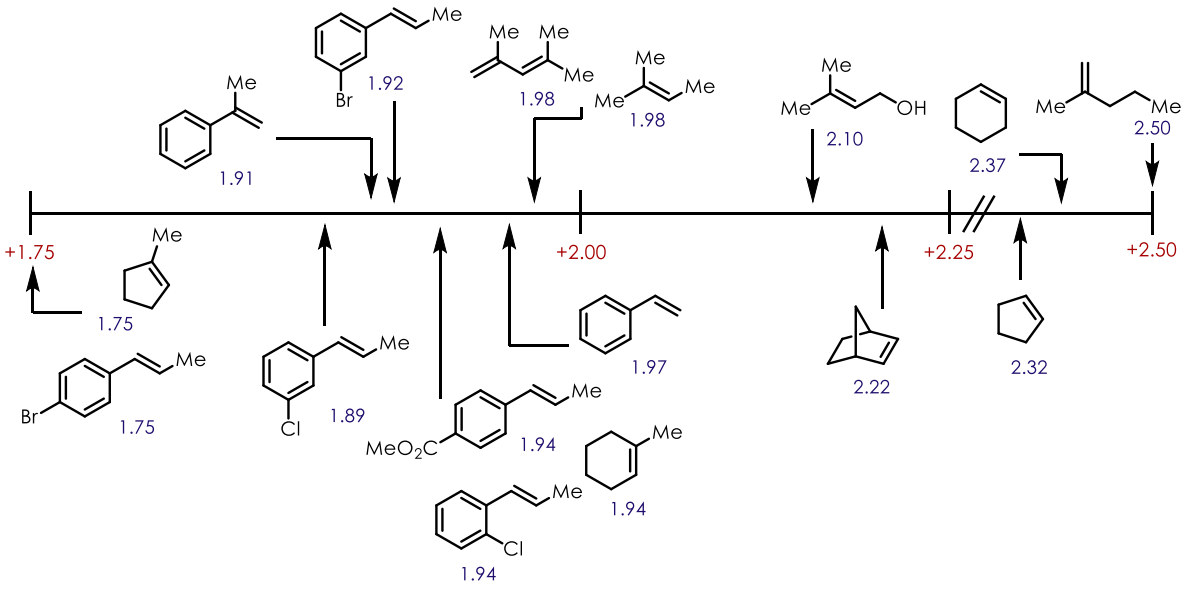


**Figure 2.5** Electrochemical Series of Alkenes between +1.75 and +2.50 V (V vs SCE)

Arenes and alkenes with oxygen, nitrogen, or sulfur-based substituents became easier to oxidize with increasing electron-donating ability, aniline < thiophenol < phenol (Figures 2.6 to

2.9). In addition, aromatic heterocycles exhibited the same general trend, indole < benzothiophene < benzofuran (Figure 2.10).

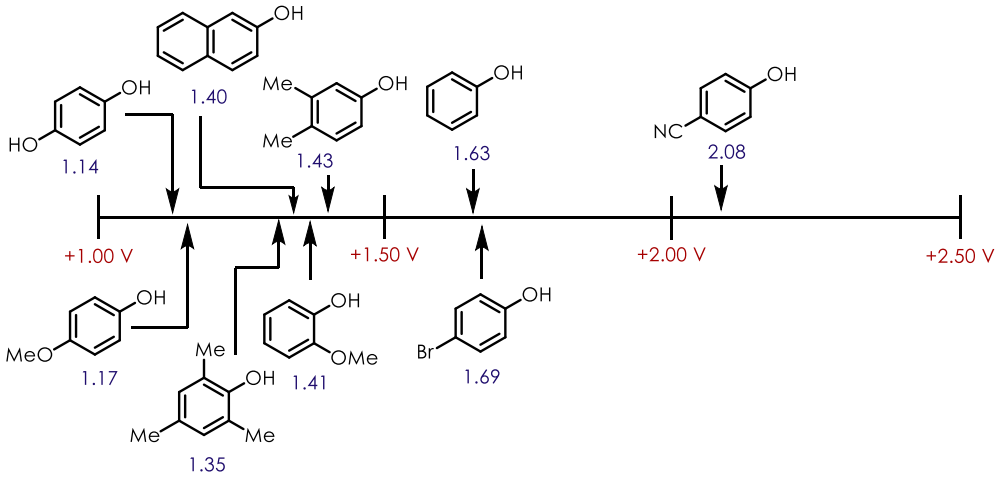


**Figure 2.6** Electrochemical Series of Phenols (V vs SCE)

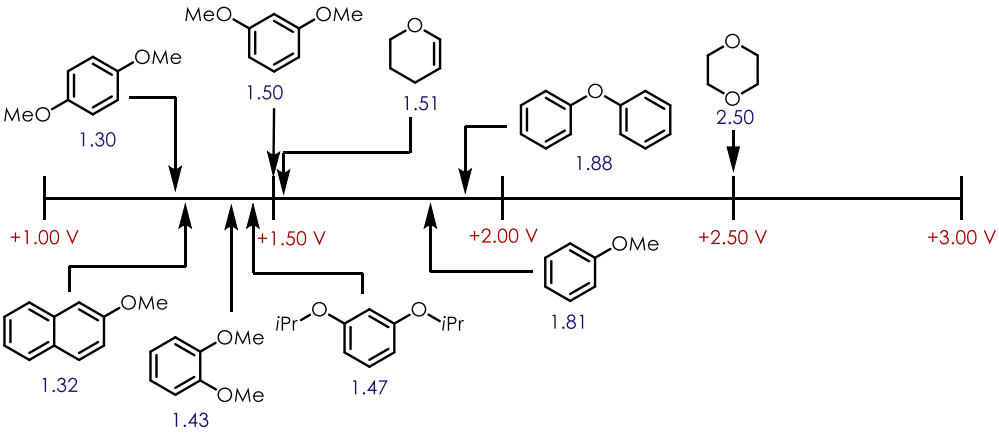


**Figure 2.7** Electrochemical Series of Ethers (V vs SCE)

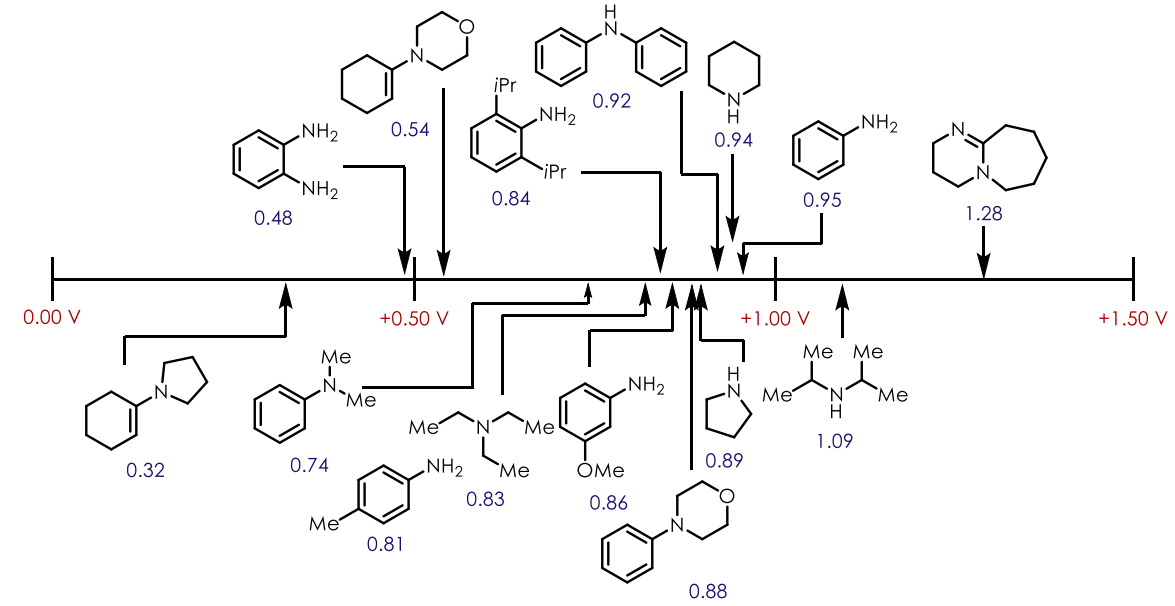


**Figure 2.8** Electrochemical Series of Amines (V vs SCE)

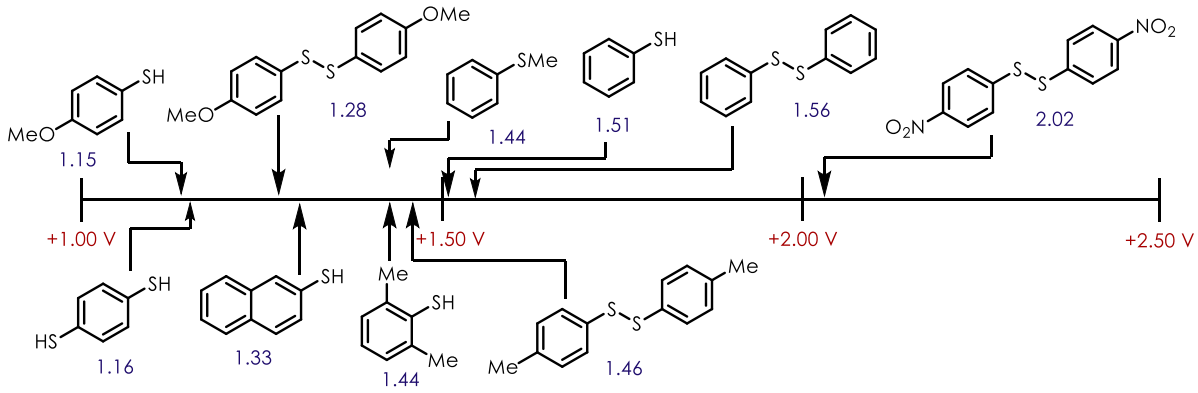


**Figure 2.9** Electrochemical Series of Thiophenols and Aryl Disulfides (V vs SCE)

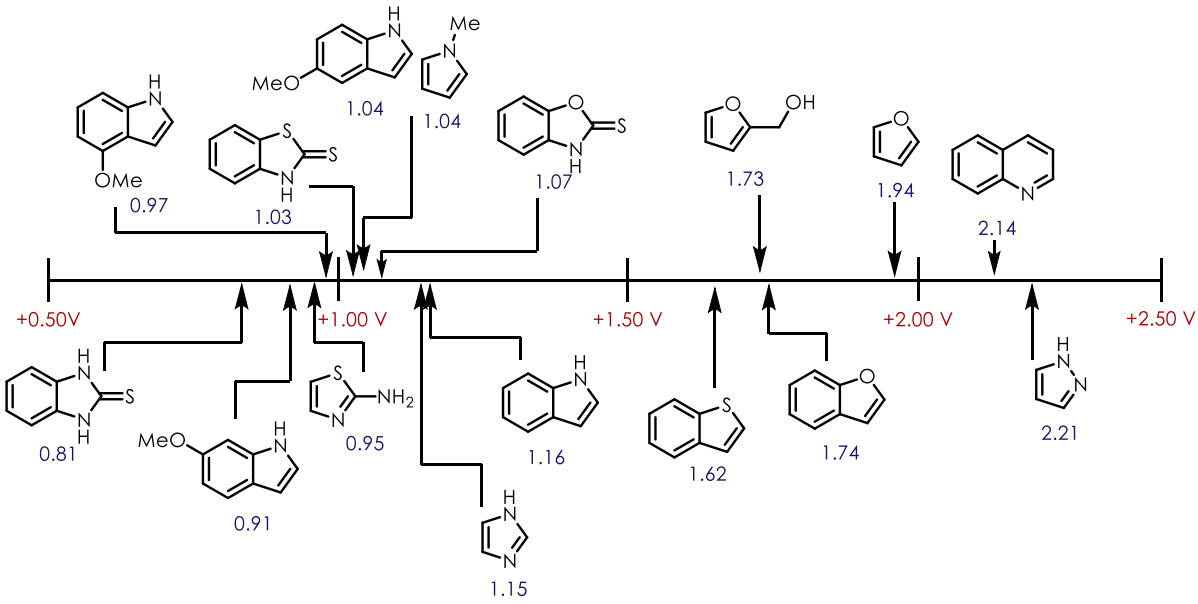


**Figure 2.10** Electrochemical Series of Aromatic Heterocycles (V vs SCE)

Electrochemical potentials for a variety of alkyl and aryl halides were also collected. In both oxidations and reductions, the same trend was observed where iodides were the easiest to oxidize/reduce followed by bromides, and lastly chlorides (Figure 2.11).

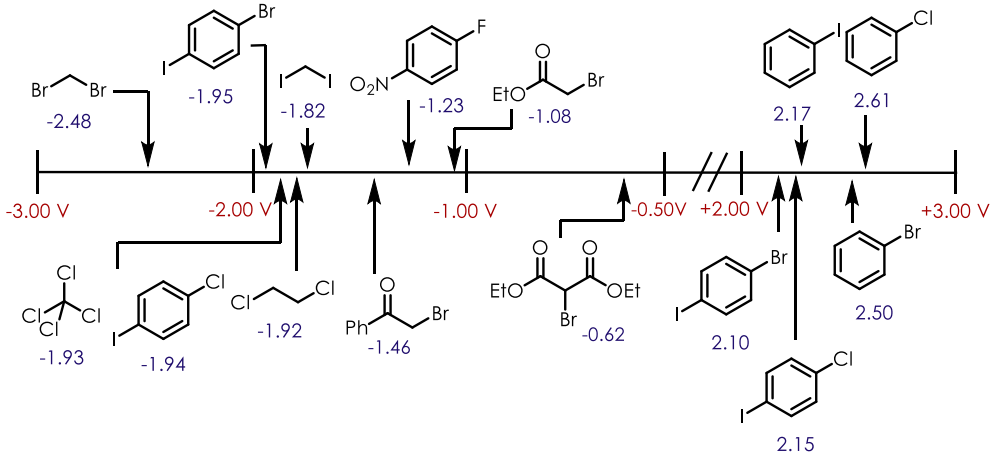


**Figure 2.11** Electrochemical Series of Alkyl and Aryl Halides (V vs SCE)

Carbonyl-containing compounds were examined, and aldehydes/ketones were found to primarily undergo reductions, unless a very electron-donating substituent was present on an aromatic ring in the molecule (Figures 2.12 and 2.13). Imines and related species typically

experienced both oxidation and reduction potentials, suggesting they could serve as versatile substrates in photoredox transformations (Figure 2.14).

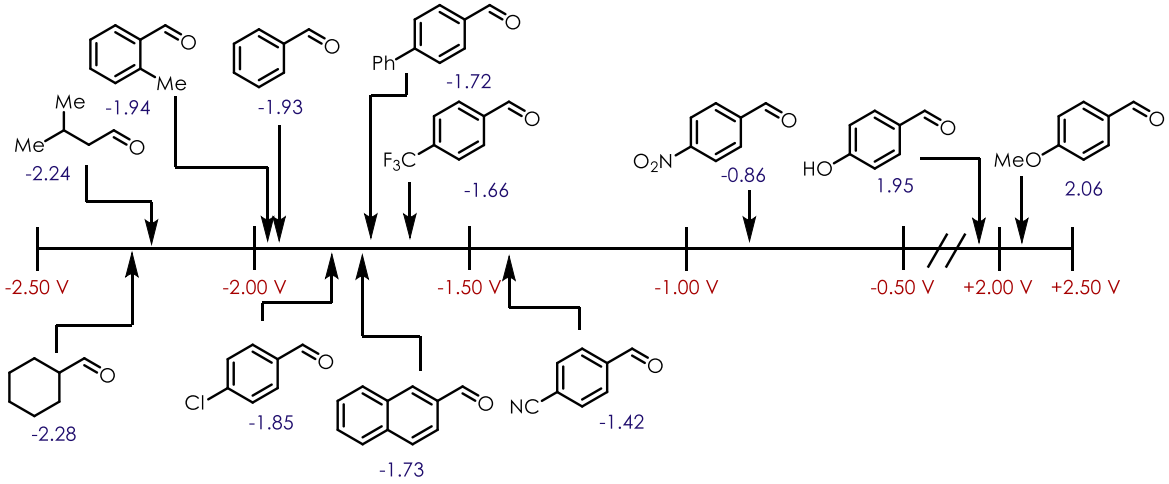


**Figure 2.12** Electrochemical Series of Aldehydes (V vs SCE)

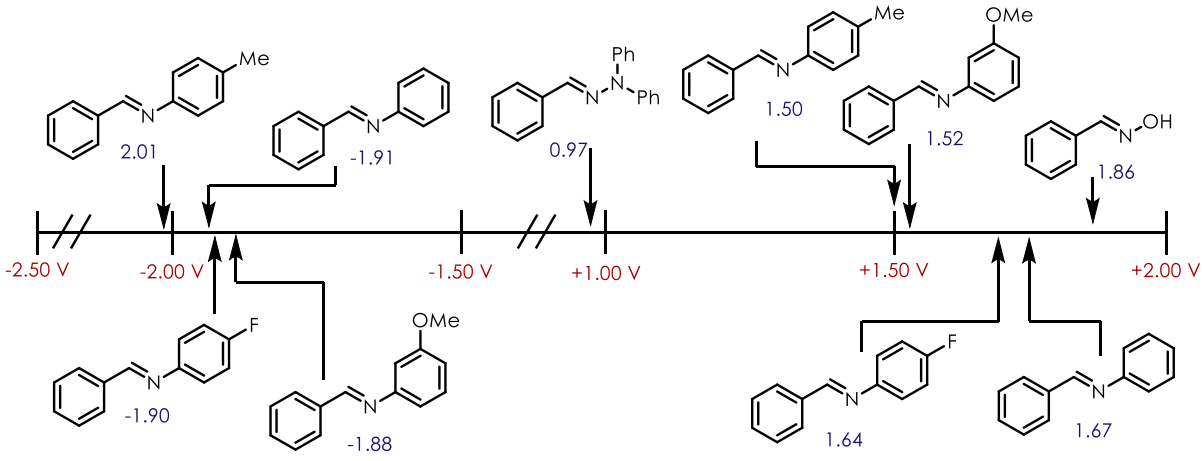


**Figure 2.13** Electrochemical Series of Imines and Related Compounds (V vs SCE)

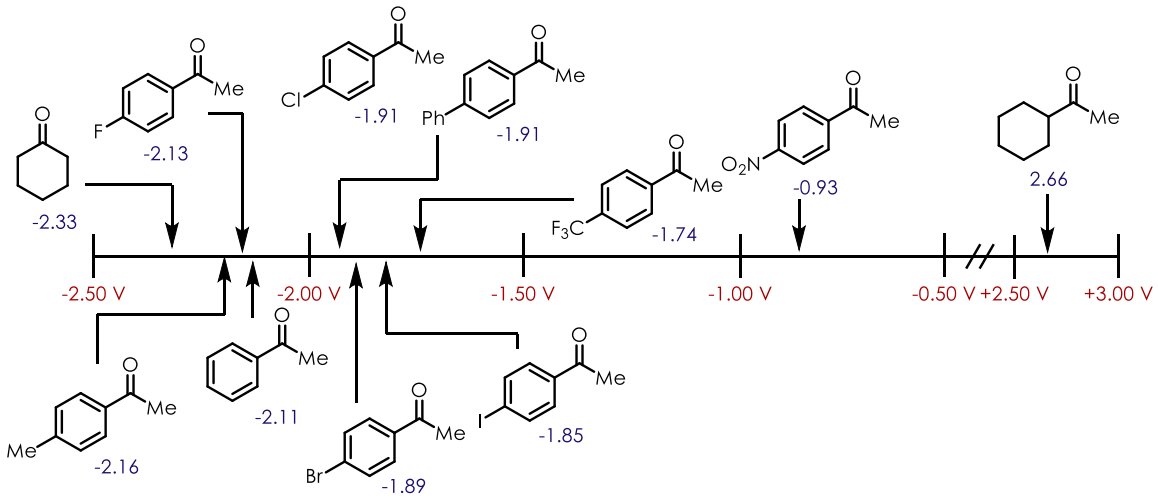


**Figure 2.14** Electrochemical Series of Ketones (V vs SCE)

Several carboxylic acids and corresponding derivatives (esters, acid chlorides, anhydrides, nitriles, amides, sulfonyl chlorides) were also examined. Again, due to the electron-withdrawing nature of these functional groups, reductions were often observed, except in the case of carboxylate salts and amides, both of which only underwent oxidation events (Figures 2.15 to 2.17).

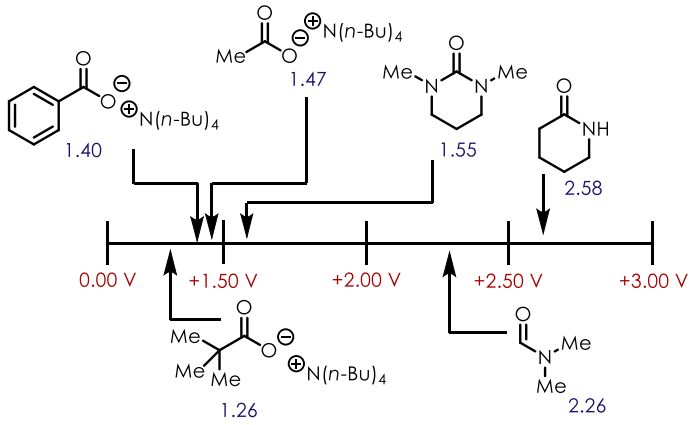


**Figure 2.15** Electrochemical Series of Amides and TBA Carboxylates (V vs SCE)

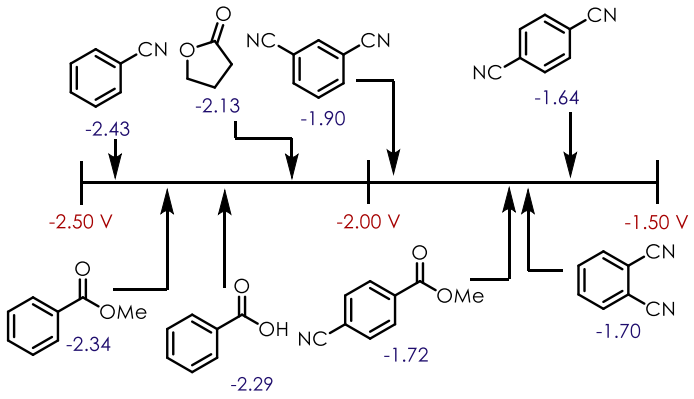


**Figure 2.16** Electrochemical Series of Carboxylic Acids and Derivatives (V vs SCE)

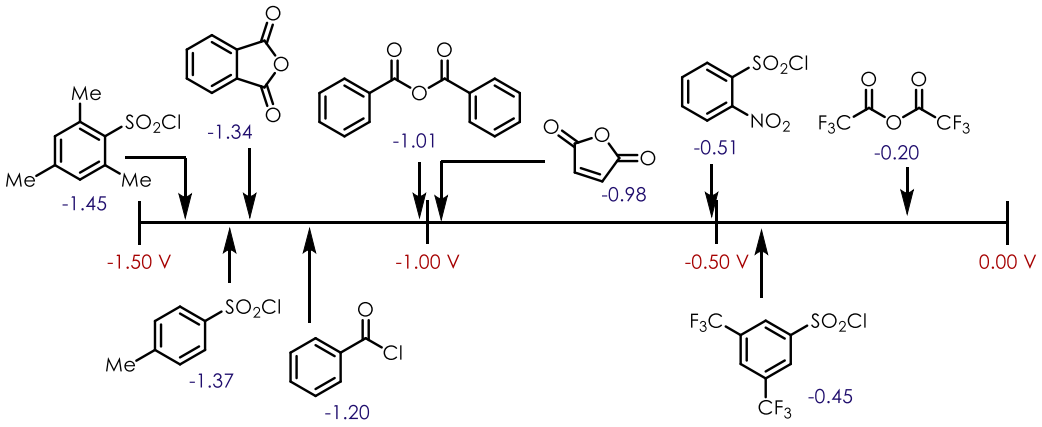


**Figure 2.17** Electrochemical Series of Acyl and Sulfonyl Chlorides and Anhydrides (V vs SCE)

Lastly, electrochemical potentials for a few miscellaneous compounds were collected including a few common oxidants, various salts, silanes, and hypervalent iodines (Figures 2.18 and 2.19).

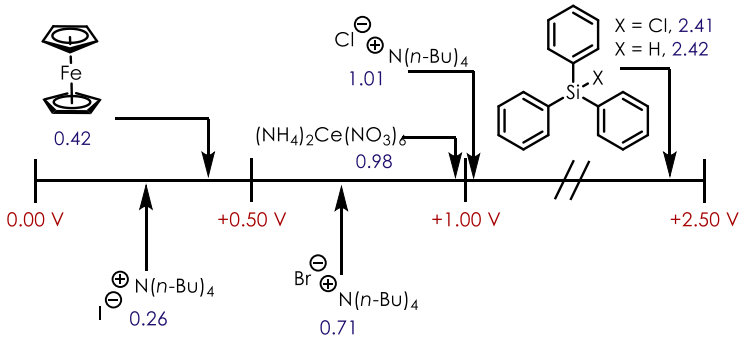


**Figure 2.18** Electrochemical Series of Inorganic Compounds, Aryl Silanes, and TBA Salts (V vs SCE)

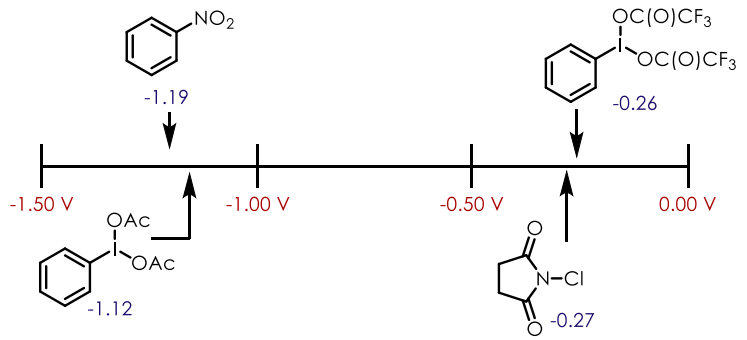


**Figure 2.19** Electrochemical Series of Hypervalent Iodine Compounds, Nitrobenzene, and NCS (V vs SCE)

## 2.3 Calculated Electrochemical Potentials

While the previous section detailed a large amount of $E_{p/2}$ values, it is by no means a comprehensive list. Our goal is that this database will serve as a starting point for chemists looking to develop or utilize a photoredox transformation in a synthesis. However, we do realize that there may be functional groups or substrates of interest that we did not report, and that many scientists may not have access to an electrochemical setup to collect their own CV data. Due to this, we also sought to provide a computational method for calculating $E_{p/2}$ values as an alternate means of assessing an organic molecule's viability in a given PET process.

The majority of this computational work was done by Nathan Romero, and as a result only the key results will be discussed here. Our approach sought to evaluate a relatively simple

method of calculating electrochemical potentials with the goal of making these values more accessible to synthetic chemists. This involved calculating the difference in free energy (Equation 2.3) between the oxidized and reduced forms of a molecule (Scheme 2.2) and relating this to the redox potential by referencing an absolute potential for a standard electrode (Equation 2.4).[32]

**Equation 2.3**

$$\Delta G_{1/2}^{\text{o, calc}} = G(\text{reduced})_{298} - G(\text{oxidized})_{298}$$

**Scheme 2.2** Half Reactions for Oxidation and Reduction

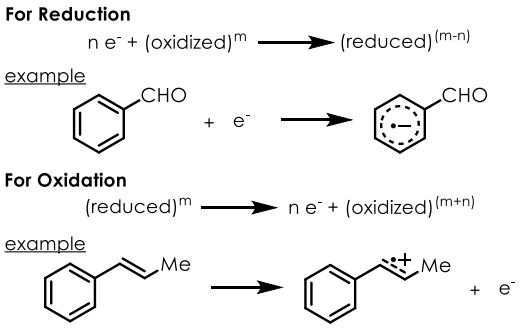


**Equation 2.4**

$$E_{1/2}^{\text{o, calc}} = -\frac{\Delta G_{1/2}^{\text{o, calc}}}{\text{n}F} - E_{1/2}^{\text{o, ref}}$$

Redox potentials were calculated using B3LYP[33,34] and M06-2X[35] functionals, the split valence basis set 6-31+G(d,p)[36,37], and the CPCM solvent continuum approach to account for solvation in MeCN.[38,39] All calculations were done in Gaussian 09[40], and structures were submitted to geometry optimization, with frequency calculations performed on the optimized structures both to verify that the geometries were true minima and to calculate free energies at 298 K. The solution-phase energies were referenced to SCE by subtraction of 4.281 V (the absolute potential of SHE) and 0.141 V to convert from SHE to SCE in MeCN.[32]

The values calculated using B3LYP and M06-2X were compared to the experimentally measured ones and $R^2$ values of 0.96 and 0.97 were obtained, respectively (Figure 2.20).

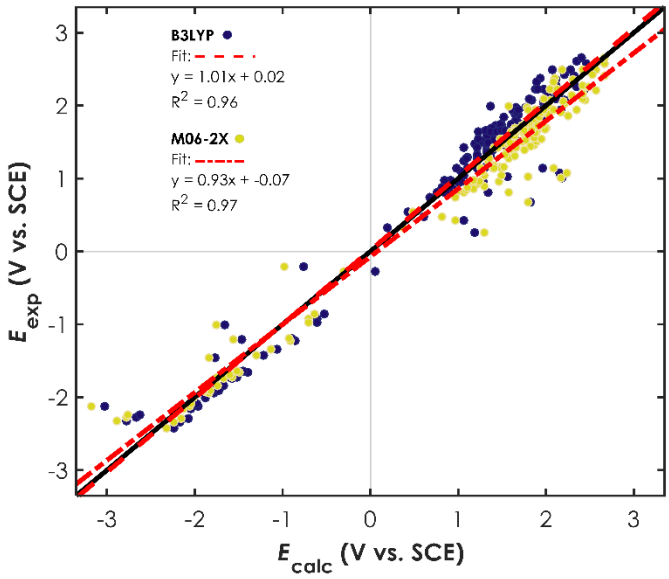


**Figure 2.20** Plot of Experimental vs. Calculated Redox Potentials

While the overall correlation is good, there are a few exceptions worth noting. These typically fall into four general categories. First, compounds that have different tautomers of equal importance such as 2-mercaptobenzothiazole and related compounds (Scheme 2.3). Second, salts with a loose cation-anion pair such as TBACl, in which case adequate solvation of the anion is likely not accounted for in the computational method. Third, molecules that undergo hybridization change (commonly $sp^2$ to $sp^3$) during the redox event, γ-butyrolactone and trifluoroacetic anhydride are two examples. Fourth, species with relatively weak C-X bonds, such as benzoyl chloride, greatly favored fragmentation of the radical anion during computational modeling, giving potentials that deviated from those measured experimentally.

**Scheme 2.3** Important Tautomers of 2-Mercaptobenzothiazole

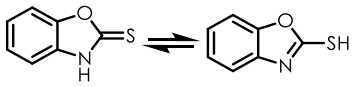


Despite these few exceptions, we are confident that the observed correlation between experimental and computational electrochemical potentials indicates one can easily obtain such a value for any organic molecule via either method and reliably use it to assess the thermodynamics of a PET.

## 2.4 Acridinium Ions as Sustainable Photoredox Catalysts

The most recent interest in photoredox catalysis began roughly a decade ago with a report from the MacMillan lab on the asymmetric alkylation of aldehydes that employed $Ru(bpy)_3^{2+}$ (**1**) as the catalyst.[41] While **1** has since been used to mediate a variety of transformations, it has largely been supplanted by iridium complexes, such as $[Ir(dF\text{-}CF_3\text{-}ppy)_2(dtbpy)]PF_6$ (**2**), due to their longer excited state lifetimes and wider redox windows.[15]

However, the low abundance of iridium in the earth's crust (0.001 ppm)[9] makes these complexes neither cost-effective, nor sustainable. Process-scale production of pharmaceuticals and agrochemicals is therefore unable to utilize these powerful transformations, and as a result there is an ongoing interest in developing organic photoredox catalysts that can mediate the same transformations.[15]

To this end, we collaborated with the research team led by Daniel DiRocco at Merck in Rahway, New Jersey, to investigate the ability of acridinium ions to replace **2** as the catalyst in the decarboxylative conjugate addition of Cbz-proline (**3**) into dimethyl maleate (**4**) (Scheme 2.4), a transformation originally been reported by the MacMillan lab.[42]

**Scheme 2.4** Decarboxylative Conjugate Addition Reported by MacMillan

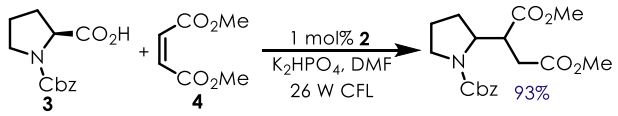


A series of substituted acridinium ions were prepared and their electrochemical and photophysical properties investigated (Table 2.1). Catalyst design focused on making the acridinium ion core more electron-rich by adding methoxy groups at various positions around the tricyclic ring system. This sought to not only increase the catalyst's resistance to nucleophilic deactivation, but also impart a more negative $E_{1/2}$ value, which would be necessary for them to serve as adequate replacements for **2**.

**Table 2.1** Electrochemical and Photophysical Properties of Photoredox Catalysts

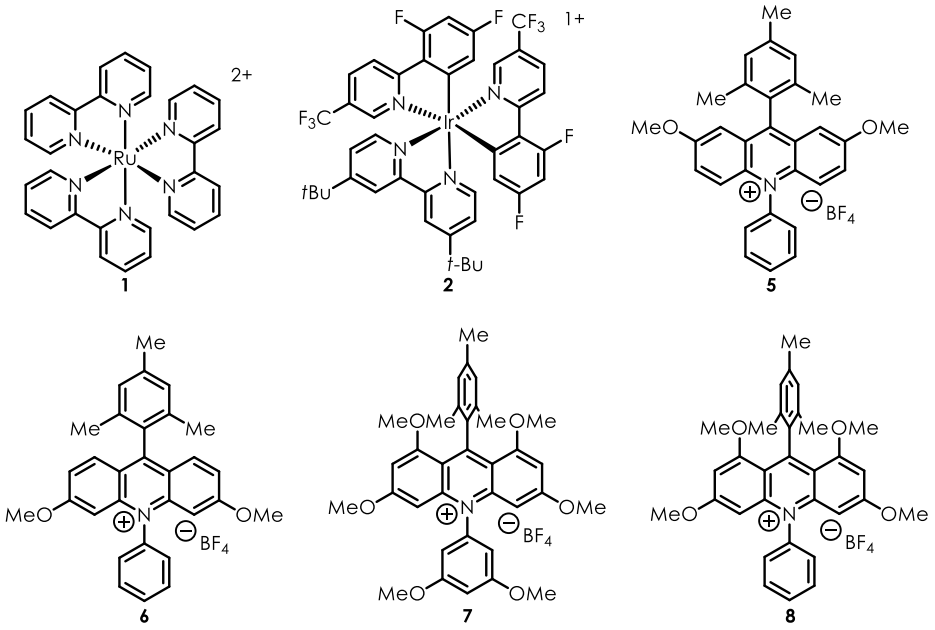


| Catalyst | *$E_{1/2}$ (V vs SCE) | $E_{1/2}$ (V vs SCE) | τ (ns) |
|---|---|---|---|
| **1** | 0.77 | -1.33 | 1100 |
| **2** | 1.21 | -1.37 | 2300 |
| **5** | 1.90 | -0.57 | 466 |
| **6** | 2.01 | -0.71 | 407 |
| **7** | 1.65 | -0.82 | 414 |
| **8** | 1.62 | -0.84 | 412 |

The mechanism of this transformation (Scheme 2.5) involves oxidation of the conjugate base of **3** by the excited-state catalyst. After decarboxylation, the α-amino radical can add into **4** to give an α-keto radical. This species has an estimated $E_{1/2}$ of -0.60 V vs SCE[42], therefore the catalyst must have a more negative $E_{1/2}$ for the turnover step to be thermodynamically favorable. Lastly, protonation of the enolate affords product.

**Scheme 2.5** Mechanism of Decarboxylative Conjugate Addition

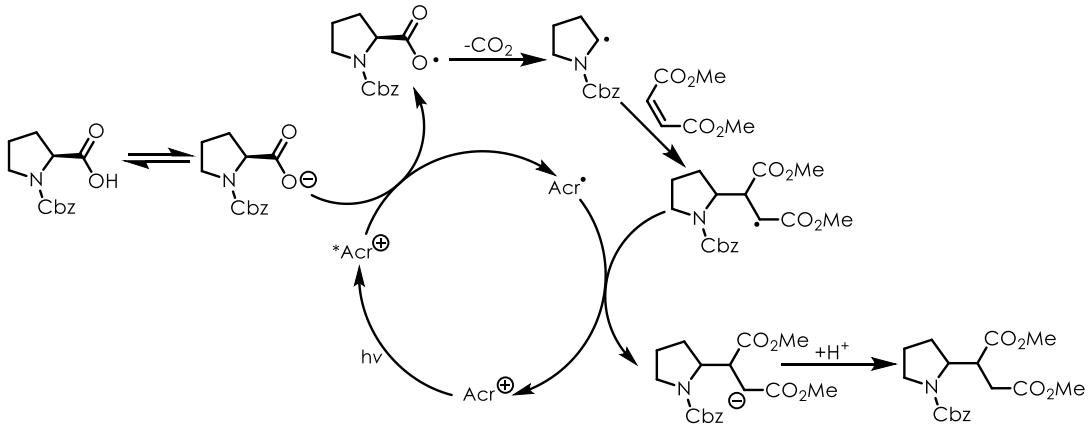


Based on the data compiled in Table 2.1, all the acridinium ion catalysts screened in this work have $E_{1/2}$ values less than -0.60 V, aside from **5**. However, all of these species were able to effectively catalyze the transformation (Table 2.2).

**Table 2.2** Decarboxylative Conjugate Addition with Acridinium Ion Catalysts

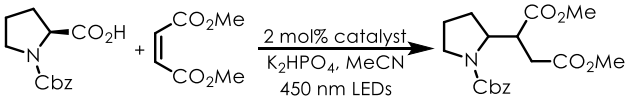


| Catalyst | % Yield |
|---|---|
| **5** | 66 |
| **6** | 69 |
| **7** | 86 |
| **8** | 88 |

While this work details only one transformation, it is still a promising result for those who are interested in utilizing an acridinium ion photoredox catalyst in place of the more expensive iridium complexes.[15]

## 2.5 Conclusion

In summary, this chapter compiles our work on electrochemical and photophysical properties of common organic molecules and acridinium ion photoredox catalysts. Our intentions are not to downplay the importance and utility of the ruthenium- and iridium-based systems that have helped pave the way for photoredox catalysis in recent years, but to demonstrate the utility of the much-less explored acridinium ion catalysts and the potential they have to greatly expand the repertoire of reactions available to organic chemists.

## 2.6 Associated Data

Appendix A: Experimental Details and Electrochemical and Photophysical Data

## 2.7 Acknowledgements

*Synlett* **2016**, *27* (5), 714-723.

This research was supported by an NSF-CAREER grant (CHE-1352490). N.A.R. is also grateful for an NSF Graduate Fellowship.

*J. Org. Chem.* **2016**, *81* (16), 7244-7249.

This research was supported by Merck Research Laboratories. Photophysical measurements were performed in the UNC-ERFC Instrumentation Facility established by the UNC-EFRC (Center for Solar Fuels, an Energy Frontier Research Center funded by the U.S. Department of Energy, Office of Science, Office of Basic Energy Sciences under Award Number DE-SC0001011).

# CHAPTER 3: SYNTHETIC STUDIES TOWARD THE SYNTHESIS OF RUBRIFLORDILACTONE B

## 3.1 Introduction

### 3.1.1 Schisandraceae Natural Products

Plants belonging to the Schisandraceae family have been used in traditional Chinese medicine for centuries. To better study the biological properties of the natural products produced by these plants, Han-Dong Sun has spent a portion of his career isolating numerous bisnortriterpenoids from these plants.[43–45] Schisandraceae natural products have been shown to exhibit beneficial pharmacological properties such as antihepatitis, antitumor, and anti-HIV-1 activity. As a result, developing efficient syntheses of these molecules is of great interest in order to further study their bioactivity.

Most of the natural products isolated by Sun and coworkers are proposed to be biosynthetically derived from the triterpene cycloartane (**1**, Figure 3.1). A few examples of these include lancifodilactone A (**2**) from *Schisandra lancifolia*, micrandilactones B (**3**) and C (**4**) from *Schisandra mircantha*, and rubriflordilactones A (**5**) and B (**6**) from *Schisandra rubriflora*. All of these molecules share common structural motifs including a 5-5-7-6-5 ring system (rings *ABCDE*), which exhibits varying degrees of substitution and saturation, and an α-methyl butenolide (ring *F*) on the eastern half (Figure 3.2).

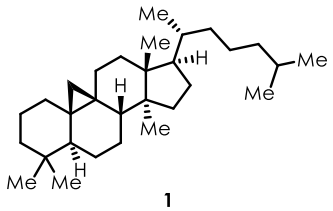

**Figure 3.1** Cycloartane

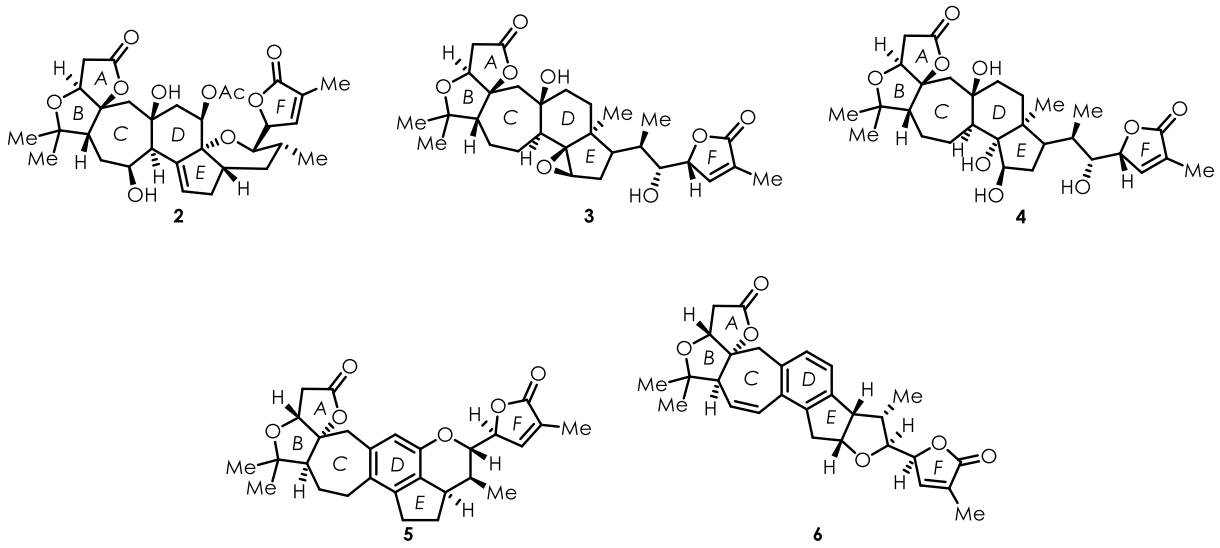

**Figure 3.2** Bisnortriterpenoids Isolated by Sun

Even though the isolation of these five compounds was reported over a decade ago, only rubriflordilactones A and B have complete syntheses in the literature.[46–49] Therefore, there is still a lot of synthetic work to be done in the area of schisandraceae natural products.

### 3.1.2 Reported Efforts Toward Rubriflordilactone B

Since the isolation of rubriflordilactone B[viii] (**6**, Figure 3.3) was reported in 2006[45], there have been a few partial syntheses and one complete route published in the literature.[48,50,51]

[viii] The ring lettering system show in Figure 3.3 will be used throughout the remainder of this chapter

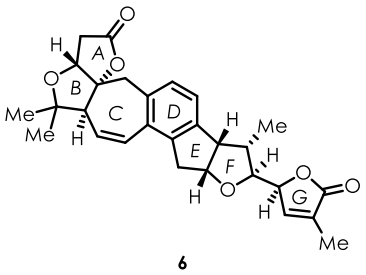


**Figure 3.3** Rubriflordilactone B

The first report by the Peng lab in 2015 details the construction of the eastern hemisphere of the natural product in just 5 steps (Scheme 3.1).[51]

**Scheme 3.1** Peng's Synthesis of the Eastern Hemisphere of Rubriflordilactone B

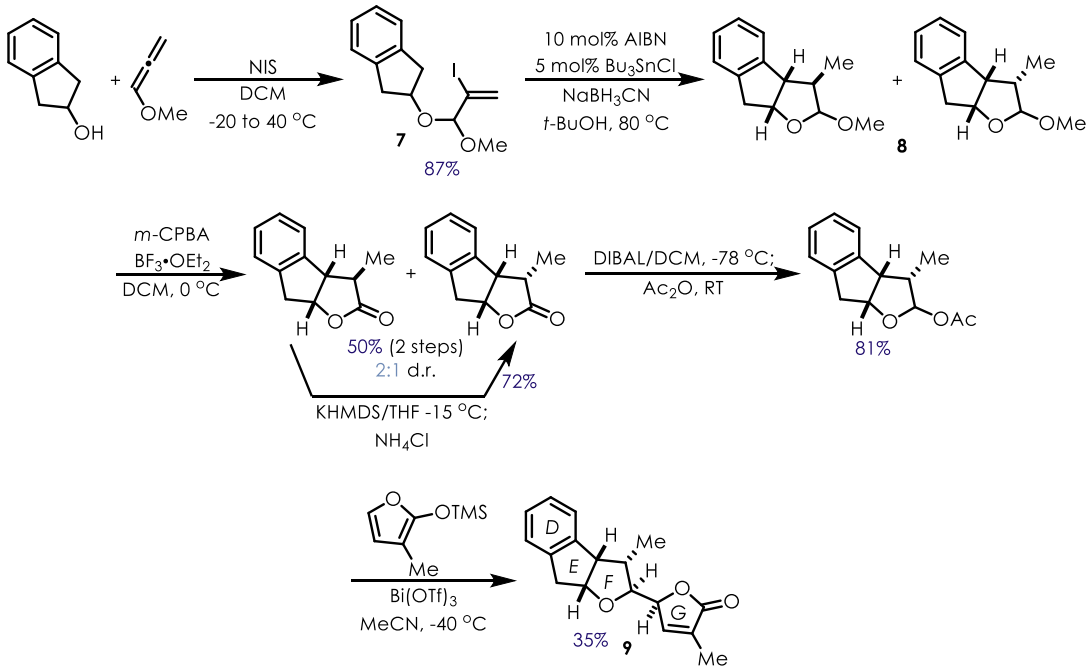


Peng's route begins by constructing vinyl iodide (**7**) from 2-indanol and 1-methoxyallene; a radical cyclization using AIBN as the initiator gives the tricyclic product (**8**) as a 2:1 mixture of diastereomers. Demethylation and oxidation of the lactol to the corresponding lactone allows them to obtain more of the product with the correct stereochemistry by epimerization of the α-position in the γ-butyrolactone. Subsequent reduction of the lactone with

DIBAL, trapping of the lactol with acetic anhydride, and nucleophilic attack on this species by a siloxyfuran gives the target (**9**).[ix]

While this is a relatively short sequence to half of a complex natural product, it suffers from poor diastereoselectivity in the radical cyclization step. As the major diastereomer is undesired, an oxidation, epimerization, and reduction sequence is necessary to obtain more of the desired diastereomer. A preferable alternative would be a radical cyclization in the correct oxidation level to give the lactone, enabling immediate epimerization if poor diastereoselectivity was still observed.

Just a year later, Xie and coworkers disclosed a route to the left-hand side of **5**.[50] This leverages an intramolecular [2+2+2] cycloaddition of a triyne to form the *D* ring. Their route (Scheme 3.2) consists of eight linear steps.

**Scheme 3.2** Xie's Synthesis of the Left Half of Rubriflordilactone B

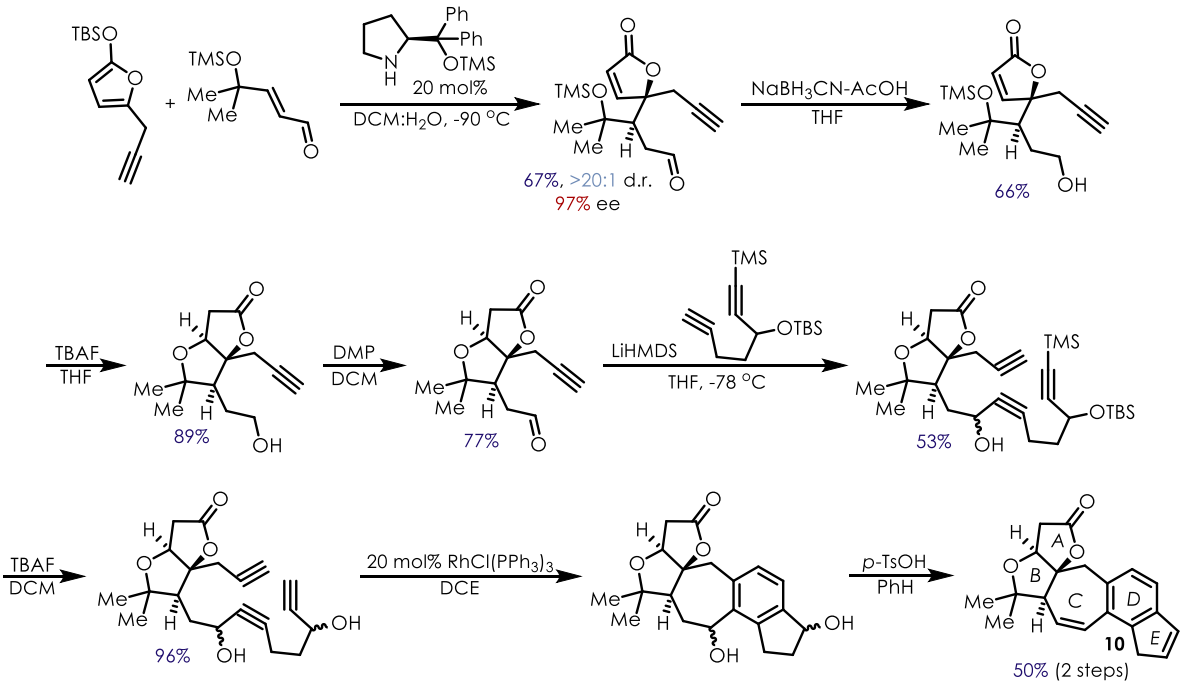


[ix] Throughout this dissertation, bold/hashed lines will be used to designate relative stereochemistry while bold/hashed wedges will be used for absolute stereochemistry

The main drawback to Peng's route is the undesired stereochemistry at the *BC* ring junction, resulting in an epimer (**10**) of the western hemisphere of **6**. While several attempts were made to correct this, none of them were successful. However, if a solution were to be discovered, **10** has the potential to be used in a complete synthesis as the alkene in ring *E* could be used to construct the remainder of the molecule.

That same year, Ang Li reported the first total synthesis of **6**.[48] The route is analogous to his lab's work on the closely related rubriflordilactone A, which was reported just two years earlier.[47] The western-portion (Scheme 3.3A) utilizes the same acetylation, intramolecular Claisen, cationic deoxygenation sequence to construct ring *A*. After synthesis of the eastern side (Scheme 3.3B), a Sonogashira coupling and a 6π-electrocyclization were used to link both halves of the molecule together and construct ring *D* (Scheme 3.3C).

**Scheme 3.3** Ang Li's Synthesis of Rubriflordilactone B

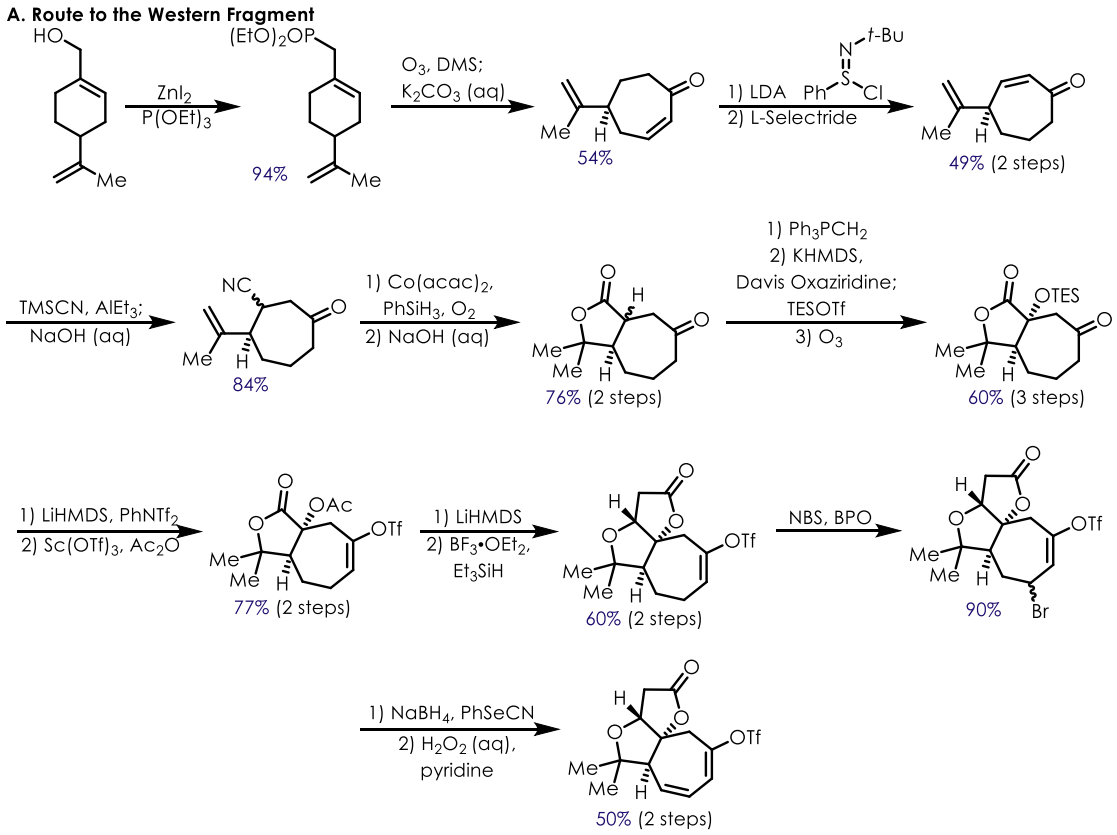

**B. Route to the Eastern Fragment**

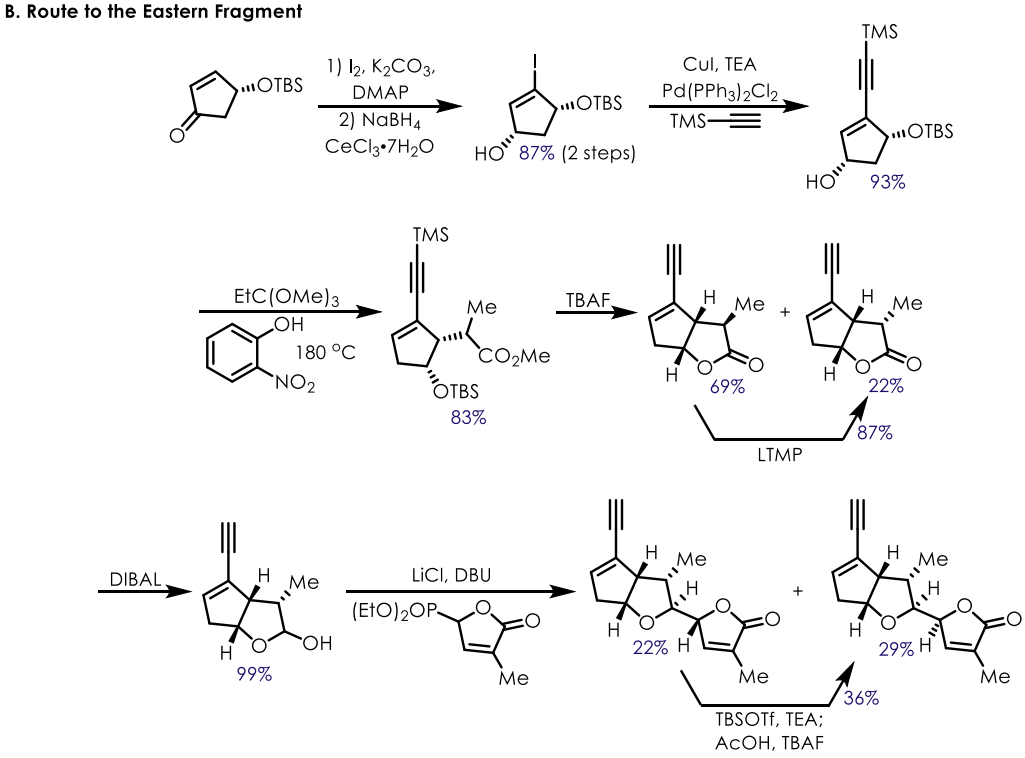


**C. Union of Western and Eastern Fragments**

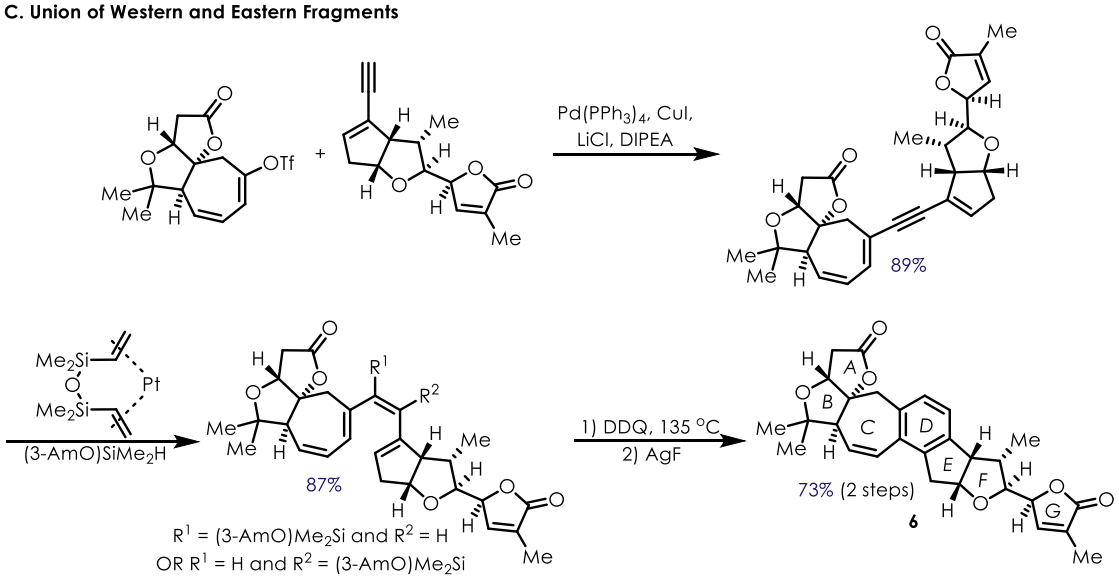


Overall Li and coworkers accomplished an efficient and convergent route to **6**, providing a benchmark for other synthetic chemists to improve upon. Li and coworkers, however, discovered that while their synthetic sample's crystal structure matched that of the authentic sample isolated by Sun, the $^{1}$H NMR data did not. This prompted them to synthesize 23-*epi*-

rubriflordilactone B (Figure 3.4), but this species did not match the original $^{1}$H NMR data either.[48]

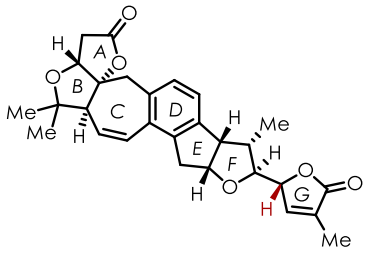


**Figure 3.4** 23-*epi*-Rubriflodilactone B

Based on this result, Li proposed Sun isolated a mixture of two closely related diastereomers. The major species, which Li termed pseudo-rubriflordilactone B, was responsible for the $^{1}$H NMR data reported by Sun, while the minor diastereomer (**6**) crystallized and produced the x-ray crystal structure.[48] Since the discrepancy between the characterization data reported by Li and Sun came to light in 2016, the stereochemistry of pseudo-rubriflordilactone B has been a topic of interest in the literature.

### 3.1.3 Stereochemistry of Rubriflordilactone B

In an effort to solve the stereochemical mystery of pseudo-rubriflordilactone B, Kaufman and Sarotti conducted a computational NMR study.[52] Based on Li's proposal that Sun isolated a mixture of 2 diastereomers, and the similarity between Li's and Sun's $^{13}$C NMR data, their study focused on stereoisomers of **6** as opposed to constitutional isomers.

Kaufman and Sarotti's work employed DP4+ probability calculations to predict $^{1}$H NMR shifts of various stereoisomers of **6** and compared them to the experimental values obtained in Sun's isolation paper. Since **6** contains eight stereocenters, a total of 128 different diastereomers are possible for pseudo-rubriflordilactone B (**11**, Figure 3.5).

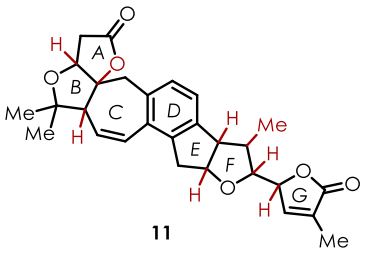


**Figure 3.5** Stereocenters in pseudo-Rubriflordilactone B

In order to limit the number of isomers to consider, they first analyzed the *ABC* ring system in **6** and various other natural products in the Schisandraceae family that have the same configuration at the associated stereocenters. By comparing the $^{1}H$ and $^{13}C$ NMR shifts, they could confidently say that **11** and **6** have the same stereochemistry around this portion of the molecule – specifically 1*R*,5*S*,10*R* (Figure 3.6).[52]

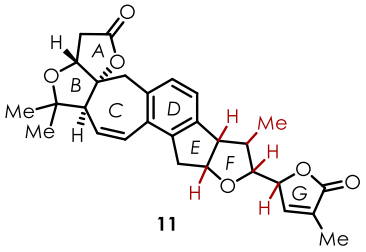


**Figure 3.6** Remaining Stereocenters to Resolve in pseudo-Rubriflordilactone B

This analysis greatly reduced the number of possible diastereomers from 128 to 32. Furthermore, NOESY analysis revealed an interesting correlation between the β-proton in ring *A* and the α-methyl protons in ring *G*. In order for this to be possible, the *EF* ring junction would need to be *syn*, specifically with a 16*R*,17*S* configuration; in addition, the point of attachment between rings *F* and *G* would need to allow the methyl group in ring *G* to approach β-hydrogen in ring *A*, or a 22*S* configuration (Figure 3.7).[52]

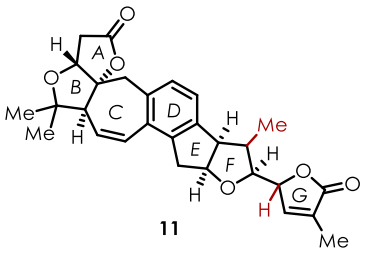


**Figure 3.7** Remaining Stereocenters to Resolve in pseudo-Rubriflordilactone B

At this point, only two stereocenters remained unknown, further reducing the possible diastereomers down to only four (Figure 3.8).

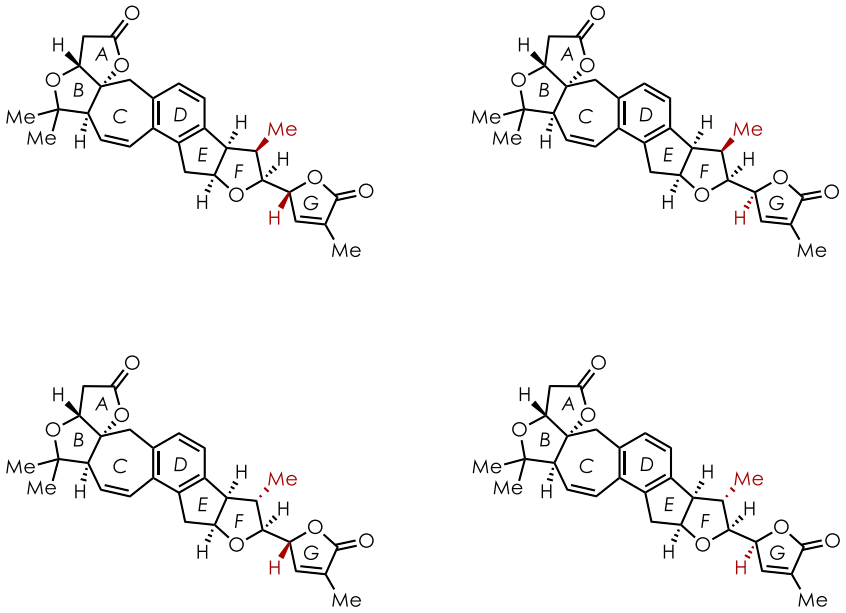

**Figure 3.8** Four Remaining Diastereomeric Possibilities

In order to decide which of these four isomers is the most likely structure of pseudo-rubriflordilactone B, computational models of conformers in which the β-proton of ring *A* and the α-methyl group of ring *G* were within 5 Å of each other were constructed and the enthalpy relative to the global minimum conformation was calculated (Figure 3.9).[52]

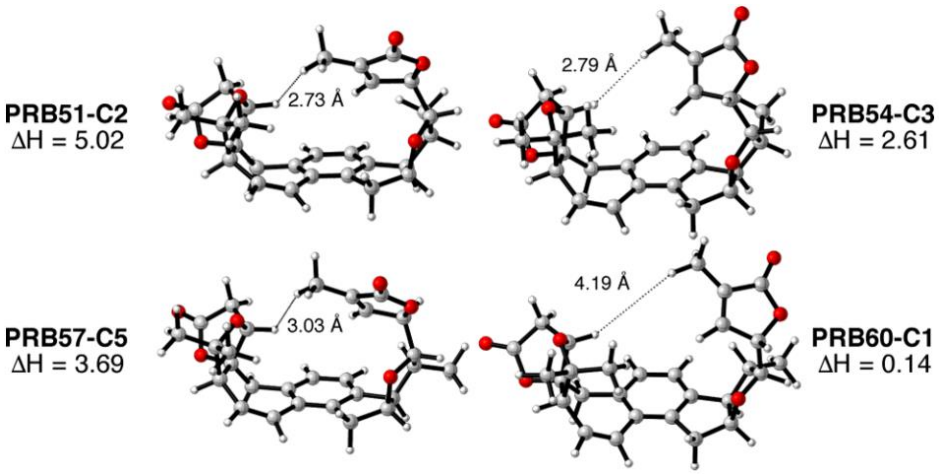


**Figure 3.9** Computational Models Reported by Kaufman and Sarotti

Based on this data, only one isomer exhibits a favorable change in enthalpy for this conformation (less than 2.5 kcal/mol above the global minimum), prompting Kaufman and Sarotti to propose a structure for **11** (Figure 3.10). These results suggest that only the stereochemistry at the *EF* ring junction differs between rubriflordilactone B and pseudo-rubriflordilactone B.

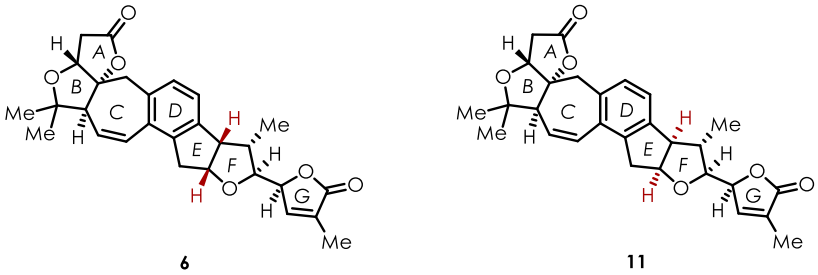


**Figure 3.10** Comparison of Rubriflordilactone B (**6**) and pseudo-Rubriflordilactone B (**11**)

While an authentic sample of **11** would be required to verify their work, Kaufman and Sarotti have made a considerable contribution to this area by providing a target for organic chemists to synthesize in order to solve this stereochemical ambiguity.

### 3.2 Synthetic Strategy for Rubriflordilactone B

Our interest in **6** stems from one of the lab's earliest publications detailing a PRCC between alkenes and unsaturated alcohols to form highly substituted tetrahydrofurans.[17] The mechanism by which this transformation occurs (Scheme 3.4) involves oxidation of the alkene by the excited-state acridinium ion to give a radical cation that is trapped by an allylic alcohol in an anti-Markovnikov manner. The resulting radical is poised to undergo a 5-*exo*-trig cyclization to give an *exo*-cyclic radical that can abstract a hydrogen atom from phenylmalononitrile (PMN), affording product. The PMN radical is then able to oxidize the acridine radical back to the acridinium ion to close the catalytic cycle.[17]

**Scheme 3.4** Mechanism for Tetrahydrofuran Synthesis via a PRCC

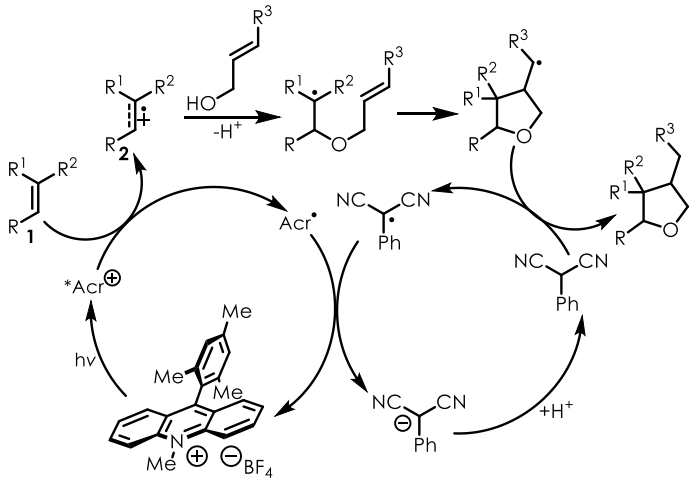


During the development of this chemistry, the product formed between indene and allyl alcohol was found to be reminiscent of the *DEF* ring system in **6**, with the reaction exhibiting a slight preference for the correct relative stereochemistry around the THF ring (Scheme 3.5). Since reporting this PRCC transformation back in 2013, we have sought to apply this chemistry to the synthesis of **6**.

**Scheme 3.5** PRCC Adduct of Indene and Allyl Alcohol and its Comparison to Rubriflordilactone B

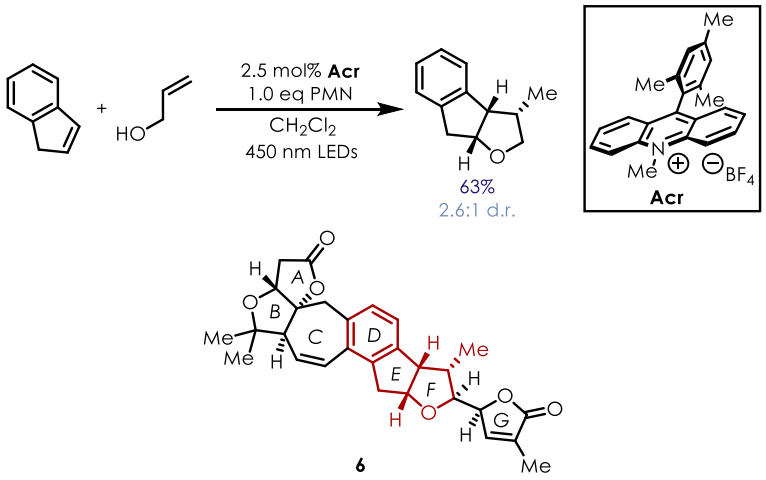





**6**

### 3.2.1 Initial Retrosynthetic Analysis

Our initial retrosynthetic analysis of **6** was inspired not only by our PRCC chemistry, but also work that has been reported on other Schisandraceae natural products. We envisioned that ring *A* could be made in a manner analogous to Li's work on rubriflordilactone A (Scheme 3.6A) [47], or Chen and Yang's investigations into micrandilactone A (Scheme 3.6B).[53] Li's route involves an intramolecular aldol condensation followed by a cationic deoxygenation, while Chen and Yang's employs an interesting HWE, oxy-Michael, lactonization cascade.

**Scheme 3.6** Reported Methods for *A* Ring Synthesis

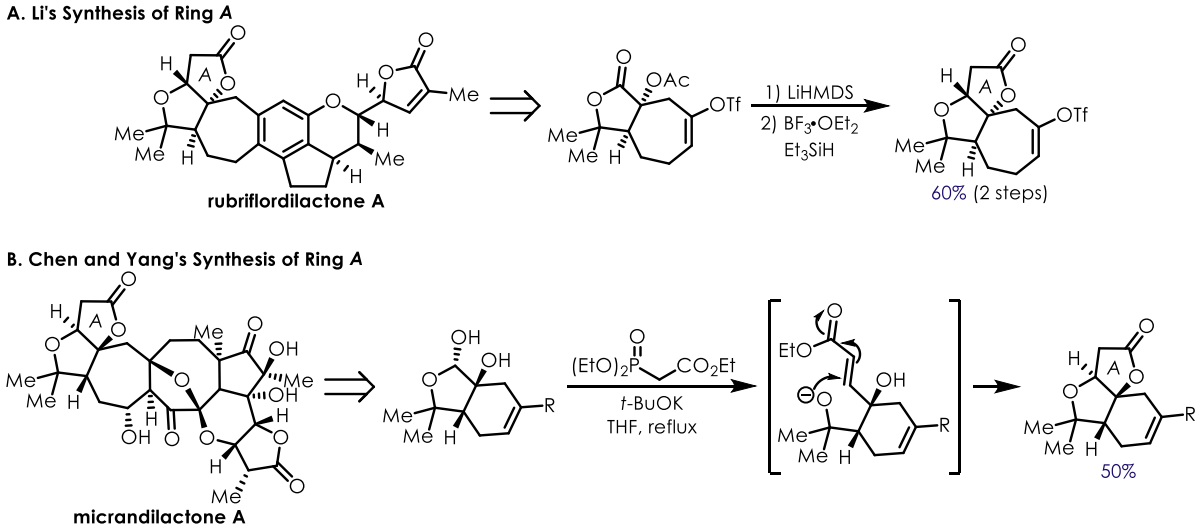


Taking this precedent into account, we devised a retrosynthesis of **6** (Scheme 3.7) which constructs the *A* ring last from the α-hydroxylactone **12** using either of the previously discussed methods. Intermediate **12** would be prepared from diene **13** via a reductive cyclization and enolate oxidation. Compound **13** would be prepared from lactone **14** via a Lindlar reduction of the alkyne to give the *Z*-alkene and an *exo*-methylenation of the lactone using Eschenmoser's salt. Lactone **14** would be synthesized from butenolide **15** and alkyne **16** via an asymmetric conjugate addition reaction. Finally, **16** would be made with a PRCC using indene **17** and allyl alcohol **18**.

**Scheme 3.7** Retrosynthetic Analysis of Rubriflordilactone B

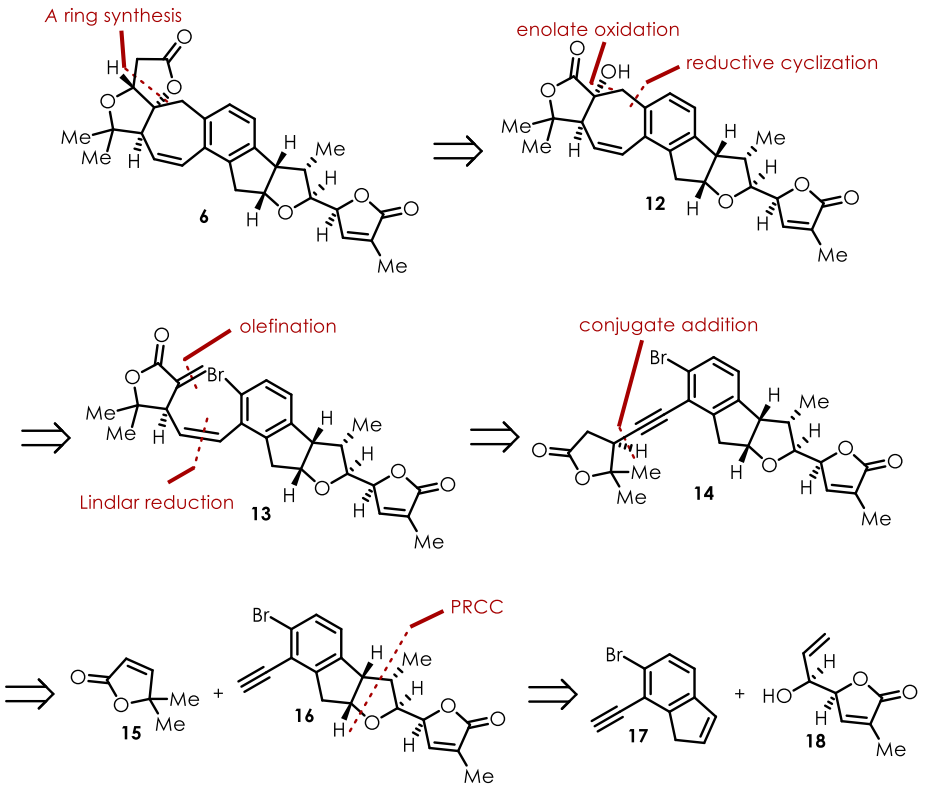


### 3.3 Synthesis of the Western Half of Rubriflordilactone B

Our first goal was to develop a model system for the western side of **6**. To accomplish this, we proposed a retrosynthesis of α-hydroxylactone **19** (Scheme 3.8).

**Scheme 3.8** Retrosynthesis of Left Side Model System

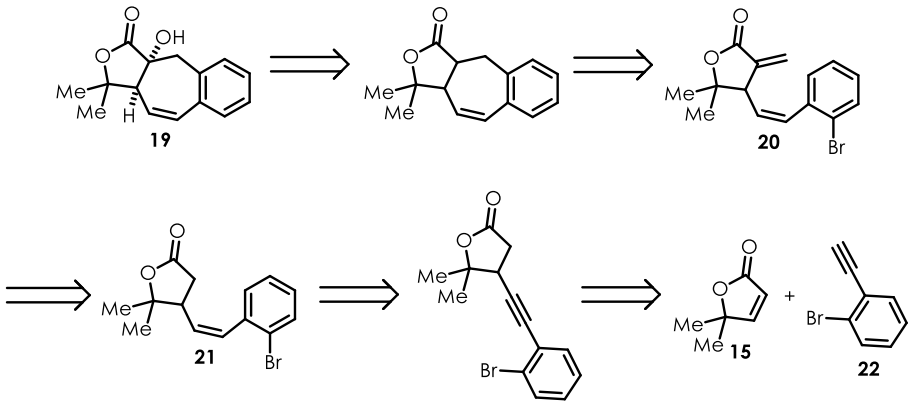

Starting from butenolide **15**, a conjugate addition of *o*-bromophenylacetylene (**22**) followed by a Lindlar reduction would afford lactone **21**. While a vinyl nucleophile could provide a more direct route to **21**, using an acetylide instead was a strategic choice. First, it prevents chemoselectivity issues in the PRCC step, as alkynes are unreactive. Second, it allows for better control over the final alkene geometry as since vinyl nucleophiles can be susceptible to erosion of configurational purity.

From lactone **21**, an *exo*-methylenation sequence with Eschenmoser's salt followed by alkylation and elimination of the β-trimethylammonium group would provide intermediate **20**. Finally, an intramolecular reductive Heck cyclization to form the seven-membered ring and an enolate oxidation with $O_2$ and triethyl phosphite would give the target compound **19**.

### 3.3.1 Conjugate Addition and Olefination

We initially attempted to synthesize **15** via a five-step route involving a HWE, saponification, isomerization, and esterification sequence to give methyl ester **23**. However, attempts at converting this species to **15** with *m*CPBA and TFA were unsuccessful (Scheme 3.9A). The second route consisted of methyl magnesium bromide addition into maleic anhydride followed by an acidic workup to achieve lactonization (Scheme 3.9B); while the first attempt at this afforded product in a 32% yield, the result was irreproducible. Fortunately, this approach could be slightly modified by first synthesizing the Diels-Alder adduct of maleic anhydride and furan (which is exclusively formed as the *exo*-isomer);[54,55] reacting this species with methyl magnesium bromdie followed by an acidic workup and distillation consistently provides **17** in a 57% yield over 2 steps (Scheme 3.9C).

**Scheme 3.9** Synthesis of Butenolide Starting Material

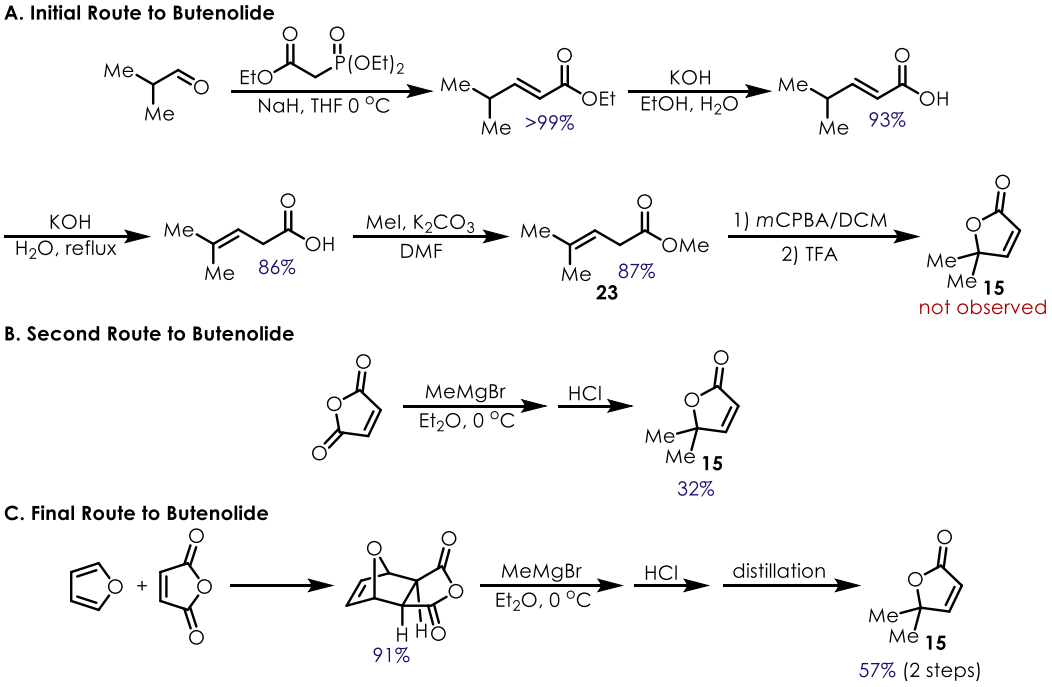


With **15** in hand, we screened conditions for the conjugate addition reaction using phenylacetylene as the nucleophile. Unfortunately, numerous attempts with various metals were unsuccessful in affording the desired product (Scheme 3.10).

**Scheme 3.10** Attempted at Conjugate Additions

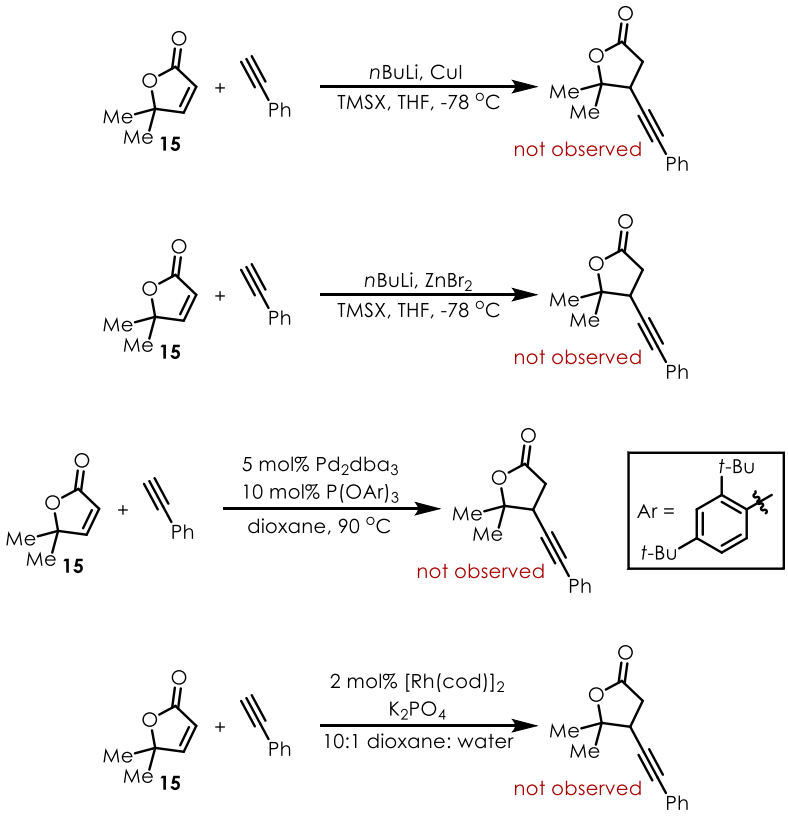


These initial results led me to suspect two issues with this conjugate addition – poor electrophilicity of the butenolide and steric hindrance of the β-position due to the geminal dimethyl group at the γ-position. In order to overcome these problems, I synthesized α-phosphonate butenolide **24** (Scheme 3.11).[56,57] Not only did I envision the additional electron-withdrawing group at the α-position would help the conjugate addition, but also the phosphonate group would allow for introduction of the *exo*-methylene moiety via an HWE with formaldehyde.

**Scheme 3.11** Synthesis of the α-Phosphonate Butenolide

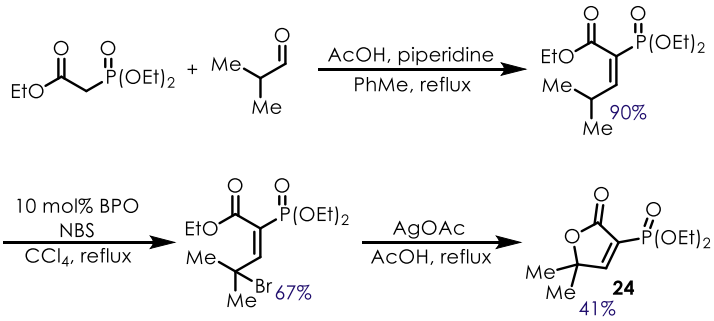


Conjugate addition of *o*-bromophenylacetylene into **24** was found to work quite well at elevated temperatures[58], suggesting that the increased electrophilicity of this species is partially responsible for achieving the desired reactivity. Lindlar reduction of the alkyne resulted in either no reduction or over-reduction to the alkane; however, a copper-mediated transfer hydrogenation process reported by the Lalic lab gave the desired *Z*-alkene in good yield.[59] Lastly, an HWE with formaldehyde afforded the *exo*-methylene lactone **25** (Scheme 3.12)

**Scheme 3.12** Route to the α-Methylene-γ-butyrolactone

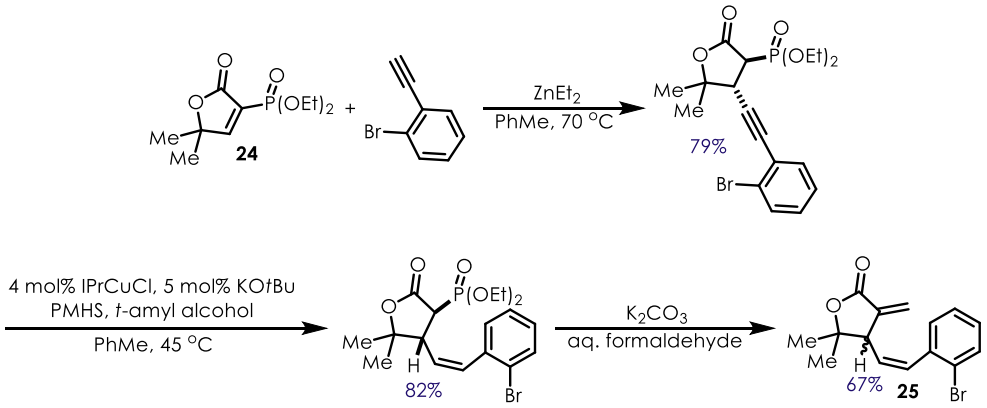


### 3.3.2 Seven-Membered Ring Formation

Initial attempts at forming ring *C* consisted of a radical cyclization and an intramolecular reductive Heck coupling; however, product was not observed in either case. Radical cyclization resulted in isomerization of **25** to the corresponding butenolide (Scheme 3.13A), which likely resulted from fast 1,5-hydrogen atom abstraction after formation of the aryl radical. Reductive

Heck conditions only afforded conjugate reduction of **25** with sodium formate serving as the hydride source (Scheme 3.13B).

**Scheme 3.13** Attempts at a Reductive Cyclization to form the Cycloheptene

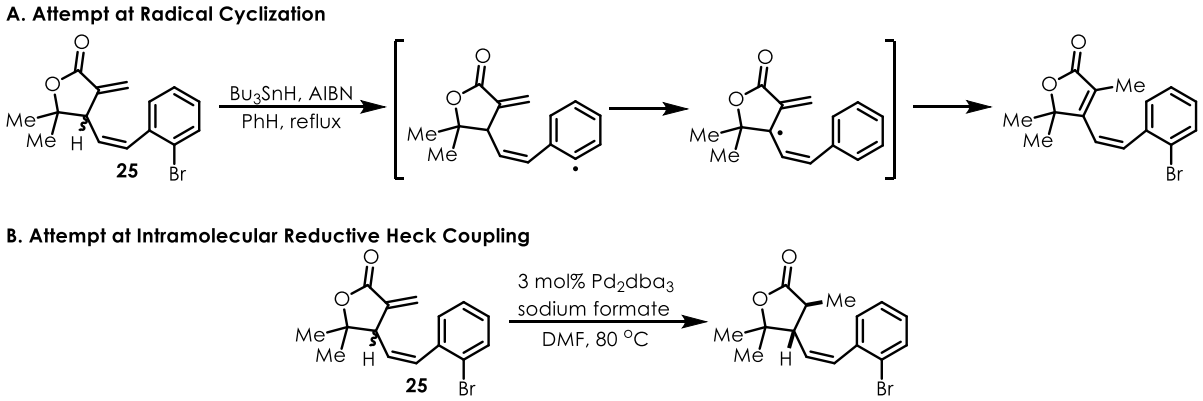


Based on these results, we opted to change the approach and first conducted a nucleophilic epoxidation on an analog of **25** to form spirocycle **26** (Scheme 3.14), we envisioned that an acid-mediated epoxide opening by the arene could form the desired seven-membered ring **19** while also introducing the α-hydroxygroup required to construct ring *A*.

**Scheme 3.14** Nucleophilic Epoxidation

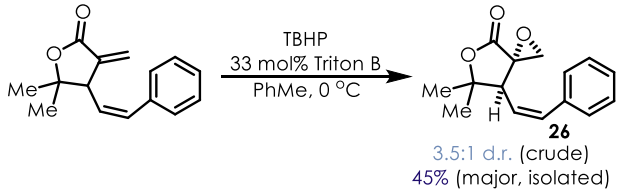


Unfortunately, after an extensive screen of Brønsted and Lewis acids (Table 3.1), the desired transformation was never observed. In the majority of cases no reaction occurred, but a few instances resulted in epoxide opening by either the conjugate base of the Brønsted acid or a ligand on the Lewis acid behaving as the nucleophile.

**Table 3.1** Attempts at an Acid-Mediated Epoxide Opening

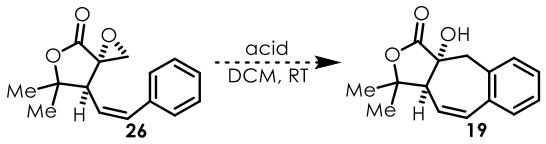


| **Brønsted Acids** | | **Lewis Acids** | |
|---|---|---|---|
| Acid | Result | Acid | Result |
| $H_3PO_4$ | No reaction | $TiCl_4$ | Epoxide opening |
| $Tf_2NH$ | Epoxide opening | $SnCl_4$ | Epoxide opening |
| TFA | No reaction | $AlCl_3$ | Epoxide opening |
| CSA | No reaction | $BF_3{\cdot}OEt_2$ | Decomposition |
| $HBF_4$ | No reaction | $Sc(OTf)_3$ | No reaction |
| *p*TsOH | Epoxide opening | $La(OTf)_3$ | Decomposition |
| $H_2SO_4$ | Decomposition | $Cu(OTf)_2$ | No reaction |
| TfOH | Decomposition | $Ti(OiPr)_4$ | No reaction |
| $HCO_2H$ | No reaction | $Sn(OTf)_2$ | No reaction |
| $MeSO_3H$ | No reaction | $Al(OTf)_3$ | No reaction |
| $HPF_6$ | No reaction | $TrBF_4$ | No reaction |

At this point, I decided to investigate formation of ring *C* via an RCM from diene **27** (Scheme 3.15A). Initially, we proposed **27** could be formed by conjugate addition of a vinyl cuprate into butenolide **15** followed by alkylation of the enolate with 2-vinylbenzylbromide. While the conjugate addition reactions did afford the desired product, a significant amount of competitive 1,2-addition was also observed (Scheme 3.15B). Due to this, we explored a route that would install the desired α-substituent prior to the conjugate addition, hoping that this would mitigate the undesired 1,2-addition.

**Scheme 3.15** Initial Plan for Diene Synthesis

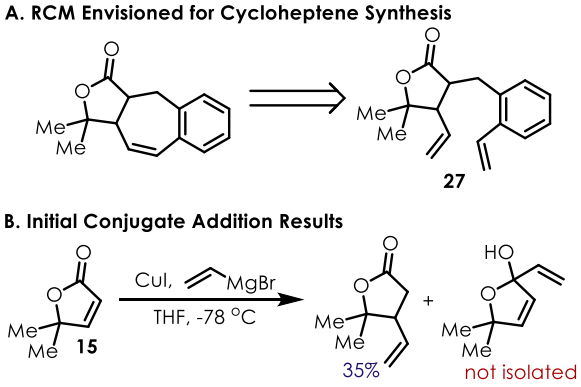


Based on the route for the synthesis of butenolide **15**, we envisioned the tricyclic lactone derived from the furan-maleic anhydride Diels-Alder adduct could first be alkylated prior to a retro-Diels-Alder to provide an α-substituted butenolide (Scheme 3.16A). However, work by Cannone which reveals this species would not undergo alkylation, but the closely related compound derived from the cyclopentadiene-maleic anhydride Diels-Alder adduct would give product (Scheme 3.16B).[60,61] This is proposed to be a result of the difference in Diels-Alder product selectivity. In the first case, furan's aromaticity allows for thermodynamic control, giving only the *exo*-product, while with cyclopentadiene kinetic control dominates, giving the *endo*-product. The resulting tricyclic lactones after Grignard addition retain their configuration at the ring junction, and as a result only the *endo*-species is able to effectively undergo alkylation since the α-position in the *exo*-species is more sterically hindered.

**Scheme 3.16** Difference in Diels-Alder Selectivity Impacts Enolate Alkylation

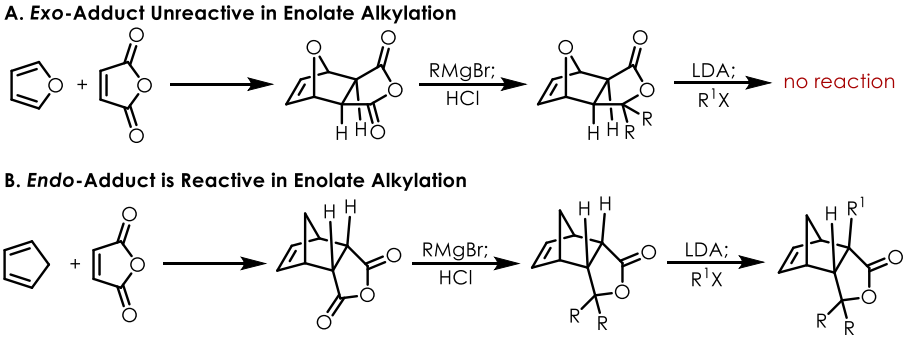


Based on this precedent, I synthesized Diels-Alder adduct **28** which could be converted to tricyclic lactone **29** via a Grignard addition, lactonization sequence. Alkylation of **29** with 2-vinylbenzyl bromide (which was prepared in 3 steps from 2-bromobenzaldehyde) followed by a retro-Diels-Alder gave the desired α-functionalized butenolide **30**. We were pleased to discover that conjugate addition of vinyl cuprate into **30** gave the desired diene **27** in good yield with minimal competitive 1,2-addition (Scheme 3.17).

**Scheme 3.17** Synthesis of the Diene for the Ring Closing Metathesis

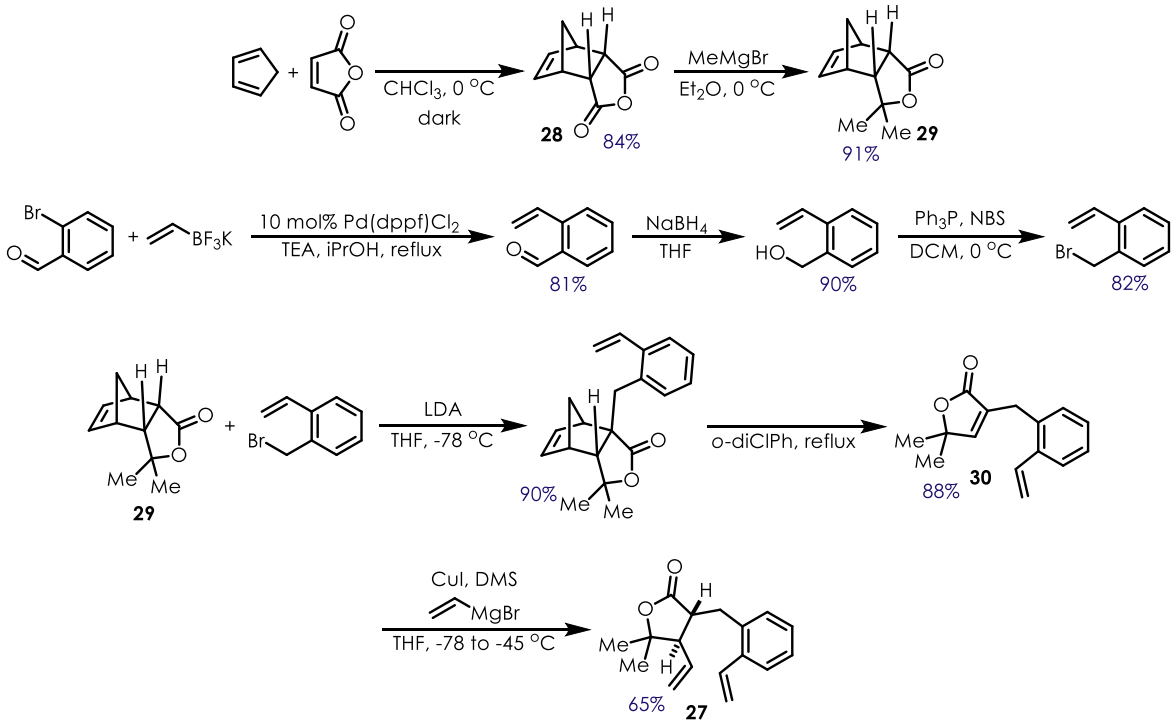

From here, two different routes could be envisioned for forming the target α-hydroxylactone **19**. Enolate oxidation could be conducted on diene **27** followed by the RCM (Scheme 3.18A), or **27** could be used in the RCM and the corresponding product in the enolate oxidation (Scheme 3.19B).[x] While both routes were successful, variations between GC retention times and $^{1}$H NMR chemical shifts indicated a different diastereomer was formed in each case.

**Scheme 3.18** Two Routes to Tricyclic α-Hydroxylactone

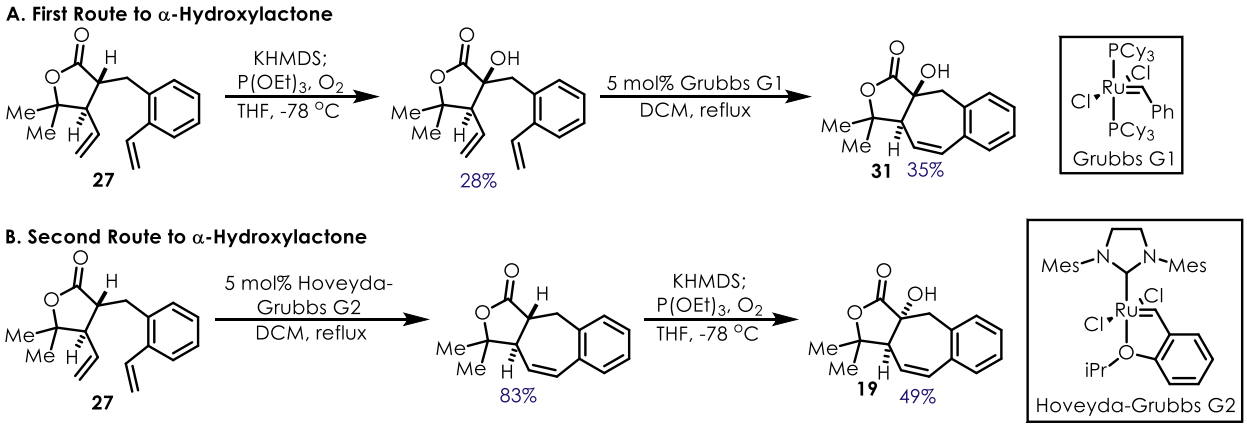


In order to determine the relative stereochemistry at the *BC* ring junction, x-ray crystallography analysis was performed on both diastereomers (Figure 3.11). In the first route, a *trans*-ring junction was formed. This is likely due to the enolate oxidation on diene **27** favoring an *anti*-relationship between the benzyl group at the α-carbon and the vinyl group at the β-position. In the second route, the desired *cis*-ring junction was produced. In this case, pre-formation of the 5-7 ring junction allows enolate oxidation to favor the more thermodynamically stable *syn*-ring junction exhibited in most fused 5-7 ring systems.[62]

[x] The RCM catalysts differ as only the route to **19** is optimized, as the other route gives the undesired diastereomer.

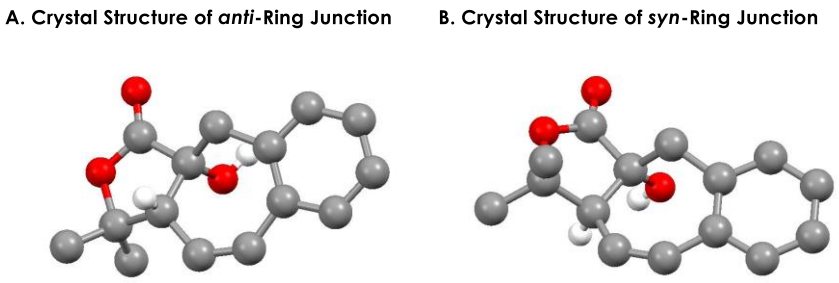


**Figure 3.11** Crystal Structures of α-Hydroxylactone Diastereomers

### 3.3.3 Synthesis of the Terminal Lactone

After confirming **19** was constructed as the correct diastereomer, we turned to optimization of the enolate oxidation followed by synthesis of the *A* ring.

Initially, we hoped that scaling-up the enolate oxidation would improve the yield from 49% due to the sensitivity of enolate chemistry on small scale; however, we were discouraged to find that the yield dropped by nearly half. After testing various conditions such as temperature and sequence of reagent addition, no major improvements to the yield were observed. Based on these results, it appears this transformation is sensitive to scale, as reactions conducted with less than 1 mmol of substrate give yields around 50%, while those employing larger amounts give an average yield of 25% (Table 3.2).

**Table 3.2** Impact of Enolate Oxidation Scale on Yield

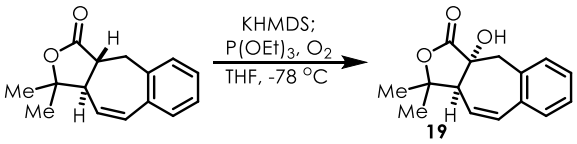


| Reaction | Scale (mmol) | % Yield |
|---|---|---|
| **1** | 0.508 | 48 |
| **2** | 1.41 | 27 |
| **3** | 1.87 | 24 |
| **4** | 2.19 | 26 |
| **5** | 0.727 | 49 |
| **6**[xi] | 0.727 | 56 |

The mechanism of this reaction involves oxidation of the enolate by triplet oxygen to give an α-carbonyl radical, which can subsequently be trapped by oxygen to give a hydroperoxide that is reduced by the trialkyl phosphite. The main byproduct observed is dieneoate **32**, which likely forms from the intermediate α-carbonyl radical by abstraction of the allylic hydrogen atom by oxygen (Scheme 3.19). Larger scale reactions may facilitate this process by either less-efficient oxygen flow or greater variations in temperature throughout the reaction medium. Due to this limitation, we turned to other oxidants that have been used in the synthesis of α-hydroxylactones.[63]

**Scheme 3.19** Mechanism of Dieneoate Formation

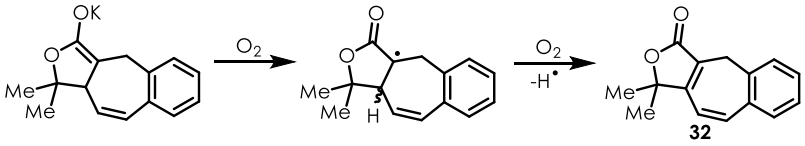


Initially, we proposed Davis's oxaziridine[64] could be used as the oxidant, but we discovered this species gave no improvement in yield (Scheme 3.20A). Furthermore, the less-widely used molybdenum(VI) complexes MoOPH[65] and MoOPD[66] were prepared and used in

[xi] Reaction run with $P(OMe)_3$ instead of $P(OEt)_3$

the transformation, but with no success in either instance (Scheme 3.20B). Based on these results, we opted to move ahead with synthesis of the *A* ring, accepting the yield that could be obtained with molecular $O_2$ as the oxidant.

**Scheme 3.20** Attempts at Enolate Oxidation with Different Oxidants

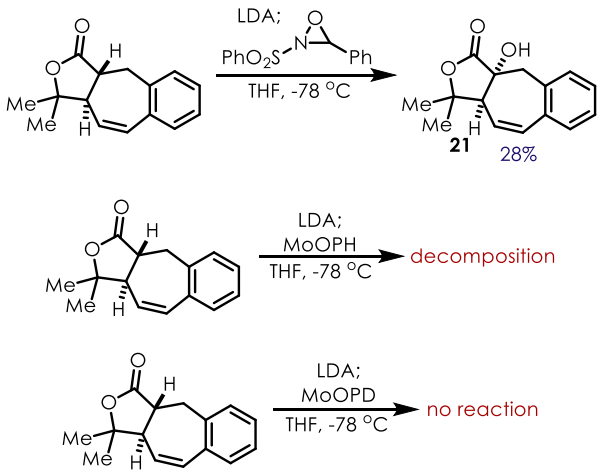


First we sought to synthesis ring *A* via the HWE, oxy-Michael, lactonization cascade reported by Chen and Yang on their work with micrandilactone A.[53] Reduction of **19** with DIBAL afforded the requisite lactol for this transformation, but we were discouraged to discover that attempting the reported cascade conditions resulted in formation of diene **33** (Scheme 3.21).

**Scheme 3.21** Initial Cascade Attempt Result

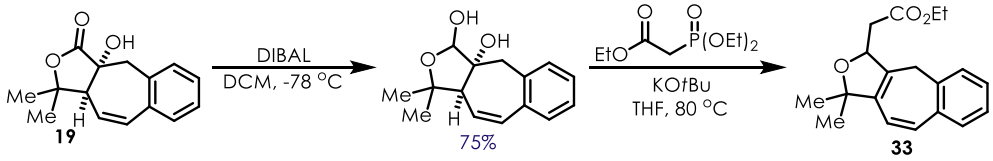


In an attempt to prevent the elimination reaction, we screened various reaction temperatures and base loadings, but found that any deviation from the conditions reported by Chen and Yang resulted in no reaction. Furthermore, attempting analogous cascades with either a Wittig salt[67] or Meldrum's acid[68] were also unsuccessful (Scheme 3.22).

**Scheme 3.22** Cascade Attempts with Wittig Salt and Meldrum's Acid

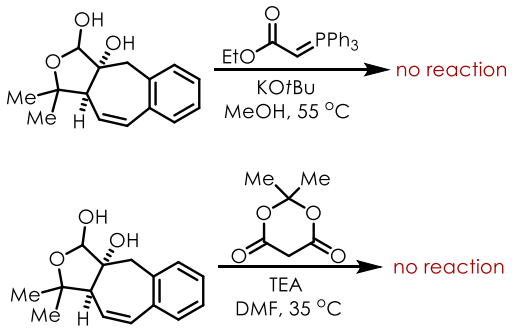


Due to these unsuccessful attempts, we turned to the approach employed by Ang Li in rubriflordilactone A.[46] Starting from **19**, we were able to conduct acetylation of the α-hydroxy group followed by an intramolecular aldol reaction to give β-hydroxylactone **34** in good yield. Cationic deoxygenation of this species with $BF_3 \cdot OEt_2$ and $Et_3SiH$ resulted in a single product that we could not conclusively identify by $^1H$ NMR (Scheme 3.23).

**Scheme 3.23** Initial Sequence for the Synthesis of Ring *A*

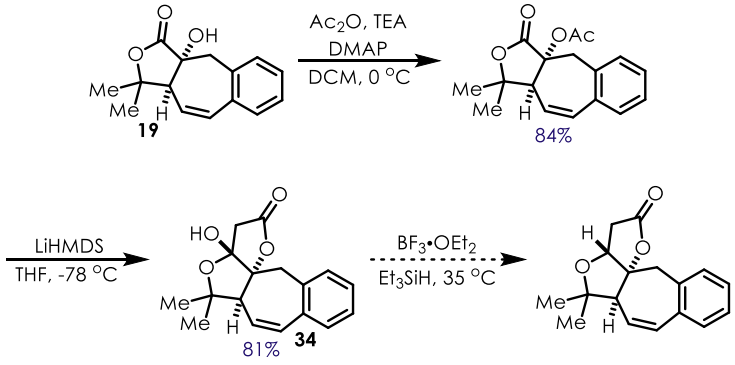


In an effort to determine the identity of the product, an alternate route to the same target was conducted (Scheme 3.24). From **34**, dehydration to the butenolide with Martin's sulfurane followed by conjugate reduction with L-selectride was carried out, resulting in a product that exhibited the same $^1H$ NMR characterization as that formed in the cationic deoxygenation.

**Scheme 3.24** Alternate Route to Ring *A*

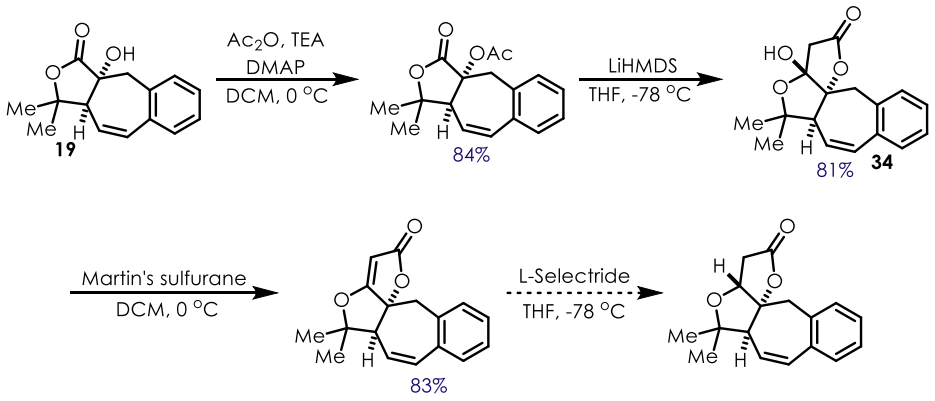


While GC-MS data showed the isolated material to have the mass of the desired product, the $^{1}$H NMR data remained a mystery. The spectrum exhibited broadening of several signals, most noticeably a methyl group that initially appears to be non-existent without careful examination (Figure 3.12). Based on this, we hypothesized that the rigidity of the molecule caused conformational changes to be slow on the NMR time-scale, resulting in unusual anisotropic effects.

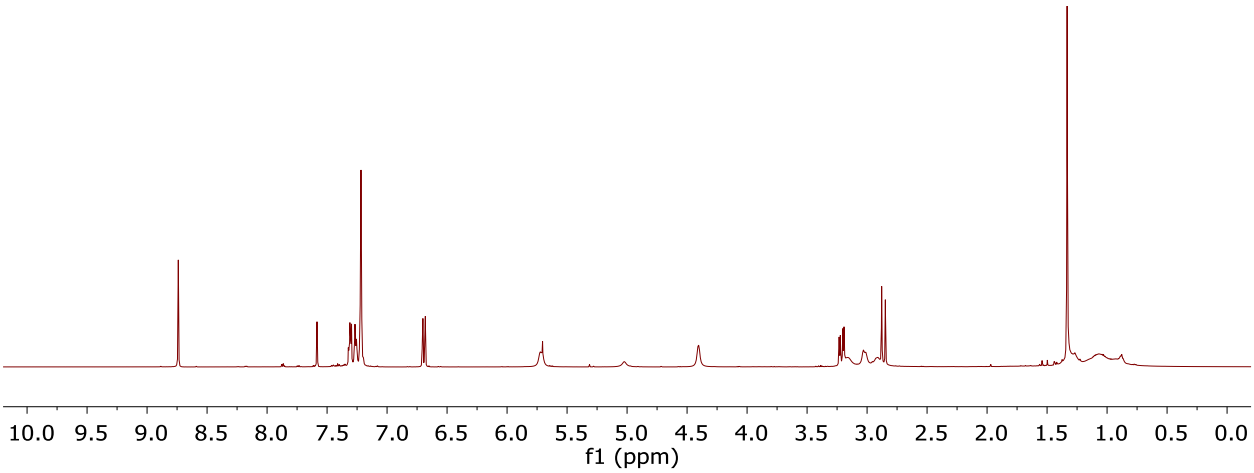


**Figure 3.12** $^{1}$H NMR (pyridine-*d*5) of Product Formed in Both Routes

In order solve this mystery, we collected $^{1}$H NMR data at 60 °C and observed increased resolution of the previously broad peaks (Figure 3.13).

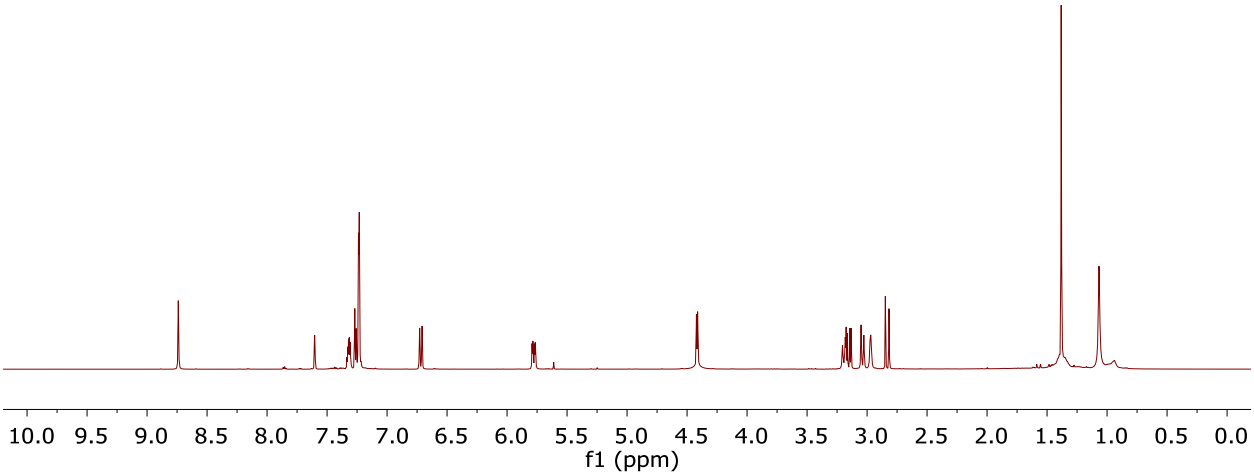


**Figure 3.13** $^{1}$H NMR (pyridine-*d*5) of Product at 60 $^{o}$C

In addition, we obtained a crystal structure of the product (Figure 3.14) and were pleased to find that it had the correct relative stereochemistry around the *ABC* ring system, indicating we successfully developed a diastereoselective synthesis for the left half of **6**.

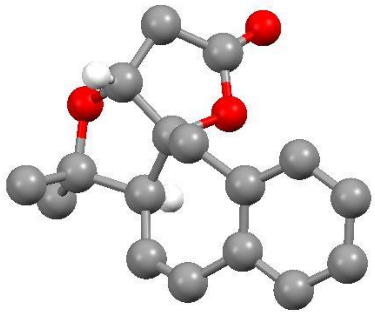

**Figure 3.14** Crystal Structure of Left Half of Rubriflordilactone B

### 3.3.4 Diastereoselective Route to the Left Half of Rubriflordilactone B

Our final diastereoselective route to the left side of rubriflordilactone B consists of 11 linear steps from maleic anhydride and an overall yield of 9% (Scheme 3.25).

**Scheme 3.25** Diastereoselective Route to the Left Half of Rubrilfordilactone B

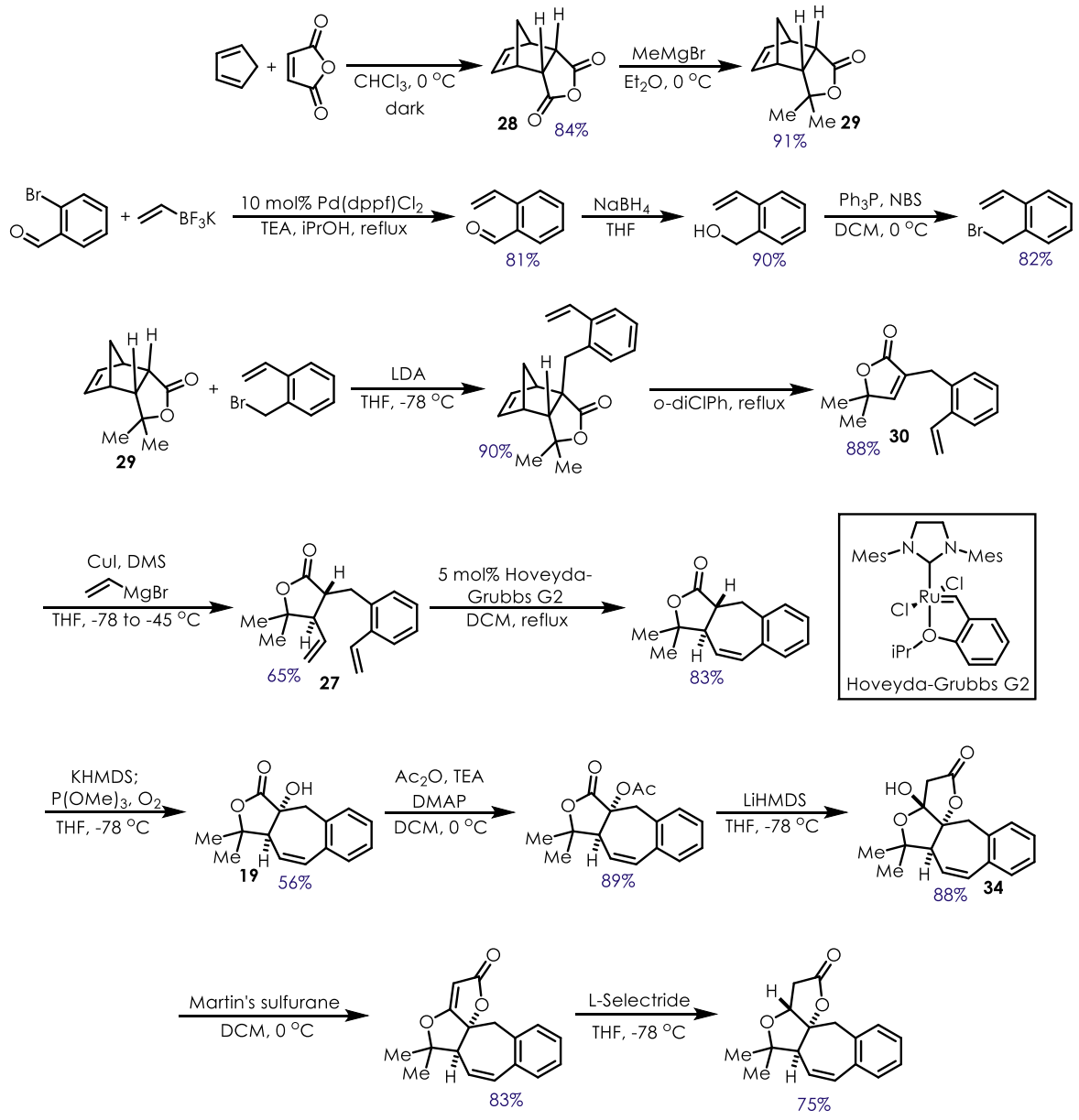


## 3.4 Progress Toward the Synthesis of the Eastern Half of Rubriflordilactone B

Our initial approach to the right side of rubriflordilactone B comprised of a PRCC reaction (Scheme 3.26) between allylic alcohol **35** and indene, the former of which could be made via a vinylogous Mukaiyama aldol between a siloxyfuran and acrolein.

**Scheme 3.26** Retrosynthesis for the Right Side of Rubriflordilactone B

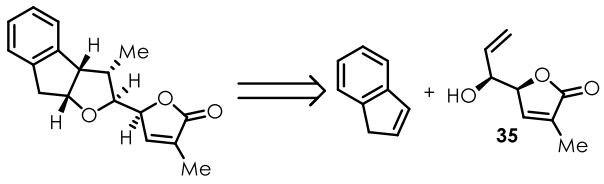


We first investigated this approach and discovered that the PRCC between indene and **35** afforded the eastern side of rubriflordilactone B, albeit in very low yield and with the undesired stereochemistry[xii] at the *EF* ring junction (Scheme 3.27).[69]

**Scheme 3.27** Initial PRCC Results

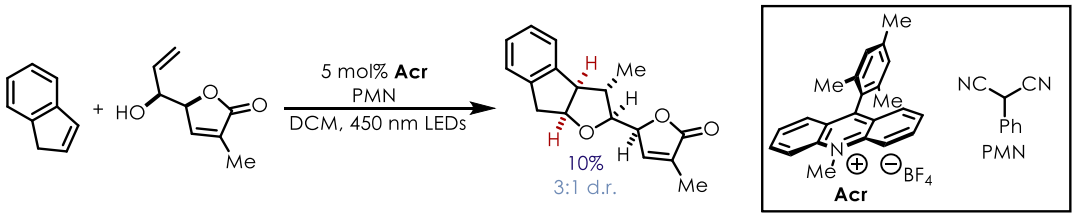


In an effort to overcome this diastereoselectivity issue, we synthesized allylic alcohol **36**, which was subsequently used in the PRCC. While the correct relative stereochemistry at the *EF* ring junction was now observed, the stereocenter bearing the methyl group was not (Scheme 3.28).[69]

**Scheme 3.28** Attempt to Alter PRCC Diastereoselectivity

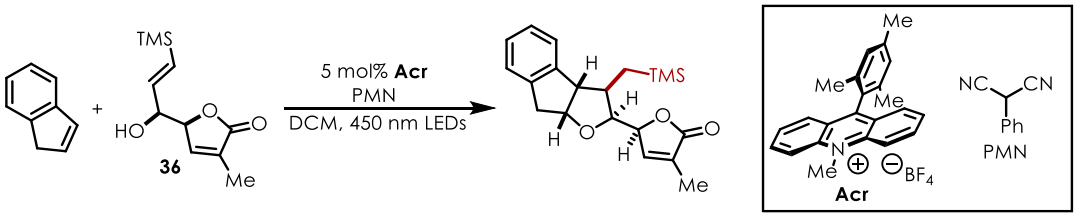


Due to the inherent challenges of trying to set four stereocenters in a single step, we slightly altered our approach and planned to conduct the PRCC with propargyl alcohol **37**. This

[xii] Though we will note this is the correct diastereomer for pseudo-rubriflordilactone B

would reduce the number of stereocenters involved to three, and we would be able to easily set the stereochemistry of the methyl group via a hydrogenation reaction, which should occur from the convex face of the molecule (Scheme 3.29).

**Scheme 3.29** Retrosynthesis Employing a Propargyl Alcohol in the PRCC

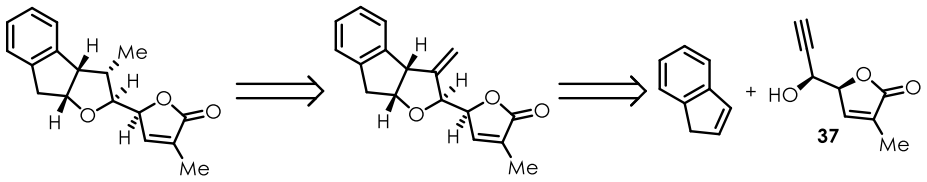


### 3.4.1 Propargyl Alcohol Synthesis

We were able to synthesize **38** using a catalyst originally reported by the Carreira lab (Scheme 3.30).[70,71] Unfortunately, the diastereoselectivity for this transformation was inconsistent with the reported work.

**Scheme 3.30** Synthesis of Propargyl Alcohol

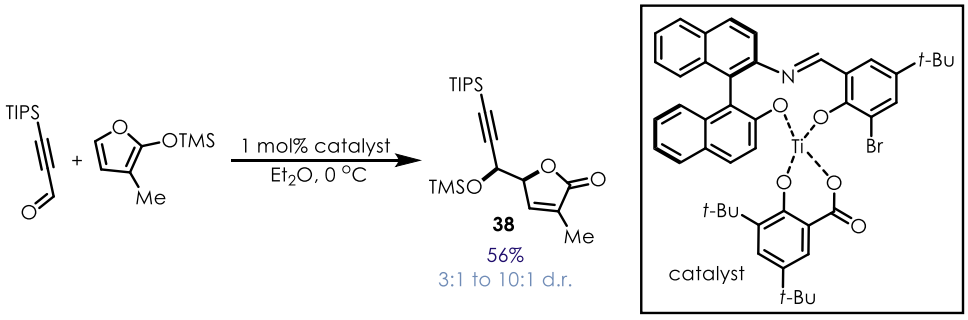


In order to optimize this transformation, we first tested the impact of the silyl groups on the diastereomeric ratio (Table 3.3). Increasing the size of the silyl group on the siloxyfuran shut down the reaction, and any deviation from the TIPS group on the propargaldehyde resulted in worse diastereoselectivity.

**Table 3.3** Impact of Silyl Group on Vinylogous Mukaiyama Aldol

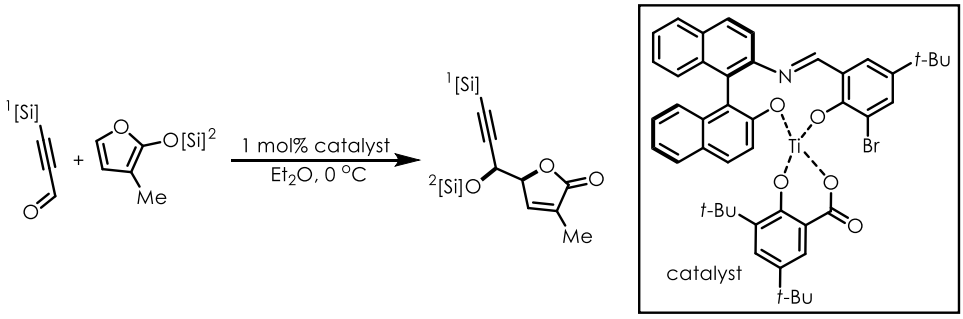


| Trial | $[Si]^1$ Group | $[Si]^2$ Group | d.r. |
|---|---|---|---|
| **1** | TIPS | TMS | 4.5:1 |
| **2** | TIPS | TBS | NA – no reaction |
| **3** | TMS | TMS | 1.1:1 |
| **4** | TES | TMS | 1.2:1 |
| **5** | TPS | TMS | 1.0:1 |

Following this up with a solvent screen, we discovered that toluene provided the best diastereoselectivity (Table 3.4).

**Table 3.4** Impact of Solvent on Vinylogous Mukaiyama Aldol

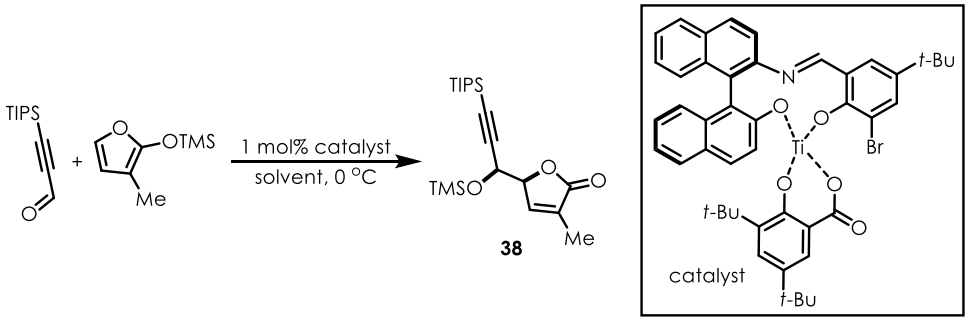


| Trial | Solvent | d.r. |
|---|---|---|
| **1** | $Et_2O$ | 6.3:1 |
| **2** | THF | 1:9.2 |
| **3** | Dioxane | 4.7:1 |
| **4** | DCM | 1.0:1 |
| **5** | $CHCl_3$ | 1.0:1 |
| **6** | DCE | 2.3:1 |
| **7** | PhH | 5.8:1 |
| **8** | PhMe | 8.7:1 |
| **9** | $PhCF_3$ | 2.6:1 |

Unfortunately, the second time we ran the reaction with these new conditions, the high d.r. previously obtained was not observed. Suspecting that the reaction is highly sensitive to moisture, extra care was taken to run the reaction in the absence of water, but in this case the reaction was completely shut down.

Based on this observation, we wondered if water was in fact playing a critical role in the transformation, likely by producing a Brønsted acid *in situ*. After coming across a report by Kobayashi in which water was found to enhance the rate of a titanium-medial vinylogous Mukaiyama aldol (Scheme 3.31),[72] we opted to test out the addition of water to our reaction.

**Scheme 3.31** Rate Enhancement by Water Observed by Kabayashi

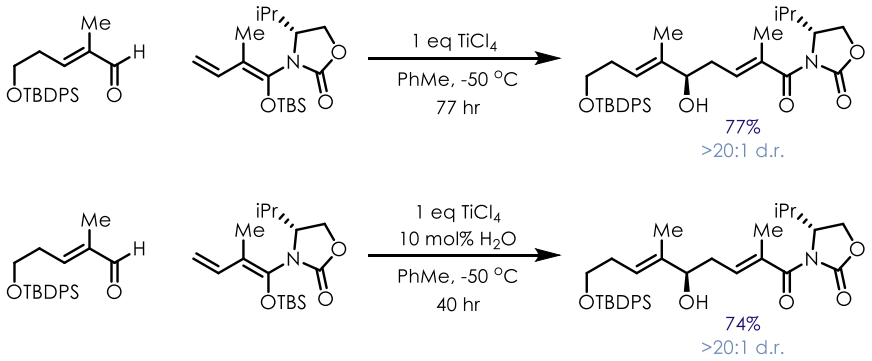


We were pleased to find that by adding a catalytic amount of water, we were able to consistently obtain high conversion and high diastereoselectivity for this transformation, which was maintained through removal of the TMS group with citric acid (Scheme 3.32).

**Scheme 3.32** Optimized Vinylogous Mukaiyama Aldol with Catalytic Water

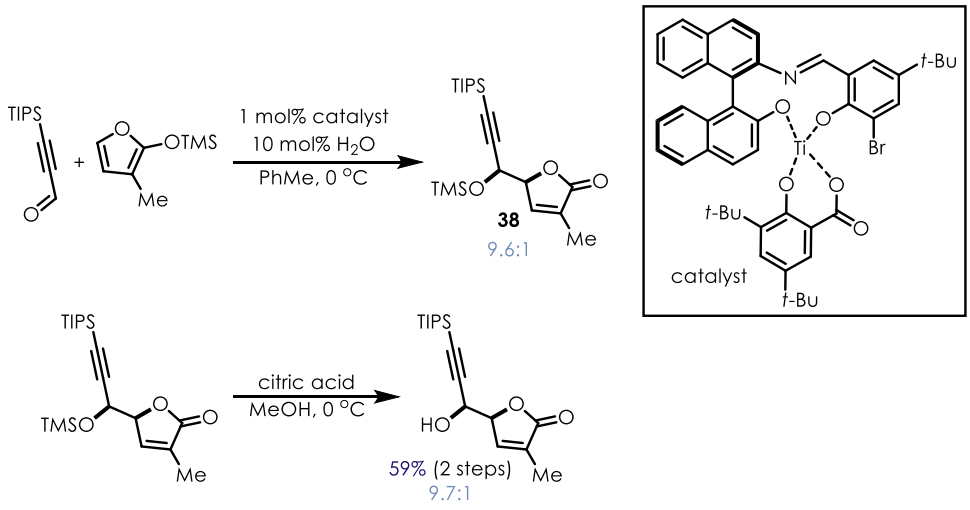


At this point, we turned our attention to removing the TIPS group and were discouraged to discover that traditional TBAF conditions resulted in complete erosion of diastereoselectivity. Furthermore, attempts at buffering the reaction with acetic acid made little to no improvements (Table 3.5).

**Table 3.5** Summary of Deprotection Conditions with TBAF

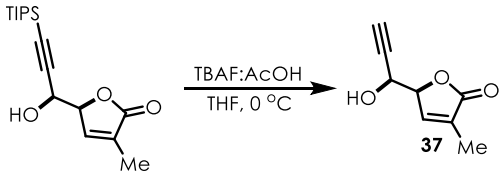


| Trial | AcOH:TBAF Ratio | d.r. |
|---|---|---|
| **1** | 1.1:1 | 2.5:1 |
| **2** | 1.3:1 | 2.4:1 |
| **3** | 1.5:1 | 2.6:1 |
| **4** | 1.6:1 | 2.8:1 |
| **5** | 1.7:1 | 1.1:1 |
| **6** | 1.8:1 | 2.5:1 |
| **7** | 2.0:1 | 2.2:1 |
| **8** | 2.5:1 | 2.4:1 |

However, based on a report by Hernádez on the deprotection of sensitive TIPS-aryl acetylenes with AgF,[73] we were able to accomplish this reaction in moderate yield with minimal impact on the diastereomeric ratio (Scheme 3.33).

**Scheme 3.33** Deprotection of TIPS-Acetylene

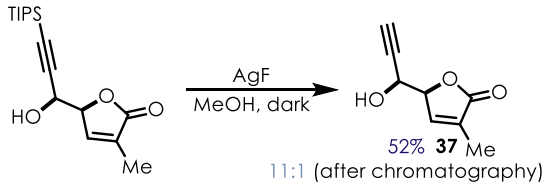


### 3.4.2 Polar Radical Crossover Cycloaddition

With propargyl alcohol **37** in hand, I turned to developing conditions for the PRCC. Due to the lack of precedent with employing secondary propargyl alcohols in this reaction[17], we initially attempted a PRCC with indene and 3-butyn-1-ol. After a hydrogen-atom donor screen (Table 3.6), we were confident enough to attempt the desired transformation with **37** as the nucleophile.

**Table 3.6** Hydrogen Atom Donor Screen for PRCC with 3-Butyn-1-ol

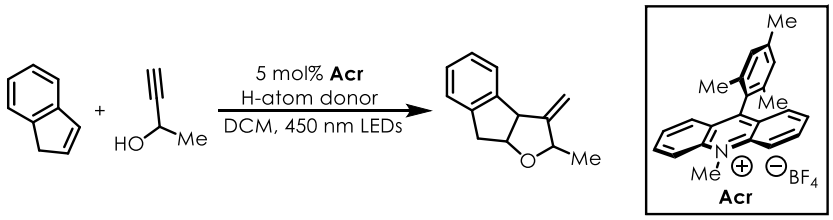


| Trial | H-atom donor[xiii] | % Yield[xiv] |
|---|---|---|
| **1** | 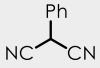 | 41 |
| **2** | 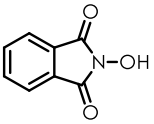 | 30 |
| **3** | 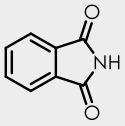 | 18 |
| **4** | 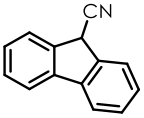 | 15 |
| **5** | 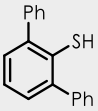 | 10 |
| **6** | 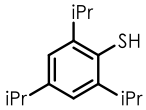 | 29 |
| **7** | 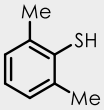 | 12 |

Unfortunately, the best conditions for the reaction with 3-butyn-1-ol did not directly translate when **38** was used instead, as no product was observed. We subsequently screened a variety of conditions with variations in stoichiometry, solvent, hydrogen atom donor, and base, but unfortunately product was never observed (Table 3.7).

[xiii] All hydrogen atom donors were used in stoichiometric quantities (1 equivalent) except for the benzenethiols, which were used with a 20 mol% loading

[xiv] Yields with thiol hydrogen atom donors are GC-MS yields using 1,3-dimethoxybenzene as an internal standard

**Table 3.7** PRCC Conditions Screened with Alcohol **37**

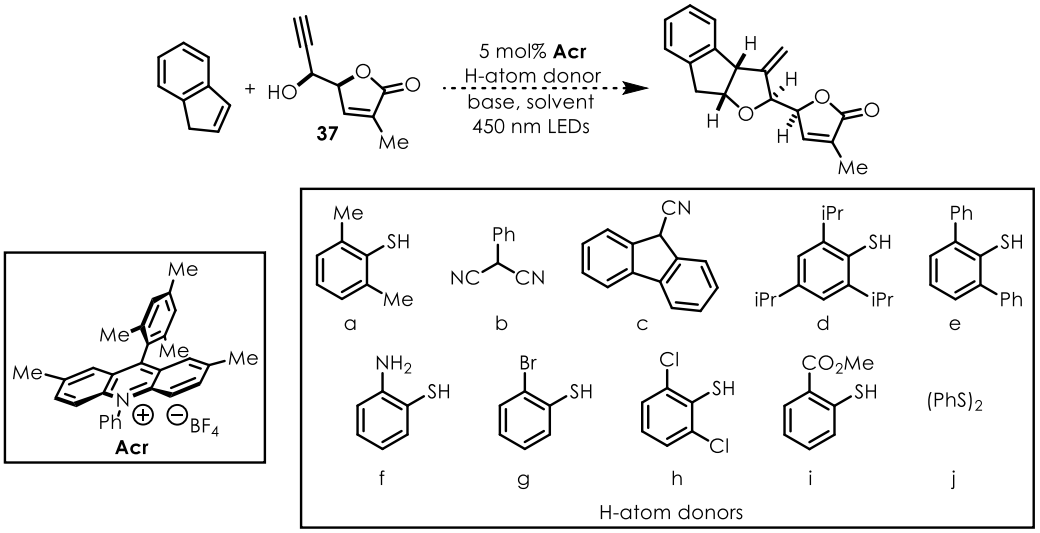


| Trial | H-donor | Stoichiometry (indene:alcohol) | Solvent | Base |
|---|---|---|---|---|
| **1** | a | 1.5:1.0 | DCM | NA |
| **2** | a | 1.5:1.0 | $MeNO_2$ | NA |
| **3** | a | 1.5:1.0 | DCE | 15 mol% 2,6-lutidine |
| **4** | a | 1.0:3.0 | DCM | 15 mol% 2,6-lutidine |
| **5** | b | 1.5:1.0 | DCM | NA |
| **6** | b | 1.5:1.0 | DCM | 15 mol% 2,6-lutidine |
| **7** | b | 1.5:1.0 | $MeNO_2$ | NA |
| **8** | b | 1.0:1.5 | DCE | NA |
| **9** | b | 1.0:3.0 | DCM | NA |
| **10** | b | 1.0:5.0 | DCM | NA |
| **11** | c | 1.0:5.0 | DCM | NA |
| **12** | d | 1.0:1.5 | DCM | NA |
| **13** | d | 1.0:1.5 | DCM | 15 mol% 2,6-lutidine |
| **14** | e | 1.0:1.5 | DCM | NA |
| **15** | e | 1.0:1.5 | DCM | 15 mol% 2,6-lutidine |
| **16** | f | 1.0:1.5 | DCM | NA |
| **17** | g | 1.0:1.5 | DCM | NA |
| **18** | h | 1.0:1.5 | DCM | NA |
| **19** | i | 1.0:1.5 | DCM | NA |
| **20** | j | 1.0:1.5 | DCE | NA |

In addition, we also attempted the reaction prior to removal of the TIPS group, as it could help stabilize the vinyl radical formed after the 5-*exo*-trig cyclization (Table 3.8), but again not product was observed.

**Table 3.8** PRCC Conditions Screened with Silylated Alkyne

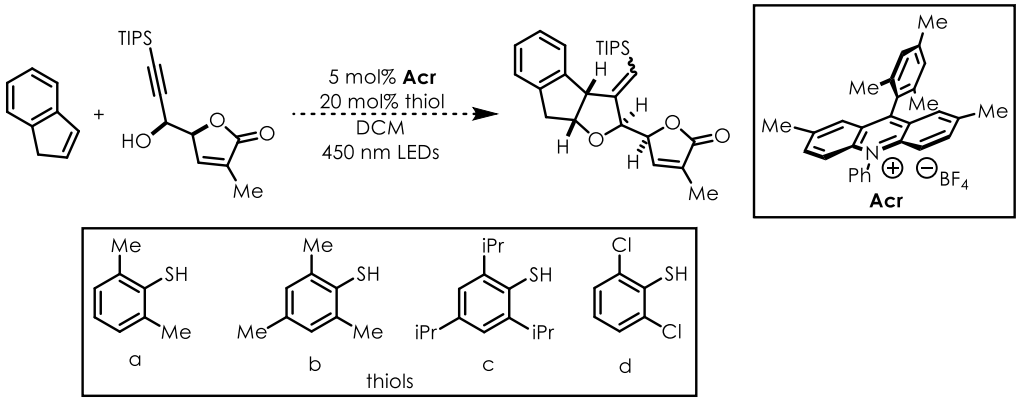


| Trial | Thiol | Stoichiometry (indene:alcohol) |
|---|---|---|
| **1** | a | 1.0:5.0 |
| **2** | a | 1.5:1.0 |
| **3** | b | 1.0:5.0 |
| **4** | b | 1.5:1.0 |
| **5** | c | 1.0:5.0 |
| **6** | c | 1.5:1.0 |
| **7** | d | 1.0:5.0 |
| **8** | d | 1.5:1.0 |

The main byproduct formed under the reaction conditions was the [2+2] homodimer of indene (Figure 3.15), which is unsurprising based on precedent from our laboratory.[13] Due to the lack of reactivity with propargyl alcohol **37** as compared to 3-butyn-1-ol, we believe the bulkiness of the butenolide greatly limits the nucleophilicity of **37**, allowing homodimerization to outcompete the desired transformation. As a result, we started to investigate smaller nucleophiles bearing functionality which we could use to introduce the butenolide after the PRCC.

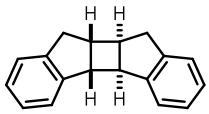

**Figure 3.15** [2+2] Homodimer of Indene

We first envisioned employing an α-silylallyl alcohol as the nucleophile since the silyl group could subsequently be oxidized with Fleming-Tamao conditions to give the corresponding lactol.[74,75] This intermediate could then be used to introduce the butenolide (Scheme 3.34) according to the procedure reported by Li in his work on rubriflordilactone B.[48]

**Scheme 3.34** Proposed Route with α-Silylallyl Alcohols

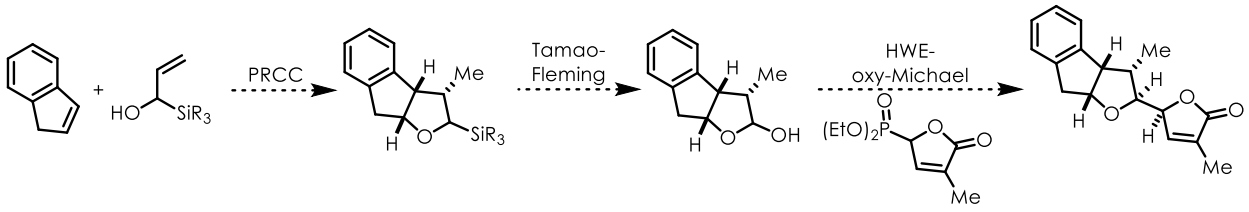


When we attempted this reaction, we were surprised to discover that the conjugate addition adduct between acrolein and the conjugate base of phenyl malononitrile somehow formed in the reaction (Scheme 3.35).

**Scheme 3.35** Results from PRCC with α-Silylallyl Alcohols

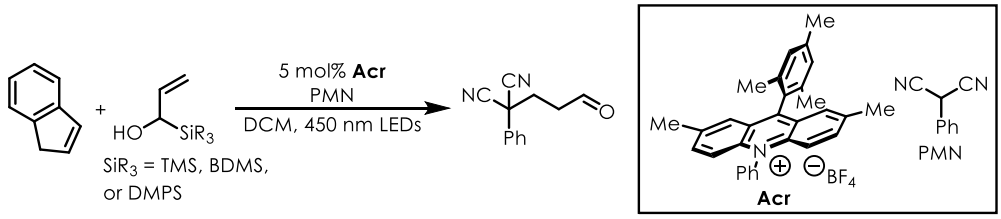


In order to elucidate how this occurred, we obtained CVs of the three alcohols used and discovered they all exhibited surprisingly low $E_{p/2}$ values (Figure 3.16). Based on this data, we believe the α-silylalcohols are competitively oxidized over indene and the resultant radical cation is converted to acrolein by silyl group and hydrogen atom loss. As a result, we opted to once again alter our approach.

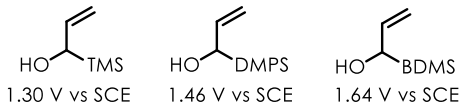


**Figure 3.16** $E_{p/2}$ Values Obtained for α-Silylalcohols

We next proposed that a diol **39** could be used as the nucleophile in the PRCC. The resultant *exo*-cyclic allylic alcohol could be converted to the butenolide via esterification followed by an RCM (Scheme 3.36), an approach that has been used in the synthesis of other natural products.[76,77]

**Scheme 3.36** Proposed Route with Diol Nucleophile

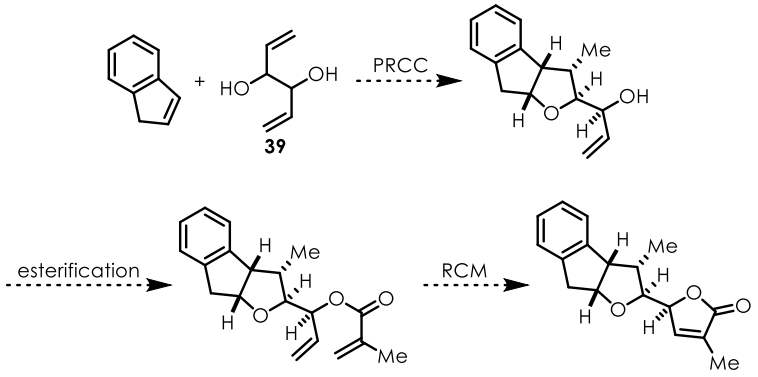


Unfortunately, we once again observed formation of the conjugate addition adduct between acrolein and phenyl malononitrile (Scheme 3.37); in this case, we suspect the acrolein is formed via a retro-pinacol reaction, which may occur before or after nucleophilic attack on the indene radical cation.

**Scheme 3.37** Results from PRCC with Diol Nucleophile

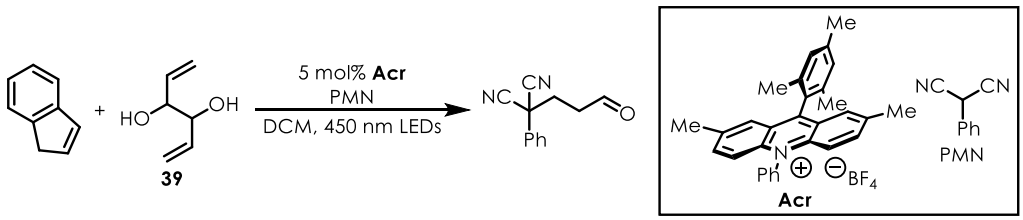

In an effort to avoid this, we mono-protected the diol with either a TBS- or acetyl group, but in these instances the PRCC reaction was completely inhibited. Therefore, we decided 1,5-hexadiene-3-ol could be a suitable replacement as an allylic oxidation after the PRCC could be used to access the same precursor to the butenolide. We were pleased to find that the PRCC reaction gave product in a modest yield and poor diastereoselectivity (Scheme 3.38).

**Scheme 3.38** Results from PRCC with 1,5-Hexadiene-3-ol

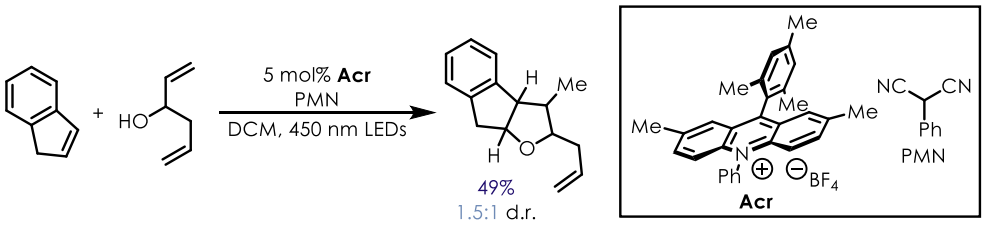


Due to the poor diastereoselectivity, we attempted the PRCC with propargyl alcohol **40**, but found that tetracycle **41** was the only product, likely forming via a second 5-*exo*-trig cyclization (Scheme 3.39). Based on the lack of success with the PRCC using indene, we decided it was time to revise our strategy.

**Scheme 3.39** Results from PRCC with Propargyl Alcohol

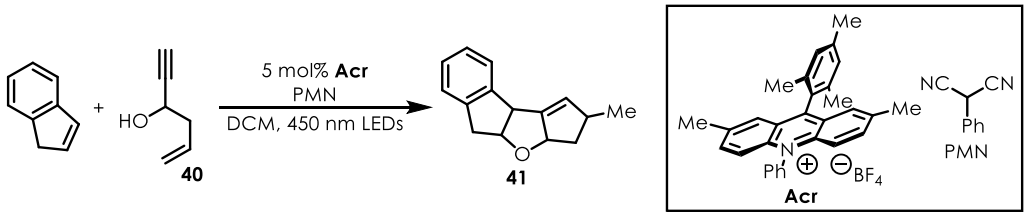


### 3.4.3 Substituted Indene Synthesis

Hunter Ripberger's contribution to this project focused on the synthesis of indene **17**. We initially envisioned using the alkene portion of this species in the PRCC step and the alkyne moiety as a nucleophile in the conjugate addition (Scheme 3.40A). By the time Hunter graduated, we had demonstrated the application of an RCM to synthesize the left portion of

rubriflordilactone B. As a result, we opted to investigate the synthesis of indene **42**, which would allow us to make the left side of the target in a similar manner (Scheme 3.40B). However, the presence of the vinyl group in **42** would prevent it from being a suitable electrophile in the PRCC step due to competitive oxidation. As a result, we devised a slightly different retrosynthesis for **6** that involved the PRCC and butenolide synthesis as the final two steps (Scheme 3.39C).

**Scheme 3.40** Altering the Retrosynthesis

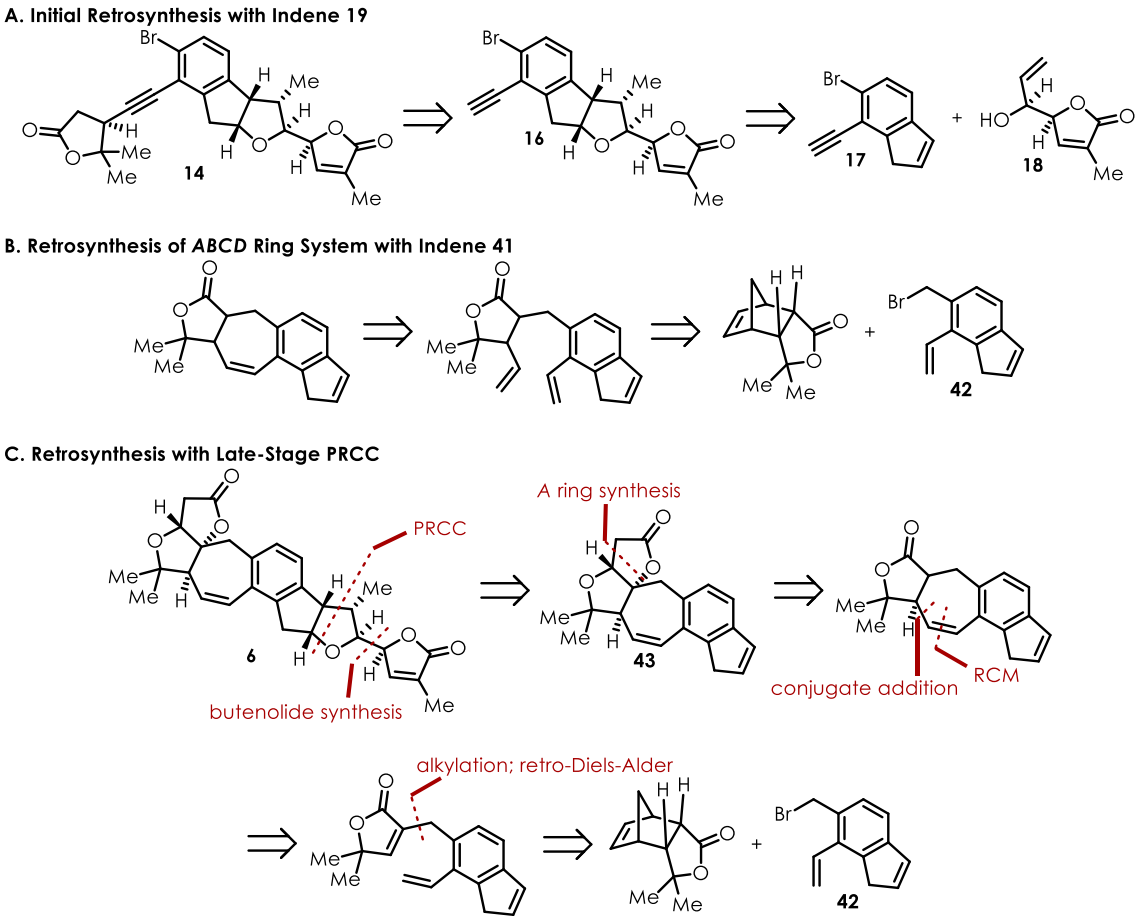


One important thing to note about this plan is that intermediate **43** would likely not present the same issues as **42** in terms of competitive oxidation. This is because the favored conformation of ring *C* in rubriflordilactone B is such that the alkene present is not in

conjugation with the arene, meaning that it cannot be oxidized by the acridinium ion photocatalyst.

In order to synthesize **42**, we began with a Friedel-Crafts acylation with 2-chromanone to give 4-hydroxyindanone, which was been reported previously in the literature.[78,79] We anticipated that the phenol moiety could be used as a directing group in an *ortho*-formylation method reported by Skattebøl[80], but no reaction was observed, likely due to the presence of the electron-withdrawing ketone *para* to the position of interest (Scheme 3.41A). We subsequently made both the indanol and indene analogs via reduction and dehydration reactions, but found that both of these species were also unreactive under the reported conditions (Scheme 3.41B).

**Scheme 3.41** Attempt at an *ortho*-Directed Formylation

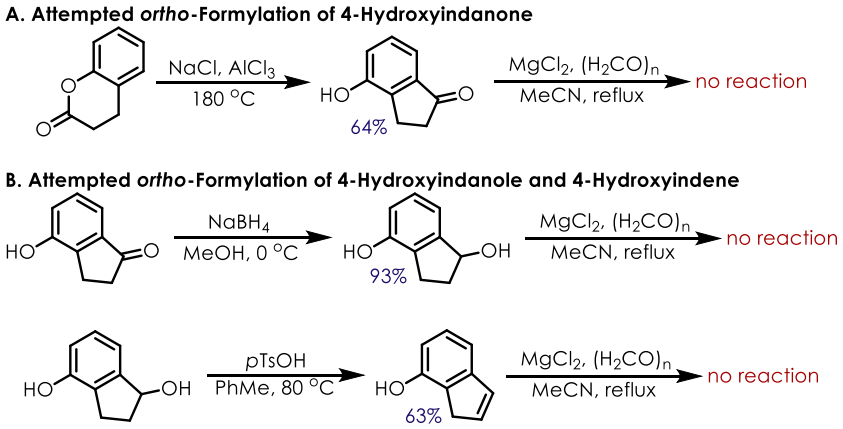


From here, we synthesized indene **44**, again starting from 2-chromanone, in a sequence that required fairly little optimization (Scheme 3.42). The only step necessitating some work was the bromination, which required a very slow addition of NBS and running the reaction in the dark to limit overbromination of the arene.[81]

**Scheme 3.42** Synthesis of Disubstituted Indene

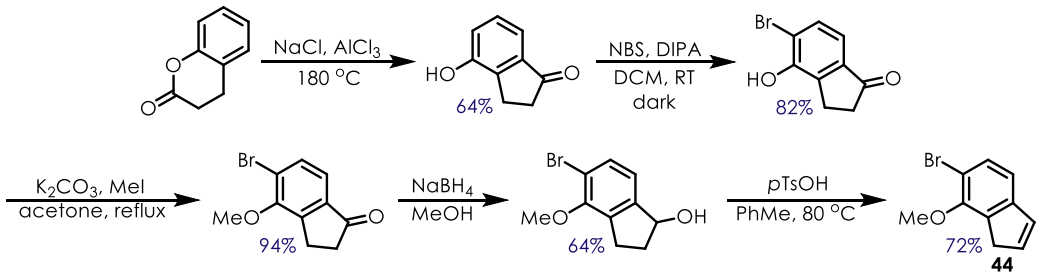


We hypothesized that the bromide and the methoxy group in **44** would allow for orthogonal reactivity to introduce the required formyl and vinyl groups. Initial attempts at a traditional lithiation-formylation sequence resulted in no reaction (Scheme 3.43). Due to the formation of an aromatic ion upon deprotonation, the benzylic position in indene is relatively acidic with a p$K_a$ of 20.1 in DMSO.[82] While the lithiation of aryl bromides is often facile, even in the presence of relatively acidic groups, we suspect that competitive deprotonation of the benzylic carbon may have been an issue due to the aromaticity that results from this process.

**Scheme 3.43** Attempted Lithiation-Formylation

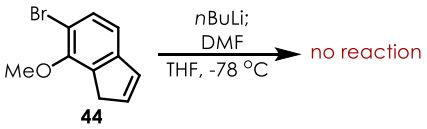


Another way the aryl bromide and aryl ether groups can be differentiated is through cross-coupling. While aryl ethers are inert under traditional palladium-catalyzed reactions, they are competent electrophiles in nickel-catalyzed processes.[83–85] Therefore, we envisioned a palladium-mediated formylation with the aryl bromide could be performed first followed by a nickel-mediated cross-coupling to introduce the vinyl group (Scheme 3.44).

**Scheme 3.44** Orthogonal Reactivity of Aryl Bromides and Aryl Ethers

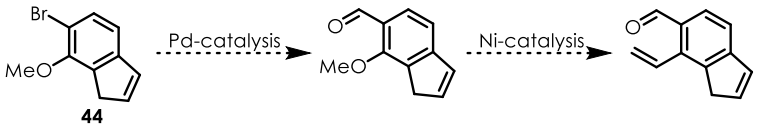

Unfortunately, the attempts we made at a palladium-catalyzed carbonylation based on reports by Beller[86] and Zhu and Ji[87] were unsuccessful (Scheme 3.45).

**Scheme 3.45** Attempts at a Palladium-Catalyzed Formylation

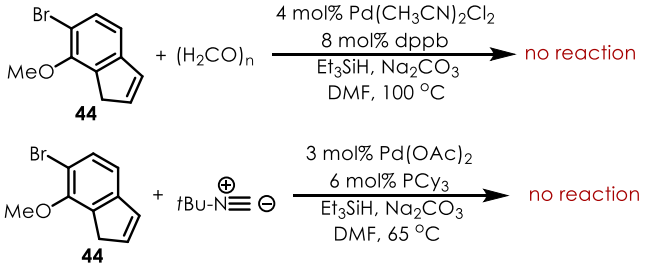


Due to the difficulty we were facing with synthesizing a substituted indene, along with the previously-discussed challenges with the PRCC reaction, we began to rethink our approach. Furthermore, some work by Xie revealed that a PRCC with advanced intermediate **43** was problematic, as their attempts to do so resulted in decomposition of this species (Scheme 3.46).[88]

**Scheme 3.46** PRCC Attempted by Xie

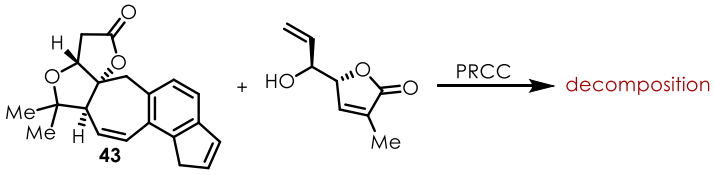


## 3.5 Investigating a Decarboxylative Diels-Alder Reaction

Due to the challenges we faced with both the substituted indene synthesis and the PRCC with indene, we wondered if Ang Li's approach to rubriflordilactone B could serve as an ideal starting point to rethink our approach. In his report, Li constructs ring *D* via an oxidative [2+2+2] electrocyclization, which also serves to link the two halves of the molecule together (Scheme 3.47).[48]

**Scheme 3.47** Electrocyclization Employed by Ang Li

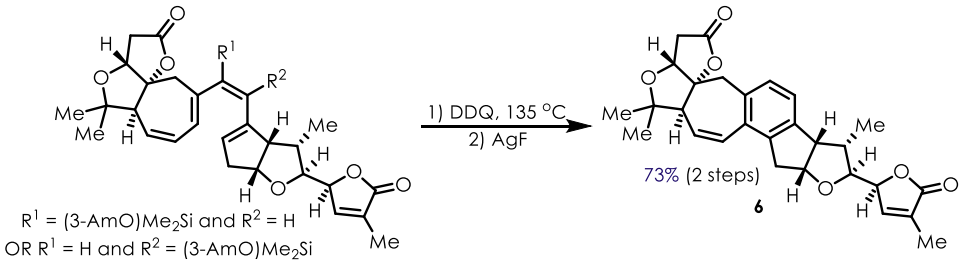


Based on this, we proposed another retrosynthesis of **6** which constructed the *D* ring via a decarboxylative Diels-Alder (Scheme 3.48).[89,90] Pyrone **45** would be made in a manner analogous to that described previously by constructing ring *C* via an RCM from intermediate **47**. Cyclopentene **46** could in turn be made from a PRCC employing cyclopentadiene as the electrophile.

**Scheme 3.48** Retrosynthesis with Decarboxylative Diels-Alder

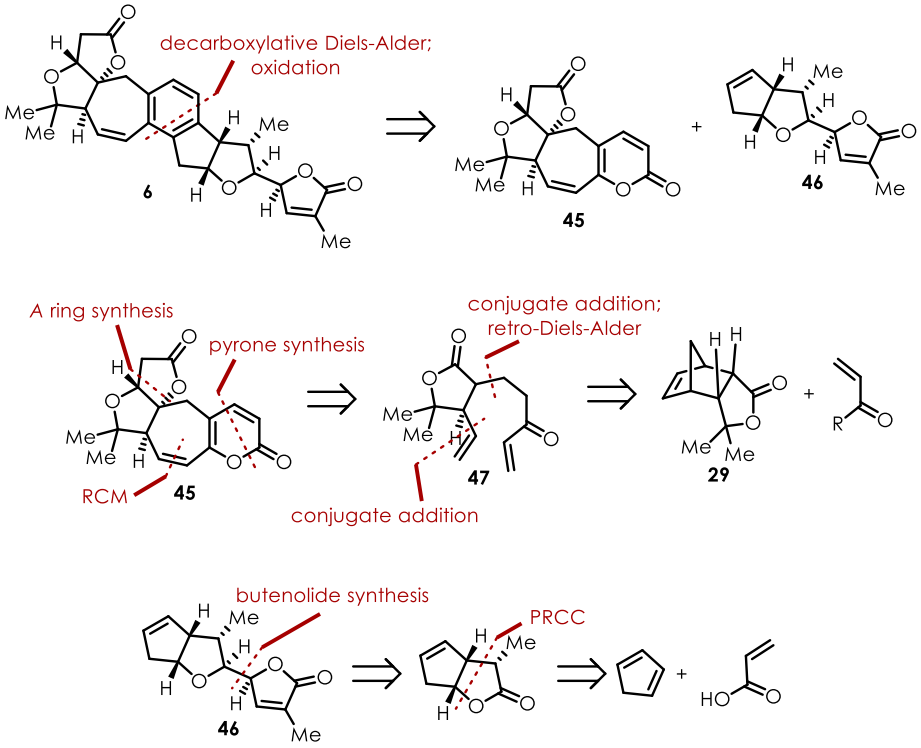

### 3.5.1 Pyrone Synthesis

Starting again from tricyclic lactone **29**, we performed a conjugate addition reaction with cinnamic acid-derived dieneone **48**, thinking that the styrene moiety could be used as one of the alkene partners in the RCM. After ketal protection, retro-Diels-Alder, and conjugate addition, diene **49** was obtained (Scheme 3.49). However, traditional RCM conditions gave no reactivity, it is possible that moving to more active Schrock-type catalysts may facilitate this transformation,[91] but we decided to alter our approach to avoid use of a protecting group.

**Scheme 3.49** Synthesis of Enone for RCM

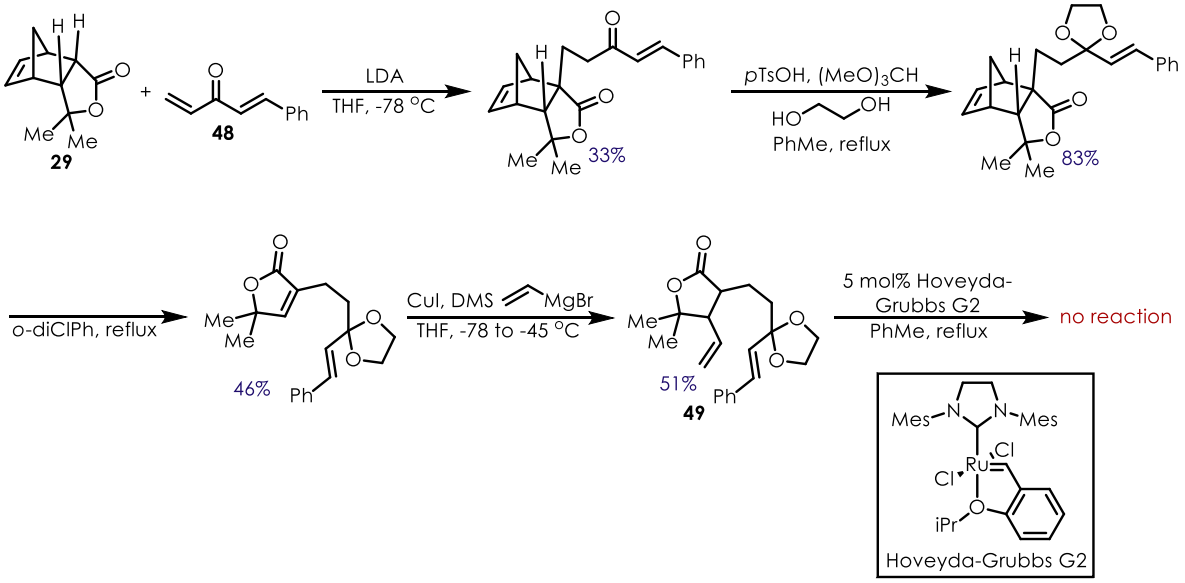


We turned our attention to the Weinreb amide derived from acrylic acid, which we hoped could be used in the conjugate addition step with **29** and subsequently converted to an enone in the same step as the conjugate addition with vinyl cuprate (Scheme 3.50A). Unfortunately, conjugate addition with this amide only produced adduct **50**, which likely forms via deprotonation of the Weinreb amide in situ to generate formaldehyde (Scheme 3.50B).

**Scheme 3.50** Conjugate Addition with Acrylic Acid Weinreb Amide

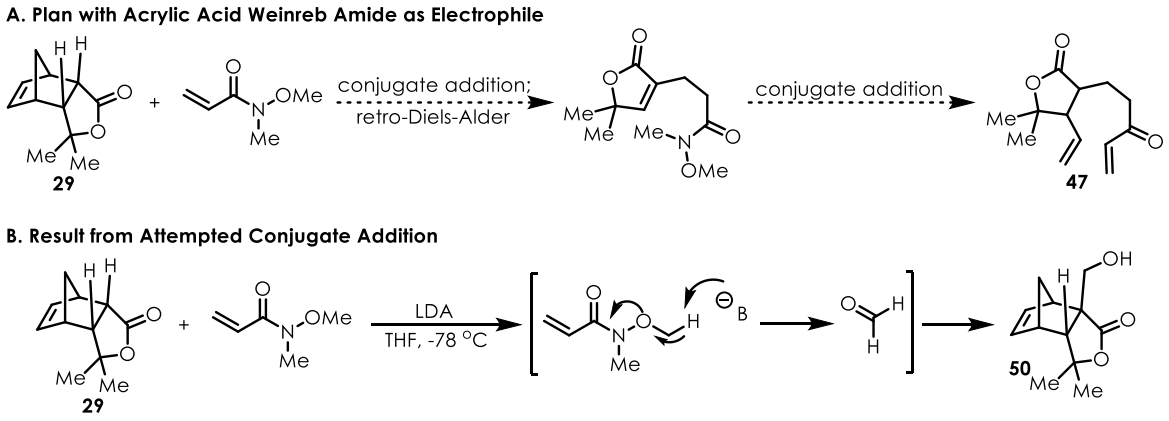


Fortunately, using the β-bromo analog of the Weinreb amide gave the desired adduct, albeit in lower yield; while this reaction was slightly improved via an in situ Finklestein reaction, competitive elimination to the acrylamide was always observed. Following this reaction up with the retro-Diels-Alder, and conjugate addition steps gave **47**, which when used in the RCM reaction provided the cycloheptenone **51** in modest yield (Scheme 3.51).

**Scheme 3.51** Synthesis of Cycloheptenone

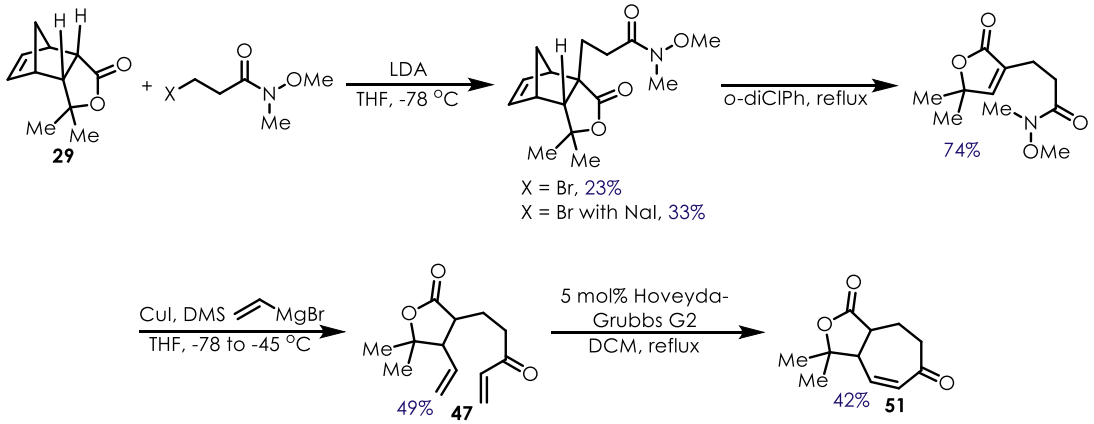


With the successful synthesis of **51**, we were fairly confident we could construct the desired pyrone in a manner analogous to that reported by Sieburth via formation of the silyl enol ether.[92] While there were concerns with competitive reactivity at the lactone, previous work on the enolate oxidation step revealed the α-position of the lactone is deprotonated very slowly

below 0 °C, leading us to believe deprotonation of the α-position to the enone could outcompete this process. However, we wanted to first assess the decarboxylative Diels-Alder reaction with a model system and opted to make pyrone **52** following the route disclosed by Sieburth (Scheme 3.52).

**Scheme 3.52** Synthesis of Pyrone for Decarboxylative Diels-Alder Model System

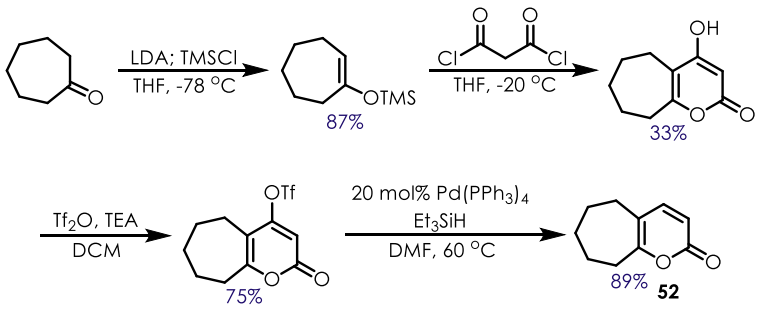


### 3.5.2 Cyclopentene Synthesis

To synthesize cyclopentene **46**, we began by screening PRCC conditions using 1,3-cyclohexadiene. Our rational for this stems from cyclopentadiene's tendency to homodimerize, and we hoped using 1,3-cyclohexadiene would help simplify the initial round of optimization. Furthermore, we used our PRCC method for the synthesis of γ-butyrolactones as a starting point,[20] proposing that the greater nucleophilicity of carboxylic acids compared to alcohols may allow the desired reaction to compete with homodimerization.

Unfortunately, our initial attempt at this reaction resulted in no product formation; however, a simple change of solvent from DCM to $MeNO_2$[17] gave product in trace yield[xv] (Table 3.9). From here we conducted typical rounds of optimization looking at catalyst loading, hydrogen atom donor loading, and base loading, all giving marginal improvements to the yield (Table 3.10).

[xv] Yields reported for optimization are $^1$H NMR yields using HMDSO as an internal standard, unless otherwise indicated

**Table 3.9** Optimization of the PRCC with 1,3-Cyclohexadiene – Solvent

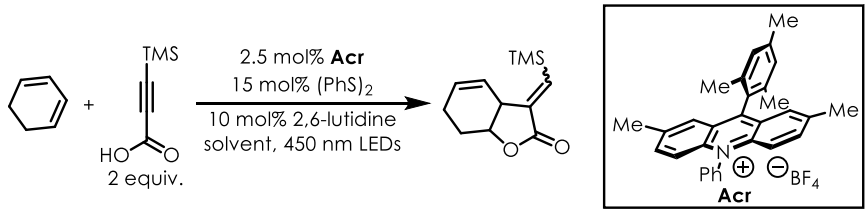


| Trial | Solvent | Concentration (M) | % Yield |
|---|---|---|---|
| **1** | DCM | 0.10 | 0% |
| **2** | $MeNO_2$ | 0.10 | <10% |
| **3** | $MeNO_2$ | 0.20 | <10% |
| **4** | $MeNO_2$ | 0.40 | <10% |
| **5** | $MeNO_2$ | 0.05 | 16% |

**Table 3.10** Optimization of the PRCC with 1,3-Cyclohexadiene – Loading

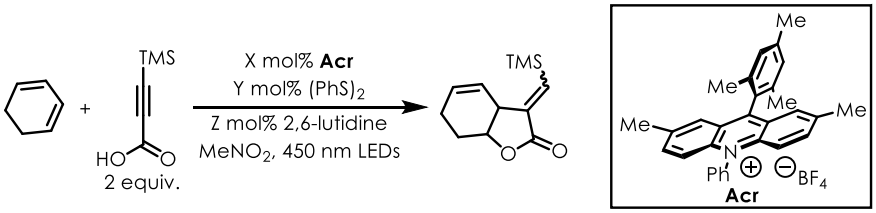


| Trial | X mol% catalyst | Y mol% $(PhS)_2$ | Z mol% 2,6-lutidine | % Yield |
|---|---|---|---|---|
| **1** | 2.5 | 15 | 10 | 15% |
| **2** | 5.0 | 15 | 10 | 11% |
| **3** | 7.5 | 15 | 10 | 12% |
| **4** | 10.0 | 15 | 10 | 11% |
| **5** | 2.5 | 10 | 10 | 14% |
| **6** | 2.5 | 15 | 10 | <10% |
| **7** | 2.5 | 20 | 10 | <10% |
| **8** | 2.5 | 30 | 10 | <10% |
| **9** | 2.5 | 10 | 10 | 11% |
| **10** | 2.5 | 10 | 20 | 13% |
| **11** | 2.5 | 10 | 50 | <10% |
| **12** | 2.5 | 10 | 100 | 20% |
| **13** | 2.5 | 10 | 200 | 13% |
| **14** | 2.5 | 10 | 300 | 23% |
| **15** | 2.5 | 10 | 400 | 21% |

In an effort to improve the reaction, we attempted slow addition of 1,3-cyclohexadiene. This would not only maintain a high nucleophile:electrophile ratio, but also limit photodimerization of the alkene.[93] We were pleased to find that this doubled the reaction yield, leaving us confident enough to start running the desired reaction with cyclopentadiene (Table 3.11).

**Table 3.11** Optimization of the PRCC with 1,3-Cyclohexadiene – Slow Addition

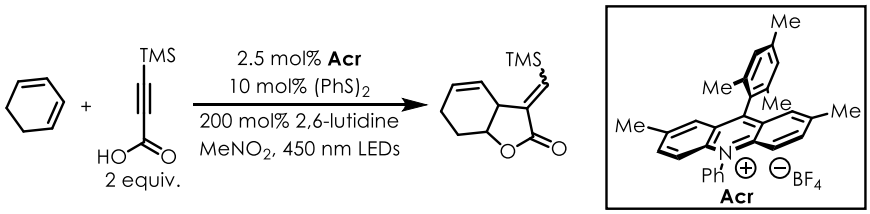


| Trial | Portions of 1,3-cylcohexadiene | % Yield |
|---|---|---|
| **1** | 1 | 24% |
| **2** | 2 | 33% |
| **3** | 4 | 45% |
| **4** | 8 | 43% |
| **5** | 8 | 47% (isolated) |

While switching out 1,3-cyclohexadiene for cyclopentadiene gave a large decrease in yield, we found that switching from 3-trimethylsilylpropiolic acid to 3-*tert*-butyldimethylsilylpropiolic acid restored the yields typically observed when employing 1,3-cyclohexadiene as the electrophile (Table 3.12). The larger TBS group likely mitigates a competitive Diels-Alder reaction between cyclopentadiene and the alkyne present in the propiolic acid. Furthermore, we found that increasing the nucleophile loading to five equivalents also improved the reaction.

**Table 3.12** Optimization of the PRCC with Cyclpentadiene

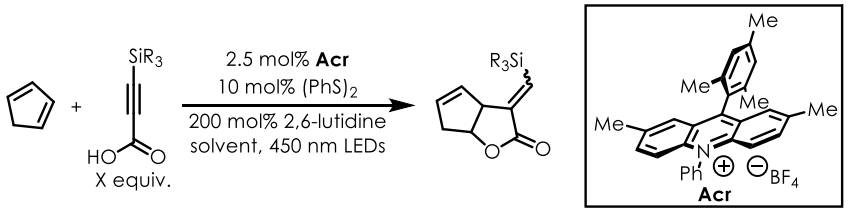


| Trial | $SiR_3$ Identity | X equiv. | % Yield; *E*:*Z* ratio |
|---|---|---|---|
| **1** | TMS | 2 | 18%; 4.0:1 |
| **2** | TBS | 2 | 40%; 1.7:1 |
| **3** | TBS | 3 | 44%; 2.7:1 |
| **4** | TBS | 4 | 48%; 5.9:1 |
| **5** | TBS | 5 | 62%; 5.9:1 |
| **6** | TBS | 5 | 63% (isolated); 4.8:1 |

### 3.5.3 Attempts at a Decarboxylative Diels-Alder

At this point, we attempted a decarboxylative Diels-Alder using pyrone **52** and cyclopentene **53** with conventional heating, but observed no formation of product. Furthermore, adding a Lewis acid to help activate the pyrone proved ineffective (Table 3.13).

**Table 3.13** Attempt at Decarboxylative Diels-Alder with Conventional Heating

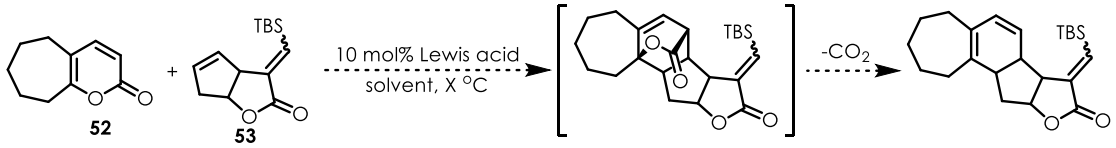


| Trial | Solvent | Temperature (°C) | Lewis Acid |
|---|---|---|---|
| **1** | xylenes | 140 | none |
| **2** | *o*-dichlorobenzene | 80 | $ZnCl_2$ |
| **3** | *o*-dichlorobenzene | 100 | $ZnCl_2$ |
| **4** | *o*-dichlorobenzene | 150 | $ZnCl_2$ |
| **5** | toluene | 120 | $Sc(OTf)_3$ |

Based on some literature precedent, we then attempted to use a microwave reactor,[94] but once again found no success with or without Lewis acid (Table 3.14).

**Table 3.14** Attempted at Decarboxylative Diels-Alder with Microwave Heating

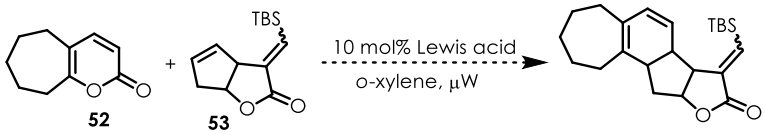


| Trial | Temperature (°C) | Power (W) | Lewis acid |
|---|---|---|---|
| **1** | 150 | 150 | none |
| **2** | 200 | 200 | none |
| **3** | 250 | 250 | none |
| **4** | 150 | 150 | $Sc(OTf)_3$ |
| **5** | 200 | 200 | $Sc(OTf)_3$ |
| **6** | 250 | 250 | $Sc(OTf)_3$ |

We questioned if the size of the TBS group on **53** could be impeding the reaction, we attempted to remove it via conjugate reduction[95] and desilylation (Scheme 3.53). While the reduction of the *exo*-cyclic double bond went well, no silyl group removal occurred, likely due to this requiring build-up of negative charge beta to the carbonyl. However, we did attempt the decarboxylative Diels-Alder after the conjugate reduction using the conditions discussed above, but once again observed no reaction.

**Scheme 3.53** Conjugate Reduction and Desilylation Attempt with PRCC Product

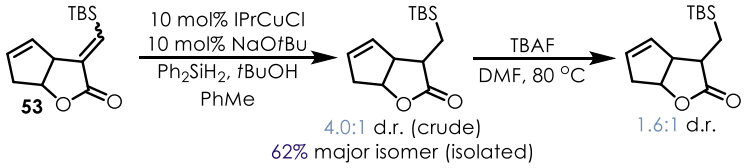


At this point, we suspected the Diels-Alder reaction was disfavored electronically. We found some evidence for this in some work by Posner where they reported a pyrone Diels-Alder using unactivated alkenes.[96] In order for their reaction to proceed, not only was a Lewis acid required, but the reaction needed to be run under high pressure.

To address the electronic effects, we synthesized electron-poor pyrone **54**. But once again, we observed no formation of product (Table 3.15); instead, we saw formation of pyrone **52**, likely via a zinc-assisted decarboxylation.

**Table 3.15** Attempt at Decarboxylative Diels-Alder with Electron-Poor Pyrone

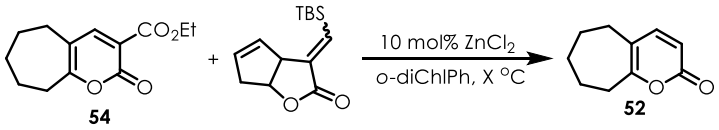


| Trial | Temperature (°C) |
|---|---|
| **1** | 80 |
| **2** | 115 |
| **3** | 150 |
| **4** | 180 |

Our last attempt at this reaction was based on our lab's work on a cation-radical Diels-Alder.[97] With the hydroxylated precursor to pyrone **52**, we attempted this reaction with a few different photocatalysts, but observed no reaction in any case (Scheme 3.54).

**Scheme 3.54** Cation-Radical Diels-Alder Attempts

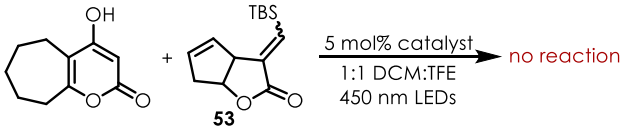


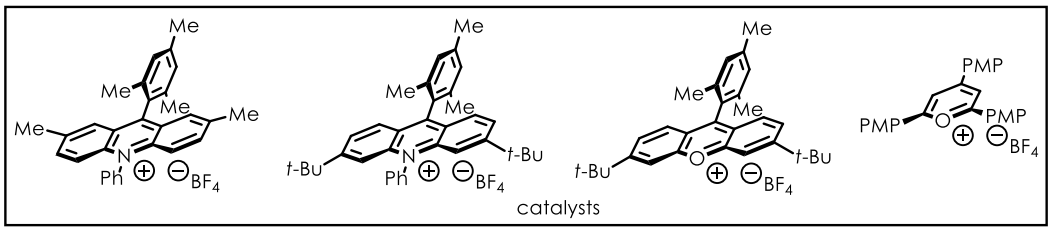


## 3.6 Conclusion

To date, we have developed a diastereoselective route to the left half of the natural product rubriflordilactone B, which hinges on an RCM and enolate oxidation sequence to set the relative stereochemistry. Furthermore, we have shown that our PRCC chemistry shows some

promise for applications to natural product synthesis. While it is limited by the steric hindrance of the nucleophile, even very reactive electrophiles such as cyclopentadiene can be utilized with minimal side-reactivity. Overall, we feel the work presented here will be a great help in determining future directions undertaken by the lab towards the synthesis of this and other natural products.

### 3.7 Associated Data

Appendix B: Experimental Details and Characterization Data of Key Intermediates

### 3.8 Acknowledgements

I would like to thank Nathan Gesmundo and Peter Morse for their contributions to the PRCC portion of this project and Hunter Ripberger for his work on the substituted indene synthesis. I would also like to thank Peter White and Chun-Hsing (Josh) Chen for collecting x-ray crystallography data and Marc ter Horst for help with higher temperature NMR experiments.

# CHAPTER 4: SYNTHETIC STUDIES TOWARD THE SYNTHESIS OF STEMOCURTISINE AND RELATED NATURAL PRODUCTS

## 4.1 Introduction

### 4.1.1 Stemonaceae Natural Products

Natural products isolated from the Stemonaceae genus of plants found throughout Asia were reported as early as the 1960s.[98] These molecules are collectively referred to as stemona alkaloids and are characterized by a pyrrolo[1,2-*a*]azepine nucleus (Figure 4.1).

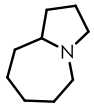


**Figure 4.1** The Pyrrolo[1,2-*a*]azepine Nucleus of Stemona Alkaloids

The Stemonaceae plants are valued in Chinese and Japanese medicine and have been used as anthelmintics for pets and anticough agents for human patients.[99] In addition, many of the isolated stemona alkaloids have exhibited antilarval effects, most notably towards mosquito larvae.[100] Due to their bioactivity and interesting molecular structures, organic chemists have sought to synthesize and study these species since their initial isolation.

To date, well over 40 stemona alkaloids have been isolated, and these are typically divided into 5 categories based on the substituents on the pyrrolo[1,2-*a*]azepine core. The corresponding parent compounds exhibit the simplest substituents associated with each subclass (Figure 4.2).

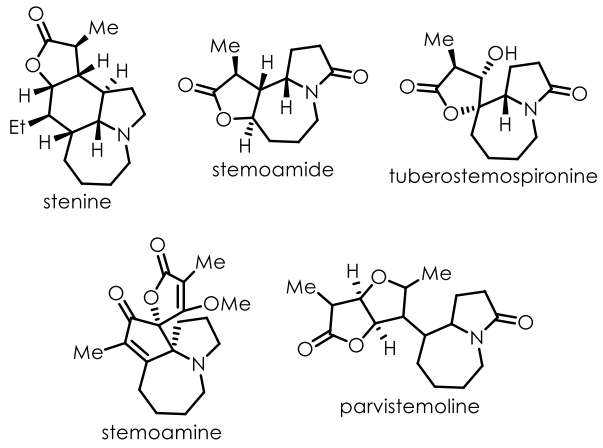


**Figure 4.2** Five Parent Compounds of Stemona Alkaloids Subclasses

While there are reports of stemona alkaloids that do not fit cleanly into the above subclasses, they are labeled as miscellaneous since there are not enough similar compounds to warrant a new class. However, work by Pyne in the early 2000s resulted in the isolation of stemona alkaloids having an unprecedented pyrido[1,2-*a*]azapine core (Figure 4.3), suggesting these species may comprise a brand new family of these natural products.[101,102]

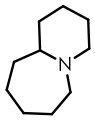

**Figure 4.3** Novel Pyrido[1,2-*a*]azapine Core

The first compound Pyne isolated from this new family was stemocuritisine (**1**), which contains a contiguous *ABC* ring system along with a butenolide off the *C* ring and an ether bridge connecting rings *C* and *A* (Figure 4.4).

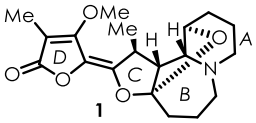

**Figure 4.4** Structure of Stemocurtisine

As the more traditional pyrrolo[1,2-*a*]azepine stemona alkaloids have been known for decades, many of them have reported syntheses that are discussed in reviews.[98,99] Due to the

interesting chemical architecture exhibited by stemocurtisine, and the lack of precedent for the synthesis of this subclass of stemona alkaloids, we began to investigate the possibility of approaching this molecule with organic photoredox catalysis.

### 4.1.2 Reported Efforts Toward Stemocurtisine

While no completed syntheses of stemocurtisine have been reported, the Pyne lab has disclosed some preliminary work.[103,104] Their first report in 2013 details a model system[97], which helped inspire their 2015 publication that details a diastereoselective synthesis of the *ABC* ring system in 19 steps.[98] To accomplish this, they first prepared lactam **2** from commercially available iodide **3**, using an epoxide-opening step to set the relative stereochemistry (Scheme 4.1).

**Scheme 4.1** Synthesis of Substituted Lactam

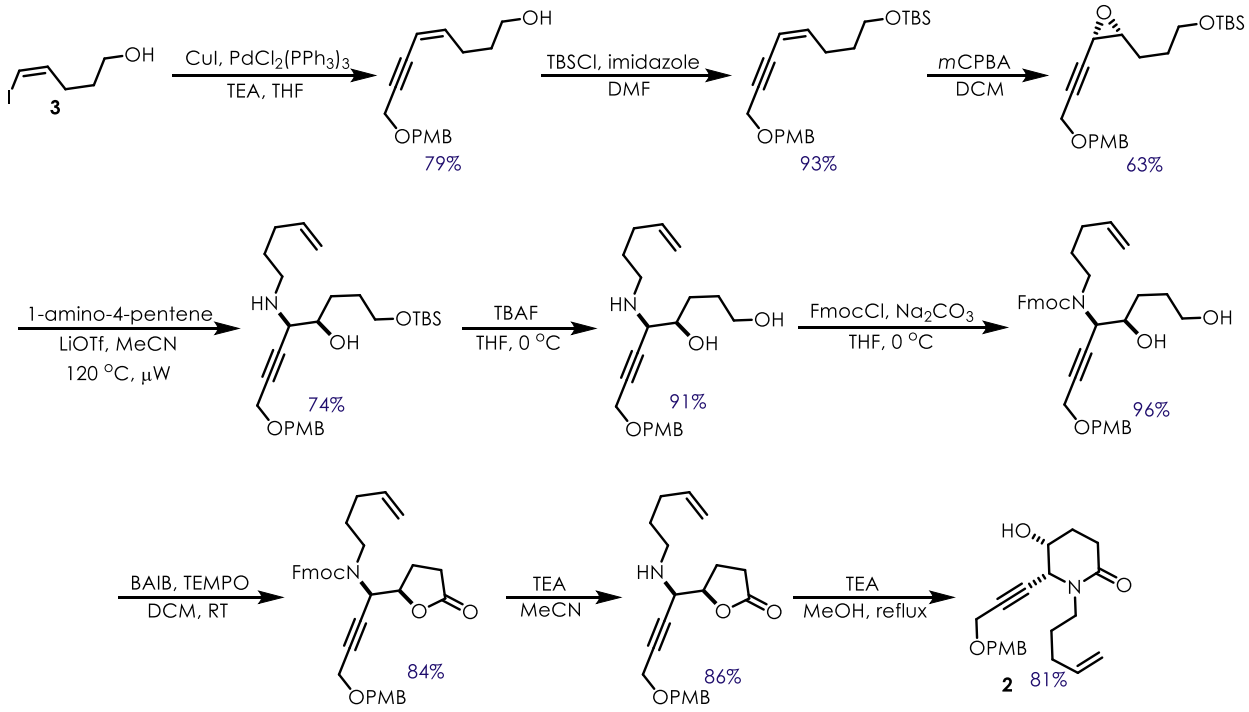


Lactam **2** was then carried on to construct the seven-membered ring present in stemocurtisine via an ene-yne RCM reaction to yield **4**.

**Scheme 4.2** Constructing the Seven-Membered Ring

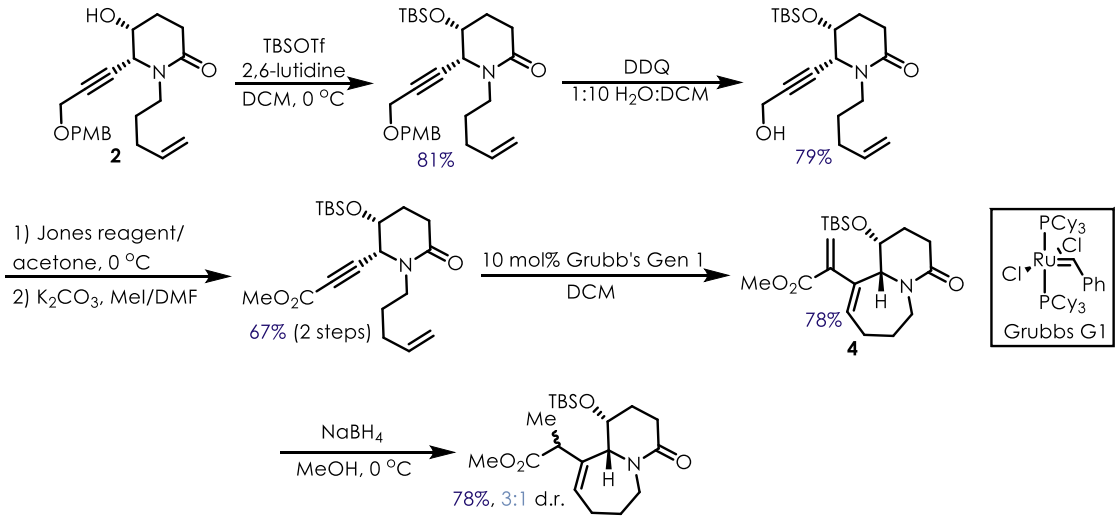


Finally, the butenolide was prepared by a bromolactonization sequence to give tricyclic intermediate **5** as a mixture of diastereomers; fortunately, the undesired diastereomer could be epimerized at the γ-position of the butenolide with DBU. Reduction of the butenolide and TBS-deprotection provided **6**, which Pyne planned to use in a photochemical oxidative cyclization.

**Scheme 4.3** Synthesizing the *C* Ring

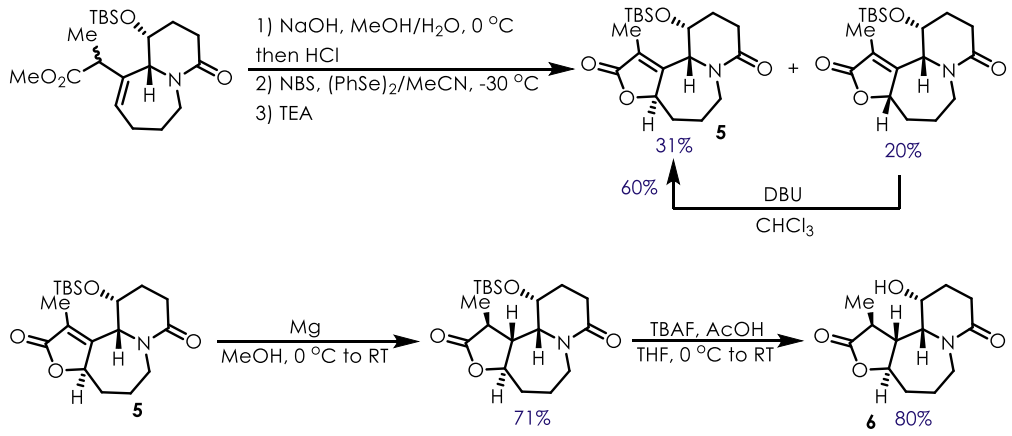


Unfortunately, their attempts at a photochemical cyclization with hypervalent iodine $PhI(OAC)_2$ resulted in opening of the *A* ring (Scheme 4.4A). Furthermore, reduction of the lactam to the cyclic amine did not facilitate this cyclization (Scheme 4.4B).

**Scheme 4.4** Attempts at a Photochemical Oxidative Cyclization

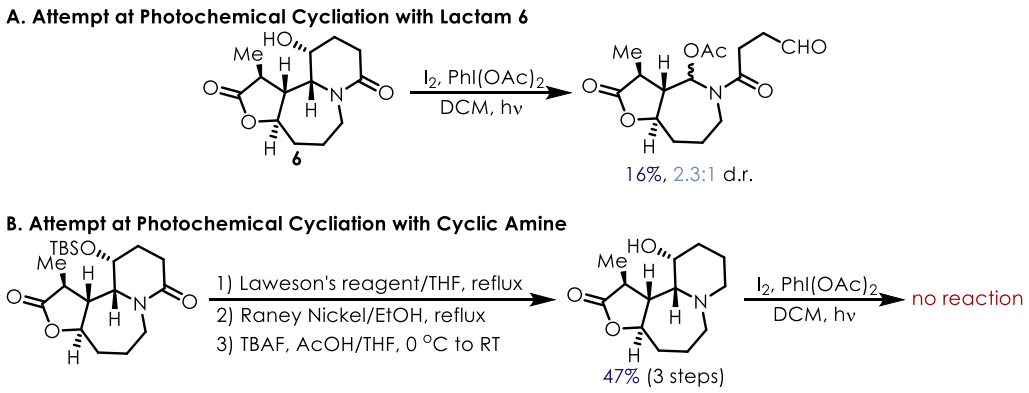


While Pyne was able to successfully synthesize a rather advanced intermediate to stemocurtisine with high diastereoselectivity, the formation of the ether bridge proved challenging. In addition, his sequence is quite lengthy, prompting us to consider if photoredox chemistry could be used to streamline the synthesis of this natural product.

## 4.2 Synthetic Approach to Stemocurtisine

Our initial approach to stemocurtisine hinged on unpublished work involving an acridinium ion and cobaloxime[105] dual catalytic system that we have used to dehydrogenate a number of simple organic molecules. Cobaloximes as dehydrogenation catalysts have been studied for quite some time, and more details on this chemistry can be found in several papers and reviews.[106,107]

The most relevant example of this chemistry to stemocurtisine is the dehydrogenation of protected piperidine **7** to the correspond enamine **8** (Scheme 4.5A)[xvi]. In addition, our lab has shown the Cbz-variant of **8** to be compatible with our anti-Markovnikov hydrofunctionalization chemistry, specifically in regards to the addition of carboxylic acids (Scheme 4.5B).[108]

[xvi] This experiment was performed by Dr. Alex White during his time as a postdoc in the lab

**Scheme 4.5** Precedent for Dehydrogenation and Hydrofunctionalization

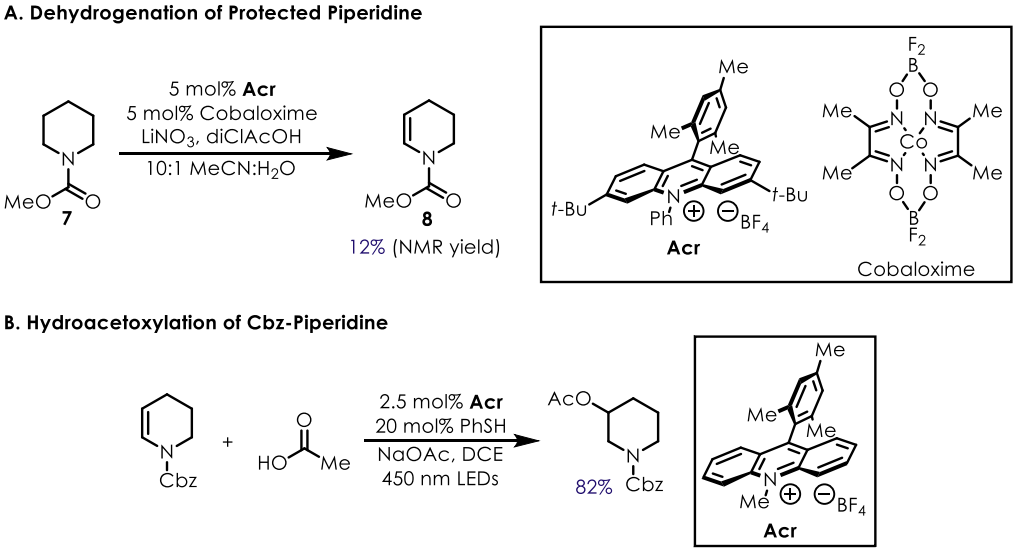


Based on this precedent, we began to consider the possibility of an organic photoredox cascade process involving dehydrogenation and anti-Markovnikov hydrofunctionalization to construct the *ABC* ring system of stemocurtisine from butenolide **9** (Scheme 4.6).

**Scheme 4.6** Proposed Organic Photoredox Cascade

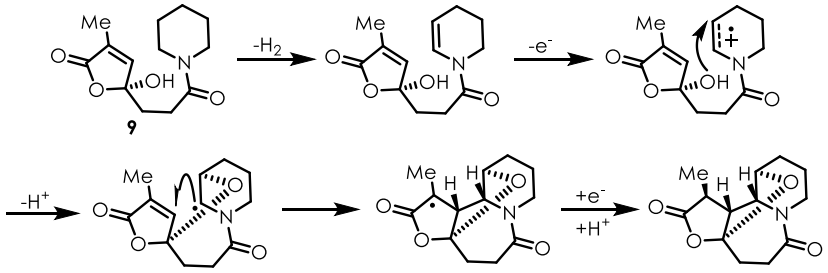


Following this process, we envisioned lactam reduction[109] and olefination of the *C* ring[110] would give **1** (Scheme 4.7).

**Scheme 4.7** Synthesis of Stemocurtisine from Cascade Product

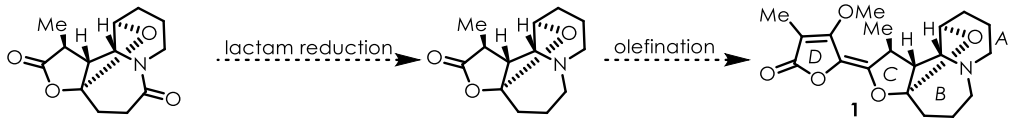

### 4.2.1 Attempting the Organic Photoredox Cascade

We first attempted to synthesize **9** via a vinylogous Mukaiyama Michael addition[111] with butenolide **10** and acrylamide **11**, but no product was observed (Scheme 4.8A). In addition, employing the lithium enolate of **10** (Scheme 4.8B) or replacing **11** with the analogous thioamide[112] (Scheme 4.8C) or methyl acrylate (Scheme 4.8D) did not yield product either.

**Scheme 4.8** Attempts at Synthesizing the Photoredox Cascade Precursor

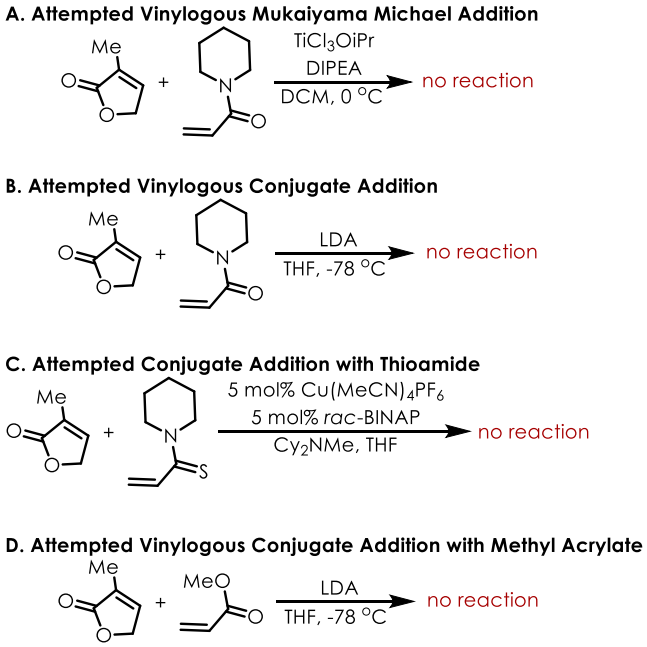


Fortunately, we found that alkylation of butenolide **10** with β-bromoamide **12** and subsequent γ-oxygenation with molecular $O_2$[113] gave **9** in modest yield (Scheme 4.9).

**Scheme 4.9** Synthesis of the Photoredox Cascade Precursor

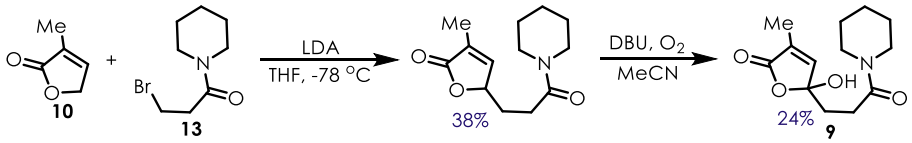


With **9** in hand, we attempted the best conditions developed in the lab for the dehydrogenation of **7** (Scheme 4.10). Interestingly, only spirocycle **13** was observed, which is likely the result of amide hydrolysis to the corresponding carboxylic acid followed by

intramolecular esterification. Based on this outcome, and the lack of optimization for the dehydrogenation conditions at the time this experiment was run, we decided to take a different approach to stemocurtisine.

**Scheme 4.10** Photoredox Cascade Results

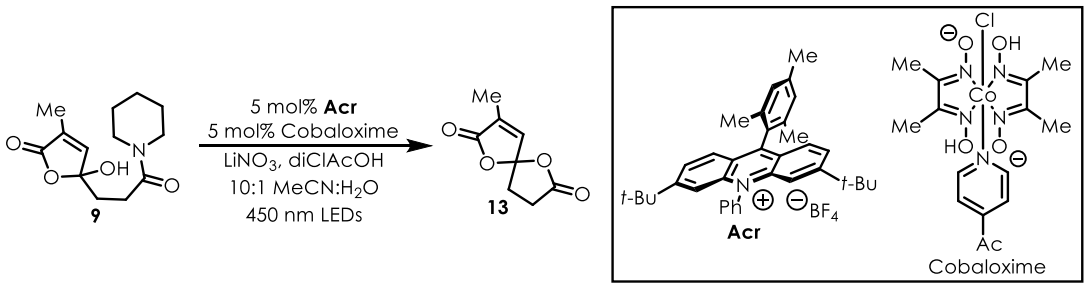


## 4.3 Synthetic Approach to seco-Stemocurtisine

After the isolation of stemocurtisine in 2003, Pyne continued to work identifying novel stemona alkaloids. One that is closely related to stemocurtisine, which will be referred to as seco-stemocurtisine (**14**), was reported by his lab in 2013 (Figure 4.5).

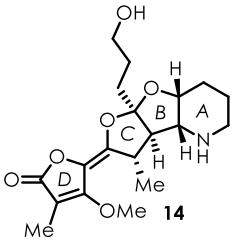


**Figure 4.5** Structure of 6-Hydroxy-5,6-seco-stemocurtisine

Not only is **14** an easier synthetic target due to the absence of the ether bridge, it could likely be converted to **1** via an oxidation, reductive-amination sequence (Scheme 4.11). Based on these two factors, we began to investigate a route to **14** utilizing the chemistry developed in our lab.

**Scheme 4.11** Proposed Synthesis of Stemocurtisine from seco-Stemocurtisine

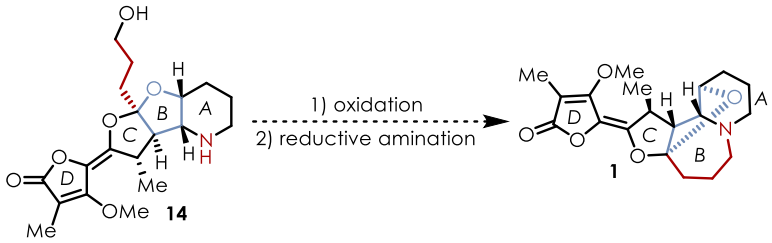


### 4.3.1 Attempt at a PRCC

Since the *B* ring in **14** is a substituted tetrahydrofuran, we proposed a PRCC reaction between γ-hydroxybutenolide **15** and protected enamine **16** could be used to access tricyclic intermediate **17**. This species would provide **14** after olefination of the lactone[110] and deprotection of the alcohol and enamine (Scheme 4.12)

**Scheme 4.12** Proposed Synthesis of seco-Stemocurtisine via a PRCC

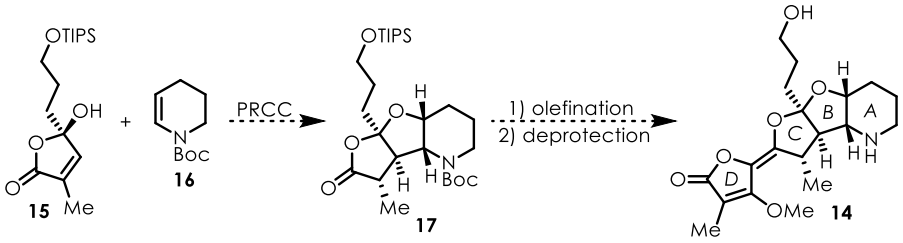


We began working on this by synthesizing **16** from δ-valerolactam in three steps (Scheme 4.13A). Next, we synthesized **15** from butenolide **10**, also in 3 steps (Scheme 4.13B).

**Scheme 4.13** Synthesis of Protected Enamine and γ-Hydroxybutenolide

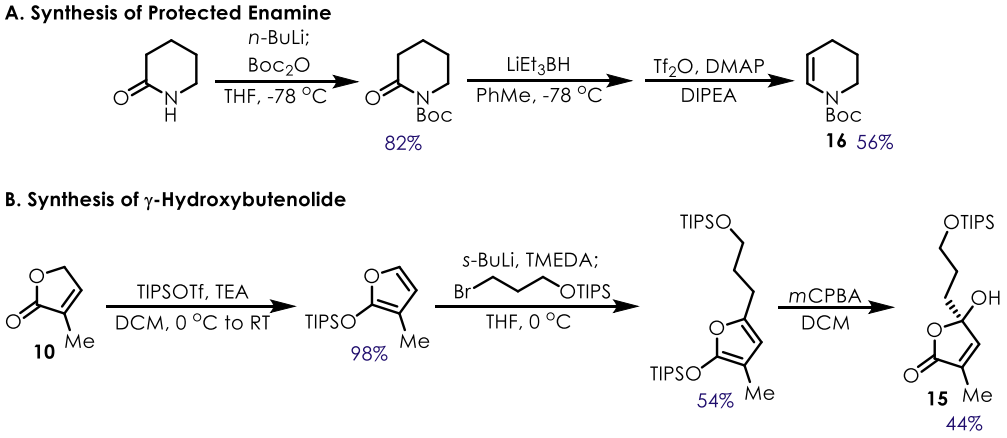


Attempts at the PRCC reaction between **15** and **16** did not yield promising results (Table 4.1). $^{1}$H NMR data collected of isolates from flash chromatography suggested either desilylation of the alcohol or conjugate addition of the thiophenol radical generated from diphenyl disulfide into the butenolide. While there are more conditions that can be explored for this reaction, such as using a bulkier hydrogen-atom donor to prevent conjugate addition or altering the alcohol protecting group, the steric environment surrounding the γ-hydroxy group on **15** is likely to limit its nucleophilicity.

**Table 4.1** Conditions Employed for PRCC Attempts

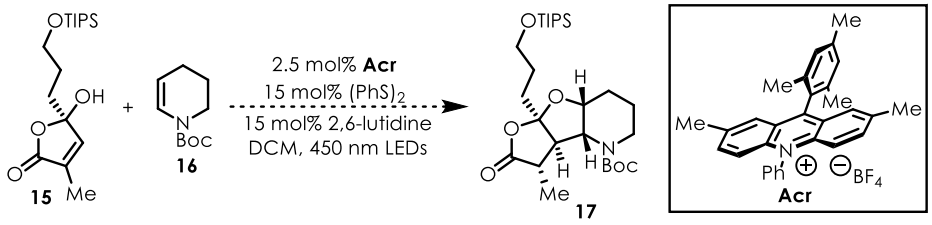


| Trial | Equiv. 15 | Equiv. 16 |
|---|---|---|
| **1** | 1.0 | 1.0 |
| **2** | 1.5 | 1.0 |
| **3** | 2.0 | 1.0 |
| **4** | 1.0 | 2.0 |

### 4.3.2 Application of α-Amino Alkylation

In addition to screening more PRCC conditions, we have undertaken another approach to access **14**, which is currently being investigated by Susanna Liang. This route is based on a more recent publication from the lab detailing the α-amino alkylation of protected amines.[14] We envision that butenolide **18** could be used to construct **17** via an intramolecular variant of this chemistry. Compound **18** could in turn be made from a silver-mediated alkoxylation of γ-bromobutenolide **19** using protected amino alcohol **20** as the nucleophile (Scheme 4.14). This type of alkylation is common in carbohydrate chemistry and has been used on both tertiary halides and with very bulky nucleophiles.[114,115]

**Scheme 4.14** Proposed Synthesis of *seco*-Stemocurtisine via Intramolecular α-Amino Alkylation

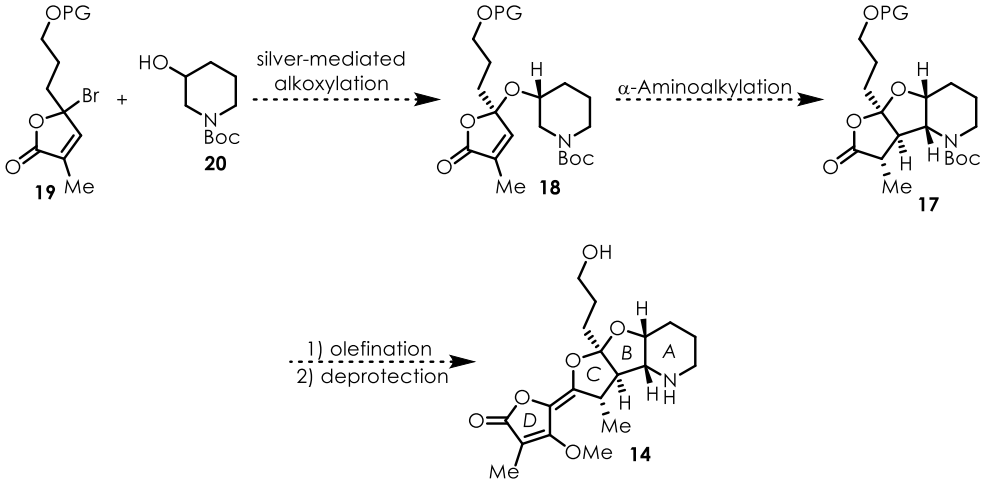


We are currently working on the synthesis of butenolide **21** as a model system for assessing the α-amino alkylation step by either an alkylation (Scheme 4.15A) or acetal formation[116,117] (Scheme 4.15B). We envision that we will see success with this approach to synthesize **14** in the near future.

**Scheme 4.15** Synthesis of α-Amino Alkylation Model System

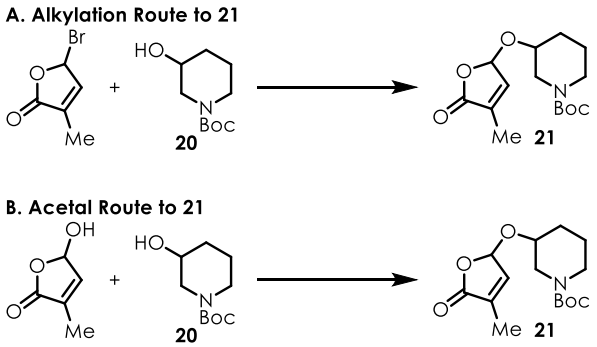


## 4.4 Conclusion

While our work on the synthesis of stemocurtisine and seco-stemocurtisine is still in its infancy, we envision that the α-amino alkylation approach will be successful in accessing these molecules.

## 4.5 Associated Data

Appendix C: Experimental Details and Characterization Data of Key Intermediates

## 4.6 Acknowledgements

I would like thank Susanna Liang for her help and contributions to this preliminary work on stemocurtisine and seco-stemocurtisine.

# APPENDIX A: EXPERIMENTAL DETAILS AND ELECTROCHEMICAL AND PHOTOCHEMICAL DATA

## A.1 Electrochemical Measurements

### A.1.1 General Information

Commercially available substrates were purchased from Sigma-Aldrich or Fisher Scientific and used without further purification. Acetonitrile was purified by passing through activated alumina under nitrogen prior to use. Cyclic amines, aldehydes, and ketones used to prepare substrates were distilled prior to use.

Imines, hydrazones, oximes, enamines, and carboxylate salts were prepared in accordance to literature procedures, and the spectral data obtained matched reported values.[8]

### A.1.2 Cyclic Voltammetry

Cyclic voltammograms were obtained with a Pine WaveNow Potentiostat. Samples were prepared with 0.05 mmol of substrate and 5 mL of 0.1 M tetra-*n*-butylammonium hexafluorophosphate in dry, degassed acetonitrile. Measurements employed a glassy carbon working electrode, platinum wire counter electrode, 3.5 M KCl silver-silver chloride reference electrode, and a scan rate of 100 mV/s. Reductions were measured by scanning potentials in the negative direction and oxidations in the positive direction; the glassy carbon electrode was polished between scans. Data was analyzed in MATLAB by subtracting a background current prior to identifying the maximum current and determining the potential at half this value ($E_{p/2}$). The obtained value was originally referenced to Ag|AgCl and converted to SCE by subtracting 0.03 V.

Representative CVs are compiled here to showcase the features present in each set of functional groups for which data was obtained.

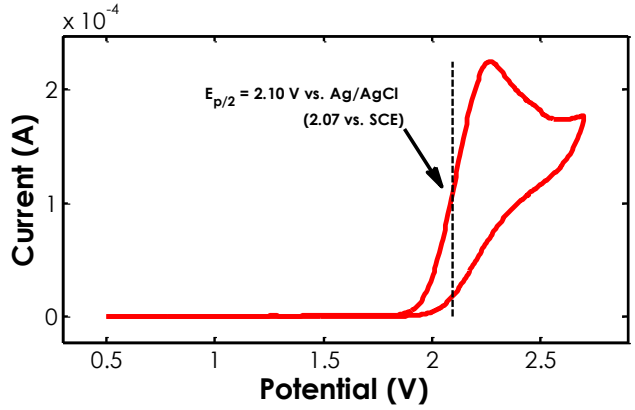


**Figure A.1** Cyclic Voltammogram of Mesitylene

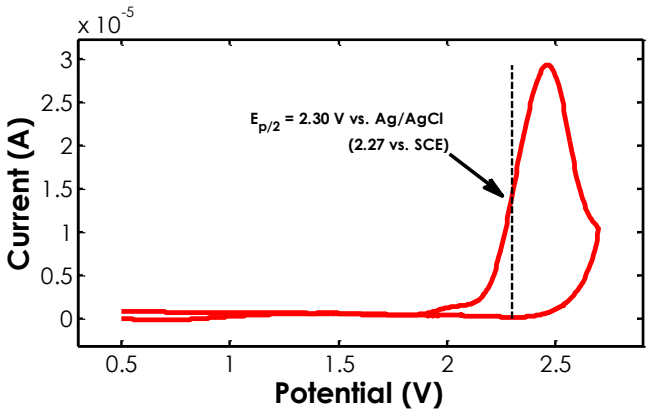


**Figure A.2** Cyclic Voltammogram of Phenylacetylene

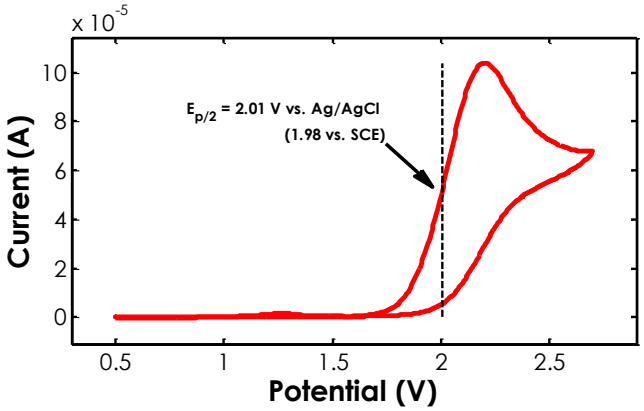


**Figure A.3** Cyclic Voltammogram of 2-Methyl-2-butene

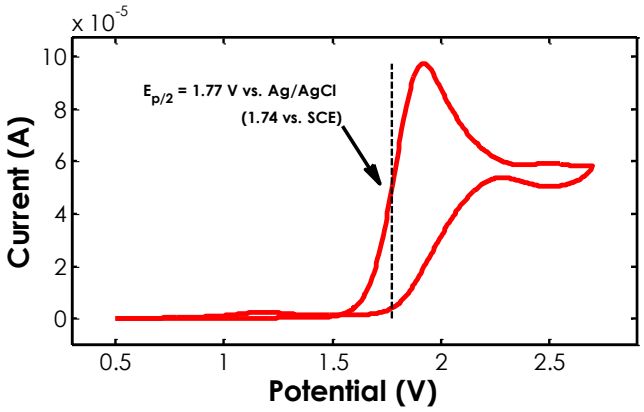


**Figure A.4** Cyclic Voltammogram of *trans*-β-methylstyrene

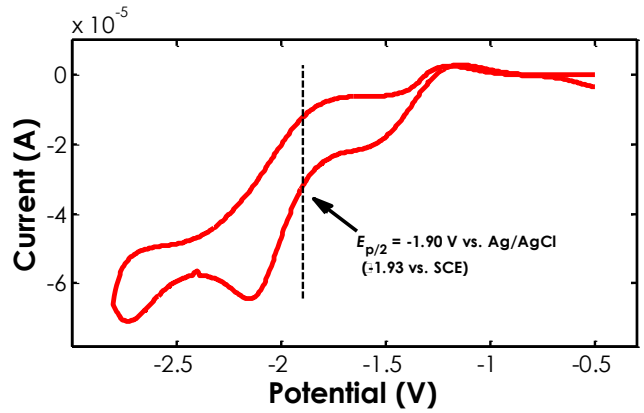


**Figure A.5** Cyclic Voltammogram of Carbon tetrachloride

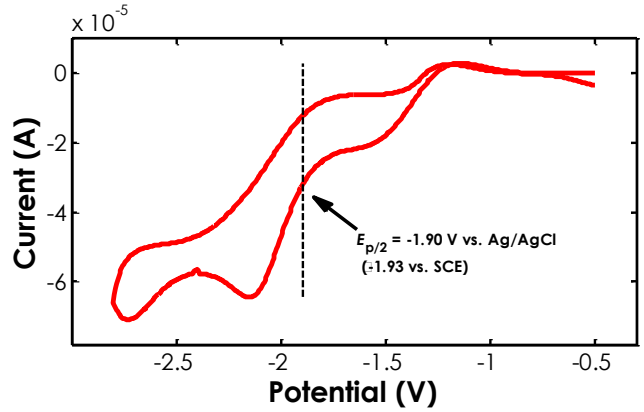


**Figure A.6** Cyclic Voltammogram of Ethyl bromoacetate

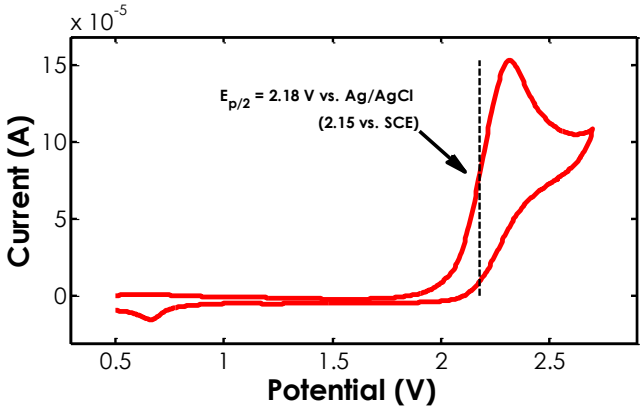


**Figure A.7** Cyclic Voltammogram of 1-Chloro-4-iodobenzene (oxidation)

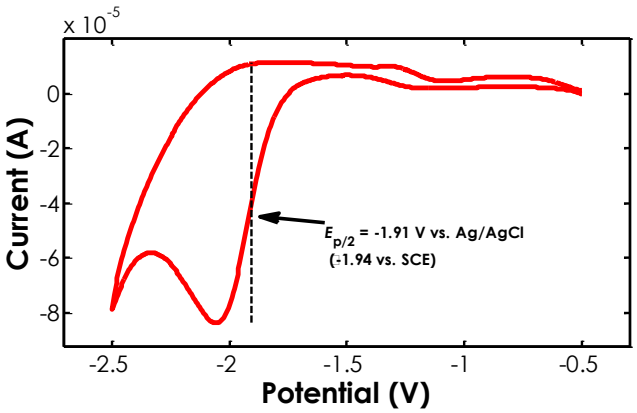


**Figure A.8** Cyclic Voltammogram of 1-Chloro-4-iodobenzene (reduction)

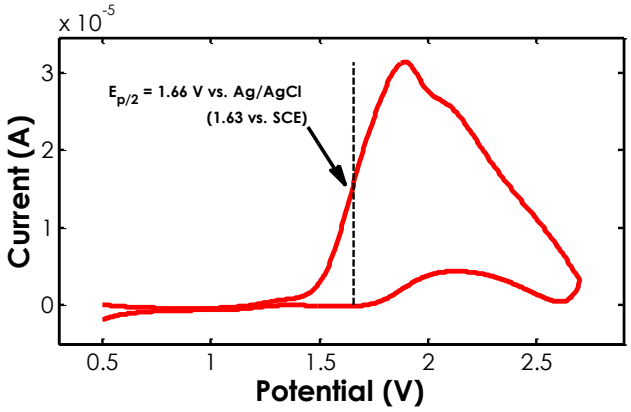


**Figure A.9** Cyclic Voltammogram of Phenol

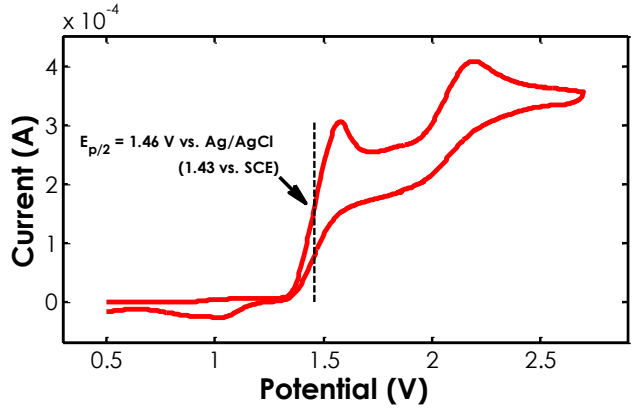


**Figure A.10** Cyclic Voltammogram of *o*-Dimethylbenzene

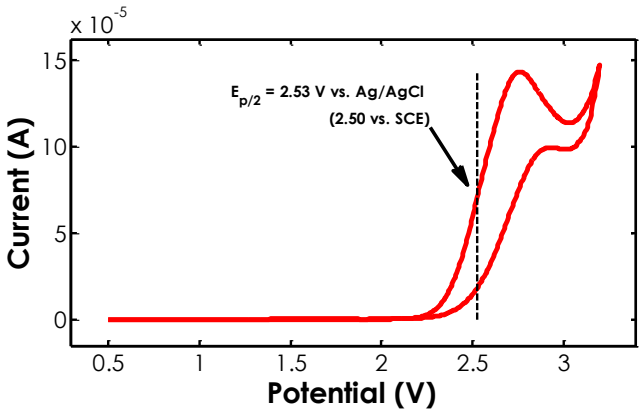


**Figure A.11** Cyclic Voltammogram of 1,4-Dioxane

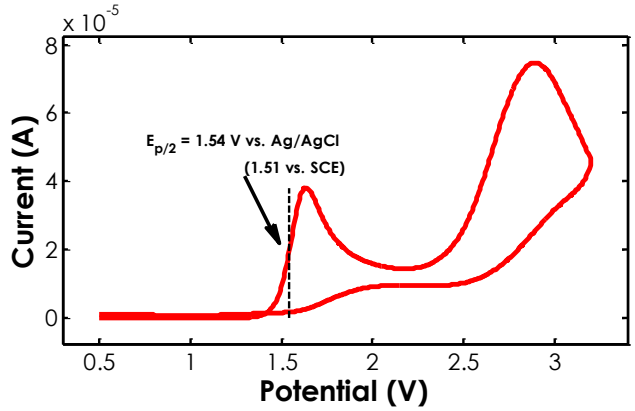


**Figure A.12** Cyclic Voltammogram of 3,4-Dihydro-2*H*-pyran

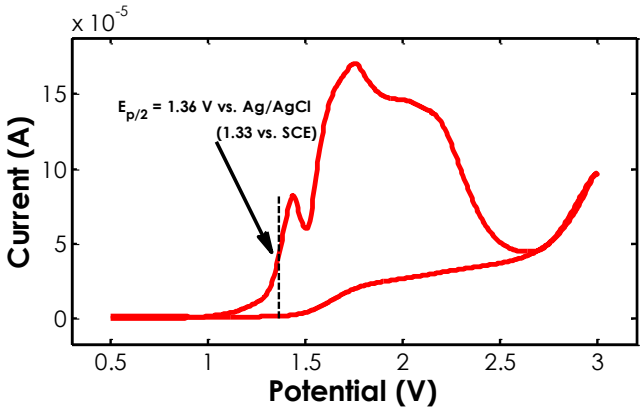


**Figure A.13** Cyclic Voltammogram of 2-Naphthalenethiol

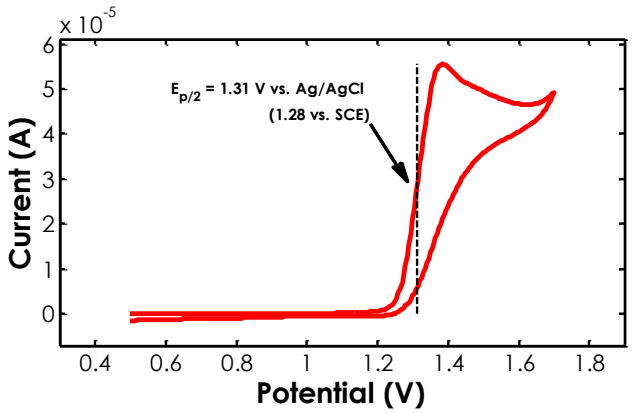


**Figure A.14** Cyclic Voltammogram of *p*-Methoxyphenyldisulfide

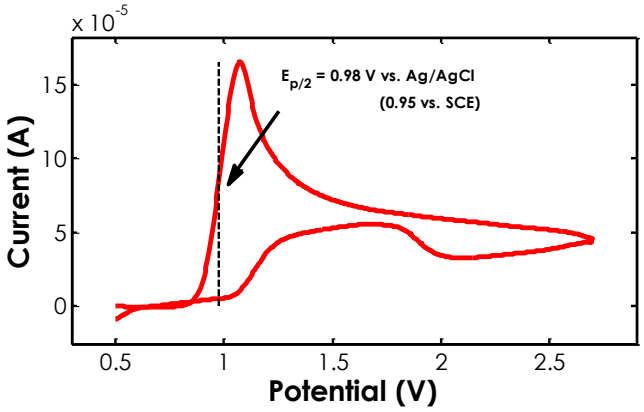


**Figure A.15** Cyclic Voltammogram of Aniline

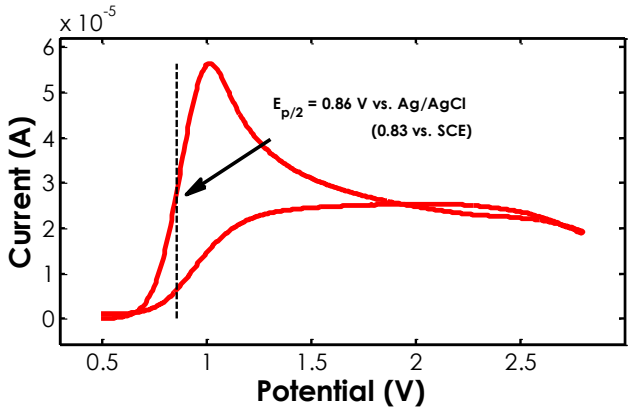


**Figure A.16** Cyclic Voltammogram of Triethylamine

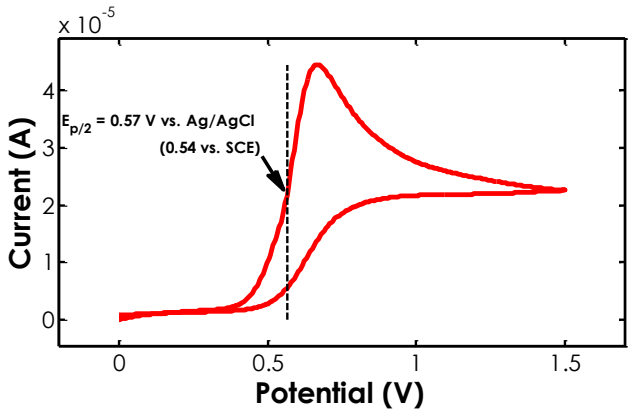


**Figure A.17** Cyclic Voltammogram of 1-Morpholinocyclohexene

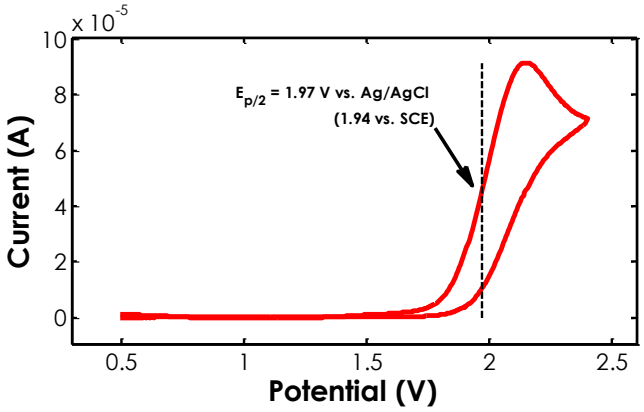


**Figure A.18** Cyclic Voltammogram of Furan

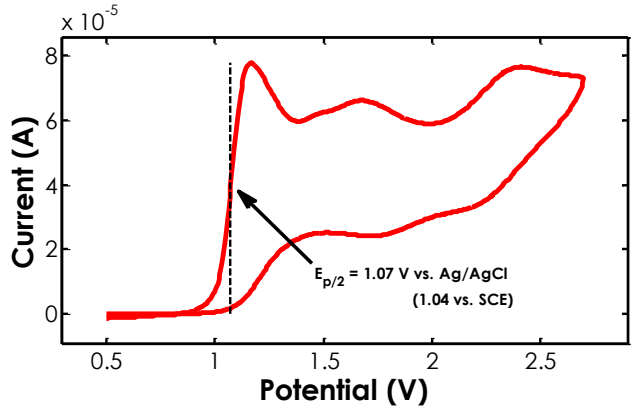


**Figure A.19** Cyclic Voltammogram of 5-Methoxyindole

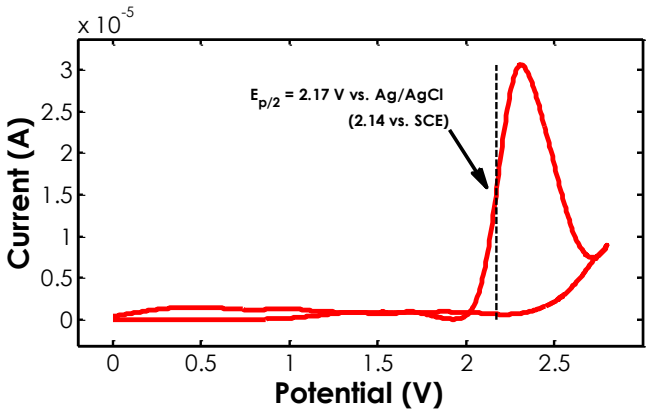


**Figure A.20** Cyclic Voltammogram of Quinoline

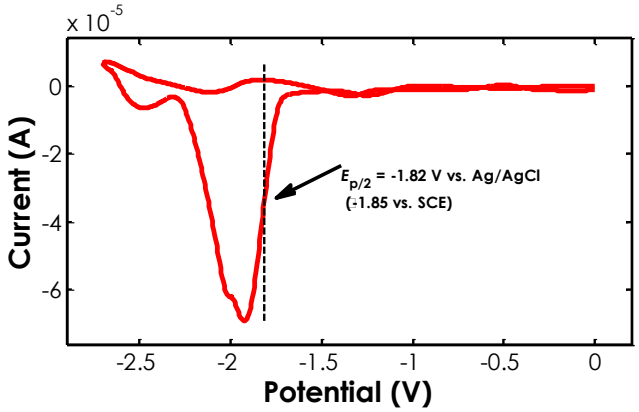


**Figure A.21** Cyclic Voltammogram of 4-Chlorobenzaldehyde

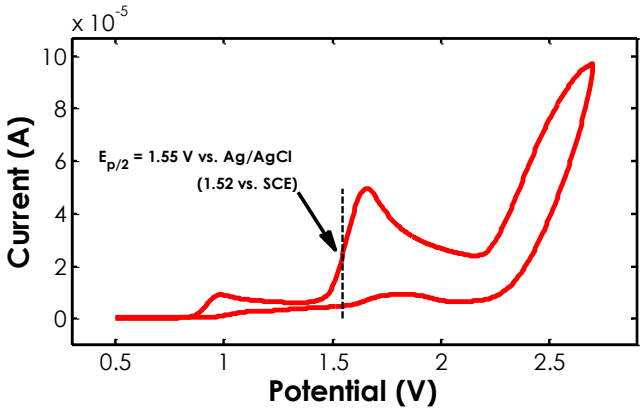


**Figure A.22** Cyclic Voltammogram of (*E*)-*N*-Benzylidene-3-methoxyaniline (oxidation)

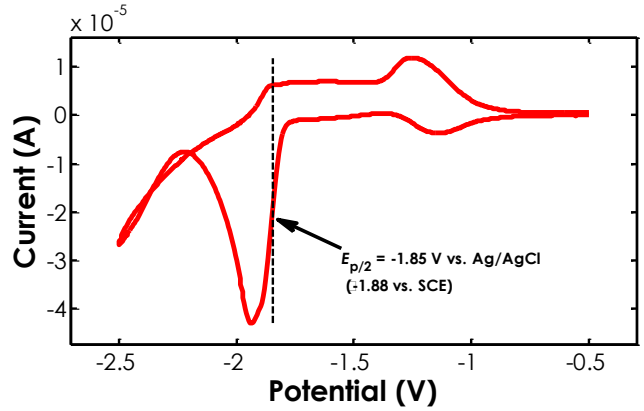


**Figure A.23** Cyclic Voltammogram of (*E*)-*N*-benzylidene-3-methoxyaniline (reduction)

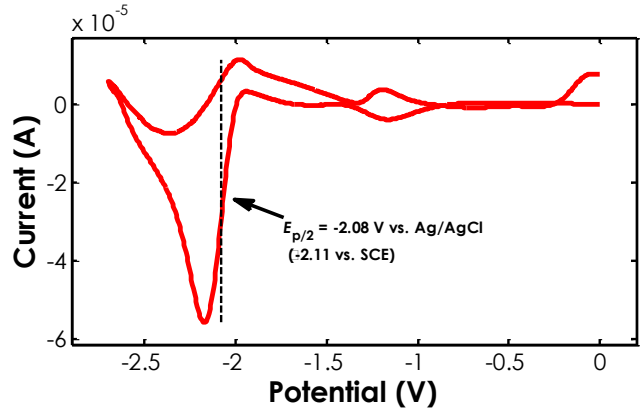


**Figure A.24** Cyclic Voltammogram of Acetophenone

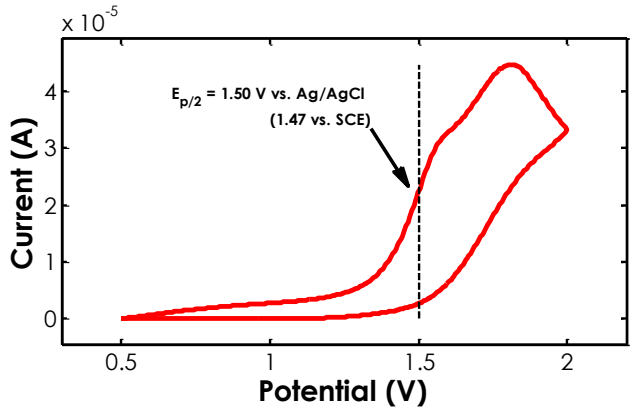


**Figure A.25** Cyclic Voltammogram of Tetra-*n*-butylammonium acetate

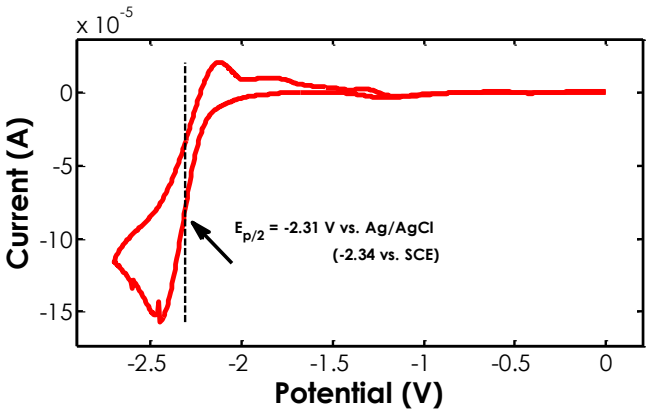


**Figure A.26** Cyclic Voltammogram of Methyl benzoate

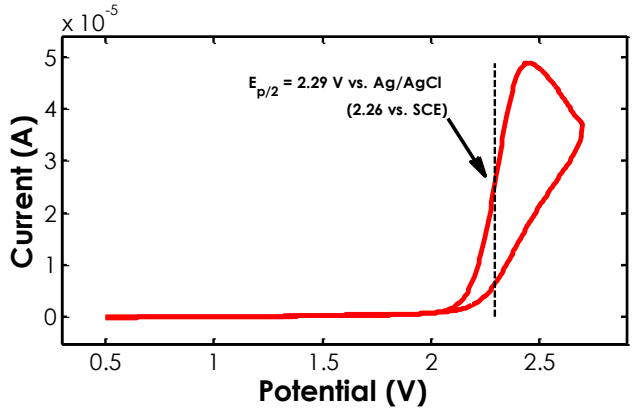


**Figure A.27** Cyclic Voltammogram of *N*,*N*-Dimethylformamide

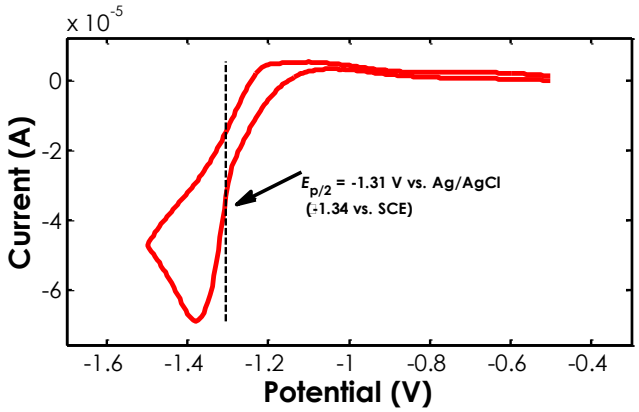


**Figure A.28** Cyclic Voltammogram of Phthalic anhydride

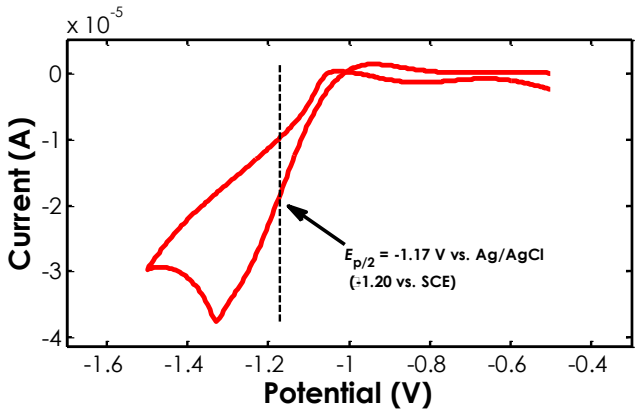


**Figure A.29** Cyclic Voltammogram of Benzoyl chloride

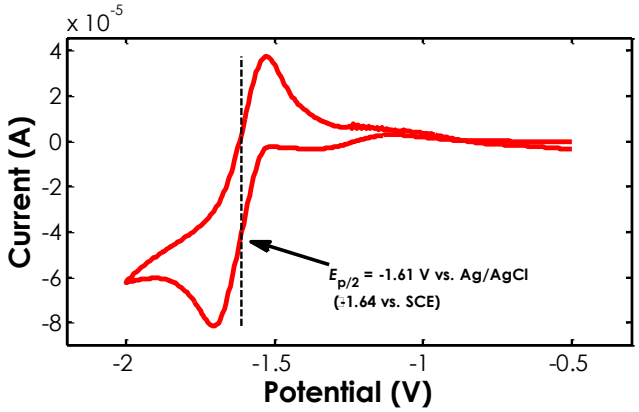


**Figure A.30** Cyclic Voltammogram of *p*-Dicyanobenzene

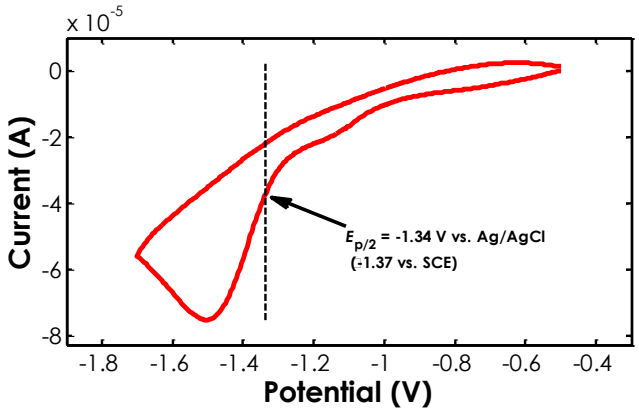


**Figure A.31** Cyclic Voltammogram of *p*-Toluenesulfonyl chloride

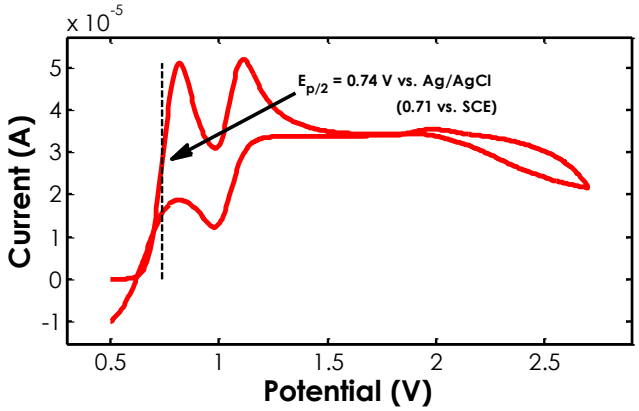


**Figure A.32** Cyclic Voltammogram of Tetra-*n*-butylammonium bromide

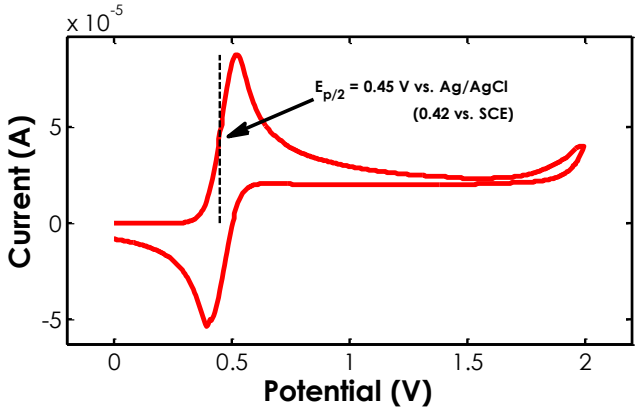


**Figure A.33** Cyclic Voltammogram of Ferrocene

## A.2 Photophysical Measurements

### A.2.1 General Information

Acridinium ion catalysts were prepared at Merck & Co. in Rahway, New Jersey and sent to the Nicewicz lab for electrochemical and photophysical data. Details on their preparation can be found in the original literature report.[15]

### A.2.2 Experimental Procedures and Data

Samples for photophysical measurements were prepared in a nitrogen-filled glovebox using spectrophotometric grade DCE, which was freshly distilled from $P_2O_5$. Stock solutions of the substrates were diluted to a concentration of 15 μM and a total volume of 4 mL before being transferred to a 4 mL quartz cell and sealed with a PTFE-lined screw cap. The solvent absorbance background was subtracted from the reported spectra. Emission spectra (1 nm step size, 5 nm bandwidth) are fully corrected for the spectral response of the instrument. Time resolved emission measurements were made by the time-correlated single photon counting (TCSPC) capability of the same instrument (FLS920) with pulsed excitation light (444.2 nm, typical pulse width = 95 ps) generated by an Edinburgh EPL-445 ps pulsed laser diode operating at a repetition rate of 5 MHz. The lifetime of fluorescence was determined by reconvolution fit with the instrument response function using the Edinburgh FS900 software. Fluorescence decay fit satisfactorily according to the function $It = A_0e^{-t/\tau}$ or $It = A_1e^{-t/\tau 1} + A_2e^{-t/\tau 2}$, where two τ-values are reported in the latter case.

Excited state reduction potentials ($^*E_{1/2}$) were calculated by subtracting the ground-state reduction potential ($E_{1/2}$), obtained by cyclic voltammetry, from the excitation energy ($E_{0,0}$). $E_{0,0}$ is determined by calculating the energy of the wavelength at which the substrate's UV-Vis absorption and emission spectra overlap.

Data (CVs, absorption/emission spectra, and fluorescence decay data) are compiled below for the four methoxy-substituted acridinium ions investigated.

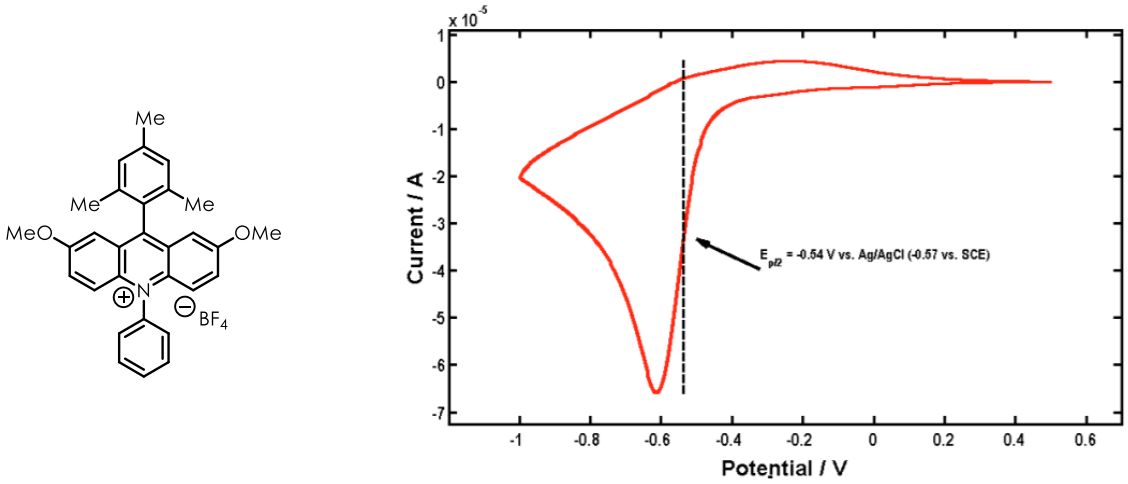


**Figure A.34** Cyclic Voltammogram of Catalyst **5**

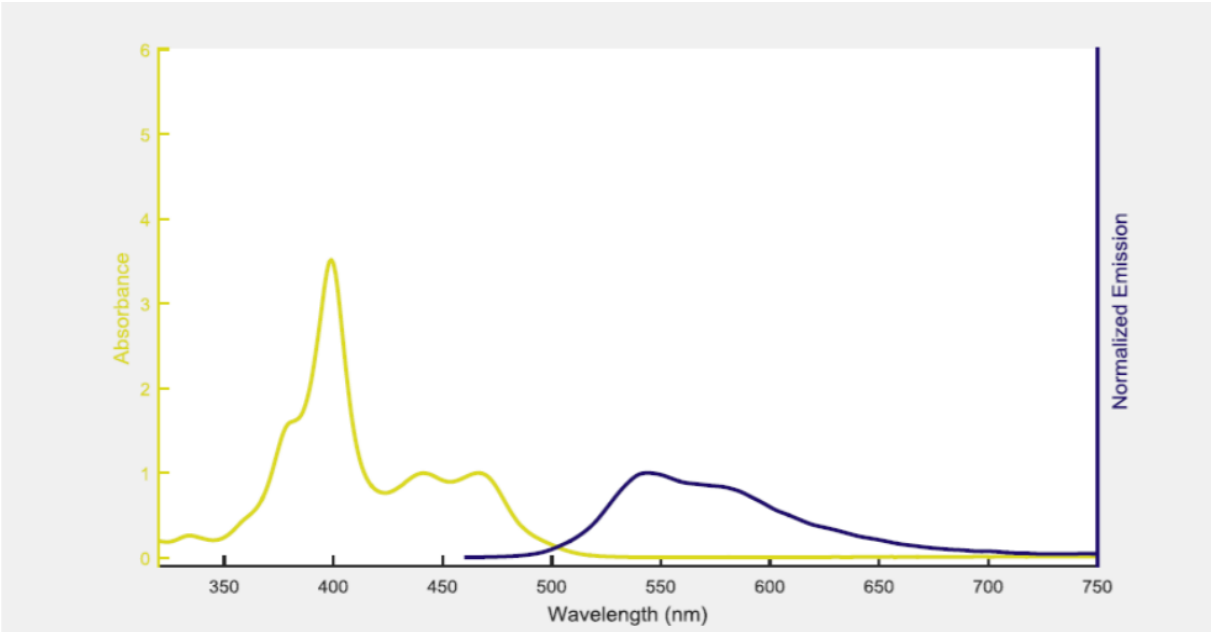


**Figure A.35** Absorption and Emission Spectra of Catalyst **5**

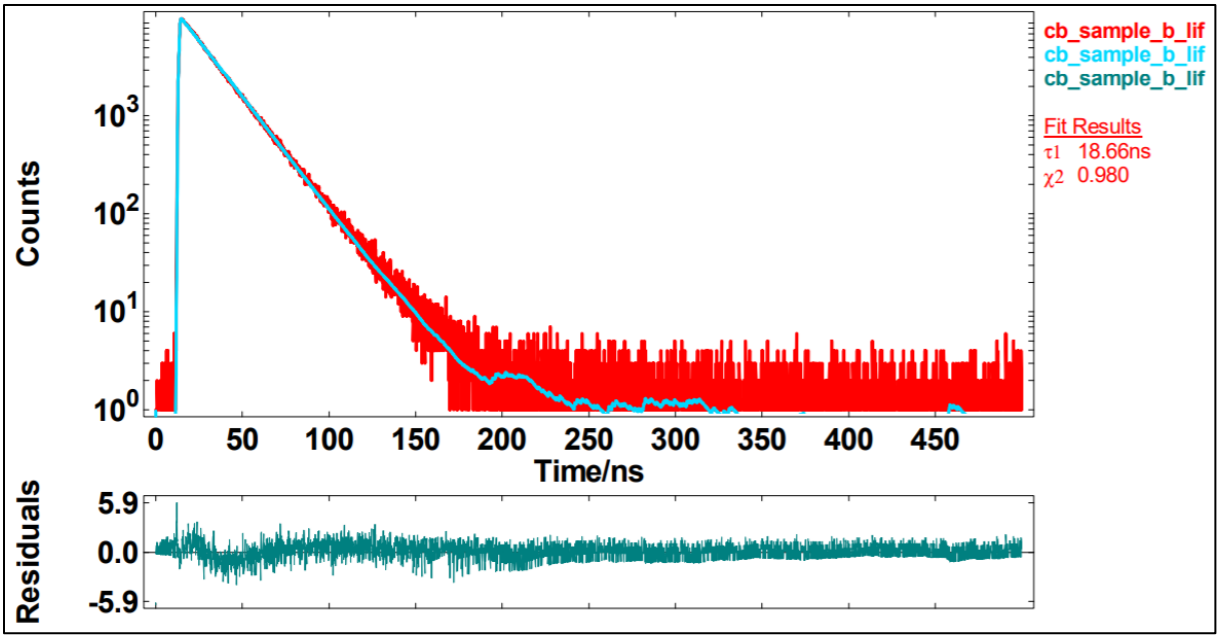


**Figure A.36** Fluorescence Decay Data of Catalyst **5**

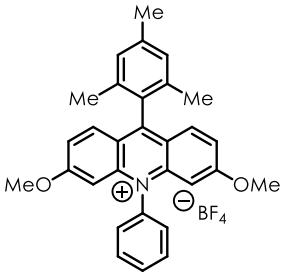


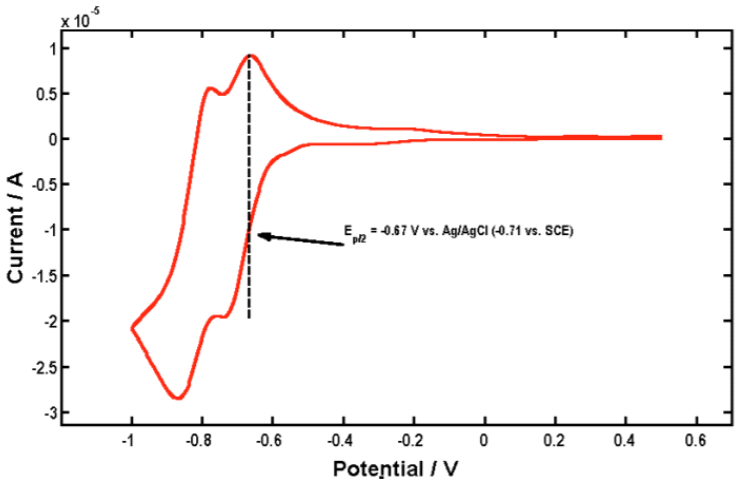


**Figure A.37** Cyclic Voltammogram of Catalyst **6**

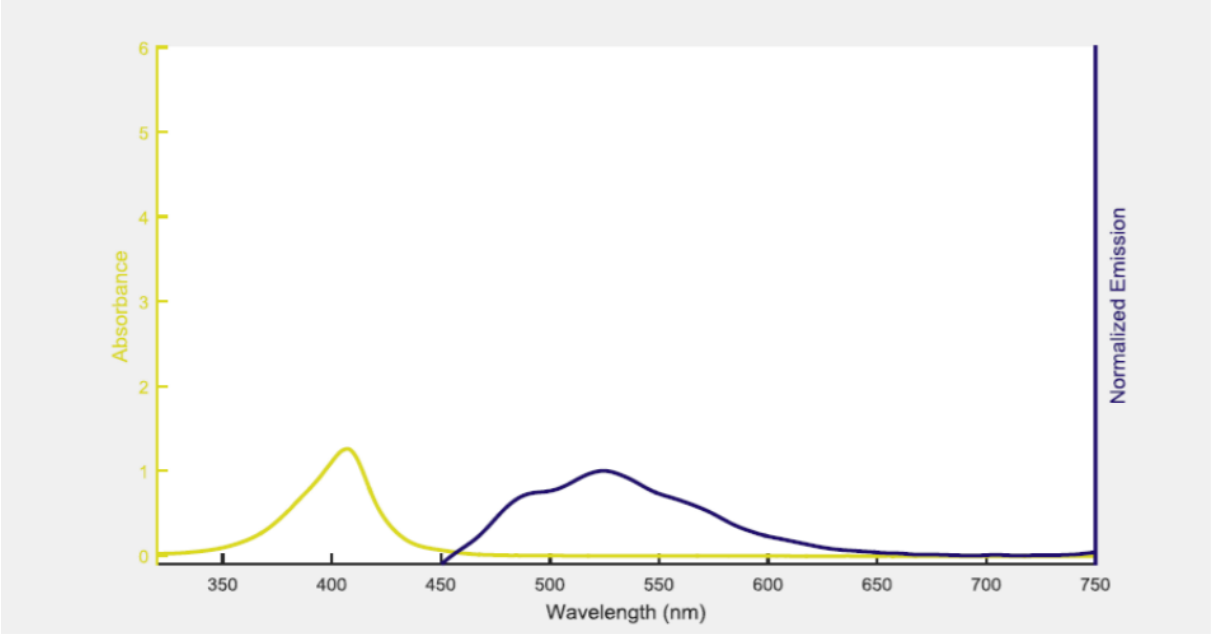


**Figure A.38** Absorption and Emission Spectra of Catalyst **6**

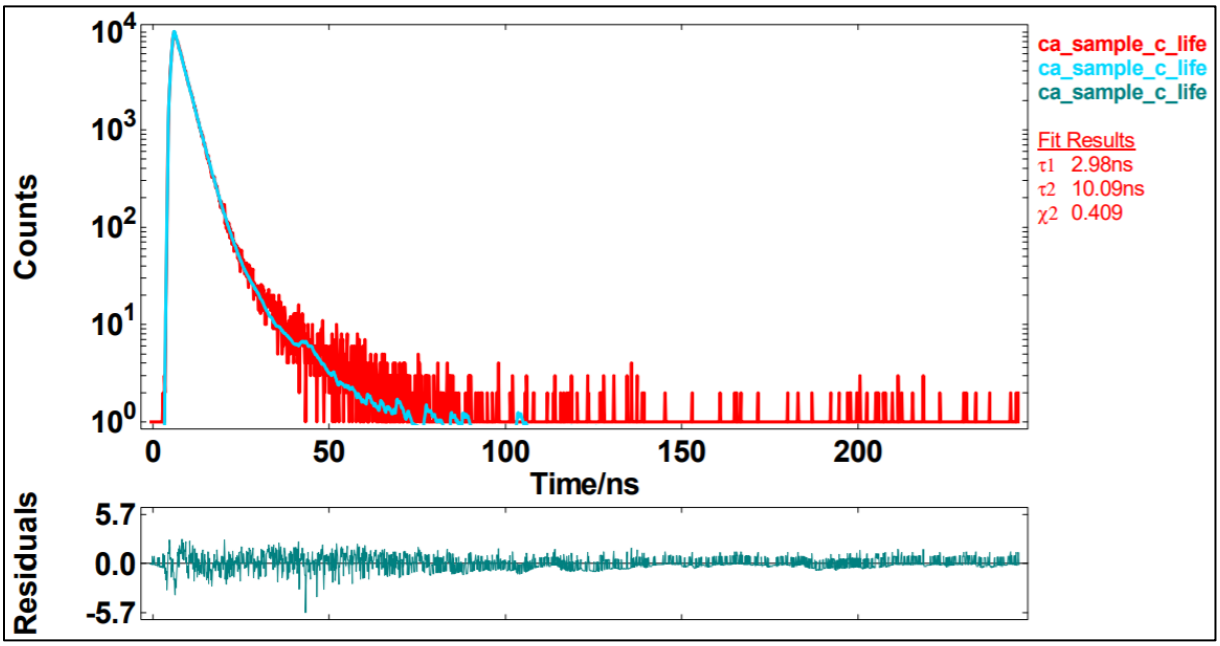


**Figure A.39** Fluorescence Decay Data of Catalyst **6**

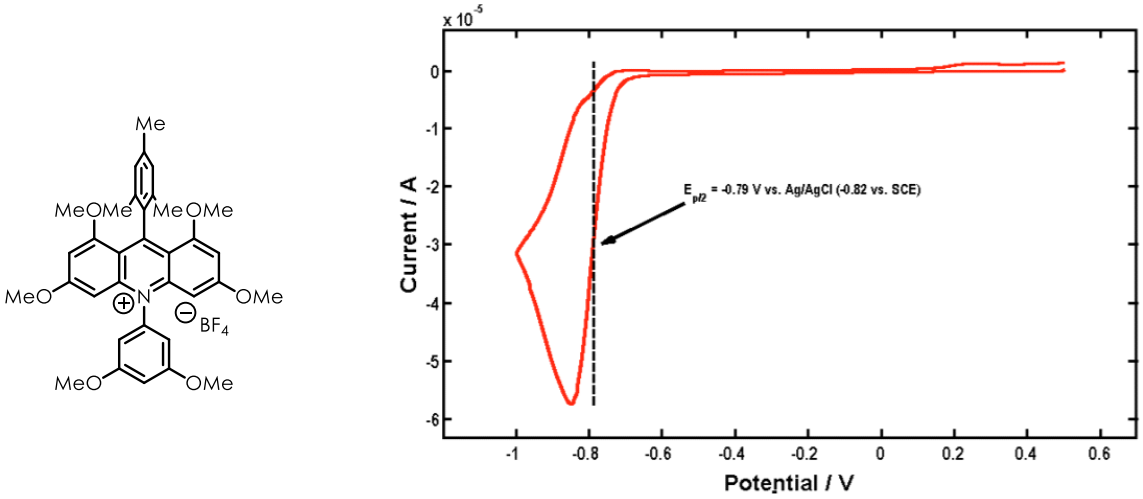


**Figure A.40** Cyclic Voltammogram of Catalyst **7**

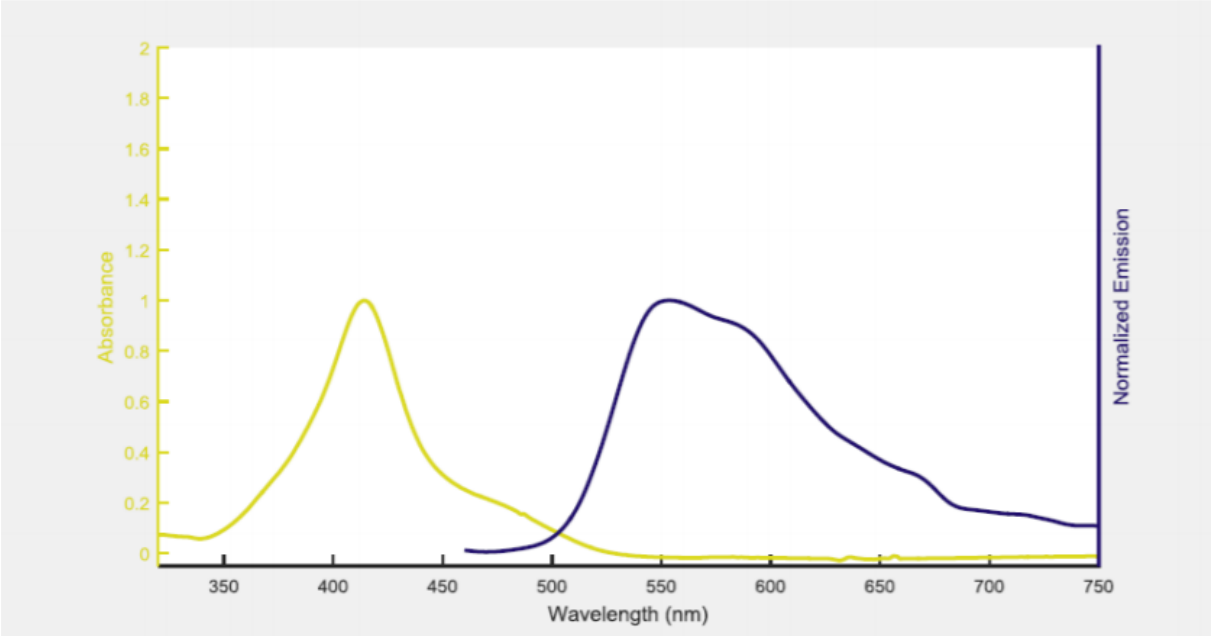


**Figure A.41** Absorption and Emission Spectra of Catalyst **7**

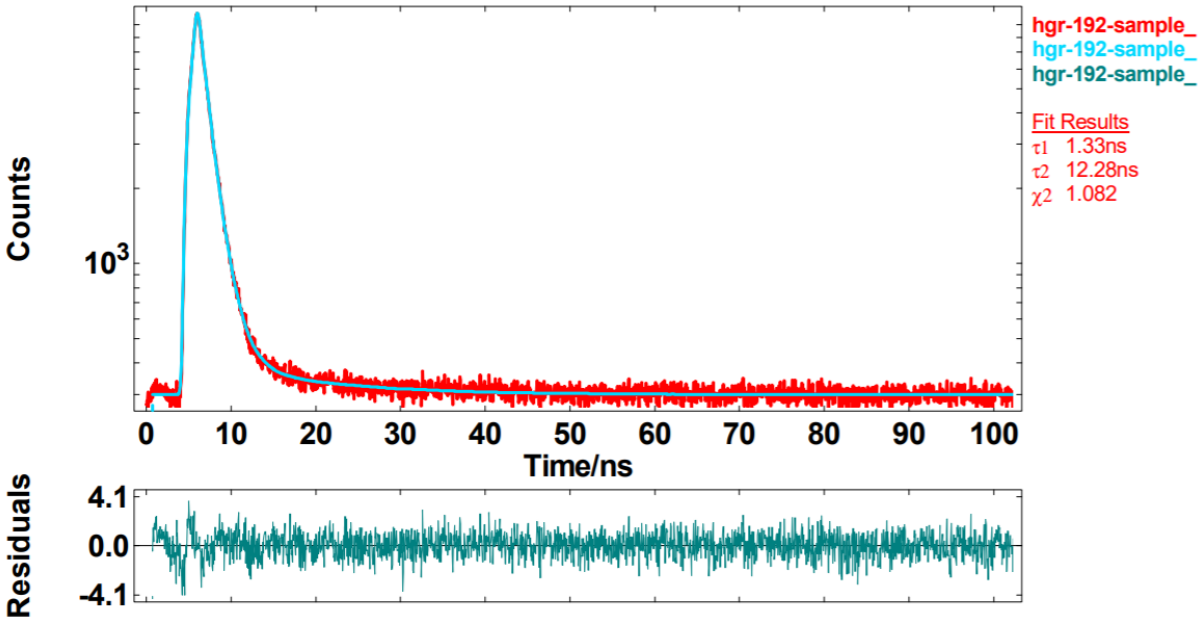


**Figure A.42** Fluorescence Decay Data of Catalyst **7**

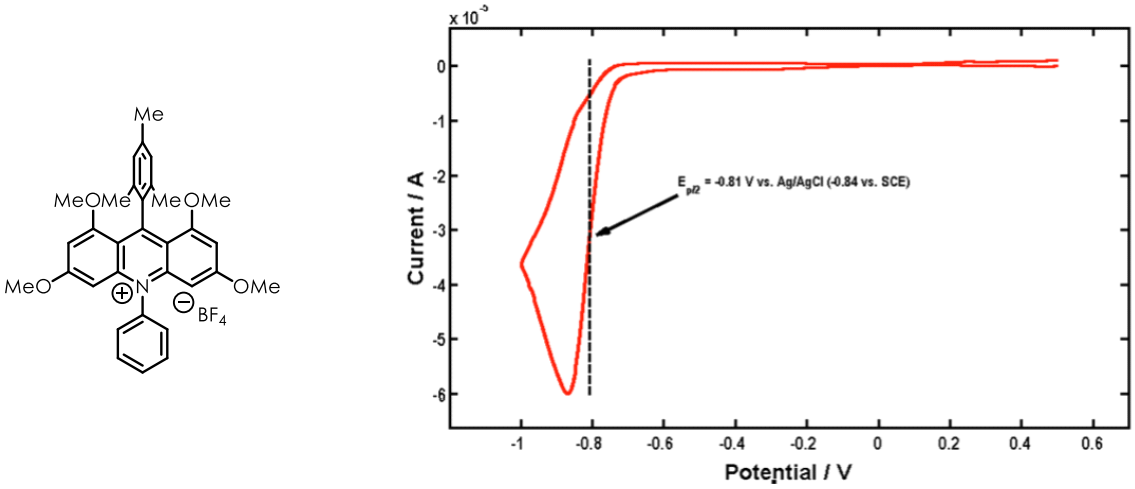


**Figure A.43** Cyclic Voltammogram of Catalyst **8**

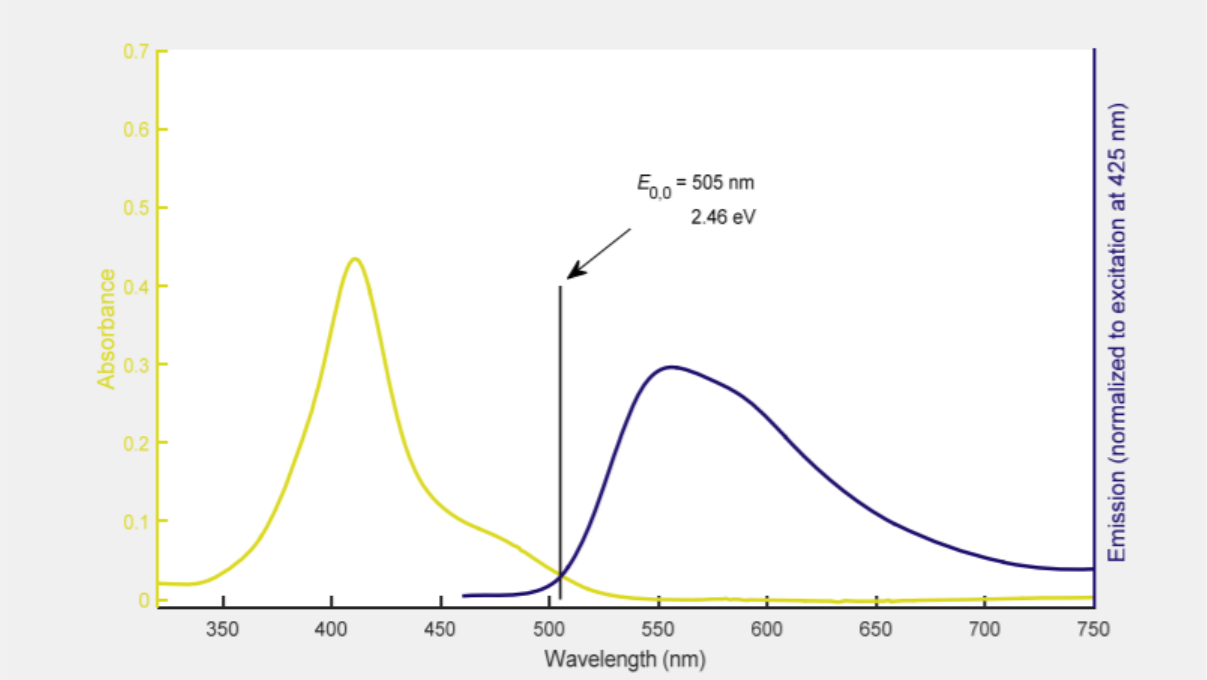


**Figure A.44** Absorption and Emission Spectra of Catalyst **8**

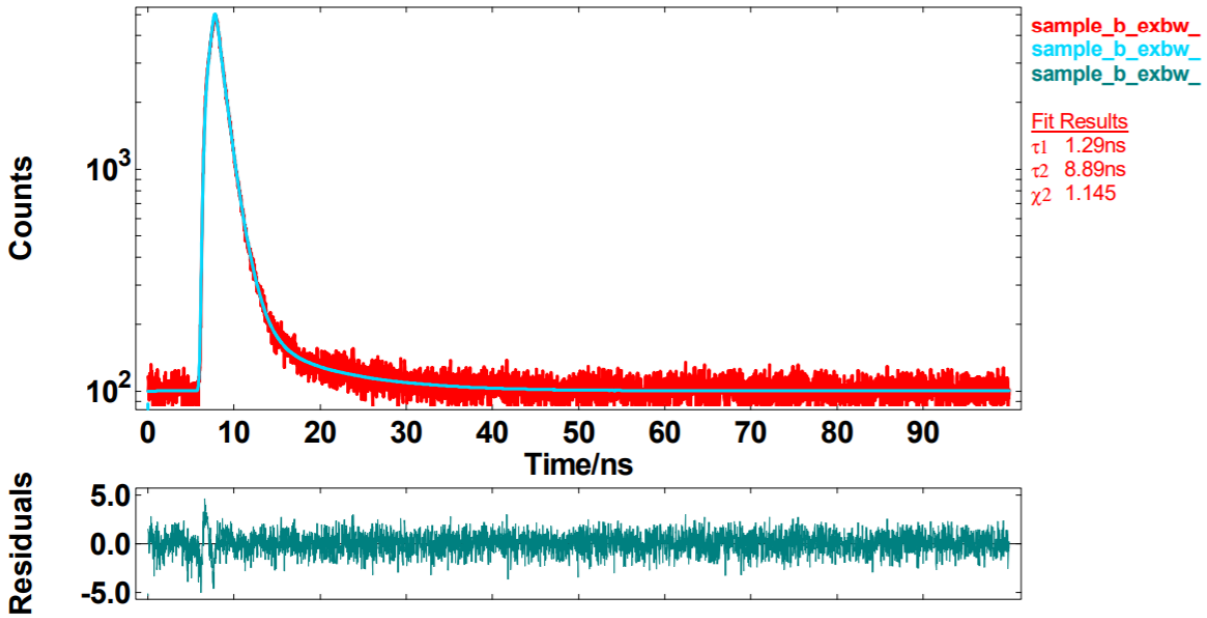


**Figure A.45** Fluorescence Decay Data of Catalyst **8**

# APPENDIX B: EXPERIMENTAL DETAILS AND CHARACTERIZATION DATA OF KEY INTERMEDIATES

## B.1 General Information

Reactions were run under nitrogen and anhydrous conditions unless otherwise stated. Commercially available reagents were purchased from Sigma-Aldrich, Acros, Alfa Aesar, Oakwood Chemical, VWR, or Fisher Scientific and purified using reported methods as needed.[118] Solvents were dried by passing through activated alumina prior to use; the exceptions to this include DIPA, which was distilled from KOH, and THF, which was distilled from LAH.

Reactions were monitored by TLC using silica plates from VWR, and UV light or $KMnO_4$ stain as a method of visualization. Flash chromatography was conducted with 40-63 μm (230-400 mesh) silica from Silicycle.

NMR spectroscopy was recorded using Bruker 400 MHz or Bruker Advance III 600 Cryoprobe ($^1$H NMR at 600 MHz, $^{13}$C NMR at 151 MHz, and $^{31}$P at 243 MHz). Solvent resonances were used as an internal standard: $CDCl_3$ (7.26 ppm for $^1$H and 77.0 ppm for $^{13}$C), DMSO-$d_6$ (2.50 ppm for $^1$H and 39.0 for $^{13}$C), or pyridine-$d_5$ (7.21, 7.58, 8.73 ppm for $^1$H and 123.3, 135.3, 149.7 ppm for $^{13}$C). Chemical shifts are reported in ppm and coupling constants in Hz. Crystal structure data was obtained with a Bruker Smart Apex II crystal x-ray diffractometer.

## B.2 Experimental Details

### B.2.1 Synthesis of the Western Half of Rubriflordilactone B

**Scheme B.1** Synthesis of **1-4**

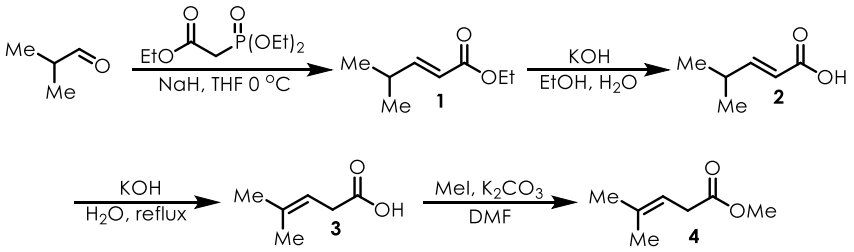


**Synthesis of 1** NaH (1.98 g, 49.5 mmol, 1.1 equiv; 60% dispersion in mineral oil) was added to a flame-dried RBF and rinsed with dry hexanes (3x) before it was suspended in THF (113 mL) and cooled to 0 °C. Triethylphosphonoacetate (9.80 mL, 49.5 mmol, 1.1 equiv) was added and the contents were stirred for 30 min before freshly distilled isobutyraldehyde (4.20 mL, 45.0 mmol, 1 equiv) was added. After stirring for 16 hr and warming to room temperature, the reaction was quenched with sat. aq. $NH_4Cl$ and the aqueous layer extracted with $Et_2O$ 3x and the combined organic layers washed with brine and dried over $MgSO_4$. Filtration and concentration gave the product as a colorless liquid (6.37 g, >99%). $^1$H NMR (400 MHz, Chloroform-*d*) δ 6.93 (dd, *J* = 15.7, 6.6 Hz, 1H), 5.75 (dd, *J* = 15.7, 1.4 Hz, 1H), 4.17 (q, *J* = 7.1 Hz, 3H), 2.44 (hd, *J* = 6.7, 1.7 Hz, 1H), 1.27 (t, *J* = 7.1 Hz, 4H), 1.05 (s, 3H), 1.04 (s, 3H).

**Synthesis of 2** KOH (7.92 g, 120 mmol, 2 equiv) was dissolved in a 1:1 mixture of $H_2O$:EtOH (30 mL of each) before **1** (8.53 g, 60 mmol, 1 equiv) was added. After stirring for 16 hr, the reaction was acidified with 2 N HCl and extracted with $Et_2O$. The combined organic layers were washed with brine and dried over $MgSO_4$. Filtration and concentration gave a colorless oil (6.40 g, 93%). $^1$H NMR (400 MHz, Chloroform-*d*) δ 11.90 (s, 1H), 7.05 (dd, *J* = 15.7, 6.6 Hz, 1H), 5.76 (dd, *J* = 15.7, 1.4 Hz, 1H), 2.47 (dqd, *J* = 13.5, 6.7, 1.2 Hz, 1H), 1.07 (s, 3H), 1.05 (s, 3H).

**Synthesis of 3** KOH (3.99 g, 71.0 mmol, 14.2 equiv) was dissolved in $H_2O$ (12 mL), then **2** (601 μL, 5.00 mmol, 1 equiv) was added dropwise. The contents were heated to reflux for 48 hr; after cooling to RT, the reaction was acidified with 2 N HCl and extracted with DCM (3x); the organic layers were dried over $MgSO_4$, filtered, and concentrated to give a yellow liquid (490 mg, 86%). $^1$H NMR (400 MHz, Chloroform-*d*) δ 10.79 (s, 1H), 5.29 (ddt, *J* = 7.2, 4.3, 1.4 Hz, 1H), 3.08 (d, *J* = 7.2 Hz, 2H), 1.75 (s, 3H), 1.64 (s, 3H).

**Synthesis of 4** $K_2CO_3$ (726 mg, 5.25 mmol, 1.1 equiv) was suspended in DMF (3.2 mL) before **3** (600 μL, 5.00 mmol, 1 equiv) was added. After 15 min, MeI (450 μL, 7.25 mmol, 1.45 equiv) was added and the solution stirred for 16 hr. The contents were diluted with $Et_2O$, washed with water (5x) (to remove DMF) and brine (1x). The organic layers were dried over $MgSO_4$, filtered, and concentrated to a yellow oil (556 mg, 87%). $^1$H NMR (400 MHz, Chloroform-*d*) δ 5.29 (ddt, *J* = 7.2, 5.8, 1.4 Hz, 1H), 3.67 (s, 3H), 3.03 (d, *J* = 7.2 Hz, 2H), 1.74 (s, 3H), 1.63 (s, 3H).

**Scheme B.2** Synthesis of **5**

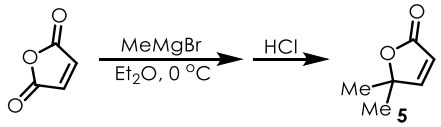


**Synthesis of 5** MeMgBr (3.0 M, 3.3 mL, 10 mmol, 2 equiv) was added to a flame-dried RBF, diluted with $Et_2O$ (5 mL), and cooled to 0 °C before maleic anhydride (490 mg, 5.00 mmol, 1 equiv) was added as a solution in $Et_2O$ (6 mL). After 3 hr, the mixture was acidified with 2 N HCl and extracted with $Et_2O$. The combined organic layers were washed with 1 N HCl, brine, and dried over $MgSO_4$. Filtration and concentration gave a pale purple oil which contained product with trace impurities (178 mg, approx. 32%). $^1$H NMR (400 MHz, Chloroform-*d*) δ 7.39 (d, *J* = 5.6 Hz, 1H), 5.97 (d, *J* = 5.6 Hz, 1H), 1.48 (s, 6H).

**Scheme B.3** Synthesis of **6** and **5**

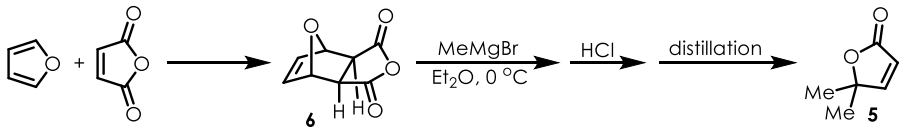


**Synthesis of 6** Maleic anhydride (1.00 g, 10.2 mmol, 1 equiv) was added to an RBF and cooled to 0 °C before furan (4.40 mL, 61.2 mmol, 6 equiv) was added dropwise in the dark. After stirring for 16 hr, the resultant white solid was filtered and washed with chilled hexanes (1.49 g, 88%). $^1$H NMR (400 MHz, Chloroform-*d*) δ 6.58 (s, 2H), 5.46 (s, 2H), 3.18 (s, 2H).

**Synthesis of 5** In a flame-dried RBF, **6** (10.6 g, 63.8 mmol, 1 equiv) was suspended in $Et_2O$ (180 mL) and cooled to 0 °C before MeMgBr (3.0 M, 64 mL, 191 mmol, 3 equiv) was added dropwise. During the addition, the reaction may clump up into a viscous material, but over time it will loosen up and stir. After stirring for 16 hr, the mixture was acidified with 2 N HCl and stirred for 30 min before it was extracted with EtOAc. The organic layers were washed with 2 N HCl, sat. aq. $NaHCO_3$, brine, and dried over $MgSO_4$. Filtration and concentration afforded an orange oil which was immediately distilled to obtain **5** as a pale-yellow liquid (4.08 g, 57%, 2 steps). $^1$H NMR (400 MHz, Chloroform-*d*) δ 7.39 (d, *J* = 5.6 Hz, 1H), 5.97 (d, *J* = 5.6 Hz, 1H), 1.48 (s, 6H).

**Scheme B.4** Synthesis of **7-9**

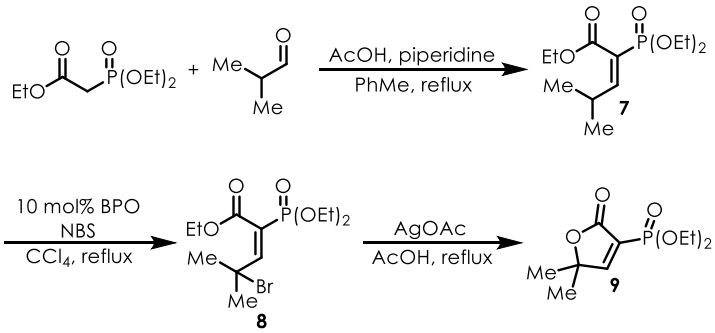

**Synthesis of 7** To a flame-dried RBF was added triethylphosphonoacetate (39.6 mL, 200 mmol, 1 equiv), isobutyraldehyde (101 mL, 1.12 mol, 5.6 equiv), acetic acid (6.00 mL, 104 mmol, 0.52 equiv), piperidine (1.40 mL, 14.0 mmol, 0.07 equiv), and PhMe (400 mL). The contents were heated to reflux with a Dean-Stark trap for 4 days, then cooled to RT, concentrated, and purified by column chromatography with 40% EtOAc/hexanes to give a yellow oil (49.9 g, 90%; small amount of alkene isomer present). $^1$H NMR (600 MHz, Chloroform-*d*) δ 6.86 (dd, *J* = 23.1, 10.2 Hz, 1H), 4.28 – 4.19 (m, 3H), 4.18 – 4.04 (m, 5H), 3.03 (dddd, *J* = 13.1, 8.7, 6.6, 3.3 Hz, 1H), 1.30 (td, *J* = 7.1, 4.9 Hz, 12H), 1.05 (dd, *J* = 6.6, 3.9 Hz, 8H).

**Synthesis of 8** To a dry flask was added NBS (41.5 g, 233.1 mmol, 1.3 equiv), $CCl_4$ (268 mL), and **7** (49.9 g, 179 mmol, 1 equiv). After adding BPO (434 mg, 1.79 mmol, 10 mol%), the contents were heated to reflux for 5 hr. After cooling to RT, the precipitate formed was filtered off and washed with chilled $CCl_4$. The filtrate was then washed with water (2x), sat. aq. $NaS_2O_3$ (1x), brine (1x), and dried over $MgSO_4$. Filtration and concentration gave an orange oil (19.4 g, 67%). $^1$H NMR (400 MHz, Chloroform-*d*) δ 6.92 (d, *J* = 24.9 Hz, 1H), 4.27 (q, *J* = 8.5, 7.1 Hz, 3H), 4.20 – 4.05 (m, 5H), 1.94 (s, 7H), 1.39 – 1.25 (m, 12H).

**Synthesis of 9** Combined **8** (16.8 g, 47.0 mmol, 1 equiv), AgOAc (7.84 g, 47.0 mmol, 1 equiv), and AcOH (70 mL) in a flask and refluxed the suspension for 6 hr. The contents were cooled to RT and concentrated. The residue was taken up in DCM and washed with water (2x) and brine (1x). Drying over $Na_2SO_4$, filtration, and concentration gave an oil which was purified by chromatography using EtOAc as the eluent to give a light-yellow oil, which solidified to a pale-yellow solid upon standing (4.82 g, 41%). $^1$H NMR (600 MHz, Chloroform-*d*) δ 8.00 (d, *J* = 9.5 Hz, 1H), 4.28 – 4.15 (m, 4H), 1.50 (s, 6H), 1.34 (t, *J* = 7.1 Hz, 6H).

**Scheme B.5** Synthesis of **10-11**

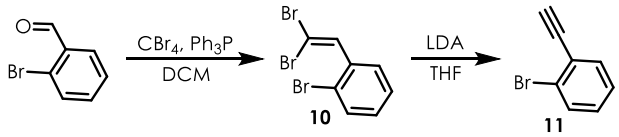


**Synthesis of 10** Within an RBF, $CBr_4$ (7.30 g, 22.0 mmol, 2 equiv) and $Ph_3P$ (11.5 g, 44.0 mmol, 4 equiv) were combined and taken up in DCM (50 mL) at 0 °C. After this solution stirred for 30 min, 2-bromobenzaldehyde (2.04 g, 11.0 mmol, 1 equiv) was added as a solution in DCM (1 mL). The contents were stirred for 2 hr, then quenched with water. The aqueous layer was extracted with DCM (3x), and the combined organic layers were washed with brine, dried over $MgSO_4$, filtered, and concentrated. The residue was purified by chromatography with hexanes as the eluent to give a yellow oil (3.16 g, 84%). $^1$H NMR (400 MHz, Chloroform-*d*) δ 7.59 (d, *J* = 8.0 Hz, 2H), 7.51 (s, 1H), 7.34 (t, *J* = 7.5 Hz, 1H), 7.21 (t, *J* = 7.7 Hz, 1H).

**Synthesis of 11** To a flame dried RBF filled with nitrogen was added DIPA (2.00 mL, 14.5 mmol, 3 equiv) and THF (37 mL). After cooling the solution to -78 °C, *n*-BuLi (1.6 M, 9.0 mL 15 mmol, 3 equiv) was added dropwise. To this freshly made LDA was added a solution of **10** (1.65 g, 4.83 mmol, 1 equiv) in THF (12 mL). After stirring the solution for 2 hrs, the reaction was quenched with sat. aq. $NH_4Cl$ and the aqueous layer extracted with DCM. The combined organic layers were dried over $MgSO_4$, filtered, and concentrated. The residual oil was purified by chromatography with hexanes as the eluent to give the product as an orange oil (600 mg, 68%). $^1$H NMR (400 MHz, Chloroform-*d*) δ 7.56 (ddd, *J* = 24.9, 7.8, 1.3 Hz, 2H), 7.31 – 7.24 (m, 1H), 7.20 (td, *J* = 7.8, 1.7 Hz, 1H), 3.38 (s, 1H).

**Scheme B.6** Synthesis of **12-14**

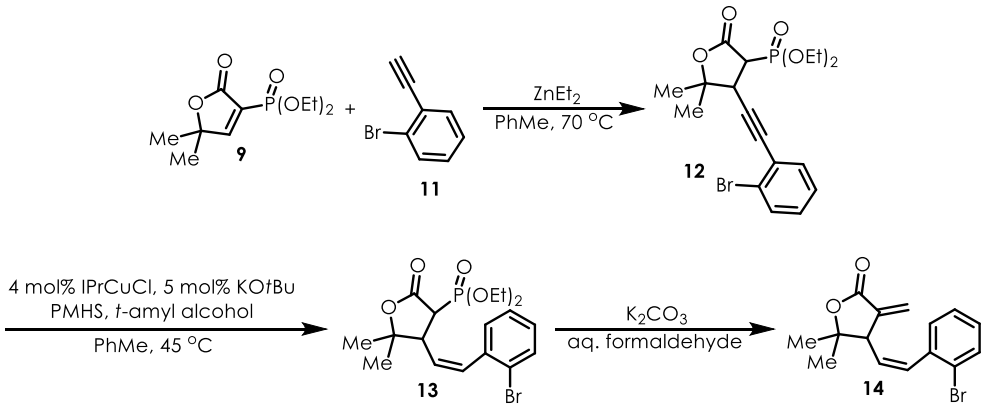


**Synthesis of 12** To a dry flask under nitrogen was added **11** (500 μL, 4.00 mmol, 2.2 equiv) and PhMe (2.5 mL). To this solution was added $ZnEt_2$ (1.5 M, 2.4 mL, 3.6 mmol, 2 equiv) and the contents were heated to 70 °C for 1.5 hr. At this point, a solution of **9** (451 mg, 1.80 mmol, 1 equiv) in PhMe (22 mL) was added and the reaction stirred at 70 °C for another 16 hr. After cooling to RT, the reaction was quenched with sat. aq. $NH_4Cl$ and the aqueous layer extracted with EtOAc. The combined organic layers were washed with brine, dried over $Na_2SO_4$, filtered, and concentrated. Purification of the residue by chromatography with 40% EtOAc/hexanes → 100% EtOAc gave the product as a pale yellow solid (611 mg, 79%). $^1$H NMR (400 MHz, Chloroform-*d*) δ 7.61 – 7.56 (m, 1H), 7.43 (dd, *J* = 7.7, 1.6 Hz, 1H), 7.30 – 7.24 (m, 2H), 7.19 (td, *J* = 7.8, 1.6 Hz, 1H), 4.39 – 4.28 (m, 2H), 4.24 (p, *J* = 7.3 Hz, 2H), 3.72 (dd, *J* = 16.3, 11.5 Hz, 1H), 3.41 (dd, *J* = 22.6, 11.5 Hz, 1H), 1.63 (s, 3H), 1.57 (s, 3H), 1.36 (dt, *J* = 11.6, 7.1 Hz, 6H). $^{13}$C NMR (151 MHz, Chloroform-*d*) δ 169.14, 133.47, 132.59, 129.94, 127.21, 125.69, 124.49, 88.90, 88.89, 85.48, 85.40, 83.86, 77.16, 64.14, 64.10, 63.12, 63.08, 46.55, 45.55, 41.32, 41.30, 27.32, 24.49, 16.57, 16.53, 16.49. $^{31}$P NMR (243 MHz, Chloroform-*d*) δ 18.90. HRMS calculated (M+Na): 451.0280; found: 451.0280.

**Synthesis of 13** Inside a nitrogen-filled glovebox, IPrCuCl (26.3 mg, 54 μmol, 4 mol%) and KO*t*-Bu (7.5 mg, 67 μmol, 5 mol%) were combined in a flask and suspended in PhMe (300 μL). The flask was sealed before removing from the glovebox and placed under a positive pressure of nitrogen. After stirring for 15 min, PMHS (280 μL, 4.00 mmol, 3 equiv) was added along with **12** (577 mg, 1.34 mmol, 1 equiv) dissolved in PhMe (1.5 mL); after an additional 5 minutes had elapsed, *t*-amyl alcohol (370 μL, 3.35 mmol, 2.5 equiv) was added. The solution was heated to 45 $^{o}$C and stirred for 16 hr. After cooling to RT, the contents were eluted through a silica plug with EtOAc and concentrated. The residue was purified by chromatography with 60% EtOAc/hexanes to give a yellow oil (470 mg, 82%). $^{1}$H NMR (400 MHz, Chloroform-*d*) δ 7.65 – 7.56 (m, 2H), 7.37 – 7.30 (m, 1H), 7.16 (td, *J* = 7.9, 1.5 Hz, 1H), 6.69 (d, *J* = 11.3 Hz, 1H), 5.62 (t, *J* = 10.9 Hz, 1H), 4.37 – 4.25 (m, 2H), 4.25 – 4.15 (m, 2H), 3.71 (dt, *J* = 15.9, 11.1 Hz, 1H), 3.15 (dd, *J* = 23.3, 11.6 Hz, 1H), 1.36 (d, *J* = 7.1 Hz, 6H), 1.30 (s, 3H), 1.14 (s, 3H). $^{13}$C NMR (151 MHz, $CDCl_3$) δ 169.90, 136.54, 134.08, 132.61, 130.38, 129.29, 128.18, 128.18, 127.63, 123.84, 86.63, 86.53, 77.16, 63.93, 63.89, 62.70, 62.66, 45.93, 45.64, 45.63, 44.93, 26.74, 22.66, 16.61, 16.57, 16.50, 16.46. $^{31}$P NMR (243 MHz, $CDCl_3$) δ 19.91. HRMS calculated (M+Na): 453.0437; found: 453.0433.

**Synthesis of 14** Within a flask, **13** (810 mg, 1.90 mmol, 1 equiv) and $K_2CO_3$ (790 mg, 5.70 mmol, 3 equiv) were combined and cooled to 0 $^{o}$C, then aqueous formaldehyde (37 wt%, 1.1 mL, 13 mmol, 7 equiv) was added. The contents were stirred for 30 min before diluting the mixture with water and extracting it with EtOAc. The combined organic layers were washed with brine, dried over $MgSO_4$, filtered, and concentrated. The residue was purified by chromatography with 20% EtOAc/hexanes to give a white solid (393 mg, 67%). $^{1}$H NMR (600 MHz, Chloroform-*d*) δ 7.61 (d, *J* = 8.0 Hz, 1H), 7.29 (t, *J* = 7.5 Hz, 1H), 7.21 – 7.15 (m, 2H),

6.84 (d, *J* = 11.2 Hz, 1H), 6.27 (d, *J* = 3.4 Hz, 1H), 5.69 – 5.63 (m, 1H), 5.62 (d, *J* = 3.0 Hz, 1H), 3.67 (dt, *J* = 10.1, 3.2 Hz, 1H), 1.32 (s, 6H). $^{13}$C NMR (151 MHz, $CDCl_3$) δ 169.23, 139.94, 136.62, 135.22, 132.96, 129.72, 129.49, 127.48, 127.07, 123.87, 122.35, 85.07, 77.16, 49.84, 27.31, 24.09. HRMS calculated (M+Na): 329.0148; found: 329.0147.

**Scheme B.7** Synthesis of **15-18**

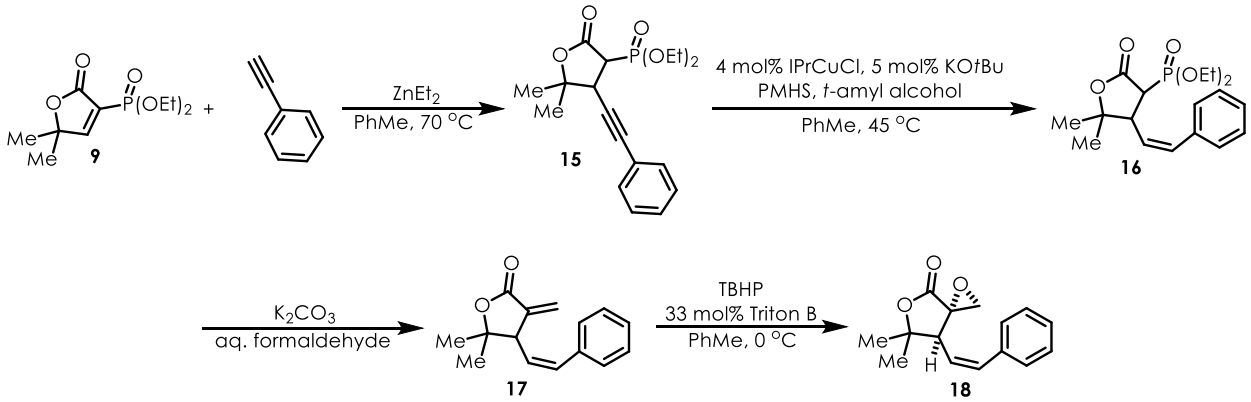


**Synthesis of 15** Made analogously to **12** on a 5 mmol scale to give a yellow oil (1.45 g, 83%). $^1$H NMR (600 MHz, Chloroform-*d*) δ 7.42 – 7.38 (m, 2H), 7.33 (t, *J* = 7.6 Hz, 3H), 4.38 – 4.27 (m, 2H), 4.23 (ddt, *J* = 10.4, 7.0, 3.1 Hz, 2H), 3.67 (dd, *J* = 16.2, 11.5 Hz, 1H), 3.37 (dd, *J* = 22.7, 11.5 Hz, 1H), 1.61 (s, 3H), 1.51 (s, 3H), 1.37 (t, *J* = 7.1 Hz, 3H), 1.34 (t, *J* = 7.0 Hz, 3H).

**Synthesis of 16** Made analogously to **13** on a 1.67 mmol scale to give a white solid (484 mg, 82%). $^1$H NMR (400 MHz, Chloroform-*d*) δ 7.43 – 7.32 (m, 3H), 7.26 (s, 2H), 6.75 (d, *J* = 11.5 Hz, 1H), 5.51 (t, *J* = 11.1 Hz, 1H), 4.28 – 4.18 (m, 2H), 4.13 (ddd, *J* = 14.5, 7.1, 2.7 Hz, 2H), 3.94 (dt, *J* = 15.8, 11.0 Hz, 1H), 3.11 (dd, *J* = 23.5, 11.4 Hz, 1H), 1.36 – 1.19 (m, 10H).

**Synthesis of 17** Made analogously to **14** on a 2.30 mmol scale to give a yellow oil (269 mg, 51%). $^1$H NMR (400 MHz, Chloroform-*d*) δ 7.38 – 7.27 (m, 3H), 7.25 – 7.20 (m, 2H), 6.90 (d, *J* = 11.5 Hz, 1H), 6.28 (d, *J* = 3.4 Hz, 1H), 5.60 – 5.48 (m, 2H), 3.96 (dt, *J* = 10.0, 2.9 Hz, 1H), 1.37 (s, 3H), 1.32 (s, 3H).

**Synthesis of 18** In a dry RBF, **17** (227 mg, 1.00 mmol, 1 equiv) was dissolved in PhMe (91 mL) and cooled to 0 °C before TBHP (400 μL, 1.95 mmol, 1.95 equiv) and Triton B (152 μL, 330 μmol mmol, 0.33 equiv) were added. After 1 hr, the contents were quenched with sat. aq. $NH_4Cl$ and extracted with EtOAc (3x). The combined organic layers were dried over $Na_2SO_4$, filtered, and concentrated. The obtained residue was purified by chromatography with 20% EtOAc/hexanes to obtain a pale-orange solid (109 mg, 45%). $^1$H NMR (600 MHz, Chloroform-*d*) δ 7.35 (t, *J* = 7.4 Hz, 2H), 7.29 (t, *J* = 7.4 Hz, 1H), 7.25 (s, 2H), 6.89 (d, *J* = 11.5 Hz, 1H), 5.46 (t, *J* = 11.1 Hz, 1H), 3.77 (d, *J* = 10.7 Hz, 1H), 3.15 (d, *J* = 6.1 Hz, 1H), 3.11 (d, *J* = 6.1 Hz, 1H), 1.46 (s, 3H), 1.39 (s, 3H).

**Scheme B.8** Synthesis of **19**

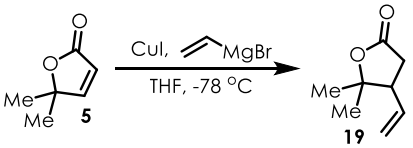


**Synthesis of 19** CuI (27.6 mg, 145 μmol, 0.58 equiv) was suspended in THF (810 μL) and cooled to -78 °C. Vinyl magnesium bromide (1.0 M, 750 μL, 750 μmol, 3 equiv) was added and contents stirred for 30 min before adding **5** (27.0 μL, 250 μmol, 1 equiv) as a solution in THF (930 μL). After 1 hr, the reaction was quenched with sat. aq. $NH_4Cl$, extracted with $Et_2O$ (3x), and the combined organic layers were washed with brine and dried over $MgSO_4$. Filtration and concentration gave a residue which was purified by chromatography with 30% EtOAc/hexanes to give a yellow oil (11 mg, 31%). $^1$H NMR (600 MHz, Chloroform-*d*) δ 5.70 (ddd, *J* = 16.9, 10.4, 8.0 Hz, 1H), 5.18 – 5.13 (m, 2H), 2.86 (dt, *J* = 11.3, 8.1 Hz, 1H), 2.61 (dd, *J* = 17.5, 8.2 Hz, 1H), 2.54 (dd, *J* = 17.5, 11.3 Hz, 1H), 1.42 (s, 3H), 1.21 (s, 3H).

**Scheme B.9** Synthesis of **20-21**

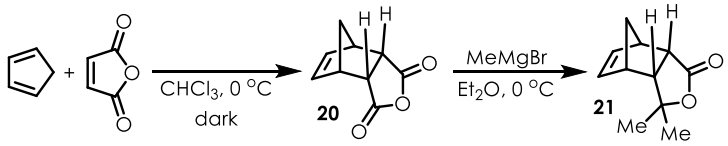


**Synthesis of 20** Maleic anhydride (24.5 g, 250 mmol, 1 equiv) was dissolved in $CHCl_3$ (147 mL) and cooled to 0 °C. In the dark, dicyclopentadiene was cracked and a portion (23.5 mL, 280 mmol, 1.1 equiv) was slowly added to the reaction vessel. The contents were stirred for 5 hrs, then concentrated down to a white solid. Recrystallization of the crude product from MeOH afforded colorless crystals (34.6 g, 84%). $^1$H NMR (400 MHz, Chloroform-*d*) δ 6.34 (s, 3H), 6.34 (d, *J* = 3.9 Hz, 2H), 3.65 – 3.49 (m, 10H), 1.81 (dt, *J* = 9.0, 1.7 Hz, 3H), 1.61 (s, 1H).

**Synthesis of 21** In a dry flask, **20** (20.0 g, 122 mmol, 1 equiv) was dissolved in $Et_2O$ (349 mL) and cooled to 0 °C before MeMgBr (3.0 M, 120 mL, 365 mmol, 3 eq) was added dropwise. The mixture was stirred for 16 hr and gradually warmed to room temperature. The contents were then cooled back to 0 °C before they were acidified with 2 N HCl. After stirring for 1 hr, the contents were extracted with EtOAc 3x and the combined organic layers were washed with 2 N HCl, sat. aq. $NaHCO_3$, brine, then dried over $MgSO_4$, filtered, and concentrated down to a light-yellow oil, which solidifies upon sitting (19.8 g, 91%). $^1$H NMR (400 MHz, Chloroform-*d*) δ 6.23 (d, *J* = 8.3 Hz, 2H), 3.46 (dd, *J* = 8.8, 5.1 Hz, 1H), 3.27 (ddt, *J* = 5.1, 2.7, 1.4 Hz, 1H), 3.07 – 2.98 (m, 1H), 2.72 (dd, *J* = 8.8, 3.7 Hz, 1H), 1.62 (dt, *J* = 8.4, 1.6 Hz, 1H), 1.42 (s, 1H), 1.37 (s, 3H), 1.35 (s, 3H). $^{13}$C NMR (151 MHz, $CDCl_3$) δ 177.55, 136.09, 134.42, 84.13, 77.16, 52.79, 49.08, 45.37, 45.31, 32.48, 23.77. HRMS calculated (M+Na): 201.0886; found: 201.0886.

**Scheme B.10** Synthesis of **22-24**

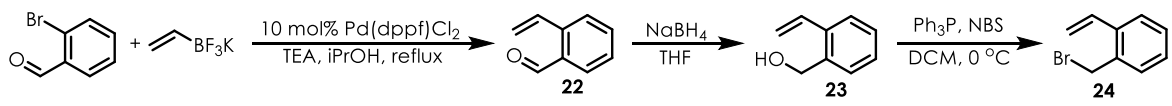

**Synthesis of 22** To a dry flask was added 2-bromobenzaldehyde (1.75 mL, 15.0 mmol, 1 equiv), triethylamine (6.20 mL, 45.0 mmol, 3 equiv), and iPrOH (150 mL). After sparging the solution with nitrogen for 1 hr, it solution was cannulated into a dry 2-neck flask fitted with a reflux condenser containing $Pd(dppf)Cl_2$ (1.10 g, 1.50 mmol, 10 mol%) and potassium vinyltrifluoroborate (4.02 g, 30.0 mmol, 2 equiv). The solution was then heated to reflux for 16 hr. The following day, the contents were cooled to room temperature and concentrated. The resultant residue was filtered through a silica plug with 4:1 hexanes:ether and the filtrate was concentrated to a red oil (1.61 g, 81%). $^1$H NMR (600 MHz, Chloroform-*d*) δ 10.30 (s, 1H), 7.84 (d, *J* = 7.6 Hz, 1H), 7.60 – 7.56 (m, 2H), 7.56 – 7.51 (m, 1H), 7.47 – 7.42 (m, 1H), 5.71 (d, *J* = 17.4 Hz, 1H), 5.52 (d, *J* = 11.0 Hz, 1H).

**Synthesis of 23** To a dry flask was added $NaBH_4$ (461 mg, 12.2 mmol, 1 equiv) and THF (24 mL). To this suspension was slowly added a solution of **22** (1.61 g, 12.2 mmol, 1 equiv) in THF (12 mL). After 1.5 hr, the reaction was quenched with 2 N HCl and extracted with DCM 3x. The combined organic layers were washed with brine then dried over $MgSO_4$. Filtration and concentration afforded an orange oil (1.56 g, 95%). $^1$H NMR (600 MHz, Chloroform-*d*) δ 7.57 – 7.52 (m, 1H), 7.36 (dd, *J* = 7.2, 1.3 Hz, 1H), 7.33 – 7.26 (m, 2H), 7.06 (dd, *J* = 17.4, 11.0 Hz, 1H), 5.71 (dd, *J* = 17.4, 1.2 Hz, 1H), 5.37 (dd, *J* = 11.0, 1.2 Hz, 1H), 4.76 (d, *J* = 4.0 Hz, 2H), 1.67 (s, 1H).

**Synthesis of 24** In a flask, **23** (4.07 g, 30.3 mmol, 1 equiv) was dissolved in DCM (152 mL) and cooled to 0 $^o$C. Triphenylphosphine (9.55 g, 36.4 mmol, 1.2 equiv) was added in one portion and the contents were stirred for 10 min, NBS (6.48 g, 36.4 mmol, 1.2 equiv) was then added in 5 portions over 5 min. After an additional 1 hr of stirring, the reaction was concentrated and purified by chromatography with 10% EtOAc/hexanes to give a yellow oil (4.92 g, 82%). $^1$H

NMR (400 MHz, Chloroform-*d*) δ 7.52 (d, *J* = 7.9 Hz, 1H), 7.35 – 7.28 (m, 2H), 7.27 – 7.21 (m, 1H), 7.10 (dd, *J* = 17.3, 11.0 Hz, 1H), 5.76 (dd, *J* = 17.3, 1.2 Hz, 1H), 5.44 (dd, *J* = 11.0, 1.2 Hz, 1H), 4.57 (s, 2H).

**Scheme B.11** Synthesis of **25-27**

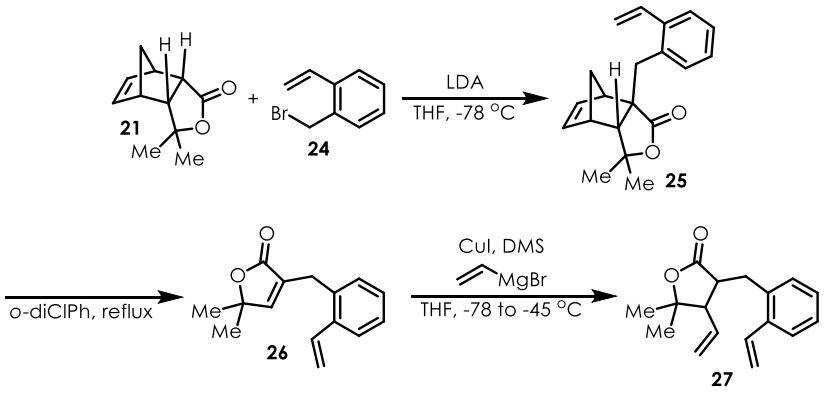


**Synthesis of 25** To a dry flask was added DIPA (1.00 mL, 7.10 mmol, 1.2 equiv) and THF (10 mL). After cooling this solution to -78 °C, *n*-BuLi (2.5 M soln, 2.6 mL, 6.5 mmol, 1.1 equiv) was added dropwise. The contents were stirred for 15 min before a solution **21** (1.05 g, 5.90 mmol, 1 equiv) in THF (2 mL) was added. After another 30 min of stirring, **24** (1.40 g, 7.1 mmol, 1.2 equiv) was added. After 3 hrs at -78 °C, the solution was quenched with sat. aq. $NH_4Cl$ and the aqueous layer extracted with EtOAc (3x). The combined organic layers were washed with brine, dried over $MgSO_4$, filtered, and concentrated down to an off-white solid (1.56 g, 90%). $^1$H NMR (400 MHz, Chloroform-*d*) δ 7.53 (d, *J* = 7.6 Hz, 1H), 7.24 (d, *J* = 5.3 Hz, 3H), 7.17 – 7.07 (m, 1H), 6.35 – 6.23 (m, 2H), 5.69 (d, *J* = 17.3 Hz, 1H), 5.38 (d, *J* = 10.9 Hz, 1H), 3.51 (d, *J* = 14.1 Hz, 1H), 3.24 (s, 1H), 2.99 (s, 2H), 2.65 (d, *J* = 3.7 Hz, 1H), 1.62 (d, *J* = 8.7 Hz, 1H), 1.50 (d, *J* = 8.7 Hz, 1H), 1.26 (s, 3H), 0.55 (s, 3H). $^{13}$C NMR (151 MHz, $CDCl_3$) δ 179.80, 137.61, 137.38, 135.84, 135.63, 135.23, 131.76, 128.46, 127.64, 126.59, 116.74, 83.60, 77.16, 63.13, 53.40, 53.00, 51.27, 46.76, 38.96, 30.25, 24.75. HRMS calculated (M+Na): 317.1512; found: 317.1511.

**Synthesis of 26** A solution of **25** (1.52 g, 5.40 mmol, 1 eq) in *o*-dichlorobenzene (38 mL) was sparged with nitrogen for 1 hr before it was heated to reflux (180 $^{o}$C) for 16 hr. After cooling the contents to room temperature, they were filtered through a silica plug using hexanes (to remove solvent) followed by ethyl acetate. The ethyl acetate filtrate was concentrated down, affording a yellow oil (1.09 g, 88%). $^{1}$H NMR (400 MHz, Chloroform-*d*) δ 7.57 – 7.50 (m, 1H), 7.31 – 7.22 (m, 3H), 7.21 – 7.15 (m, 1H), 6.79 (dd, *J* = 17.3, 11.0 Hz, 1H), 6.55 (t, *J* = 1.8 Hz, 1H), 5.64 (dd, *J* = 17.3, 1.0 Hz, 1H), 5.28 (dd, *J* = 11.0, 1.0 Hz, 1H), 3.61 (d, *J* = 1.6 Hz, 2H), 1.38 (s, 6H). $^{13}$C NMR (151 MHz, $CDCl_3$) δ 172.79, 155.06, 136.82, 134.90, 134.25, 131.97, 130.38, 128.19, 127.48, 126.15, 116.27, 84.81, 77.16, 29.41, 25.63. HRMS calculated (M+Na): 251.1042; found: 251.1042.

**Synthesis of 27** A suspension of CuI (1.36 g, 7.16 mmol, 1.5 equiv) in THF (48 mL) was cooled to -78 $^{o}$C before vinyl magnesiumbromide (1.0 M, 14 mL, 14 mmol, 3 equiv) was added. After stirring for 10 min, dimethylsulfide (351 μL, 4.77 mmol, 1 equiv) was added to the solution. Once 90 min had passed, a solution of **26** (1.09 g, 4.77 mmol, 1 equiv) in THF (48 mL) was added via cannula. The solution was then warmed to -45 $^{o}$C and stirred for 5 hr before quenching it with sat. aq. $NH_4Cl$. The aqueous layer was extracted with EtOAc (3x) and the combined organic layers were washed with brine and dried over $MgSO_4$. Filtration and concentration followed by chromatography with 10% acetone/hexanes gave a yellow oil (765 mg, 65%). $^{1}$H NMR (400 MHz, Chloroform-*d*) δ 7.47 – 7.41 (m, 1H), 7.24 – 7.12 (m, 3H), 6.98 (dd, *J* = 17.3, 10.9 Hz, 1H), 5.64 (dd, *J* = 17.3, 1.3 Hz, 1H), 5.43 – 5.33 (m, 1H), 5.31 (dd, *J* = 10.9, 1.4 Hz, 1H), 4.95 (d, *J* = 3.9 Hz, 1H), 4.92 (s, 1H), 3.35 (dd, *J* = 13.9, 5.2 Hz, 1H), 2.93 – 2.84 (m, 1H), 2.80 (dd, *J* = 13.9, 7.7 Hz, 1H), 2.54 (dd, *J* = 11.6, 8.9 Hz, 1H), 1.37 (s, 3H), 1.18 (s, 3H). $^{13}$C NMR (151 MHz, $CDCl_3$) δ 176.73, 136.84, 135.66, 134.63, 133.40, 131.02, 127.61, 127.02,

125.80, 119.15, 116.08, 84.35, 77.16, 56.70, 45.56, 32.66, 26.93, 22.68. HRMS calculated (M+Na): 279.1355; found: 279.1354.

**Scheme B.12** Synthesis of **28-29**

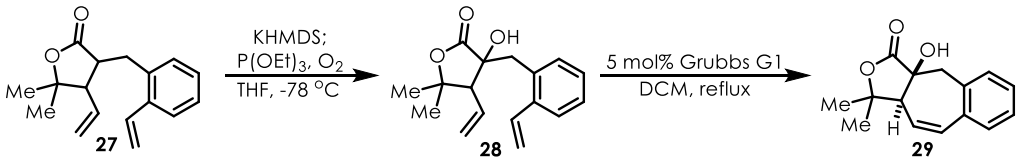


**Synthesis of 28** A solution of **27** (205 mg, 800 μmol, 1 equiv) in THF (2.4 mL) was cooled to -78 °C before KHMDS (0.5 M, 2.1 mL, 1.1 mmol, 1.3 equiv) was added. After stirring this mixture for 30 min at -78 °C and 1 hr at 0 °C, triethylphosphite (275 μL, 1.6 mmol, 2 equiv) was added and the nitrogen atmosphere replaced with oxygen at -78 °C. After 3.5 hr, the mixture was quenched with sat. aq. $NH_4Cl$ and extracted with EtOAc (4x). The combined organic layers were washed with brine, dried over $MgSO_4$ and concentrated to a yellow oil (61 mg, 28%). $^1$H NMR (600 MHz, Chloroform-*d*) δ 7.51 (d, *J* = 7.7 Hz, 1H), 7.31 (d, *J* = 7.5 Hz, 1H), 7.26 – 7.19 (m, 2H), 7.04 (dd, *J* = 17.3, 10.9 Hz, 1H), 5.87 (dt, *J* = 17.2, 9.9 Hz, 1H), 5.65 (d, *J* = 17.3 Hz, 1H), 5.32 (d, *J* = 10.9 Hz, 1H), 5.22 (dd, *J* = 10.2, 1.4 Hz, 1H), 5.11 (dd, *J* = 17.3, 1.6 Hz, 1H), 3.16 (d, *J* = 3.2 Hz, 1H), 2.52 (d, *J* = 9.5 Hz, 1H), 2.30 (s, 1H), 1.38 (s, 3H), 1.26 (s, 3H). $^{13}$C NMR (151 MHz, $CDCl_3$) δ 177.17, 138.18, 135.38, 131.98, 131.88, 130.08, 127.96, 127.71, 126.20, 121.19, 116.48, 86.41, 78.82, 77.16, 56.85, 39.00, 27.54, 24.26. HRMS calculated (M+Na): 295.1305; found: 295.1303.

**Synthesis of 29** Dissolved **28** (61.0 mg, 223 μmol, 1 equiv) in DCM (46 mL) and sparged the solution with nitrogen for 1 hr before adding Grubb's G1 catalyst (9.20 mg, 11.2 μmol, 5 mol%). The solution was refluxed for 16 hr, then cooled to RT and eluted through a silica plug with DCM. The filtrate was concentrated and purified by chromatography with15% acetone/hexanes to give a white solid (19.0 mg, 35%). $^1$H NMR (600 MHz, Chloroform-*d*) δ 7.26 – 7.21 (m, 4H),

6.59 (d, *J* = 14.9 Hz, 1H), 5.58 (d, *J* = 14.3 Hz, 1H), 3.60 (d, *J* = 17.2 Hz, 1H), 3.41 (d, *J* = 17.2 Hz, 1H), 3.14 (s, 1H), 2.34 (s, 1H), 1.60 (s, 3H), 1.54 (s, 3H). $^{13}$C NMR (151 MHz, $CDCl_3$) δ 175.17, 134.44, 134.38, 133.91, 133.01, 132.37, 128.71, 127.28, 120.37, 85.18, 77.16, 73.31, 56.44, 44.75, 28.61, 23.49. HRMS calculated (M+Na): 267.0992; found: 267.0990.

**Scheme B.13** Synthesis of **30-31**

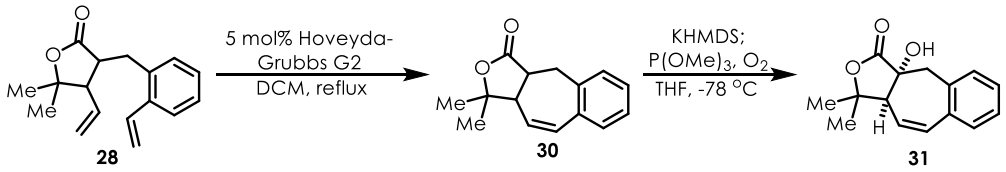


**Synthesis of 30** Dissolved **28** (100 mg, 390 μmol, 1 equiv) in DCM (32 mL) and sparged the solution with nitrogen for 1 hr before heating to reflux. Once reflux was achieved, a solution of Hoveyda-Grubbs G2 catalyst (12.2 mg, 19.5 μmol, 5 mol%) in DCM (2 mL) was added. After 4 hr, the contents were cooled to RT, filtered through a silica plug with DCM and the filtrate concentrated. The resultant residue was purified via chromatography with 10% acetone/hexanes to obtain a light pink oil (74 mg, 83%). $^{1}$H NMR (600 MHz, Chloroform-*d*) δ 7.24 – 7.14 (m, 4H), 6.45 (d, *J* = 12.3 Hz, 1H), 5.64 (d, *J* = 12.1 Hz, 1H), 3.52 (d, *J* = 16.3 Hz, 1H), 3.15 (dt, *J* = 16.3, 5.7 Hz, 1H), 3.05 (d, *J* = 6.4 Hz, 2H), 1.56 (s, 3H), 1.32 (s, 3H). $^{13}$C NMR (151 MHz, $CDCl_3$) δ 175.98, 136.99, 134.38, 134.31, 133.76, 130.96, 128.15, 126.98, 124.19, 83.78, 77.16, 55.24, 42.22, 36.41, 27.30, 21.63. HRMS calculated (M+Na): 251.1042; found: 251.1042.

**Synthesis of 31** KHMDS (0.5 M, 1.9 mL, 945 μmol, 1.3 equiv) was added to a dry flask and cooled to -78 $^{o}$C before adding a solution of **30** (166 mg, 727 μmol, 1 equiv) in THF (2.2 mL). After stirring the solution for 30 min at -78$^{o}$C and 30 min at 0 $^{o}$C, trimethyl phosphite (172 μL, 1.45 mmol, 2 equiv) and the nitrogen atmosphere replaced with $O_2$ at -78 $^{o}$C. After stirring the mixture for 30 min, it was quenched with sat. aq. $NH_4Cl$ and extracted aqueous with EtOAc (4x). The combined organic layers were washed with brine and dried over $MgSO_4$. Filtration and

concentration gave a residue which was purified via column chromatography with 15% aceton/hexanes to give a white solid (100 mg, 56%). $^{1}$H NMR (400 MHz, Chloroform-*d*) δ 7.32 (dd, *J* = 8.4, 3.8 Hz, 1H), 7.27 (d, *J* = 4.3 Hz, 3H), 6.71 (dd, *J* = 12.4, 2.4 Hz, 1H), 5.75 (dd, *J* = 12.4, 3.6 Hz, 1H), 3.15 (s, 2H), 3.05 (s, 1H), 2.33 (s, 1H), 1.64 (s, 3H), 1.42 (s, 3H). $^{13}$C NMR (151 MHz, $CDCl_3$) δ 178.27, 135.38, 133.64, 131.75, 131.28, 130.76, 127.97, 127.72, 125.00, 84.21, 78.60, 77.16, 56.94, 42.13, 29.85, 25.49. HRMS calculated (M+Na): 267.0992; found: 267.0990.

**Scheme B.14** Synthesis of **32**

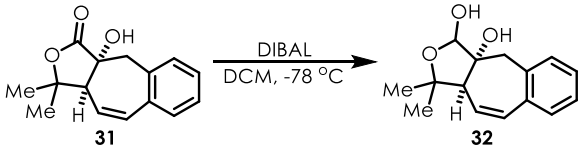


**Synthesis of 32** A solution of **31** (141 mg, 577 μmol, 1 equiv) in DCM (3.9 mL) was cooled to -78 °C before adding DIBAL (1.0 M, 1.4 mL, 1.4 mmol, 2.5 equiv). After stirring the mixture for 2 hr, it was quenched with 2 N HCl at -78 °C and extracted with EtOAc (3x). The combined organic layers were washed with brine, dried over $Na_2SO_4$, filtered, and concentrated. The obtained residue purified with 40% EtOAc/hexanes to give a white solid (100 mg, 70%). $^{1}$H NMR (600 MHz, Chloroform-*d*) δ 7.31 – 7.27 (m, 1H), 7.23 (d, *J* = 17.5 Hz, 3H), 6.61 (dd, *J* = 12.4, 2.2 Hz, 1H), 5.73 (dd, *J* = 12.4, 3.9 Hz, 1H), 5.05 (d, *J* = 6.2 Hz, 1H), 3.63 (d, *J* = 6.3 Hz, 1H), 3.10 (d, *J* = 13.9 Hz, 1H), 2.92 (d, *J* = 13.9 Hz, 1H), 2.78 (s, 1H), 2.26 (s, 1H), 1.51 (s, 3H), 1.22 (s, 3H). $^{13}$C NMR (151 MHz, $CDCl_3$) δ 135.96, 134.78, 131.27, 130.50, 129.93, 127.55, 127.53, 127.36, 101.14, 82.87, 82.07, 77.16, 58.92, 42.89, 31.48, 25.81. HRMS calculated (M+Na): 269.1148; found: 269.1147.

**Scheme B.15** Synthesis of **33-35**

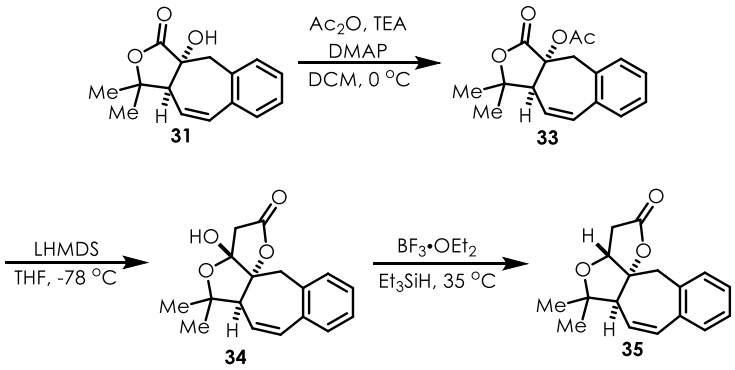


**Synthesis of 33** Dissolved **31** (115 mg, 471 μmol, 1 equiv) and DMAP (34.5 mg, 282 μmol, 0.6 equiv) in DCM (4.7 mL) and cooled to 0 °C before adding $Ac_2O$ (133 μL, 1.41 mmol, 3 equiv) and TEA (650 μL, 4.71 mmol, 10 equiv). After 2 hr, the contents were quenched with sat. aq. $NH_4Cl$ and extracted with EtOAc (3x). The combined organic layers were washed with brine and dried over $Na_2SO_4$. Filtration and concentration gave a residue that was by chromatography with 10% acetone/hexanes to yield a white solid (120 mg, 89%). $^1$H NMR (600 MHz, Chloroform-*d*) δ 7.33 – 7.21 (m, 4H), 6.68 (dd, *J* = 12.5, 2.4 Hz, 1H), 5.67 (dd, *J* = 12.5, 3.8 Hz, 1H), 3.62 – 3.50 (m, 1H), 3.28 (d, *J* = 14.0 Hz, 1H), 3.10 (d, *J* = 13.9 Hz, 1H), 1.89 (s, 3H), 1.68 (s, 3H), 1.42 (s, 3H). $^{13}$C NMR (151 MHz, $CDCl_3$) δ 174.15, 170.27, 134.98, 133.98, 131.50, 130.94, 130.16, 127.78, 127.34, 124.86, 84.41, 83.82, 77.16, 52.09, 40.93, 29.42, 26.27, 21.02. HRMS calculated (M+Na) 309.1097; found: 309.1096.

**Synthesis of 34** A solution of **33** (93.0 mg, 325 μmol, 1 equiv) in THF (11.2 mL) was cooled to -78 °C before LiHMDS (1.0 M, 810 μL, 810 μmol, 2.5 equiv) was added slowly. After 1 hr, the mixture was quenched with sat. aq. $NH_4Cl$ and extracted with EtOAc (3x). The organic layers were washed with brine, dried over $Na_2SO_4$, filtered, and concentrated to give a residue which was purified by chromatography with 15% acetone/hexanes to yield a white solid (75.0 mg, 81%). $^1$H NMR (600 MHz, Chloroform-*d*) δ 7.28 (d, *J* = 8.9 Hz, 1H), 7.19 (dq, *J* = 16.7, 7.5 Hz,

3H), 6.68 (dd, *J* = 12.0, 2.8 Hz, 1H), 5.76 (dd, *J* = 12.0, 3.1 Hz, 1H), 3.23 (d, *J* = 14.2 Hz, 1H), 3.07 – 2.99 (m, 2H), 2.97 – 2.89 (m, 2H), 2.74 (s, 1H), 1.42 (s, 3H), 1.40 (s, 3H). $^{13}$C NMR (151 MHz, $CDCl_3$) δ 172.31, 135.75, 134.51, 131.27, 131.09, 129.18, 127.66, 127.19, 126.34, 107.96, 104.82, 86.40, 77.16, 58.57, 43.50, 39.58, 29.92, 26.43. HRMS calculated (M+Na): 309.1097; found 309.1095.

**Synthesis of 35** A mixture of **34** (53 mg, 185 μmol, 1 equiv), DCM (1 mL), and $Et_3SiH$ (440 μL, 2.78 mmol, 15 equiv) was prepared the addition of $BF_3{\cdot}OEt_2$ (293 μL, 2.31 mmol, 12.5 equiv). The contents were heated to 35 °C for 16 hr, then cooled to RT and quenched with sat. aq. $NaHCO_3$. The aqueous layer was extracted with DCM (3x) and the combined organic layers were washed with brine, dried over $Na_2SO_4$, filtered, and concentrated. The obtained residue was purified with chromatography using 10% acetone/hexanes to give a colorless oil, which solidified upon standing (19.0 mg, 38%). $^1$H NMR (600 MHz, Pyridine-$d_5$) δ 7.32 (dq, *J* = 7.7, 4.3 Hz, 1H), 7.25 (d, *J* = 18.6 Hz, 4H), 6.72 (dd, *J* = 12.1, 2.0 Hz, 1H), 5.78 (dd, *J* = 12.1, 4.4 Hz, 1H), 4.42 (d, *J* = 6.0 Hz, 1H), 3.23 – 3.12 (m, 2H), 3.04 (d, *J* = 13.7 Hz, 1H), 2.97 (s, 1H), 2.83 (d, *J* = 18.3 Hz, 1H), 1.38 (s, 3H), 1.07 (s, 3H). $^{13}$C NMR (151 MHz, Pyridine-$d_5$) δ 175.11, 150.35, 137.33, 135.08, 131.72, 131.53, 130.10, 128.21, 128.01, 103.24, 85.55, 79.91, 60.70, 41.96, 36.43, 30.40, 29.09, 22.74. HRMS calculated (M+Na): 293.1148; found 293.1146.

**Scheme B.16** Synthesis of **36** and **35**

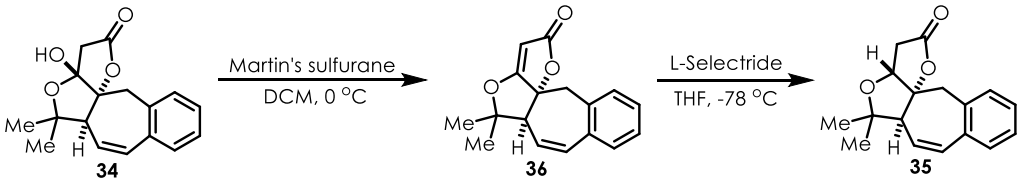


**Synthesis of 36** A solution of **34** (98.3 mg, 343 μmol, 1 equiv) in DCM (11.5 mL) was prepared and cooled to 0 °C before the addition of Martin's sulfurane (346 mg, 515 μmol, 1.5 equiv).

After 1 hr, the reaction was quenched with sat. aq. $NH_4Cl$ and extracted with EtOAc (3x). The combined organic layers were washed with brine, dried over $Na_2SO_4$, filtered, and concentrated. The resultant residue was purified with chromatography using 30% EtOAc/hexanes to obtain a white solid (76.0 mg, 83%). $^1$H NMR (600 MHz, Chloroform-*d*) δ 7.28 (d, *J* = 6.7 Hz, 1H), 7.24 – 7.19 (m, 2H), 7.16 (d, *J* = 7.4 Hz, 1H), 6.70 (dd, *J* = 12.3, 1.9 Hz, 1H), 5.61 (dd, *J* = 12.3, 3.8 Hz, 1H), 5.02 (s, 1H), 3.44 (d, *J* = 13.7 Hz, 1H), 2.94 – 2.85 (m, 2H), 1.65 (s, 3H), 1.61 (s, 3H). $^{13}$C NMR (151 MHz, $CDCl_3$) δ 187.42, 173.79, 135.24, 134.16, 132.45, 131.33, 131.05, 128.34, 127.42, 123.22, 102.19, 87.89, 87.01, 77.16, 54.02, 44.19, 31.35, 25.98. HRMS calculated (M+Na): 291.0992; found: 291.0989.

**Synthesis of 35** A solution of **34** (70.0 mg, 261 μmol, 1 equiv) in THF (4.7 mL) was cooled to -78 °C before adding L-selectride (1.0 M, 780 μL, 780 μmol, 3 equiv). After 15 min, the reaction was quenched with sat. aq. $NH_4Cl$, extracted with EtOAc (3x). The combined organic layers were washed with brine, dried over $Na_2SO_4$, filtered, and concentrated. Purification of the obtained residue with chromatography using 30% EtOAc/hexanes gave a white solid (53.0 mg, 75%). $^1$H NMR (600 MHz, Pyridine-$d_5$) δ 7.32 (dq, *J* = 7.7, 4.3 Hz, 1H), 7.25 (d, *J* = 18.6 Hz, 4H), 6.72 (dd, *J* = 12.1, 2.0 Hz, 1H), 5.78 (dd, *J* = 12.1, 4.4 Hz, 1H), 4.42 (d, *J* = 6.0 Hz, 1H), 3.23 – 3.12 (m, 2H), 3.04 (d, *J* = 13.7 Hz, 1H), 2.97 (s, 1H), 2.83 (d, *J* = 18.3 Hz, 1H), 1.38 (s, 3H), 1.07 (s, 3H). $^{13}$C NMR (151 MHz, Pyr) δ 175.11, 150.35, 137.33, 135.08, 131.72, 131.53, 130.10, 128.21, 128.01, 103.24, 85.55, 79.91, 60.70, 41.96, 36.43, 30.40, 29.09, 22.74. HRMS calculated (M+Na): 293.1148; found 293.1146.

### B.2.2 Progress Toward the Synthesis of the Eastern Half of Rubriflordilactone B

**Scheme B.17** Synthesis of **37**

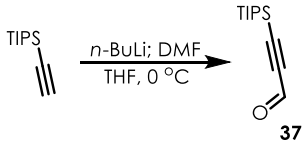


**Synthesis of 37** A solution of TIPS-acetylene (3.40 mL, 15.0 mmol, 1 equiv) and THF (25 mL). was cooled to 0 °C before *n*-BuLi (1.6 M, 10 mL, 16 mmol, 1.1 equiv) was added dropwise; after stirring for 1 hr, DMF (2.20 mL, 30.0 mmol, 2 equiv) was added to the solution. After 1.5 hrs, the contents were poured into a 1:1 mixture of 10% $KH_2PO_4$:$Et_2O$ (82 mL) and stirred vigorously for 30 min before transferring to a separatory funnel. The aqueous layer was extracted with $Et_2O$ (3x) and the combined organic layers were washed with water and brine. The combined organic layers were dried over $MgSO_4$ and concentrated down to an oil which was filtered through a silica plug with DCM, and the filtrate concentrated to a pale-yellow oil (2.96 g, 94%). $^1$H NMR (400 MHz, Chloroform-*d*) δ 9.20 (s, 1H), 1.11 (s, 22H).

**Scheme B.18** Synthesis of **38-41**

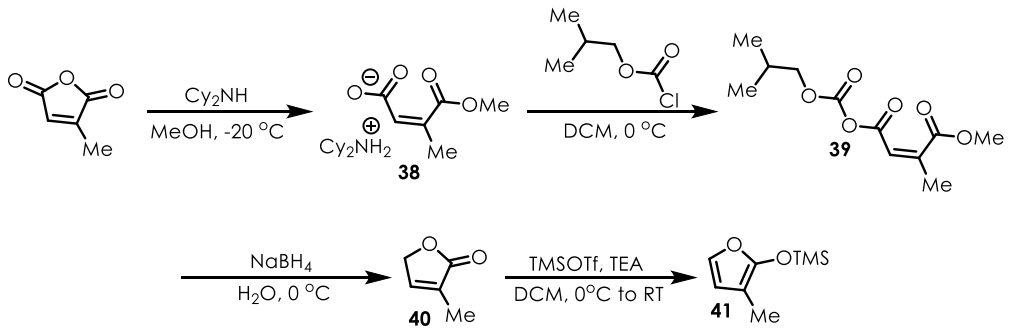


**Synthesis of 38** To a flame-dried flask containing methanol (180 mL) cooled to -20 °C was slowly added citraconic anhydride (25.0 g, 223 mmol, 1 equiv) via an addition funnel. After stirring for 45 min, dicyclohexylamine (49.0 mL, 245 mmol, 1.1 equiv) was added dropwise via a separate addition funnel. The cooling bath was removed and the solution stirred for an

additional 2 hr at room temperature before being concentrated. The resultant off-white solid was suspended in ethyl acetate (156 mL) and stirred vigorously for 1 hr before filtering off the solid and washing it with additional ethyl acetate (62.3 g, 86%).

**Synthesis of 39** Within a dry flask, **38** (62.3 g, 191 mmol, 1 equiv) was dissolved in DCM (144 mL) and cooled to 0 $^{o}$C. Isobutyl chloroformate (27.3 mL, 211 mmol, 1.1 equiv) was added dropwise and the solution was allowed to stir for 3 hr and gradually warm to room temperature, during which time a very thick slurry formed. The following day, THF (182 mL) was added and the flask was placed in the freezer for an hour before the solid was filtered off and washed with additional THF while keeping the filtrate at 0 $^{o}$C. The filtrate was used directly in the next reaction.

**Synthesis of 40** To the cooled filtrate containing **39** (approx. 191 mmol) was added $NaBH_4$ (14.5 g, 382 mmol, 2 equiv) as a solution in water (29 mL). This addition must be done very slowly, as there is a brief induction period before hydrogen gas begins to form. Once all the $NaBH_4$ was added, the mixture was stirred for an additional 2 hr. The contents were filtered, concentrated, suspended in $Et_2O$, and filtered again. The filtrate was dried over $MgSO_4$, filtered, and concentrated once again to a pale-yellow oil. Distillation of this material afforded a clear/colorless oil (14.2 g, 76% over 2 steps). $^{1}$H NMR (400 MHz, Chloroform-*d*) δ 7.13 (q, *J* = 1.6 Hz, 1H), 4.75 (p, *J* = 2.1 Hz, 2H), 1.93 (q, *J* = 2.1 Hz, 3H).

**Synthesis of 41** To a flame-dried flask was added **40** (2.60 mL, 30.0 mmol, 1 equiv), TEA (5.00 mL, 36.0 mmol, 1.2 equiv) and DCM (60 mL). After cooling the solution to 0 $^{o}$C, TMSOTf (5.42 mL, 30.0 mmol, 1 equiv) was added and the contents stirred at 0 $^{o}$C for 60 min and room temperature for 30 min before diluting with pentanes (120 mL). Contents were transferred to a separatory funnel and washed with pH 7 aq. phosphate buffer (60 mL), 0.5 M aq. $CuSO_4$ (60

mL) and brine (2x) (60 mL). The organic layer was dried over $Na_2SO_4$, filtered, and concentrated at 200 mbar and room temperature; distillation of the obtained residue afforded a clear and colorless liquid (3.32 g, 65%). $^1$H NMR (400 MHz, Chloroform-*d*) δ 6.76 (d, *J* = 2.2 Hz, 1H), 6.10 (d, *J* = 2.1 Hz, 1H), 1.82 (s, 3H), 0.27 (s, 9H).

**Scheme B.19** Synthesis of **42-45**

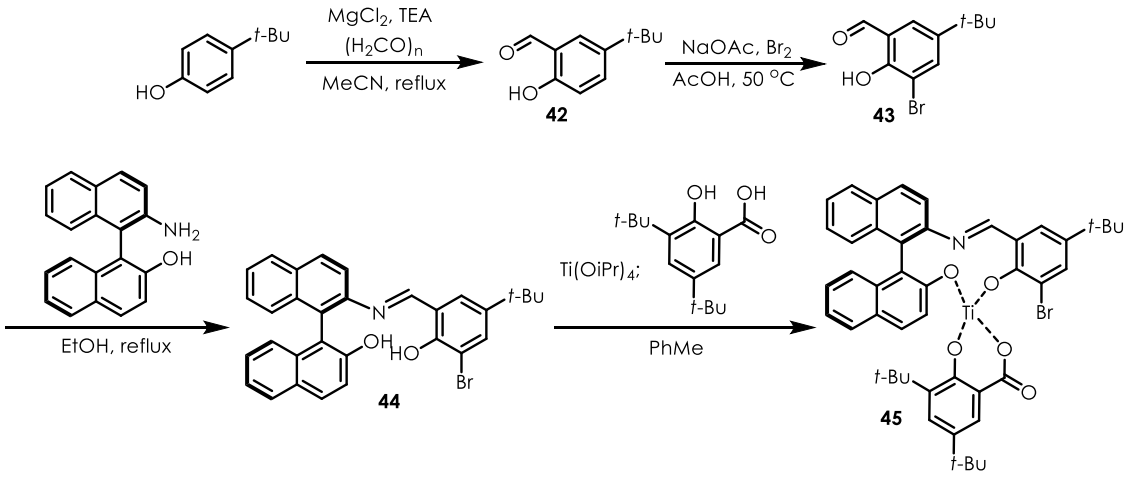


**Synthesis of 42** To a dry flask was added 4-*tert*-butylphenol (15.0 g, 100 mmol, 1 equiv), $MgCl_2$ (14.3 g, 150 mmol, 1.5 equiv), TEA (53.0 mL, 380 mmol, 3.8 equiv), paraformaldehyde (20.4 g, 680 mmol, 6.8 equiv) and MeCN (500 mL). The mixture was was heated to reflux for 3 hr, then cooled to room temperature and quenched with 2 N HCl. The aqueous layer was extracted with $Et_2O$, dried over $MgSO_4$, and concentrated down to a yellow oil (15.9 g, 89%). $^1$H NMR (400 MHz, Chloroform-*d*) δ 10.86 (s, 1H), 9.89 (s, 1H), 7.58 (dd, *J* = 8.7, 2.5 Hz, 1H), 7.51 (d, *J* = 2.5 Hz, 1H), 6.94 (d, *J* = 8.7 Hz, 1H), 1.33 (s, 10H).

**Synthesis of 43** NaOAc (6.70 g, 81.1 mmol, 1.83 equiv) and **42** (7.90 g, 44.3 mmol, 1 equiv) were taken up in AcOH (193 mL) before a mixture of $Br_2$ (2.30 mL, 44.3 mmol, 1 equiv) and AcOH (75 mL) was added dropwise via addition funnel. Once the addition was complete, the contents were heated to 50 °C for 16 hr. After cooling the contents to room temperature, the AcOH was removed under vacuum and the residue diluted with water and extracted with DCM.

The organic layers were combined, washed with sat. aq. $Na_2S_2O_3$, sat. aq. $NaHCO_3$, brine, and dried over $MgSO_4$. Filtration and concentration gave an oil which was purified using chromatography with 25% EtOAc/hexanes, yielding a tan solid (10.1 g, 89%). $^1$H NMR (400 MHz, Chloroform-*d*) δ 11.41 (s, 1H), 9.85 (s, 1H), 7.81 (d, *J* = 2.3 Hz, 1H), 7.51 (d, *J* = 2.3 Hz, 1H), 1.33 (s, 10H).

**Synthesis of 44** Combined **43** (517 mg, 2.00 mmol, 1.2 equiv) and (*R*)-NOBIN (485 mg, 1.70 mmol, 1 equiv) in EtOH (6 mL) and heated the mixture at reflux for 16 hr. After cooling the mixture to room temperature, it was concentrated, and the resultant residue purified with chromatography using 20% EtOAc/hexanes to give a bright orange solid (581 mg, 65%). $^1$H NMR (600 MHz, Chloroform-*d*) δ 12.50 (s, 1H), 8.57 (s, 1H), 8.12 (d, *J* = 8.8 Hz, 1H), 7.98 (d, *J* = 8.2 Hz, 1H), 7.93 (d, *J* = 8.9 Hz, 1H), 7.86 (d, *J* = 8.1 Hz, 1H), 7.61 (d, *J* = 8.8 Hz, 1H), 7.51 (s, 2H), 7.35 (d, *J* = 8.8 Hz, 3H), 7.32 – 7.27 (m, 1H), 7.22 – 7.18 (m, 1H), 7.15 (s, 1H), 6.97 (d, *J* = 8.4 Hz, 1H), 4.86 (s, 1H), 1.24 (s, 9H).

**Synthesis of 45** To a dry Schlenk flask was added **44** (116 mg, 220 μmol, 2.2 equiv), PhMe (13.2 mL) and Ti(O*i*-Pr)$_4$ (29.6 μL, 100 μmol, 1 equiv). After stirring the contents for 1 hr, a solution of 3,5-di-*tert*-butylsalicylic acid (50.8 mg, 200 μmol, 2 equiv) in PhMe (4.2 mL) was added. Once another hour had elapsed, the contents were dried under vacuum and used directly in the synthesis of **46**.

**Scheme B.20** Synthesis of **46-48**

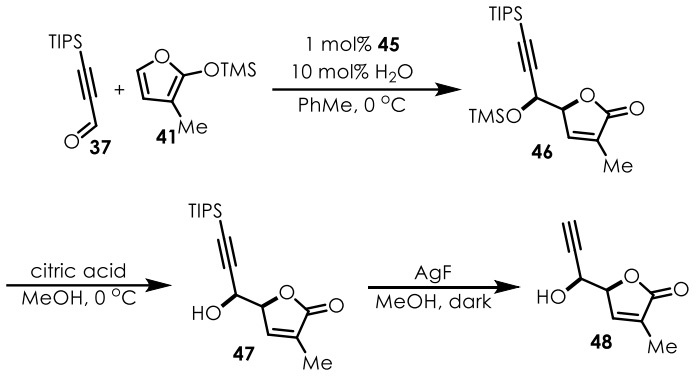


**Synthesis of 46** Complex **45** (approx. 100 μmol, 1 mol%) was dissolved in PhMe (46 mL) and cooled to 0 °C before **37** (2.36 mL, 10.0 mmol, 1 equiv), **41** (2.16 mL, 12.0 mmol, 1.2 equiv), and water (18.0 μL, 1.00 mmol, 10 mol%) were added. The contents were stirred overnight at 0 °C, then quenched with 10% aq. $NaHCO_3$. The aqueous layer was extracted with $Et_2O$ (3x) and the combined organic layers were dried over $MgSO_4$, filtered, and concentrated. The orange oil obtained was eluted through a silica plug with DCM, and the filtrate concentrated down to a yellow oil which was immediately used to make **47**.

**Synthesis of 47** Crude **46** (approx. 10.0 mmol, 1 equiv) was dissolved in MeOH (10 mL) and stirred with citric acid (2.11 g, 11.0 mmol, 1.1 equiv) for 10 min before it was diluted with water and extracted with $Et_2O$ (3x). The combined organic layers were washed with water and brine, then dried over $MgSO_4$ and filtered. The solvent was removed in vacuo and the residual oil purified by chromatography using 15% EtOAc/hexanes to obtain a yellow oil (1.81g, 59% over 2 steps, 9.7:1 d.r.). $^1$H NMR (400 MHz, Chloroform-*d*) δ 7.11 (s, 1H), 4.96 (d, *J* = 4.7 Hz, 1H), 4.52 (t, *J* = 5.2 Hz, 1H), 2.25 (d, *J* = 4.7 Hz, 1H), 1.96 (s, 3H), 1.06 (s, 21H).

**Synthesis of 48** Within a flask, **47** (1.81 g, 5.87 mmol, 1 equiv) was dissolved in MeOH (58.7 mL) and stirred with AgF (1.12 g, 8.80 mmol, 1.5 equiv) in the dark for 2 hrs. The contents were quenched with 2 N HCl and stirred for 10 min before pouring into a separatory funnel. The

aqueous layer was extracted with EtOAc (3x) and the combined organic layers were washed with brine and dried over $Na_2SO_4$. Filtration and concentration gave an oil that was purified by chromatography with 40% EtOAc/hexanes to yield a yellow oil (0.420 g, 47%, 15:1 d.r.). $^1$H NMR (400 MHz, Chloroform-*d*) δ 7.13 (p, *J* = 1.5 Hz, 1H), 5.00 – 4.94 (m, 1H), 4.45 (d, *J* = 5.8 Hz, 1H), 2.58 (s, 1H), 1.97 (t, *J* = 1.8 Hz, 3H).

**Scheme B.21** Synthesis of **49**-**50**

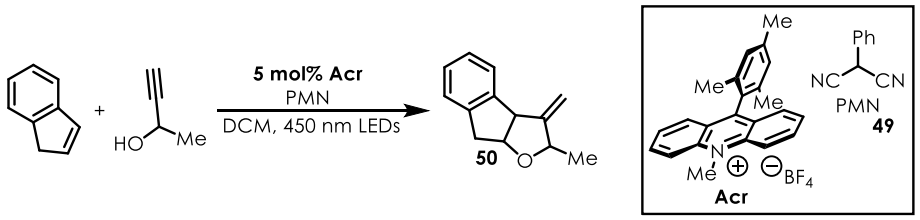


**Synthesis of 49** Malononitrile (4.90 g, 73.6 mmol, 2 equiv) was dissolved in DMSO (100 mL) and sparged with $N_2$ for 1 hr. This solution was then cannulated into a separate flask containing $K_2CO_3$ (20.3 g, 147 mmol, 4 equiv) and CuI (700 mg, 3.70 mmol, 10 mol%). Lastly, iodobenzne (4.10 mL, 36.8 mmol, 1 equiv) was added before the contents were heated to 120 $^o$C for 16 hr. After cooling to RT, the mixture was quenched with 2 N HCl, and extracted with $Et_2O$ (3x). The combined organic layers were washed with water (5x) and brine (3x), then dried over $MgSO_4$, filtered, and concentrated down to a white solid (3.35 g, 64%). $^1$H NMR (400 MHz, Chloroform-*d*) δ 7.51 (s, 5H), 5.07 (s, 1H).

**Synthesis of 50** To a dry 2-dram vial was added 9-mesityl-10-phenylacridin-10-ium tetrafluoroborate (11.5 mg, 25.0 μmol, 2.5 mol%), **49** (85.0 mg, 1.00 mmol, 2 equiv), indene (58.0 μL, 500 μmol, 1 equiv), 3-butyn-2-ol (200 μL, 2.50 mmol, 5 equiv), and DCM (1 mL). The vial was sealed with a septum cap and electrical tape, then the solution was sparged with $N_2$ for 15 min before it was irradiated with 450 nm LEDs for 5 days. The reaction was concentrated and purified by chromatography with 30% $Et_2O$/hexanes to obtain a purple oil (41%, 1.3:1 d.r.). $^1$H

NMR (600 MHz, Chloroform-*d*) δ 7.36 – 7.28 (m, 2H), 7.28 – 7.18 (m, 8H), 5.33 (d, *J* = 2.2 Hz, 1H), 5.30 (d, *J* = 2.1 Hz, 1H), 4.98 – 4.93 (m, 2H), 4.93 – 4.88 (m, 1H), 4.49 (td, *J* = 6.2, 4.2 Hz, 1H), 4.42 – 4.35 (m, 1H), 4.18 (d, *J* = 5.5 Hz, 1H), 4.14 (d, *J* = 4.9 Hz, 1H), 3.22 (dd, *J* = 17.3, 5.7 Hz, 1H), 3.16 – 3.08 (m, 3H), 1.30 (d, *J* = 6.3 Hz, 4H), 1.14 (d, *J* = 6.3 Hz, 3H).

**Scheme B.22** Synthesis of **51-53**

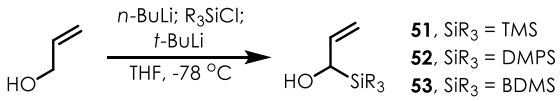


**Synthesis of 51** Combined allyl alcohol (1.36 mL, 20.0 mmol, 1 equiv) and THF (50 mL) in a flask and cooled to -78 °C. To this solution was added *n*-BuLi (2.5 M, 8.6 mL, 22 mmol, 1.1 equiv) contents were stirred for 1 hr before adding TMSCl (2.54 mL, 20.0 mmol, 1 equiv). After another 1.5 hr, *t*-BuLi (1.7 M, 16 mL, 27 mmol, 1.36 equiv) was added and solution was stirred for 1.5 hr before it was quenched with sat. aq. $NH_4Cl$. The aqueous layer was extracted with $Et_2O$, and the combined organic layers were washed with water (4x), brine (3x), then dried over $MgSO_4$. Filtration and concentration afforded a colorless liquid (1.49 g, 57%). $^1$H NMR (400 MHz, Chloroform-*d*) δ 6.01 (ddd, *J* = 16.5, 10.7, 5.3 Hz, 1H), 5.05 (d, *J* = 17.2 Hz, 1H), 4.97 (d, *J* = 10.7 Hz, 1H), 4.00 (s, 1H), 1.49 (s, 1H), 0.04 (s, 9H).

**Synthesis of 52** Made analogously to **51** on same scale but using DMPSCl (3.60 mL, 21.6 mmol, 1.1 equiv) in place of TMSCl. Product was purified by chromatography with 20% $Et_2O$/hexanes to give a pale-yellow oil (1.61 g, 42%). $^1$H NMR (600 MHz, Chloroform-*d*) δ 7.58 (dd, *J* = 7.6, 1.8 Hz, 2H), 7.47 – 7.34 (m, 3H), 6.01 (ddd, *J* = 17.1, 10.7, 5.2 Hz, 1H), 5.07 (dt, *J* = 17.2, 1.8 Hz, 1H), 5.01 (dt, *J* = 10.7, 1.7 Hz, 1H), 4.32 – 4.12 (m, 1H), 1.31 (s, 1H), 0.35 (d, *J* = 10.3 Hz, 6H).

**Synthesis of 53** Made analogously to **51** on a 15 mmol scale using BDMSCl (2.94 mL, 16.2 mmol, 1.1 equiv) in place of TMSCl. Product was purified by chromatography with 20%

$Et_2O$/hexanes to give a light-yellow oil (2.36 g, 76%). $^1$H NMR (400 MHz, Chloroform-*d*) δ 7.28 – 7.17 (m, 2H), 7.11 – 7.01 (m, 3H), 6.02 (ddd, *J* = 16.3, 10.7, 5.2 Hz, 1H), 5.11 (d, *J* = 17.2 Hz, 1H), 5.03 (d, *J* = 10.7 Hz, 1H), 4.12 – 4.01 (m, 1H), 2.21 (q, *J* = 13.7 Hz, 2H), 1.32 (s, 1H), 0.02 (d, *J* = 10.3 Hz, 6H).

**Scheme B.23** Synthesis of **54-56**

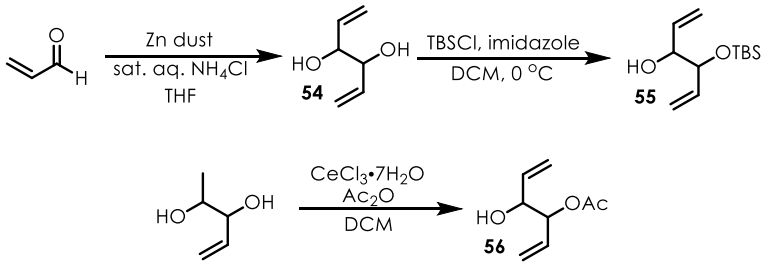


**Synthesis of 54** Acrolein (6.67 mL, 100 mmol, 1 equiv) and Zn dust (13.1 g, 207 mmol, 2.07 equiv) were added to a biphasic mixture of THF (250 mL) and sat. aq. $NH_4Cl$ (150 mL). After stirring for 16 hr, the contents were filtered through celite with DCM and the filtrate was washed with water, brine, then dried over $Na_2SO_4$. Filtration and concentration afforded a golden oil (3.3 g, 58%). $^1$H NMR (400 MHz, Chloroform-*d*) δ 5.92 – 5.80 (m, 2H), 5.35 (dd, *J* = 17.2, 6.7 Hz, 2H), 5.29 – 5.20 (m, 2H), 4.20 (d, *J* = 4.7 Hz, 1H), 4.06 – 3.93 (m, 1H), 2.74 (s, 1H), 2.53 (s, 1H).

**Synthesis of 55** A mixture of **54** (1.15 g, 10.1 mmol, 1 equiv) in DCM (51 mL) was prepared and cooled to 0 °C before adding imidazole (1.03 g, 15.1 mmol, 1.5 equiv) and TBSCl (1.52 g, 10.1 mmol, 1 equiv). After stirring for 16 hr and warming to RT, the contents were quenched with water and extracted with DCM. The combined organic layers were washed with 2 N HCl and brine, then dried over $Na_2SO_4$. Filtration, concentration, and purification of the residue by chromatography with 10% acetone/hexanes gave a colorless liquid (656 mg, 28%). $^1$H NMR (400 MHz, Chloroform-*d*) δ 5.91 – 5.72 (m, 3H), 5.36 – 5.29 (m, 1H), 5.28 (s, 1H), 5.20 (dd, *J* =

10.6, 5.3 Hz, 4H), 4.17 – 4.10 (m, 1H), 4.07 (q, *J* = 4.3 Hz, 1H), 3.96 (dt, *J* = 11.0, 5.6 Hz, 1H), 2.53 (d, *J* = 4.5 Hz, 1H), 2.27 (d, *J* = 4.3 Hz, 1H), 0.91 (s, 17H), 0.07 (d, *J* = 10.9 Hz, 11H).

**Synthesis of 56** Combined **54** (1.11 g, 9.72 mmol, 1 equiv), $CeCl_3 \cdot 7H_2O$ (362 mg, 972 μmol, 10 mol%), $Ac_2O$ (10.6 mL, 112 mmol, 11.5 equiv) and DCM (49 mL) in a flask and let stir for 16 hr. The mixture was then quenched with water and the organic layer was washed with sat. aq. $NaHCO_3$ and brine. After drying the organic layers over $Na_2SO_4$, they were concentrated and the obtained residue was purified by chromatography using 20% EtOAc/hexanes to obtain a colorless liquid (685 mg, 45%). $^1$H NMR (400 MHz, Chloroform-*d*) δ 5.91 – 5.76 (m, 5H), 5.41 – 5.20 (m, 12H), 4.32 – 4.25 (m, 1H), 4.22 (t, *J* = 5.5 Hz, 1H), 2.11 (s, 9H).

**Scheme B.24** Synthesis of **57-58**

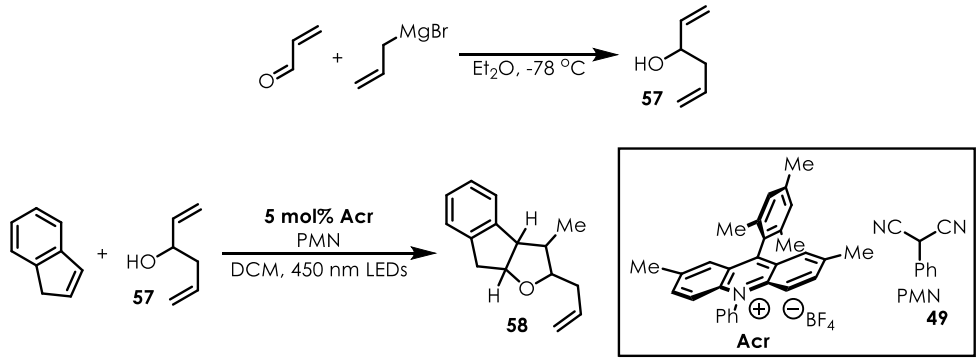


**Synthesis of 57** Acrolein (2.00 mL, 30.0 mmol, 1 equiv) was added to a mixture of allyl Grignard (1.0 M, 25 mL, 25 mmol, 0.83 equiv) and THF (50 mL). The solution was stirred for 16 hr, then quenched with 2 N HCl, and extracted with $Et_2O$. The combined organic layers were washed with brine and dried over $MgSO_4$. Filtration, concentration, and distillation of the residue gave a colorless liquid (1.33 g, 54%). $^1$H NMR (400 MHz, Chloroform-*d*) δ 5.93 – 5.71 (m, 2H), 5.23 (d, *J* = 17.2 Hz, 1H), 5.18 – 5.04 (m, 3H), 4.15 (q, *J* = 5.7 Hz, 1H), 3.72 (t, *J* = 5.5 Hz, 3H), 2.29 (tq, *J* = 14.0, 7.3, 6.6 Hz, 2H), 2.03 (s, 2H), 1.83 (s, 3H).

**Synthesis of 58** To a dry 2-dram vial was added 9-mesityl-2,7-dimethyl-10-phenylacridin-10-ium tetrafluoroborate (4.6 mg, 10 μmol, 5 mol%), **49** (28.4 mg, 400 μmol, 2 equiv), indene (23.0 μL, 200 μmol, 1 equiv), **57** (63.3 μL, 1 mmol, 5 equiv), and DCM (400 μL). The vial was sealed with a septum cap and electrical tape, before the solution was sparged with $N_2$ for 15 min. After irradiating the mixture with 450 nm LEDs for 5 days, it was concentrated and purified by chromatography with 5% $Et_2O$/hexanes to obtain a colorless liquid (21 mg, 49%, 1.5:1 d.r.). $^1$H NMR (600 MHz, Chloroform-*d*) δ 7.25 – 7.09 (m, 6H), 5.90 – 5.74 (m, 2H), 8.52 – 0.37 (m, 52H), 5.14 – 4.97 (m, 4H), 4.80 (td, *J* = 6.7, 1.8 Hz, 1H), 3.83 – 3.78 (m, 1H), 3.53 (td, *J* = 7.8, 4.6 Hz, 1H), 3.34 (t, *J* = 6.2 Hz, 1H), 3.29 – 3.25 (m, 1H), 3.20 (dd, *J* = 11.3, 6.8 Hz, 1H), 3.16 (d, *J* = 6.6 Hz, 1H), 3.10 (d, *J* = 1.5 Hz, 1H), 3.09 – 3.05 (m, 1H), 2.39 (dd, *J* = 15.5, 4.1 Hz, 1H), 2.25 – 2.11 (m, 3H), 1.87 (dt, *J* = 13.5, 6.8 Hz, 1H), 1.25 (d, *J* = 6.8 Hz, 3H), 1.06 (d, *J* = 7.0 Hz, 3H).

**Scheme B.25** Synthesis of **59-62**

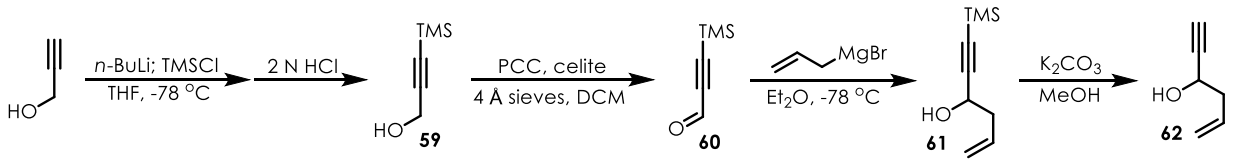


**Synthesis of 59** *n*-BuLi (2.5 M, 44 mL, 110 mmol, 2.2 equiv) was added to a solution of propargyl alcohol (2.91 mL, 50.0 mmol, 1 equiv) in THF (168 mL) at -78 °C and the contents were stirred for 30 min before adding TMSCl (14.3 mL, 112.5 mmol, 2.25 equiv). The mixture was stirred for 16 hr and allowed to warm to RT before it was quenched with 2 N HCl and then neutralized with sat. aq. $NaHCO_3$. The aqueous layer was extracted with $Et_2O$, and the combined organic layers were washed with water, brine, and dried over $MgSO_4$. Filtration and concentration gave a residue which was purified with 15% EtOAc/hexanes to obtain a yellow

liquid (4.65 g, 73%). $^1$H NMR (400 MHz, Chloroform-*d*) δ 4.27 (d, *J* = 5.6 Hz, 2H), 1.63 (d, *J* = 13.0 Hz, 1H), 0.18 (s, 8H).

**Synthesis of 60** A suspension of **59** (2.00 g, 15.6 mmol, 1 equiv), DCM (59 mL), celite (6.83 g), and 4 Å sieves (5.84 g) was prepared then cooled to 0 $^o$C before the addition of PCC (6.10 g, 28.2 mmol, 1.8 equiv). After stirring for 16 hr, the mixture was filtered through silica with DCM and the filtrate concentrated to obtain a yellow liquid (1.89 g, 96%). $^1$H NMR (400 MHz, Chloroform-*d*) δ 9.16 (s, 1H), 0.26 (s, 9H).

**Synthesis of 61** Allyl Grignard (1.0 M, 17 mL, 17 mmol, 1.3 equiv) was added to a solution of **60** (1.66 g, 13.2 mmol, 1 equiv) in $Et_2O$ (66 mL) cooled to -78 $^o$C. The solution was warmed to 0 $^o$C and stirred for 15 min before warming to RT. After 1 hr of stirring at RT, the reaction was quenched with sat. aq. $NH_4Cl$ and the aqueous layer was extracted with $Et_2O$. The combined organic layers were washed with brine, dried over $MgSO_4$, filtered, and concentrated to a pale-yellow liquid (2.10 g, 95%). $^1$H NMR (400 MHz, Chloroform-*d*) δ 5.96 – 5.80 (m, 1H), 5.27 – 5.07 (m, 2H), 4.41 (q, *J* = 6.0 Hz, 1H), 2.47 (t, *J* = 6.5 Hz, 2H), 1.90 (d, *J* = 6.0 Hz, 1H), 0.17 (s, 9H).

**Synthesis of 62** A suspension of **61** (2.10 g, 12.5 mmol, 1 equiv) and $K_2CO_3$ (2.08 g, 15.0 mmol, 1.25 equiv) in MeOH (25 mL) was stirred for 30 min before it was diluted with $Et_2O$ and transferred to a separatory funnel. The organic layer was washed with water and brine, dried over $MgSO_4$, filtered, and concentrated. The crude residue was purified with 20% $Et_2O$/hexanes to obtain a pale-yellow liquid (217 mg, 18%). $^1$H NMR (400 MHz, Chloroform-*d*) δ 6.03 – 5.77 (m, 1H), 5.30 – 5.13 (m, 2H), 4.52 – 4.36 (m, 1H), 2.56 – 2.41 (m, 3H), 2.05 – 1.89 (m, 1H).

**Scheme B.26** Synthesis of **63-65**

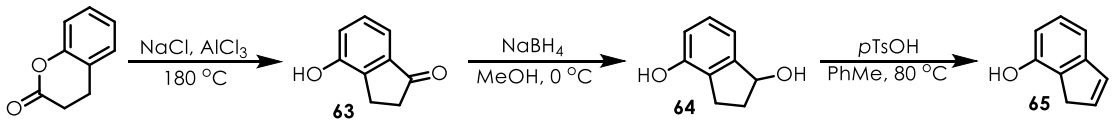


**Synthesis of 63** Dihydrocoumarin (12.7 mL, 100 mmol, 1 equiv) was added to a molten mixture of $AlCl_3$ (73.6 g, 552 mmol, 5.5 equiv) and NaCl (18.9 g, 324 mmol, 3.25 equiv) at 150 °C before increasing the temperature of the mixture to 180 °C. After 1 hr, the contents were cooled to RT and poured into a mixture of ice and conc. HCl. After stirring overnight, the precipitated product was filtered off washed with water and ethanol (9.47 g, 64%). $^1$H NMR (400 MHz, DMSO-$d_6$) δ 9.94 (s, 1H), 7.24 (t, $J$ = 7.6 Hz, 1H), 7.07 (dd, $J$ = 18.1, 7.6 Hz, 2H), 3.08 – 2.76 (m, 2H), 2.66 – 2.53 (m, 2H).

**Synthesis of 64** $NaBH_4$ (730 mg, 19.3 mmol, 2.2 equiv) was added to a suspension of **63** (1.30 g, 8.77 mmol, 1 equiv) in MeOH (30 mL) at 0 °C. After stirring this mixture for 3 hr, it was concentrated and the obtained residue was diluted with 2 N HCl. The aqueous layer was extracted with $Et_2O$ and the combined organic layers were washed with water, brine, and dried over $MgSO_4$. Filtration and concentration gave a tan solid (1.23 g, 93%). $^1$H NMR (600 MHz, Chloroform-$d$) δ 7.14 – 7.06 (m, 2H), 6.96 (d, $J$ = 7.4 Hz, 1H), 6.74 (d, $J$ = 7.9 Hz, 1H), 5.22 (d, $J$ = 5.1 Hz, 1H), 3.01 (ddd, $J$ = 15.6, 8.6, 4.7 Hz, 1H), 2.74 (dt, $J$ = 15.4, 7.3 Hz, 1H), 2.47 (td, $J$ = 13.1, 6.2 Hz, 1H), 2.11 (d, $J$ = 5.6 Hz, 1H), 1.95 (td, $J$ = 13.7, 5.6 Hz, 1H).

**Synthesis of 65** A mixture of **64** (2.60 g, 17.3 mmol, 1 equiv), $MgSO_4$ (2.08 g, 17.3 mmol, 1 equiv), $p$TsOH·$H_2O$ (362 mg, 1.90 mmol, 11 mol%), and dioxane (260 mL) was heated to 80 °C for 2 hr then cooled to RT and quenched with sat. aq. $NaHCO_3$. The dioxane was removed *in vacuo* and the aqueous layer was extracted with $Et_2O$. The combined organic layers were washed with brine and dried over $MgSO_4$. Concentration and purification of the residue by

chromatography with 30% $Et_2O$/hexanes gave a white solid (1.42 g, 62%). $^1$H NMR (400 MHz, Chloroform-*d*) δ 7.19 (t, *J* = 7.7 Hz, 1H), 7.04 (d, *J* = 7.4 Hz, 1H), 6.90 – 6.85 (m, 1H), 6.67 (d, *J* = 7.9 Hz, 1H), 6.60 – 6.54 (m, 1H), 3.36 (s, 2H).

**Scheme B.27** Synthesis of **66-69**

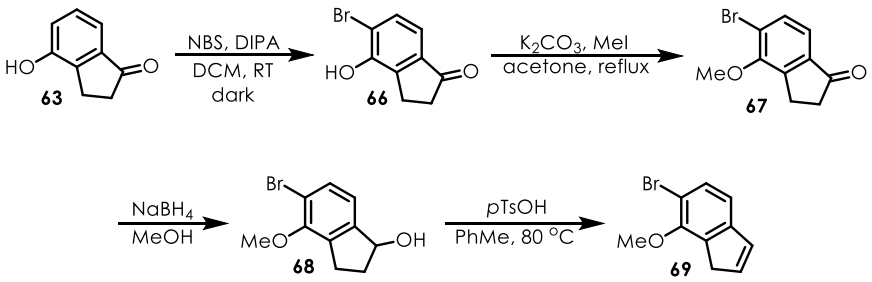


**Synthesis of 66** A solution of **63** (4.55 g, 30.7 mmol, 1.1 equiv), DCM (290 mL) and DIPA (5.6 mL, 39.9 mmol, 1.3 equiv) was prepared before a solution of NBS (4.93 g, 27.7 mmol, 1 equiv) in DCM (290 mL) was added over the course of 4 hr in the dark. The mixture was stirred for 12 hr, then quenched with 2 N HCl. The organic layer was washed with water and brine then dried over $MgSO_4$. Filtration and concentration gave a residue that was purified by chromatography with 60% EtOAc/hexanes to obtain a tan solid (5.75 g, 82%). $^1$H NMR (400 MHz, Chloroform-*d*) δ 8.78 (s, 1H), 7.31 (d, *J* = 8.1 Hz, 1H), 6.95 (d, *J* = 8.1 Hz, 1H), 2.98 – 2.90 (m, 2H), 2.49 (d, *J* = 11.6 Hz, 3H).

**Synthesis of 67** A mixture of **66** (6.34 g, 27.9 mmol, 1 equiv), acetone (121 mL), $K_2CO_3$ (4.63 g, 33.5 mmol, 1.2 equiv), and MeI (1.80 mL, 27.9 mmol, 1 equiv) was heated to reflux for 16 hr. After cooling to RT, the acetone was removed *in vacuo*. The resultant residue was taken up in water and extracted with DCM. The combined organic layers were dried over $MgSO_4$, filtered, and concentrated to a tan solid (6.32 g, 94%). $^1$H NMR (400 MHz, Chloroform-*d*) δ 7.57 (d, *J* = 8.1 Hz, 1H), 7.40 – 7.29 (m, 1H), 3.95 (s, 3H), 3.26 – 3.16 (m, 2H), 2.74 – 2.67 (m, 2H).

**Synthesis of 68** $NaBH_4$ (550 mg, 14.1 mmol, 1.1 equiv) was added to a solution of **67** (3.08 g, 12.8 mmol, 1 equiv) in MeOH (44 mL) cooled to 0 °C. After stirring for 3 hr, the mixture was concentrated and the residue diluted with 2 N HCl, then extracted with $Et_2O$. The combined organic layers were washed with water, brine, and dried over $MgSO_4$ Filtration and concentration gave a tan solid which was recrystallized from toluene to afford a white solid (1.98 g, 64%). $^1$H NMR (400 MHz, Chloroform-*d*) δ 7.43 (d, *J* = 7.9 Hz, 1H), 7.04 (d, *J* = 7.9 Hz, 1H), 5.20 (q, *J* = 6.3 Hz, 1H), 3.86 (s, 3H), 3.15 (dd, *J* = 14.9, 9.9 Hz, 1H), 2.88 (t, *J* = 15.5 Hz, 1H), 2.62 – 2.44 (m, 1H), 2.02 – 1.92 (m, 1H), 1.76 (d, *J* = 6.7 Hz, 1H).

**Synthesis of 69** A suspension of **68** (3.70 g, 15.2 mmol, 1 equiv), PhMe (34 mL), and *p*TsOH·$H_2O$ (318 mg, 1.67 mmol, 10 mol%) was heated to 80 °C for 1 hr. After cooling to RT and quenching with sat. aq. $NaHCO_3$, the organic layer was washed with brine and dried over $Na_2SO_4$. Filtration and concentration gave a residue that was purified by chromatography with 5% $Et_2O$/hexanes to obtain a pale-yellow liquid (2.44 g, 71%). $^1$H NMR (400 MHz, Chloroform-*d*) δ 7.46 (d, *J* = 7.9 Hz, 1H), 7.02 (d, *J* = 7.9 Hz, 1H), 6.90 – 6.79 (m, 1H), 6.55 (d, *J* = 5.3 Hz, 1H), 3.97 (s, 3H), 3.51 (s, 2H).

### B.2.3 Investigating a Decarboxylative Diels-Alder Reaction

**Scheme B.28** Synthesis of **70-71**

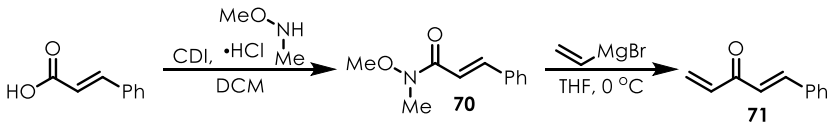


**Synthesis of 70** CDI (7.78 g, 48.0 mmol, 1.2 equiv) was added to a solution of cinnamic acid (5.93 g, 40.0 mmol, 1 equiv) in DCM (400 mL) at 0 °C. After 30 min, *N*,*O*-dimethylhydroxylamine hydrochloride (9.75 g, 100 mmol, 2.5 equiv) was added and the mixture was stirred for another 16 hr. The contents were quenched with water and the organic layer was

washed with 2 N HCl, water, and brine, then dried over $MgSO_4$, filtered, and concentrated. The crude residue was purified by chromatography with 40% EtOAc/hexanes to give a colorless oil (4.92 g, 64%). $^1$H NMR (400 MHz, Chloroform-*d*) δ 7.74 (d, *J* = 15.8 Hz, 1H), 7.63 – 7.52 (m, 2H), 7.38 (d, *J* = 7.2 Hz, 3H), 7.04 (d, *J* = 15.8 Hz, 1H), 3.77 (s, 3H), 3.31 (s, 3H).

**Synthesis of 71 V**inyl Grignard (0.7 M, 73 mL, 51 mmol, 1 equiv) was added to a solution of **70** (4.91 g, 25.7 mmol, 1 equiv) in THF (172 mL) at -78 °C. After 4 hr, the solution was quenched with sat. aq. $NH_4Cl$ and extracted with DCM. The combined organic layers were dried over $Na_2SO_4$, filtered, and concentrated. The crude residue was purified with 40% EtOAc/hexanes to give a yellow oil (1.23 g, 30%). $^1$H NMR (400 MHz, Chloroform-*d*) δ 7.68 (d, *J* = 16.0 Hz, 1H), 7.58 (d, *J* = 5.9 Hz, 2H), 7.51 – 7.36 (m, 3H), 7.01 (d, *J* = 16.0 Hz, 1H), 6.72 (dd, *J* = 17.4, 10.6 Hz, 1H), 6.39 (d, *J* = 17.4 Hz, 1H), 5.89 (d, *J* = 10.6 Hz, 1H).

**Scheme B.29** Synthesis of **72-75**

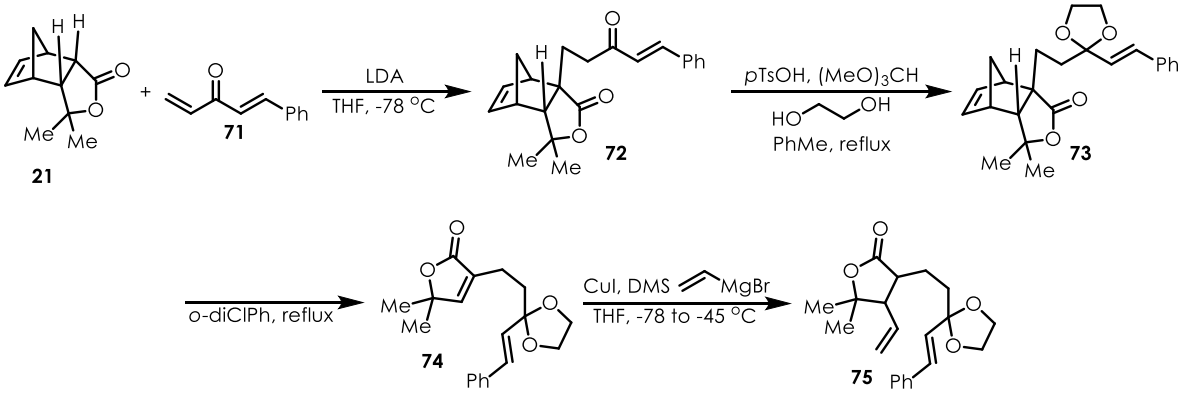


**Synthesis of 72** A solution of LDA was prepared by adding *n*-BuLi (2.5 M, 3.0 mL, 7.6 mmol, 0.98 equiv) to a solution of DIPA (1.10 mL, 7.69 mmol, 0.99 equiv) in THF (6 mL) at -78 °C. After 15 min, a solution of **21** (1.38 g, 7.77 mmol, 1 equiv) in THF (10 mL) was added to the fresh LDA. After another 30 min, the contents were warmed to 0 °C and **71** (1.23 g, 7.77 mmol, 1 equiv) was added as a solution in THF (10 mL). After 2 hr, the mixture was quenched with sat. aq. $NH_4Cl$ and extracted with EtOAc. The combined organic layers were washed with brine and

dried over $MgSO_4$, filtered, and concentrated. The crude residue was purified with chromatography using 20% EtOAc/hexanes to obtain a colorless oil (865 mg, 33%). $^1$H NMR (600 MHz, Chloroform-*d*) δ 7.62 (d, *J* = 16.3 Hz, 1H), 7.59 – 7.51 (m, 2H), 7.43 – 7.37 (m, 3H), 6.77 (d, *J* = 16.2 Hz, 1H), 6.29 (d, *J* = 5.7 Hz, 1H), 6.24 (dd, *J* = 9.6, 6.5 Hz, 3H), 3.46 (dd, *J* = 8.8, 5.1 Hz, 1H), 3.36 – 3.24 (m, 2H), 3.07 – 2.99 (m, 2H), 2.93 (s, 1H), 2.72 (d, *J* = 3.8 Hz, 1H), 2.52 – 2.41 (m, 2H), 2.19 – 2.09 (m, 1H), 1.48 (s, 3H), 1.36 (s, 3H).

**Synthesis of 73** A solution of **72** (865 mg, 2.57 mmol, 1 equiv), ethylene glycol (719 μL, 12.9 mmol, 5 equiv), *p*TsOH·$H_2O$ (48.9 mg, 257 μmol, 10 mol%), trimethoxymethane (560 μL, 5.14 mmol, 2 equiv) and PhMe (64 mL) were refluxed under Dean-Stark conditions for 36 hr. There mixture was cooled to RT, quenched with sat. aq. $NaHCO_3$ and extracted with EtOAc. The combined organic layers were washed with brine and dried over $MgSO_4$ then filtered and concentrated. The crude residue was purified with chromatography using 15% acetone/hexanes to give a yellow oil (810 mg, 83%). $^1$H NMR (400 MHz, Chloroform-*d*) δ 7.39 (d, *J* = 11.0 Hz, 2H), 7.32 (t, *J* = 7.4 Hz, 2H), 6.69 (d, *J* = 16.0 Hz, 1H), 6.24 (s, 6H), 6.09 (d, *J* = 16.0 Hz, 1H), 3.99 (d, *J* = 5.0 Hz, 2H), 3.95 (d, *J* = 4.8 Hz, 2H), 3.46 (dd, *J* = 8.8, 5.1 Hz, 2H), 3.27 (d, *J* = 3.3 Hz, 3H), 3.03 (s, 3H), 2.72 (dd, *J* = 8.8, 3.7 Hz, 3H), 1.37 (s, 6H), 1.36 (s, 6H).

**Synthesis of 74** A solution of **73** (810 mg, 2.13 mmol, 1 equiv) in *o*-dichlorobenzene (18.5 mL) was heated to reflux for 18 hr. After cooling to RT, the contents were filtered through a pad of silica with hexanes and then EtOAc. The EtOAc filtrate was concentrated and the residue purified residue by chromatography with 10% acetone/hexanes to give a pale-yellow oil (300 mg, 42%). $^1$H NMR (600 MHz, Chloroform-*d*) δ 7.39 (d, *J* = 9.1 Hz, 2H), 7.32 (t, *J* = 7.6 Hz, 2H), 7.26 (s, 2H), 6.93 (t, *J* = 1.6 Hz, 1H), 6.71 (d, *J* = 16.0 Hz, 1H), 6.10 (d, *J* = 16.0 Hz, 1H), 4.04 – 3.89 (m, 4H), 2.43 (d, *J* = 17.6 Hz, 2H), 2.06 (d, *J* = 16.2 Hz, 2H), 1.42 (s, 6H).

**Synthesis of 75** Vinyl Grignard (1.0 M, 5.7 mL, 5.7 mmol, 6 equiv) was added to a suspension of CuI (545 mg, 2.86 mmol, 3 equiv) in THF (13.6 mL) and cooled to -78 °C. After 10 min, DMS (140 μL, 1.91 mmol, 2 equiv) was added and the reaction stirred for 90 min before **74** (300 mg, 954 μmol, 1 equiv) was added as a solution in THF (6.4 mL). The mixture was warmed to -45 °C and quenched with sat. aq. $NH_4Cl$ after an additional 2 hr. The aqueous layer was extracted with EtOAc, and the combined organic layers were washed with brine and dried over $MgSO_4$. Filtration, concentration, and purification of residue with 20% EtOAc/hexanes gave a pale-yellow oil (166 mg, 51%). $^1$H NMR (400 MHz, Chloroform-*d*) δ 7.39 (d, *J* = 7.3 Hz, 2H), 7.32 (d, *J* = 14.9 Hz, 2H), 6.68 (d, *J* = 16.0 Hz, 1H), 6.08 (d, *J* = 16.0 Hz, 1H), 5.69 (dd, *J* = 26.4, 9.5 Hz, 1H), 5.27 – 5.18 (m, 2H), 3.96 (dd, *J* = 16.4, 6.9 Hz, 4H), 2.63 (d, *J* = 5.7 Hz, 1H), 2.57 – 2.47 (m, 1H), 1.95 – 1.84 (m, 1H), 1.77 – 1.65 (m, 1H), 1.39 (s, 3H), 1.24 (s, 3H).

**Scheme B.30** Synthesis of **76-77**

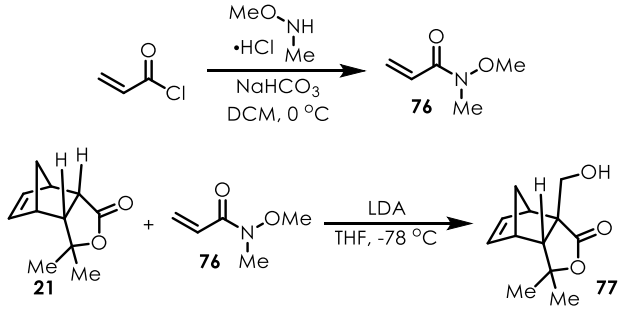


**Synthesis of 76** *N*,*O*-Dimethylhydroxylamine hydrochloride (1.25 g, 12.8 mmol, 1 equiv) and $NaHCO_3$ (2.15 g, 25.6 mmol, 2.2 equiv) were stirred in DCM (40 mL) for 30 min before cooling to 0 °C and adding acryloyl chloride (1.05 mL, 12.8 mmol, 1 equiv). After 1.5 hr, $MgSO_4$ was added to dry the reaction. The solids present were filtered off and the filtrate was concentrated to a pale-yellow liquid (606 mg, 41%). $^1$H NMR (400 MHz, Chloroform-*d*) δ 6.72 (dd, *J* = 17.1, 10.4 Hz, 1H), 6.42 (dd, *J* = 17.1, 2.0 Hz, 1H), 5.74 (dd, *J* = 10.4, 2.0 Hz, 1H), 3.70 (s, 3H), 3.25 (s, 3H).

**Synthesis of 77** LDA was freshly prepared at -78 °C using DIPA (1.80 mL, 12.3 mmol, 1.2 equiv), *n*-BuLi (2.5 M, 4.5 mL, 11 mmol, 1.1 equiv) and THF (10 mL). A solution of **21** (1.83 g, 10.3 mmol, 1 equiv) in THF (11 mL) was added and the contents stirred for 30 min before adding a solution of **76** (1.30 g, 11.3 mmol, 1.1 equiv) in THF (14 mL). The mixture was stirred for 5 hr, then quenched with sat. aq. $NH_4Cl$ and extracted with EtOAc. The combined organic layers were washed with brine, dried over MgSO4, filtered, and concentrated. The crude residue was purified by chromatography with 20% EtOAc/hexanes to obtain a yellow oil. $^1$H NMR (400 MHz, Chloroform-*d*) δ 6.36 (dd, *J* = 5.6, 2.8 Hz, 1H), 6.27 (dd, *J* = 5.7, 3.2 Hz, 1H), 4.06 (d, *J* = 11.7 Hz, 1H), 3.85 (d, *J* = 11.7 Hz, 1H), 3.10 (s, 1H), 2.99 – 2.92 (m, 1H), 2.72 (d, *J* = 3.8 Hz, 1H), 1.76 (d, *J* = 8.9 Hz, 1H), 1.69 – 1.64 (m, 1H), 1.51 (s, 3H), 1.38 (s, 3H), 0.87 (td, *J* = 7.5, 7.0, 3.2 Hz, 2H).

**Scheme B.31** Synthesis of **78-79**

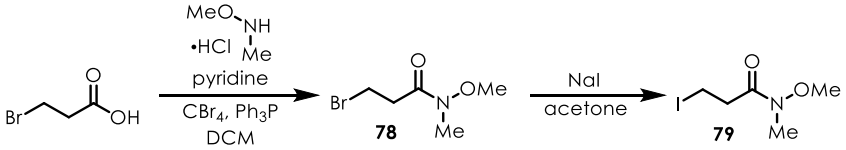


**Synthesis of 78** 3-Bromopropanoic acid (4.59 g, 30.0 mmol, 1 equiv), $CBr_4$ (10.9 g, 33.0 mmol, 1.1 equiv), *N*,*O*-dimethylhydroxylamine hydrochloride (3.22 g, 33.0 mmol, 1.1 equiv), and pyridine (2.67 mL, 33.0 mmol, 1.1 equiv) were dissolved in DCM (75 mL). Triphenylphosphine (8.66 g, 33.0 mmol, 1.1 equiv) was added to the mixture over 10 min. After 20 min of stirring, the contents were diluted with 150 mL of a 1:1 mixture of EtOAc:hexanes and filtered. The filtrate was concentrated, and the residue purified by chromatography with 40% EtOAc/hexanes to obtain a colorless liquid (4.67 g, 79%). $^1$H NMR (400 MHz, Chloroform-*d*) δ 3.71 (s, 3H), 3.63 (t, *J* = 7.0 Hz, 2H), 3.20 (s, 3H), 3.04 (t, *J* = 6.8 Hz, 2H).

**Synthesis of 79** NaI (3.81 g, 25.4 mmol, 2 equiv) and **78** (2.49 g, 12.7 mmol, 1 equiv) were dissolved in acetone (35 mL) and stirred for 16 hr. The mixture was then filtered and concentrated. The residue was dissolved in EtOAc and washed with water and dried over $Na_2SO_4$. Filtration and concentration gave an orange oil (2.42 g, 78%). $^1$H NMR (400 MHz, Chloroform-*d*) δ 3.70 (s, 3H), 3.37 (t, *J* = 7.2 Hz, 2H), 3.20 (s, 3H), 3.09 (t, *J* = 7.1 Hz, 2H).

**Scheme B.32** Synthesis of **80-83**

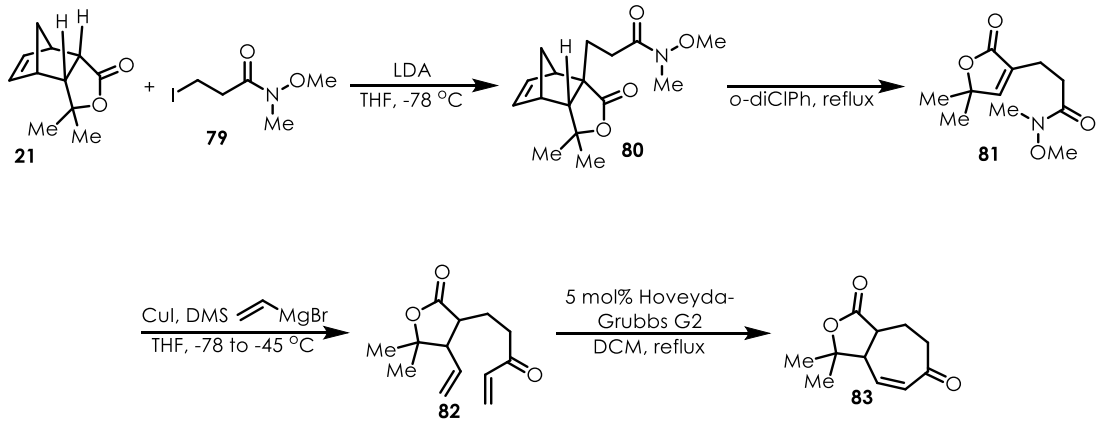


**Synthesis of 80** LDA was freshly prepared at -78 °C using DIPA (1.40 mL, 9.96 mmol, 1.2 equiv), *n*-BuLi (2.5 M, 3.7 mL, 9.1 mmol, 1.1 equiv) and THF (14 mL). A solution of **21** (1.48 g, 8.30 mmol, 1 equiv) in THF (2 mL) was added to the LDA and the contents were stirred for 30 min. A solution of **79** (2.42 g, 9.96 mmol, 1.2 equiv) in THF (2 mL) was then added and the cooling bath was removed. The contents were stirred at RT for 36 hr then quenched with sat. aq. $NH_4Cl$ and extracted with EtOAc. The combined organic layers were washed with brine, dried over $MgSO_4$, filtered, and concentrated. The crude residue was purified by chromatography with 40% EtOAc/hexanes to obtain a colorless oil (798 mg, 33%). $^1$H NMR (400 MHz, Chloroform-*d*) δ 6.29 (s, 1H), 6.25 – 6.17 (m, 1H), 3.72 (s, 3H), 3.19 (s, 3H), 3.01 (s, 2H), 2.93 (s, 1H), 2.80 – 2.66 (m, 1H), 2.50 – 2.36 (m, 2H), 2.11 (d, *J* = 10.7 Hz, 1H), 1.65 (d, *J* = 1.7 Hz, 2H), 1.46 (s, 3H), 1.34 (s, 3H).

**Synthesis of 81** Dissolved **80** (1.03 g, 3.51 mmol, 1 equiv) in *o*-dichlorobenzene (10 mL) and the contents were heated to reflux for 18 hr. After cooling to RT, the mixture was filtered through a plug of silica with hexanes and then EtOAc. The ethyl acetate filtrate was concentrated down to an orange oil (592 mg, 74%). $^1$H NMR (400 MHz, Chloroform-*d*) δ 7.05 (s, 1H), 3.68 (s, 3H), 3.17 (s, 3H), 2.70 (d, *J* = 6.9 Hz, 2H), 2.61 (t, *J* = 7.2 Hz, 2H), 1.44 (s, 6H).

**Synthesis of 82** Vinyl Grignard (1.0 M, 16 mL, 16 mmol, 6 equiv) was added to a suspension of CuI (1.49 g, 7.81 mmol, 3 equiv) in THF (37 mL) cooled to -78 $^o$C. After 10 min, DMS (383 μL, 5.21 mmol, 2 equiv) was added and contents were stirred for 90 min before **81** (592 mg, 2.60 mmol, 1 equiv) was added as a solution in THF (17 mL). The mixture was warmed to -45 $^o$C and stirred for 2 hr at which point is was quenched with sat. aq. $NH_4Cl$. The aqueous layer was extracted with EtOAc, and the combined organic layers were washed with brine, dried over $MgSO_4$, filtered, and concentrated. The crude residue was purified by chromatography with 20% acetone/hexanes to give a yellow oil (287 mg, 50%). $^1$H NMR (400 MHz, Chloroform-*d*) δ 6.43 – 6.17 (m, 2H), 5.85 (d, *J* = 10.1 Hz, 1H), 5.70 (dd, *J* = 26.4, 9.4 Hz, 1H), 5.32 – 5.21 (m, 2H), 3.01 – 2.87 (m, 2H), 2.69 – 2.55 (m, 1H), 2.52 – 2.41 (m, 1H), 2.03 – 1.77 (m, 2H), 1.41 (s, 3H), 1.24 (s, 2H).

**Synthesis of 83** Compound **82** was dissolved in DCM (50 mL) and sparged with $N_2$ for 45 min before a solution of Hoveyda-Grubbs Generation II catalyst (21.0 mg, 33.5 μmol, 5 mol%) was added as a solution in DCM (1 mL). The contents were heated to reflux for 14 hr, then cooled to RT and concentrated. The crude residue was purified by chromatography using 20% acetone/hexanes to give a pale red solid (55.0 mg, 42%). $^1$H NMR (600 MHz, Chloroform-*d*) δ 6.45 (dd, *J* = 11.7, 2.3 Hz, 1H), 6.21 (dd, *J* = 11.7, 3.1 Hz, 1H), 3.05 – 3.00 (m, 1H), 2.83 – 2.71 (m, 2H), 2.71 – 2.62 (m, 1H), 2.37 – 2.30 (m, 1H), 1.96 – 1.87 (m, 1H), 1.59 (s, 3H), 1.35 (s, 3H).

**Scheme B.33** Synthesis of **84-87**

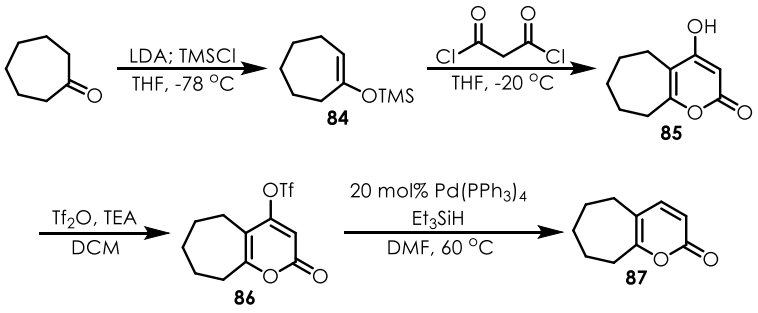


**Synthesis of 84** LDA was freshly prepared by adding *n*-BuLi (2.5 M, 8.8 mL, 22 mmol, 1.1 equiv) to a solution of DIPA (3.36 mL, 24.0 mmol, 1.2 equiv) in THF (48 mL) at -78 °C. After 15 min, cycloheptanone (2.36 mL, 20.0 mmol, 1 equiv) was added as a solution in THF (20 mL). After another 30 min, a solution of TMSCl (2.79 mL, 22.0 mmol, 1.1 equiv) in THF (22 mL) was added. Once 3 hr had elapsed, the mixture was diluted with pentanes and washed with pH 7 aq. phosphate buffer, 0.5 M aq. $CuSO_4$, and brine. The organic layer was dried over $Na_2SO_4$, filtered, and concentrated to a yellow oil (3.21 g, 87%). $^1$H NMR (400 MHz, Chloroform-*d*) δ 5.02 (t, *J* = 6.6 Hz, 1H), 2.26 – 2.18 (m, 2H), 2.02 – 1.94 (m, 2H), 1.68 (p, *J* = 6.0, 5.4 Hz, 2H), 1.54 (dp, *J* = 17.0, 5.9 Hz, 4H), 0.16 (s, 9H).

**Synthesis of 85** Dissolved **84** (3.21 g, 17.4 mmol, 1 equiv) in THF (40 mL) and cooled to -20 °C before adding malonyl dichloride (847 µL, 8.7 mmol, 0.5 equiv). After stirring for 16 hr, the mixture was quenched with water and extracted with EtOAc. The combined organic layers were washed with brine, dried over $Na_2SO_4$, filtered, and concentrated to an oil which was triturated with EtOAc/hexanes. The resultant solid was recrystallized from dioxane to obtain a light brown solid (1.2 g, 38%). $^1$H NMR (600 MHz, Chloroform-*d*) δ 10.89 (s, 1H), 3.50 (s, 2H), 2.57 – 2.38 (m, 2H), 2.38 – 2.25 (m, 2H), 1.61 (p, *J* = 6.0 Hz, 2H), 1.46 (dt, *J* = 11.4, 4.6 Hz, 2H), 1.37 (p, *J* = 5.9 Hz, 2H).

**Synthesis of 86** Combined **85** (903 mg, 5.01 mmol, 1 equiv), TEA (820 µL, 5.91 mmol, 1.18 equiv), and DCM (30 mL) in a flask then added $Tf_2O$ (974 µL, 5.76 mmol, 1.15 equiv) to the solution. After the contents stirred for 45 min, they were quenched with sat. aq. $NH_4Cl$ and the aqueous layer was extracted with DCM. The combined organic layers were dried over $Na_2SO_4$, filtered, and concentrated. The crude residue was purified by chromatography with 10% acetone/hexanes to give an orange oil (1.18 g, 75%). $^1$H NMR (400 MHz, Chloroform-*d*) δ 6.15 (s, 1H), 2.83 – 2.77 (m, 2H), 2.59 – 2.49 (m, 2H), 1.89 – 1.79 (m, 2H), 1.71 (p, *J* = 6.1 Hz, 2H), 1.65 (q, *J* = 5.6 Hz, 2H).

**Synthesis of 87** Combined **86** (1.18 g, 3.78 mmol, 1 equiv), $Pd(PPh_3)_4$ (873 mg, 756 µmol, 20 mol%), $Et_3SiH$ (1.21 mL, 7.56 mmol, 2 equiv) and DMF (25 mL) and heated the mixture to 60 °C for 2 hr. The contents were then cooled to RT, diluted with water, and extracted with EtOAc. The combined organic layers were washed with water, dried over $MgSO_4$, filtered, and concentrated. The crude residue was purified with 50% EtOAc/hexanes to give a yellow oil (550 mg, 89%). $^1$H NMR (600 MHz, Chloroform-*d*) δ 7.15 (d, *J* = 9.3 Hz, 1H), 6.08 (d, *J* = 9.3 Hz, 1H), 2.74 – 2.66 (m, 2H), 2.50 – 2.43 (m, 2H), 1.81 (p, *J* = 5.9 Hz, 2H), 1.67 (p, *J* = 6.0 Hz, 2H), 1.62 (p, *J* = 5.9 Hz, 2H).

**Scheme B.34** Synthesis of **88-89**

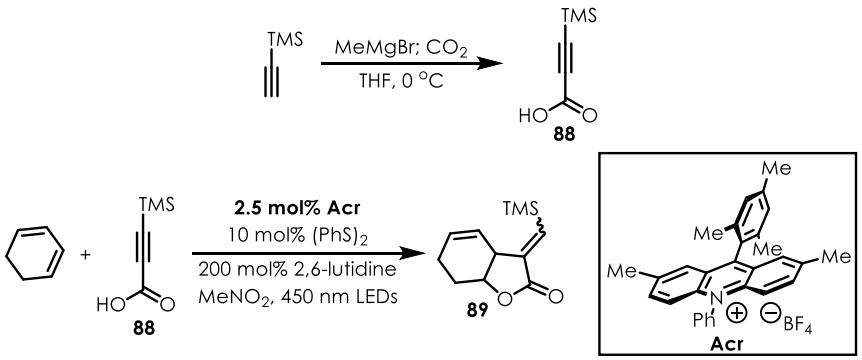

**Synthesis of 88** To MeMgBr (3.0 M, 21 mL, 63 mmol, 1.3 equiv) in a dry flask at 0 $^{o}$C was added a solution of trimethylsilylacetylene (6.90 mL, 50.0 mmol, 1 equiv) in THF (38 mL). After stirring for 1 hr at room temperature, the suspension was cooled to -20 $^{o}$C and $CO_2$ was bubbled through at this temperature for 30 min and then 2 hrs at room temperature. The mixture was quenched with 2 N HCl at 0 $^{o}$C and extracted with hexanes. The combined organic layers were washed with brine and dried over $MgSO_4$. Filtration and concentration gave a yellow oil (5.80 g, 82%). $^{1}$H NMR (400 MHz, Chloroform-*d*) δ 10.33 (bs, 1H), 0.26 (s, 9H).

**Synthesis of 89** The following procedure was repeated 3x to setup a total of 4 identical reactions. To a flame-dried 2-dram vial was added 9-mesityl-2,7-dimethyl-10-phenylacridin-10-ium tetrafluoroborate (3.7 mg, 7.5 μmol, 2.5 mol%), $(PhS)_2$ (9.8 mg, 45 μmol, 15 mol%), **88** (90.0 μL, 600 μmol, 2 equiv), 2,6-lutidine (70.0 μL, 600 μmol, 2 equiv), and $MeNO_2$ (6 mL). The solution was sparged with nitrogen for 10 min before placing it under irradiation (Kessil 455 nm LEDs) for 48 hrs. During the reaction time, 1,3-cyclohexadiene was added in 8 equal portions of 3.60 μL (total 28.6 μL, 300 μmol, 1 equiv) – 4 during the first 24 hrs and 4 during the second 24 hrs. The solutions were combined, concentrated down, and purified by chromatography with 10% $Et_2O$/hexanes to give a yellow oil (125 mg, 47%, 1:1 *E*:*Z*). $^{1}$H NMR (400 MHz, Chloroform-*d*) δ 6.84 (d, *J* = 1.5 Hz, 1H), 6.35 (d, *J* = 2.0 Hz, 1H), 5.93 – 5.84 (m, 2H), 5.55 (d, *J* = 13.7 Hz, 1H), 5.36 (d, *J* = 10.1 Hz, 1H), 4.80 – 4.70 (m, 2H), 3.57 (d, *J* = 5.4 Hz, 1H), 3.42 (s, 1H), 2.30 (s, 1H), 2.20 (s, 2H), 2.07 – 1.92 (m, 4H), 1.83 (d, *J* = 8.9 Hz, 1H), 1.72 (d, *J* = 14.0 Hz, 1H), 0.23 (s, 8H), 0.21 (s, 9H).

**Scheme B.35** Synthesis of **90-91**

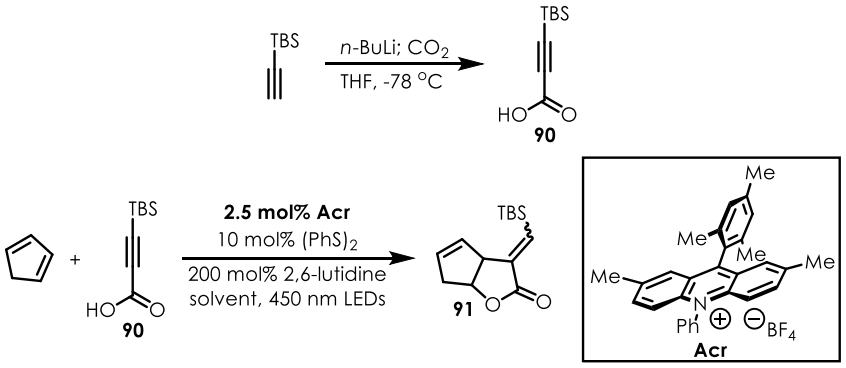


**Synthesis of 90** To a dry flask was added *tert*-butyldimethylsilylacetylene (2.66 mL, 14.3 mmol, 1 equiv) and THF (100 mL). After cooling to 0 °C, *n*-BuLi (2.5 M, 7.4 mL, 19 mmol, 1.3 equiv) was added and the solution was stirred for 1 hr before $CO_2$ was bubbled through the reaction for 3 hrs at room temperature. The mixture was quenched with 2 N HCl and the aqueous layer extracted with $Et_2O$. The combined organic layers were washed with brine, dried over $MgSO_4$, filtered, and concentrated down to a yellow oil (2.61 g, 99%). $^1$H NMR (600 MHz, Chloroform-*d*) δ 0.97 (s, 9H), 0.19 (s, 6H).

**Synthesis of 91** Made analogously to **89** with the following reagents: 1,3-cyclpentadiene (24.4 µL, 300 µmol, 1 equiv), **90** (276 mg, 1.50 mmol, 5 equiv), 9-mesityl-2,7-dimethyl-10-phenylacridin-10-ium tetrafluoroborate (3.7 mg, 7.5 µL, 2.5 mol%), $(PhS)_2$ (9.8 mg, 45 µmol, 15 mol%), 2,6-lutidine (70.0 uL, 600 µmol, 2 equiv), and $MeNO_2$ (6 mL). Product was purified by chromatography with 10% $Et_2O$/hexanes; both isomers were obtained as light brown oils (collective mass of 190 mg, 67%). *Z*-Isomer (33.0 mg) $^1$H NMR (400 MHz, Chloroform-*d*) δ 6.50 (s, 1H), 5.76 (dd, *J* = 5.5, 2.5 Hz, 1H), 5.54 (dd, *J* = 5.5, 2.5 Hz, 1H), 5.09 (t, *J* = 6.1 Hz, 1H), 3.96 (dd, *J* = 4.0, 2.1 Hz, 1H), 2.82 – 2.66 (m, 3H), 0.93 (s, 17H), 0.20 (d, *J* = 10.4 Hz, 8H). *E*-isomer (157 mg) $^1$H NMR (400 MHz, Chloroform-*d*) δ 6.92

(d, *J* = 1.8 Hz, 1H), 5.82 – 5.77 (m, 1H), 5.52 (d, *J* = 7.9 Hz, 1H), 5.05 (t, *J* = 5.6 Hz, 1H), 4.06 (d, *J* = 5.8 Hz, 1H), 2.85 – 2.69 (m, 2H), 0.94 (s, 9H), 0.20 (s, 6H).

**Scheme B.36** Synthesis of **92**

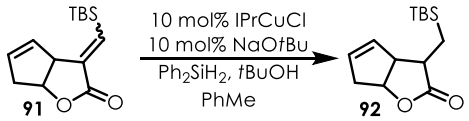


**Synthesis of 92** IPrCuCl (77.5 mg, 159 μmol, 10 mol%) and NaO*t*-Bu (15.3 mg, 159 μmol, 10 mol%) were stirred in PhMe (8 mL) for 10 min before adding $Ph_2SiH_2$ (390 μL, 2.12 mmol, 1.3 equiv). Another 5 min of stirring, more $Ph_2SiH_2$ (780 μL, 4.24 mmol, 2.6 equiv) and PhMe (8 mL) were added followed by a solution of **91** (398 mg, 1.59 mmol, 1 equiv), *t*-BuOH (608 μL, 6.36 mmol, 4 equiv), and PhMe (8 mL). The contents were stirred overnight at room temperature, then diluted with water and EtOAc. The aqueous layer was extracted with EtOAc, and the combined organic layers washed with brine and dried over $MgSO_4$. Filtration and concentration gave a residue that was purified by chromatography using 20% $Et_2O$/hexanes to give a pale-yellow oil (143 mg, 35%). $^1$H NMR (400 MHz, Chloroform-*d*) δ 5.84 (d, *J* = 7.8 Hz, 1H), 5.66 – 5.60 (m, 1H), 4.98 (t, *J* = 4.7 Hz, 1H), 3.57 – 3.49 (m, 1H), 2.70 (d, *J* = 4.7 Hz, 3H), 1.25 (dd, *J* = 15.1, 3.6 Hz, 1H), 0.92 (s, 9H), 0.68 (dd, *J* = 15.1, 11.7 Hz, 1H), 0.05 (s, 6H).

**Scheme B.37** Synthesis of **93**

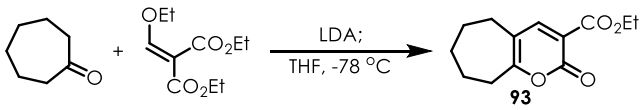


**Synthesis of 93** LDA was freshly prepared at -78 °C with DIPA (1.62 mL, 11.6 mmol, 1.3 equiv), THF (23 mL) and *n*-BuLi (2.5 M, 4.3 mL, 10.7 mmol, 1.2 equiv). A solution of cycloheptanone (1.05 mL, 8.92 mmol, 1 equiv) in THF (9 mL) was added and the mixture stirred for 30 min before the addition of diethyl 2-(ethoxymethylene)malonate (2.16 mL, 10.7 mmol, 1.2

equiv). After stirring for 16 hr, the solution was quenched with 2 N HCl and extracted with $Et_2O$. The combined organic layers were washed with brine, dried over $MgSO_4$, filtered, and concentrated to give a residue that was purified with 40% EtOAc/hexanes to obtain a peach-colored oil (1.74 g, 83%). $^1$H NMR (400 MHz, Chloroform-*d*) δ 8.05 (s, 1H), 4.34 (q, *J* = 7.1 Hz, 2H), 2.82 – 2.70 (m, 2H), 2.61 – 2.49 (m, 2H), 1.82 (p, *J* = 6.0 Hz, 2H), 1.73 – 1.58 (m, 4H), 1.36 (t, *J* = 7.1 Hz, 3H).

### B.3 Characterization Data

This section contains NMR and crystallography data (as relevant) for compounds **5-14** and **20-36**, which are associated with our final diastereoselective route to the *ABCD* ring system of rubriflordilactone B. As compounds **5-11**, **20**, **22-24** are known, only $^1$H NMR data is presented.

#### B.3.1 NMR Spectra

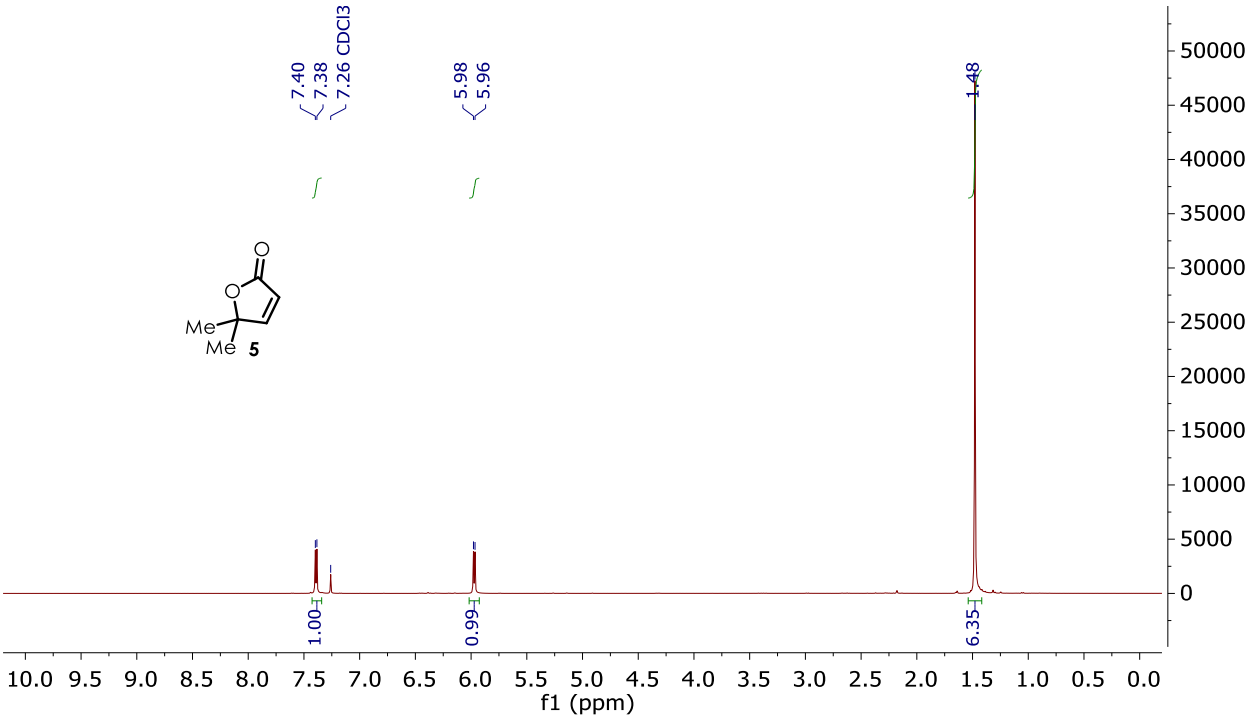


**Figure B.1** $^1$H NMR Spectrum of **5**

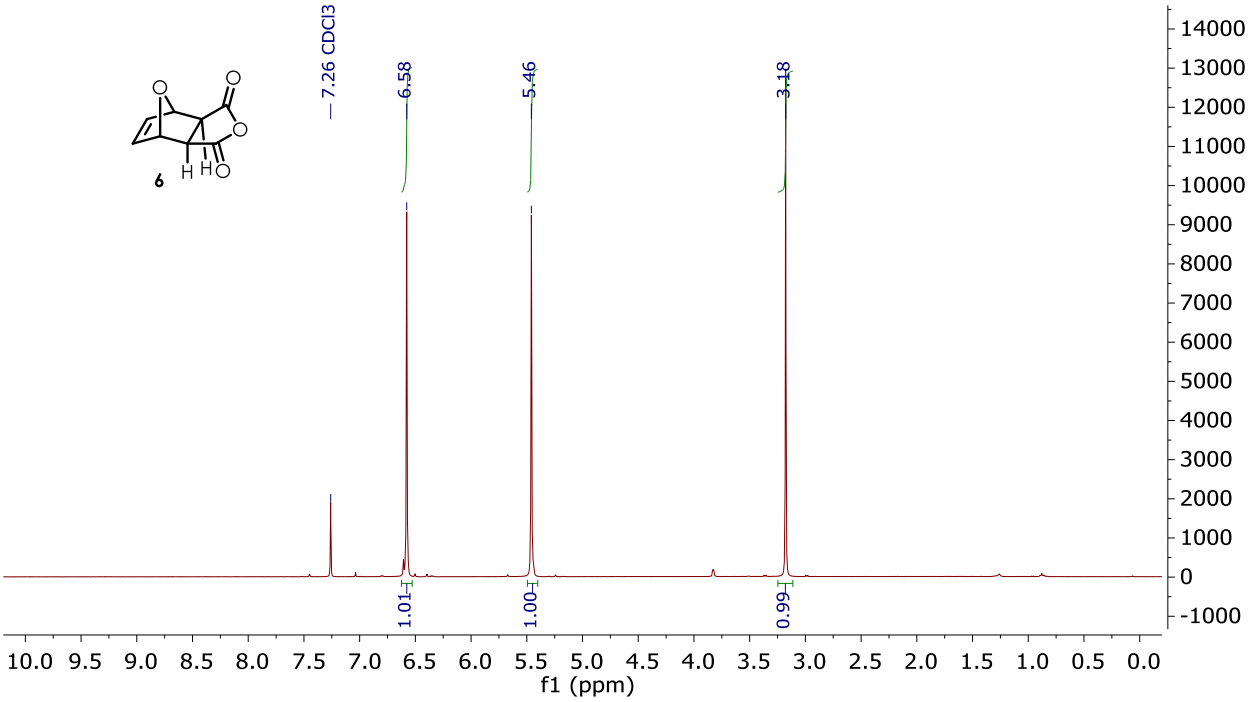


**Figure B.2** $^{1}$H NMR Spectrum of **6**

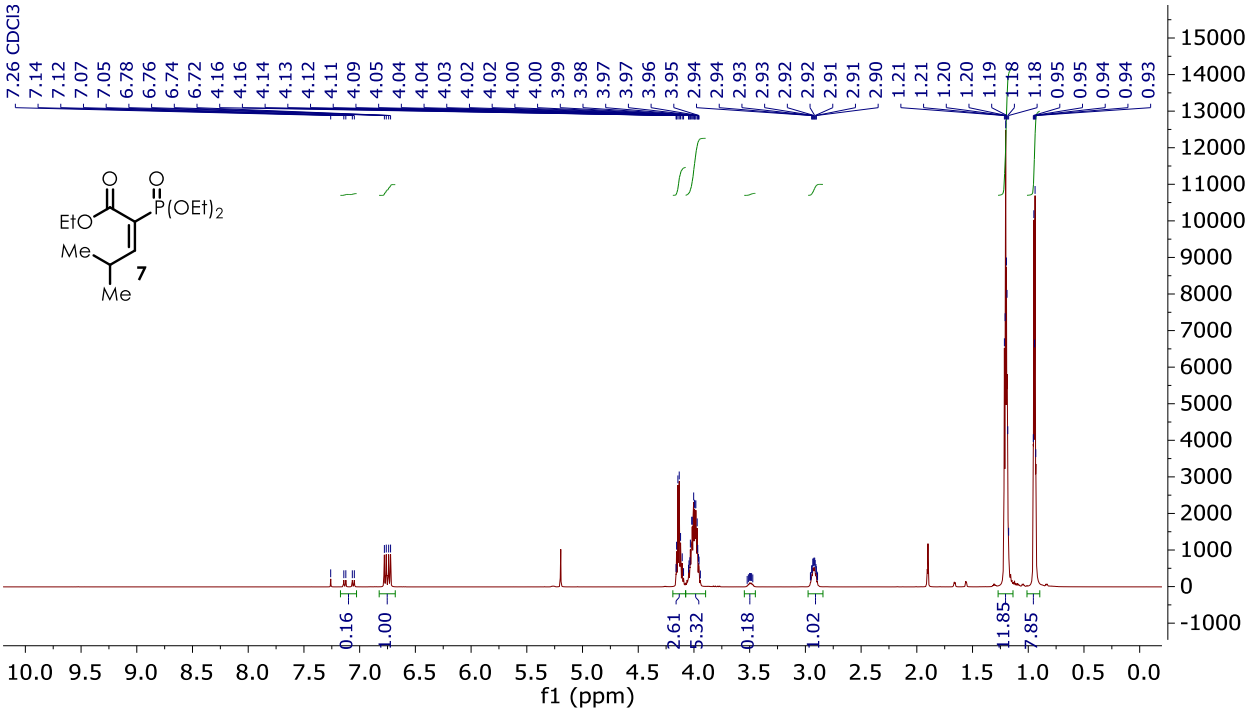


**Figure B.3** $^{1}$H NMR Spectrum of **7**

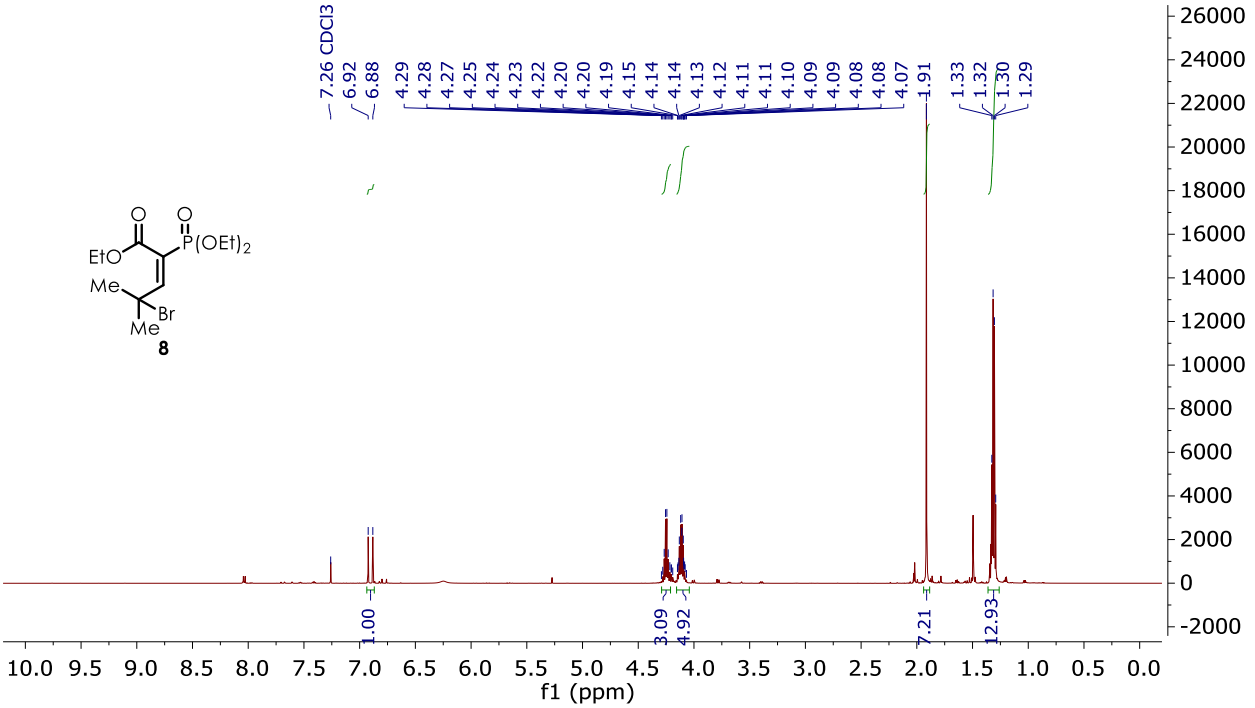


**Figure B.4** $^{1}$H NMR Spectrum of **8**

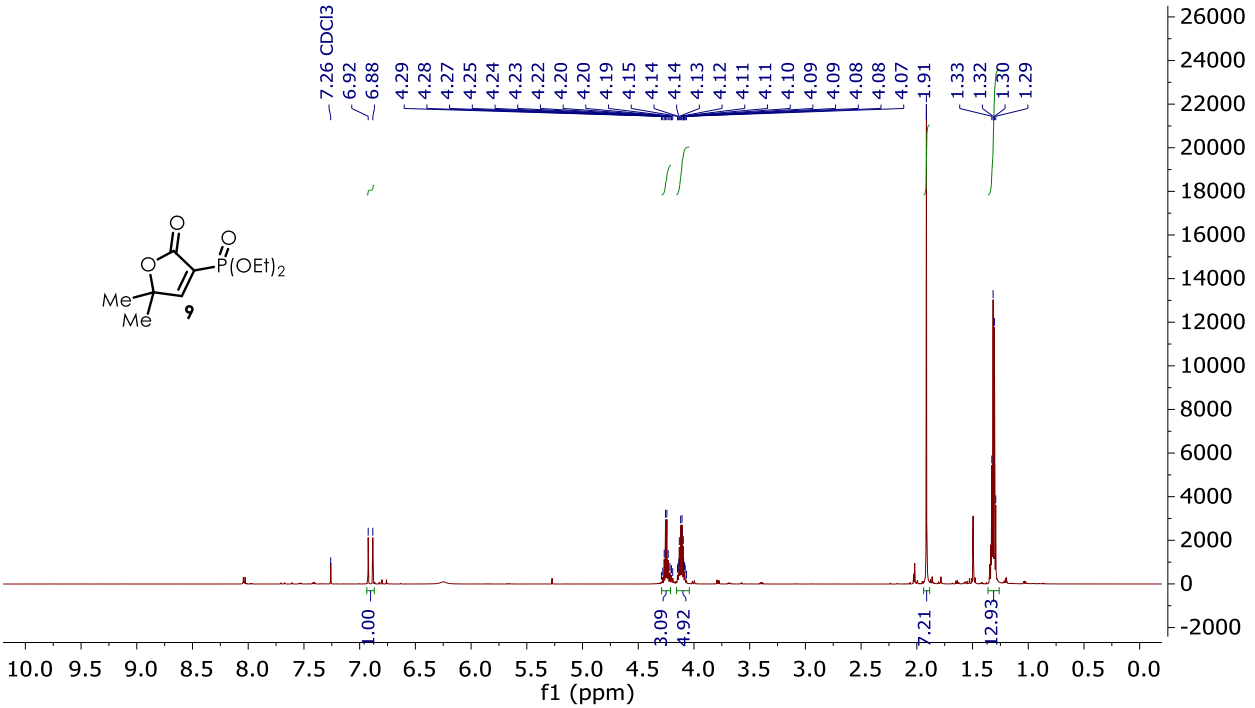


**Figure B.5** $^{1}$H NMR Spectrum of **9**

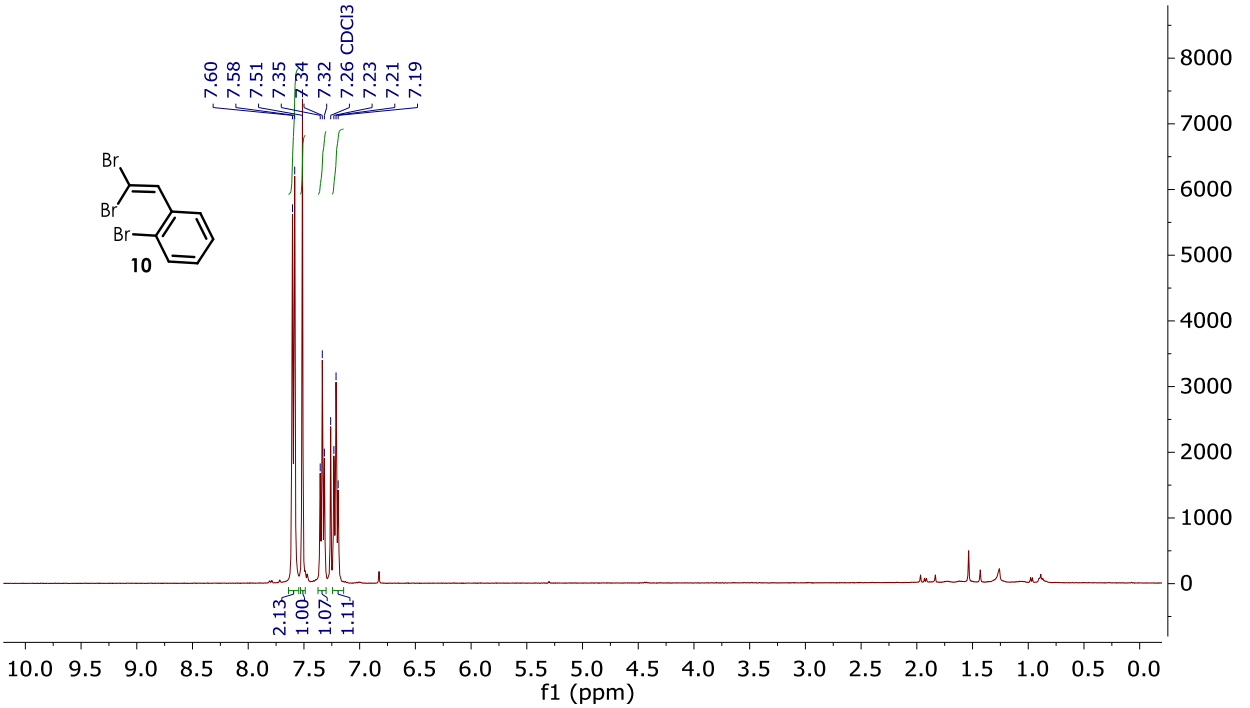


**Figure B.6** $^{1}$H NMR Spectrum of **10**

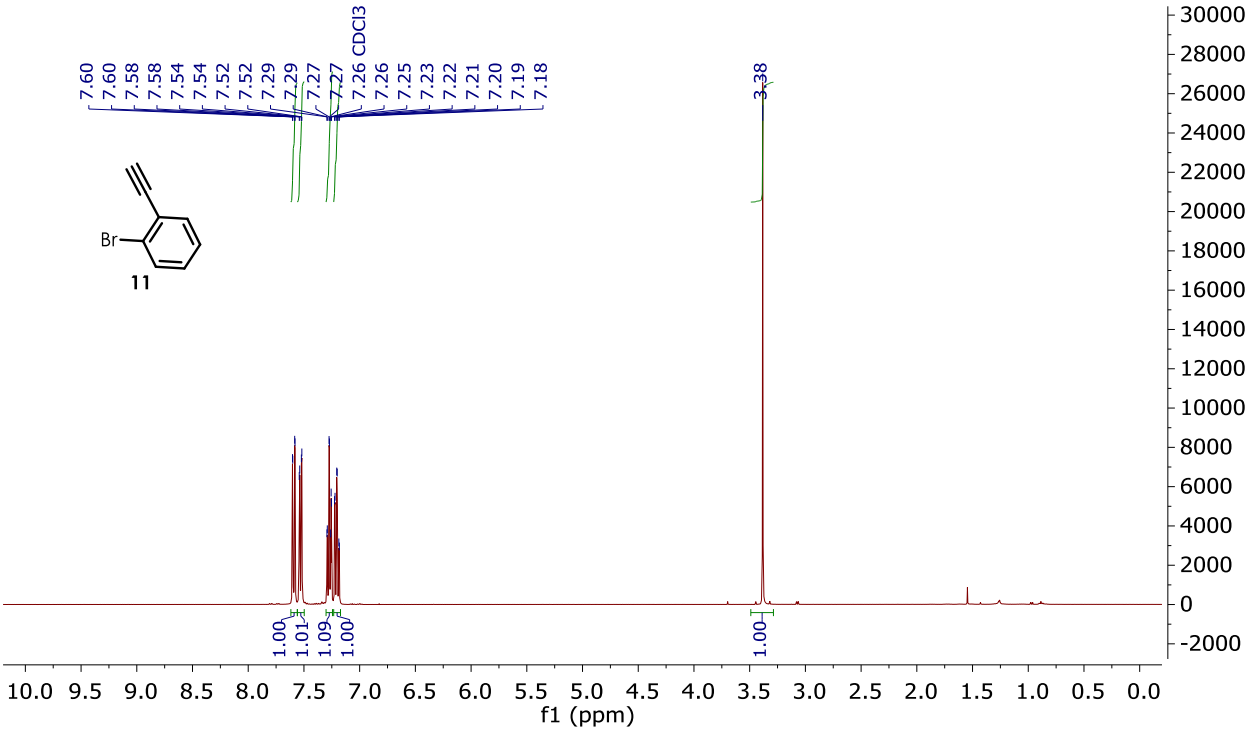


**Figure B.7** $^{1}$H NMR Spectrum of **11**

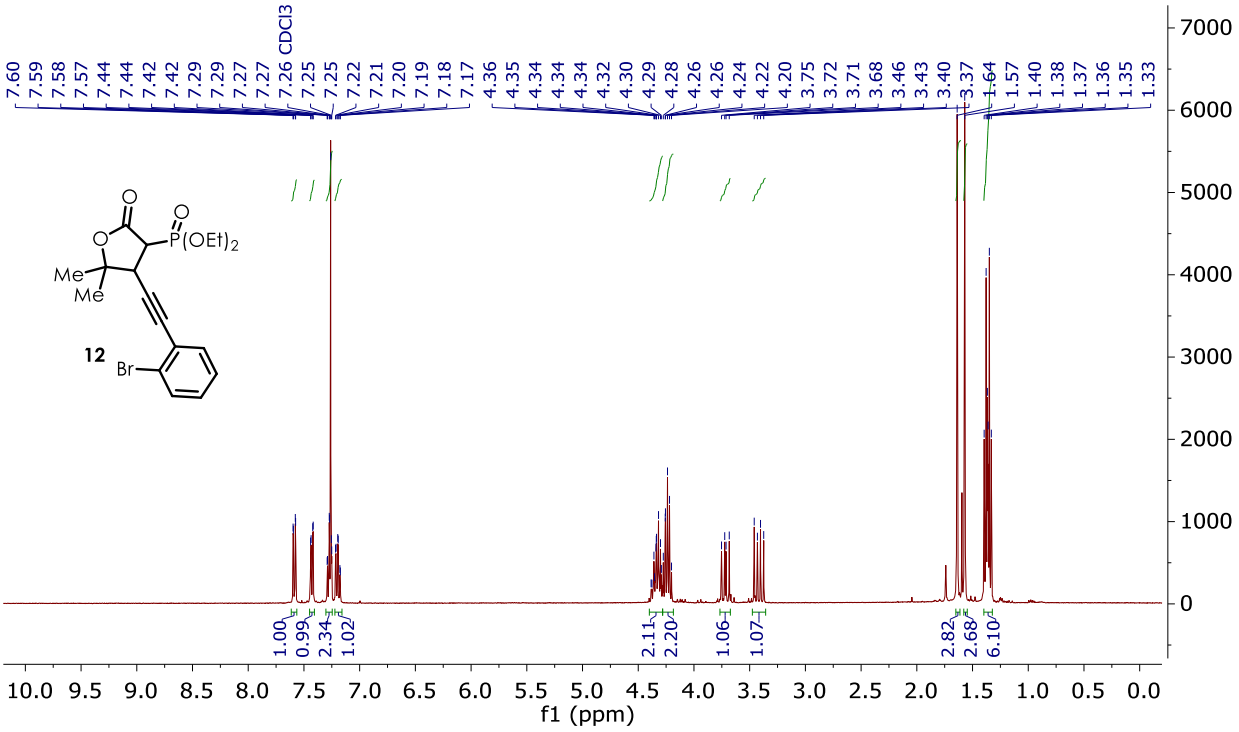


**Figure B.8** $^{1}$H NMR Spectrum of **12**

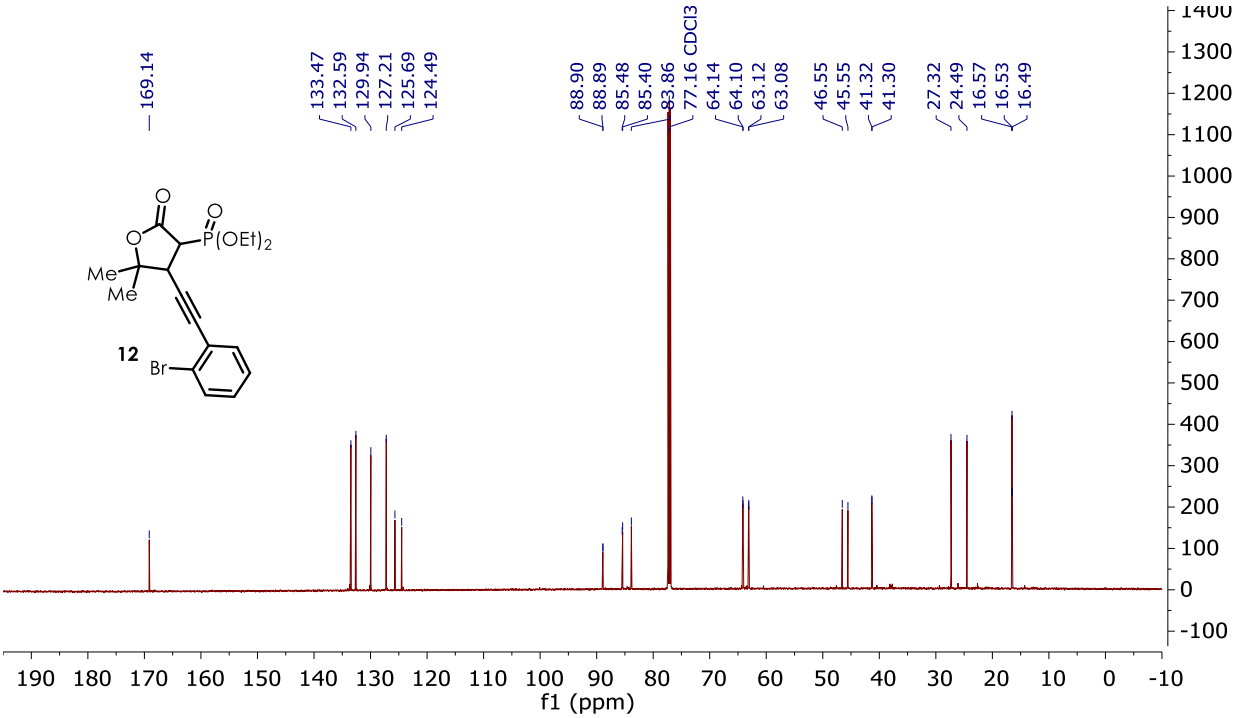


**Figure B.9** $^{13}$C NMR Spectrum of **12**

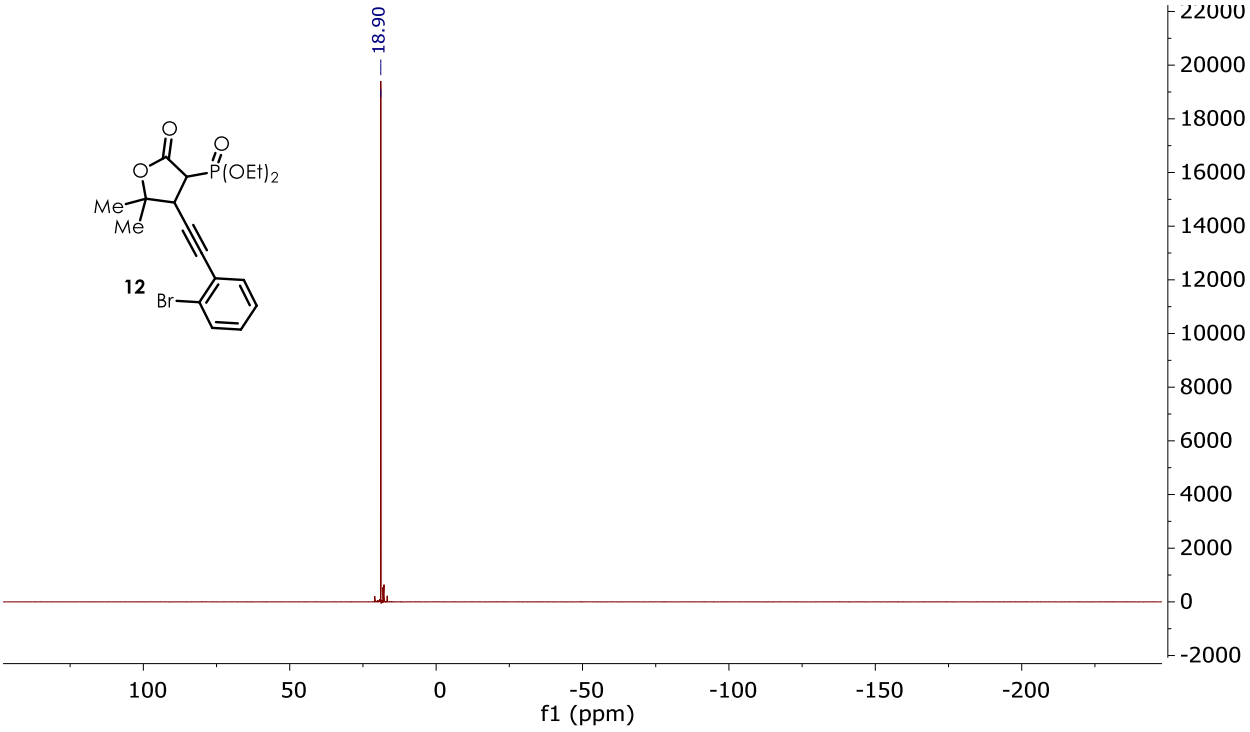


**Figure B.10** $^{31}$P NMR Spectrum of **12**

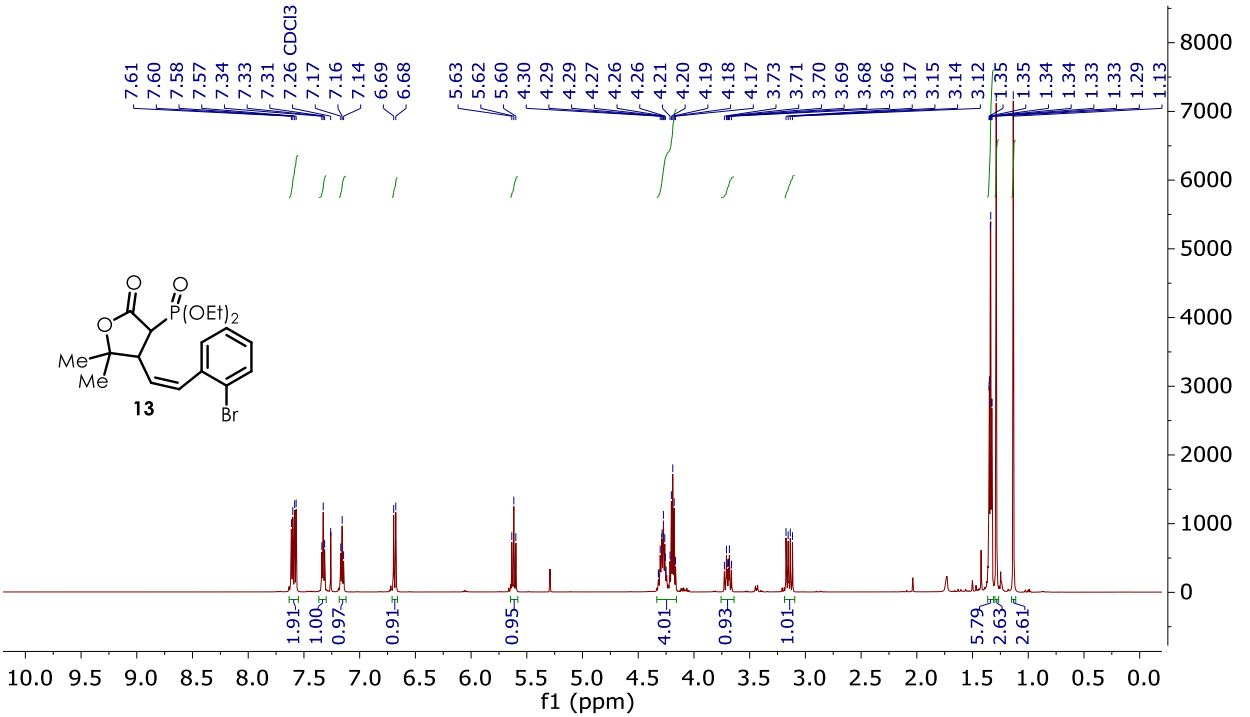


**Figure B.11** $^{1}$H NMR Spectrum of **13**

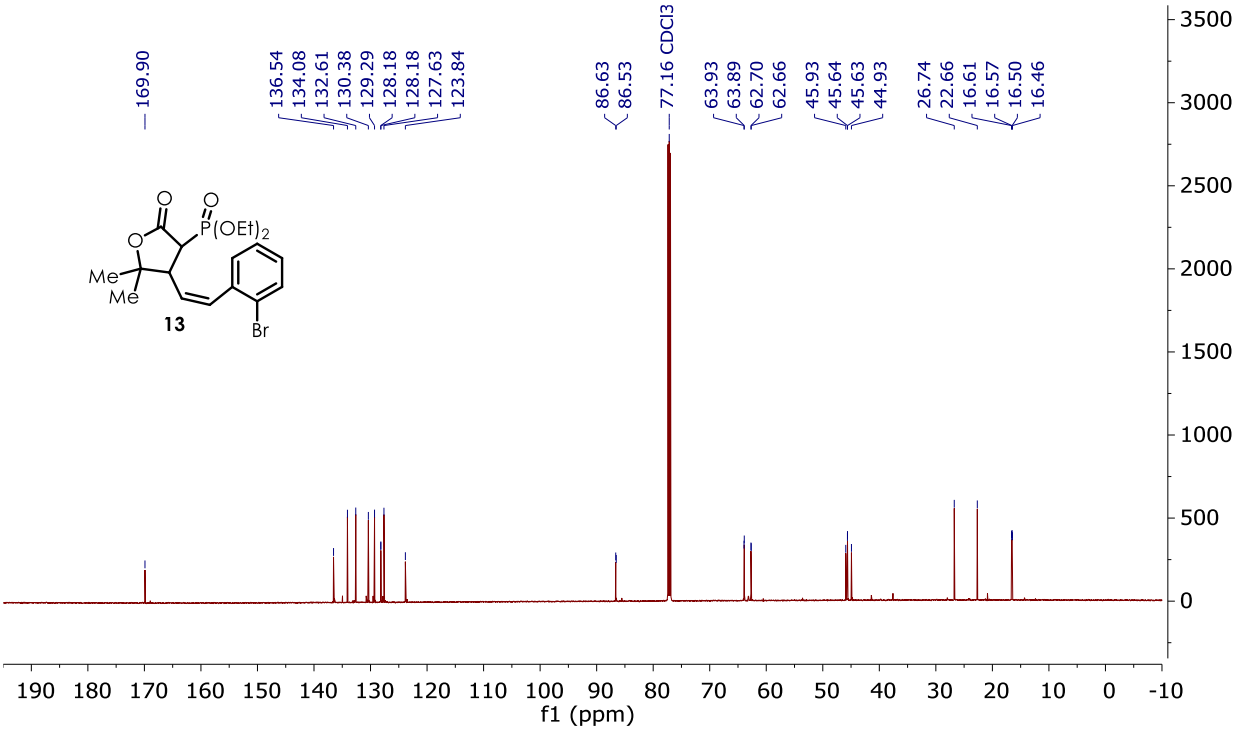


**Figure B.12** $^{13}$C NMR Spectrum of **13**

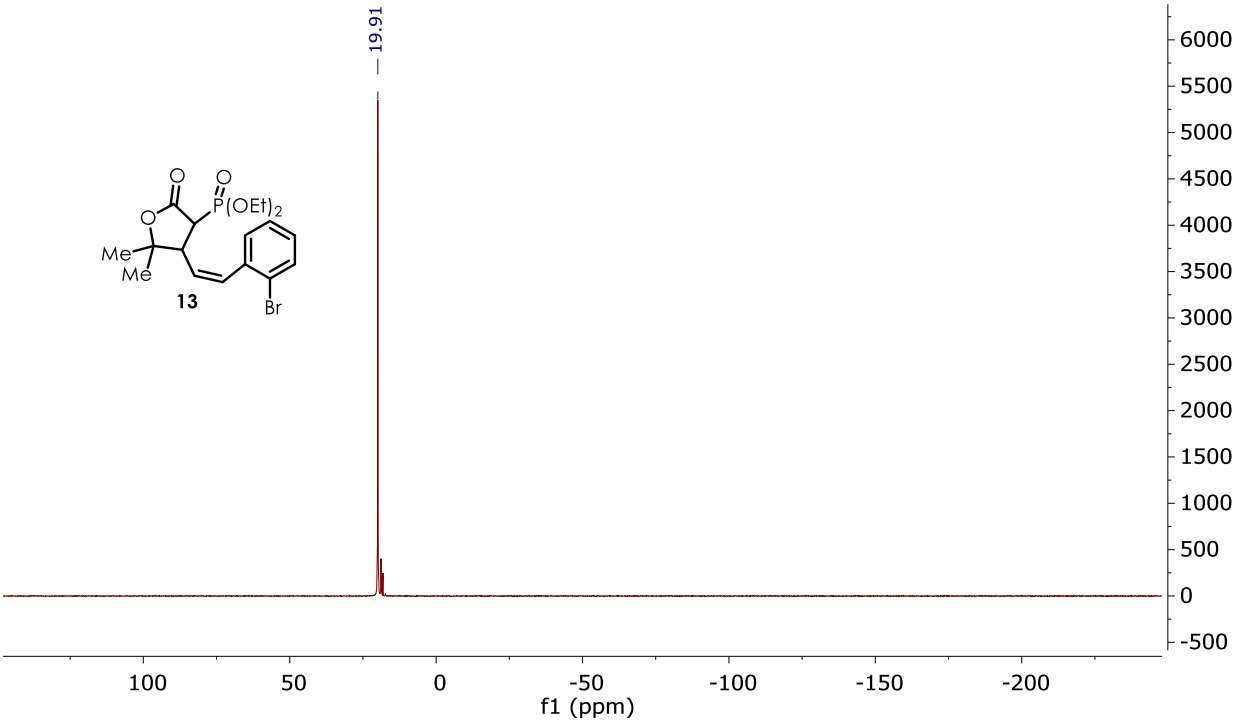


**Figure B.13** $^{31}$P NMR Spectrum of **13**

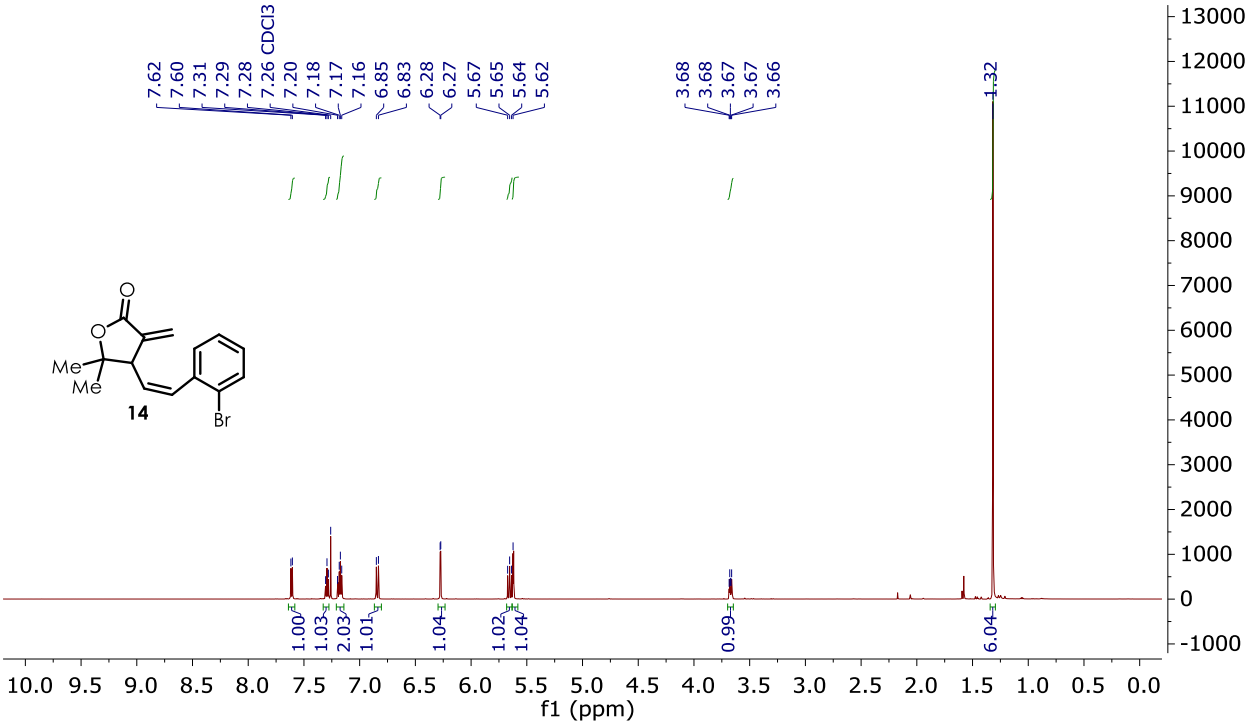


**Figure B.14** $^{1}$H NMR Spectrum of **14**

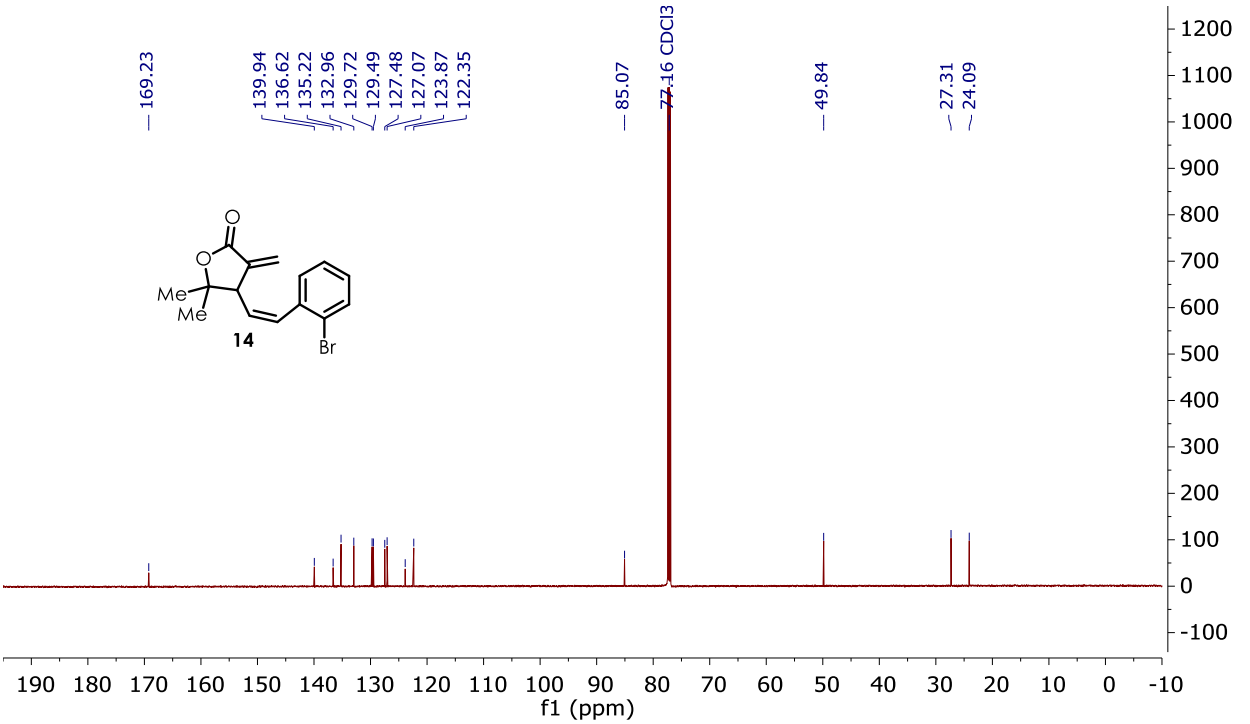


**Figure B.15** $^{13}$C NMR Spectrum of **14**

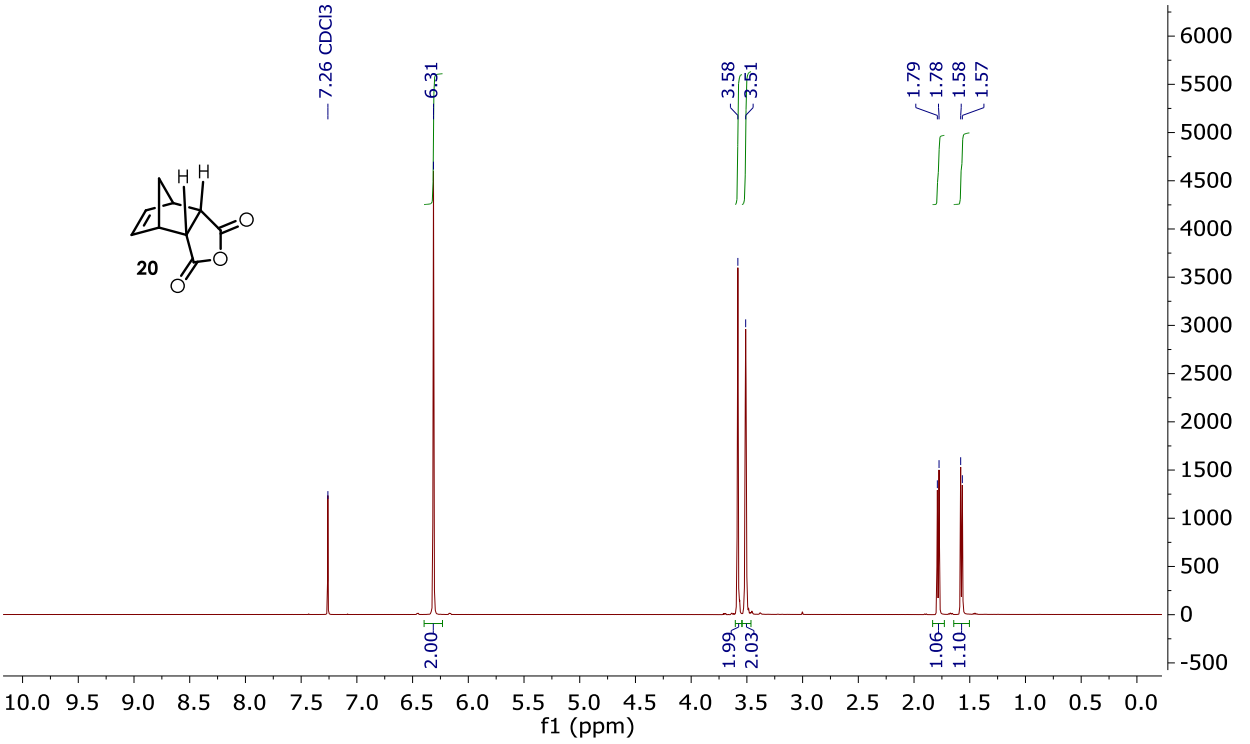


**Figure B.16** $^{1}$H NMR Spectrum of **20**

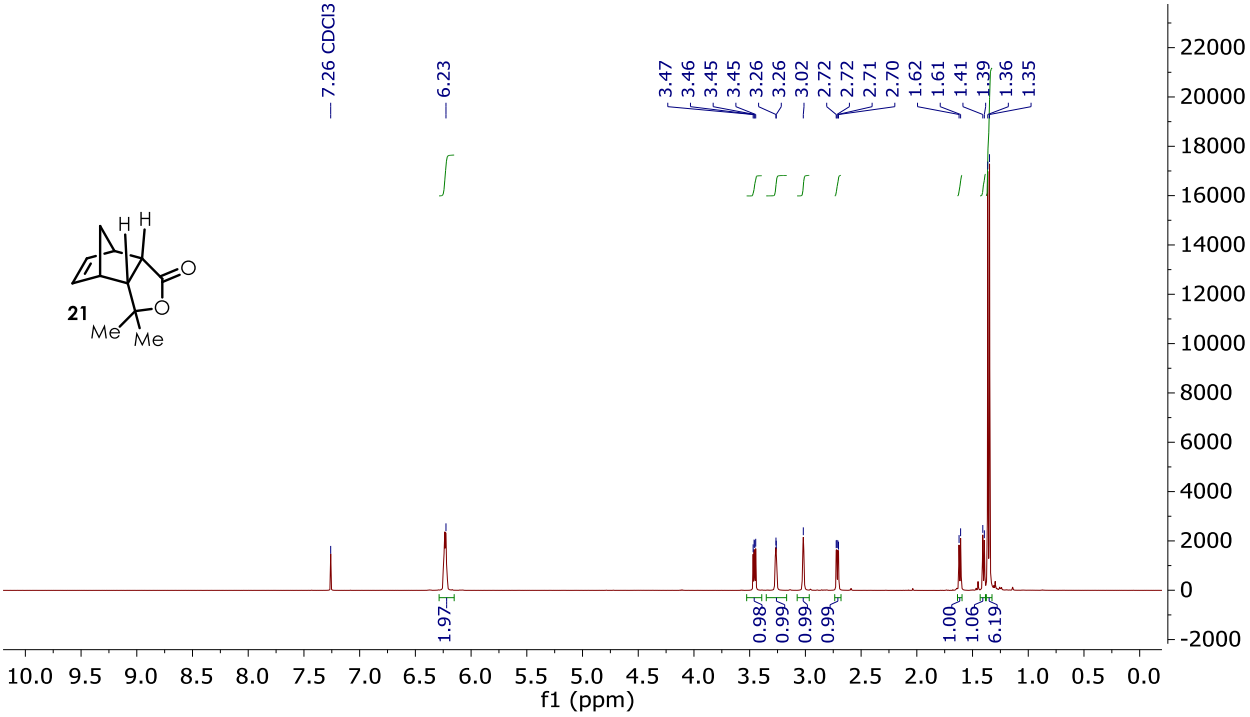


**Figure B.17** $^{1}$H NMR Spectrum of **21**

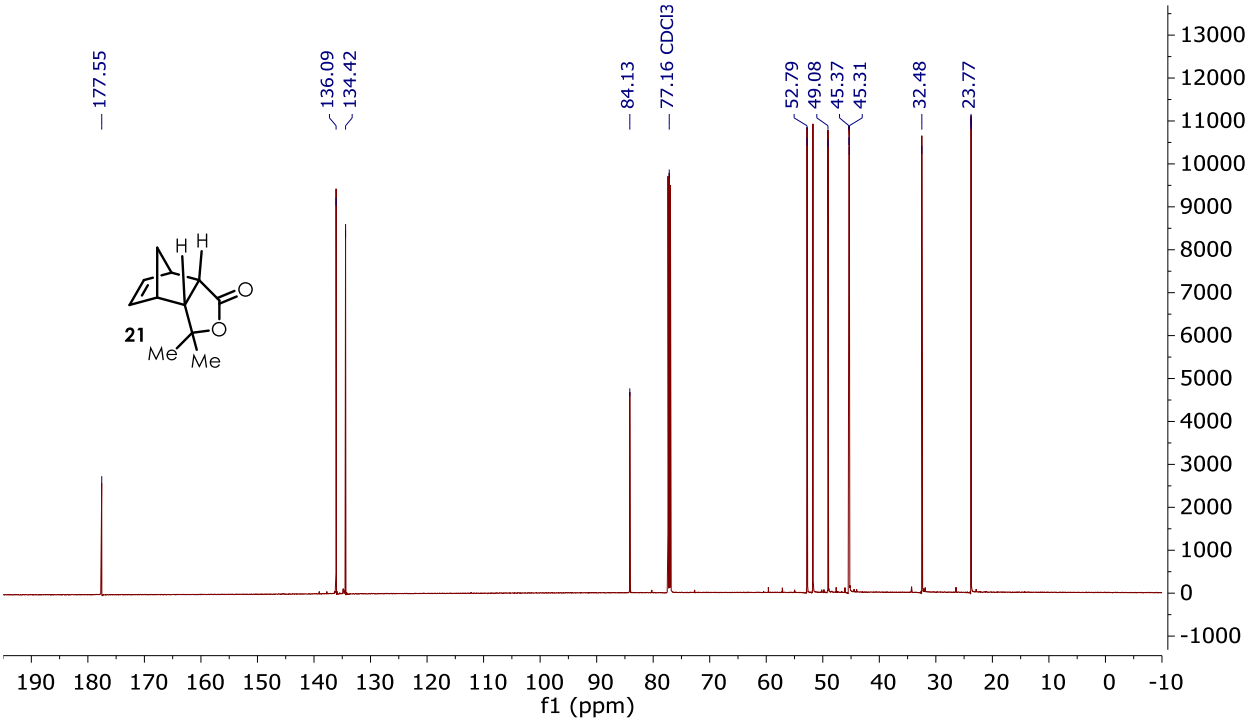


**Figure B.18** $^{13}$C NMR Spectrum of **21**

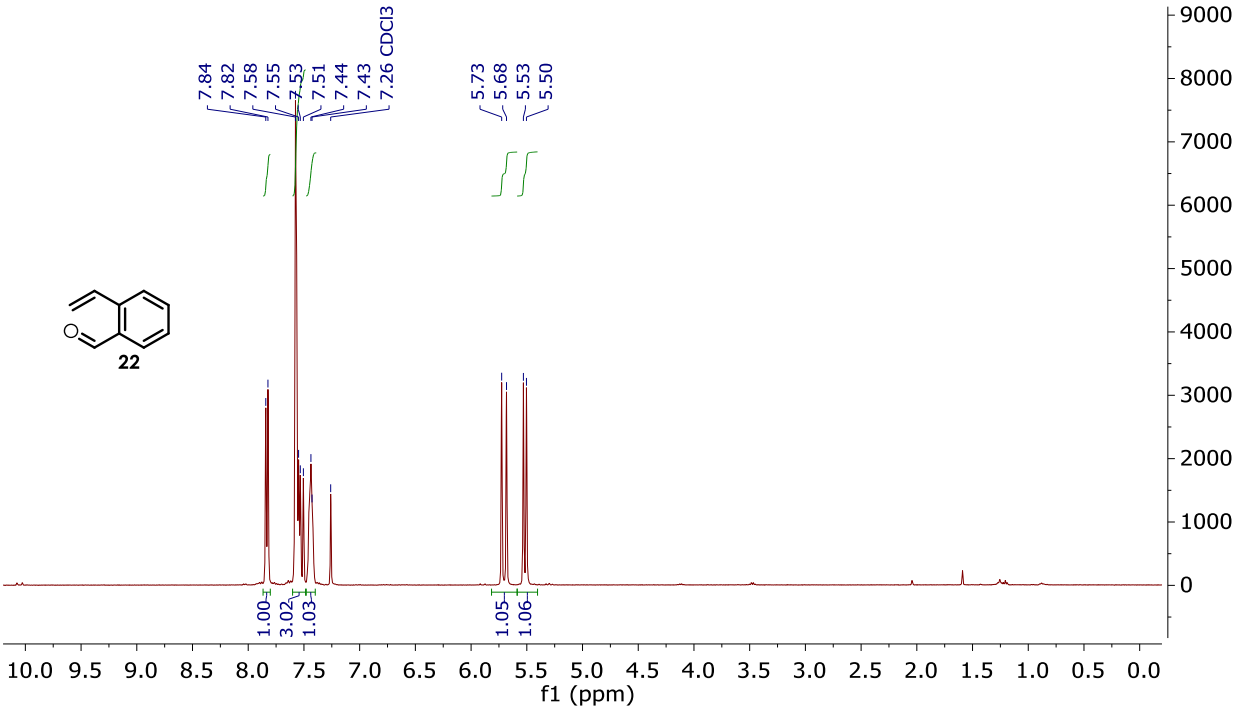


**Figure B.19** $^{1}$H NMR Spectrum of **22**

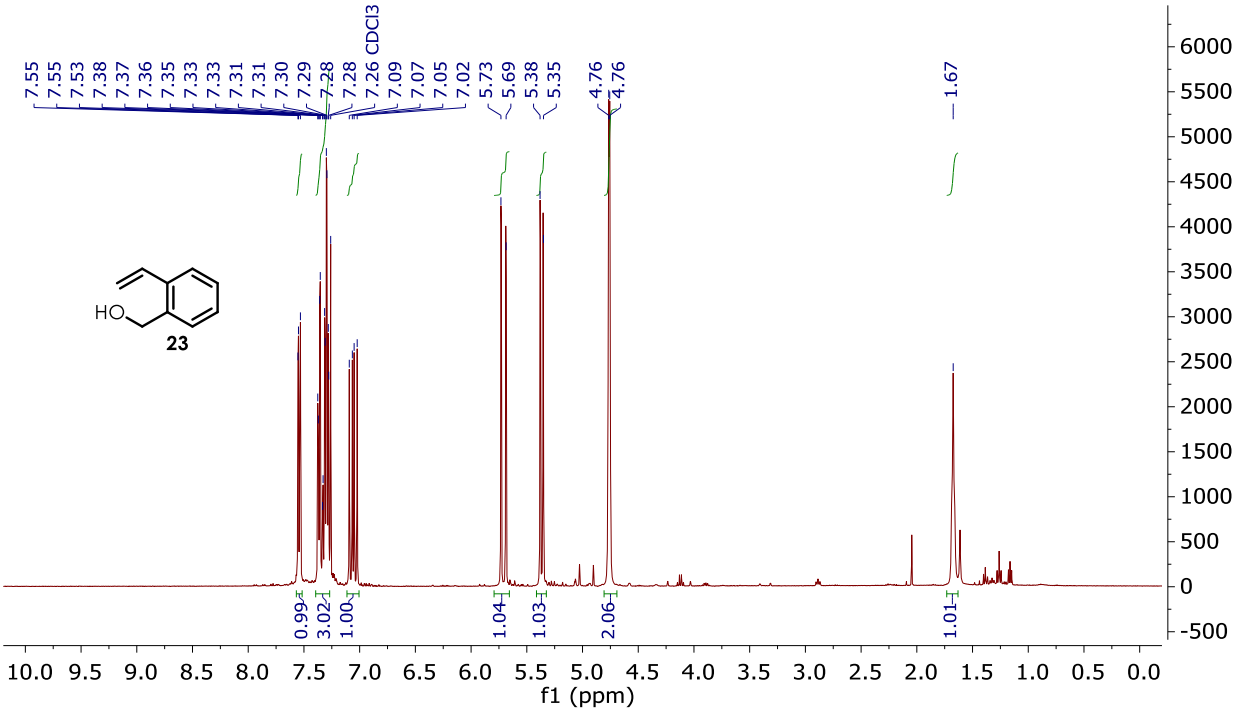


**Figure B.20** $^{1}$H NMR Spectrum of **23**

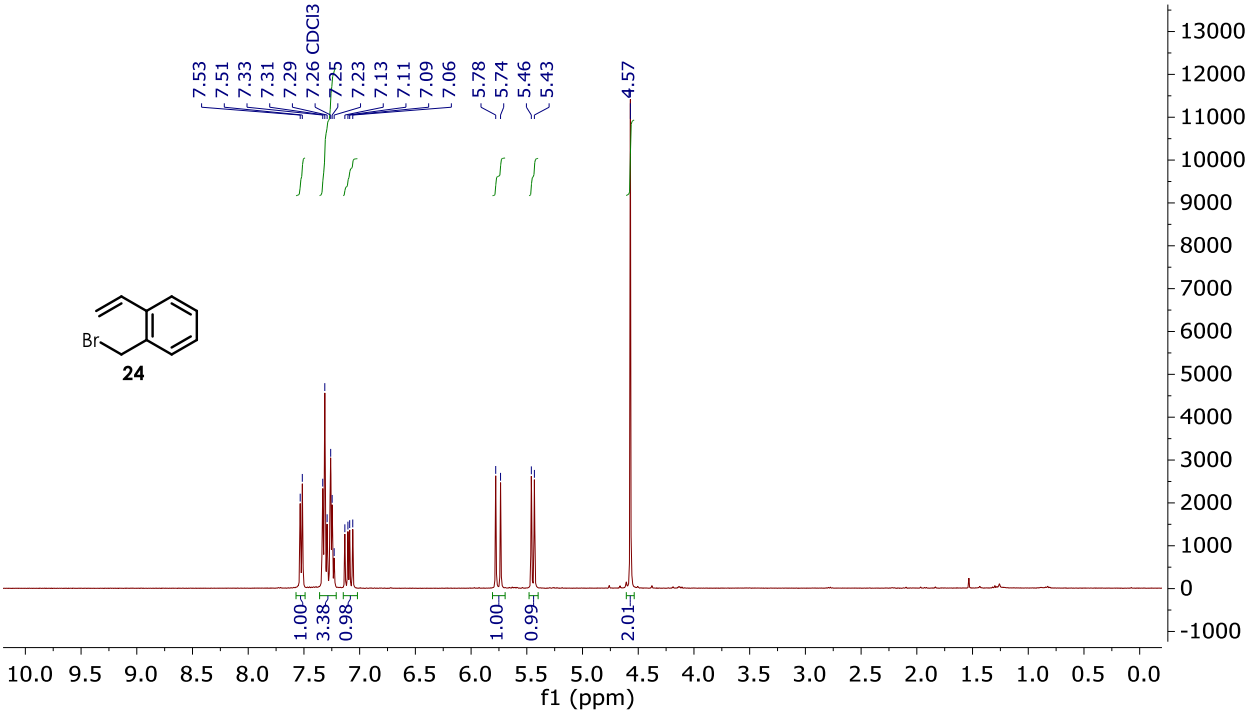


**Figure B.21** $^{1}$H NMR Spectrum of **24**

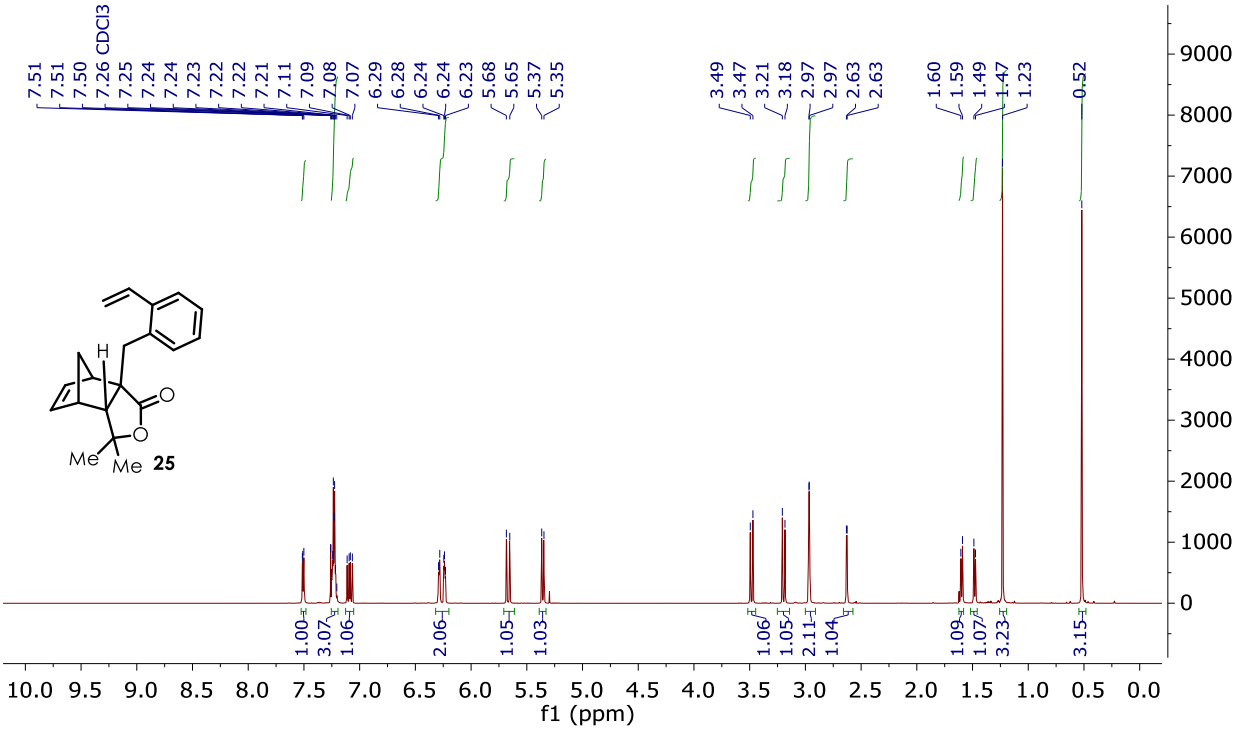


**Figure B.22** $^{1}$H NM Spectrum of **25**

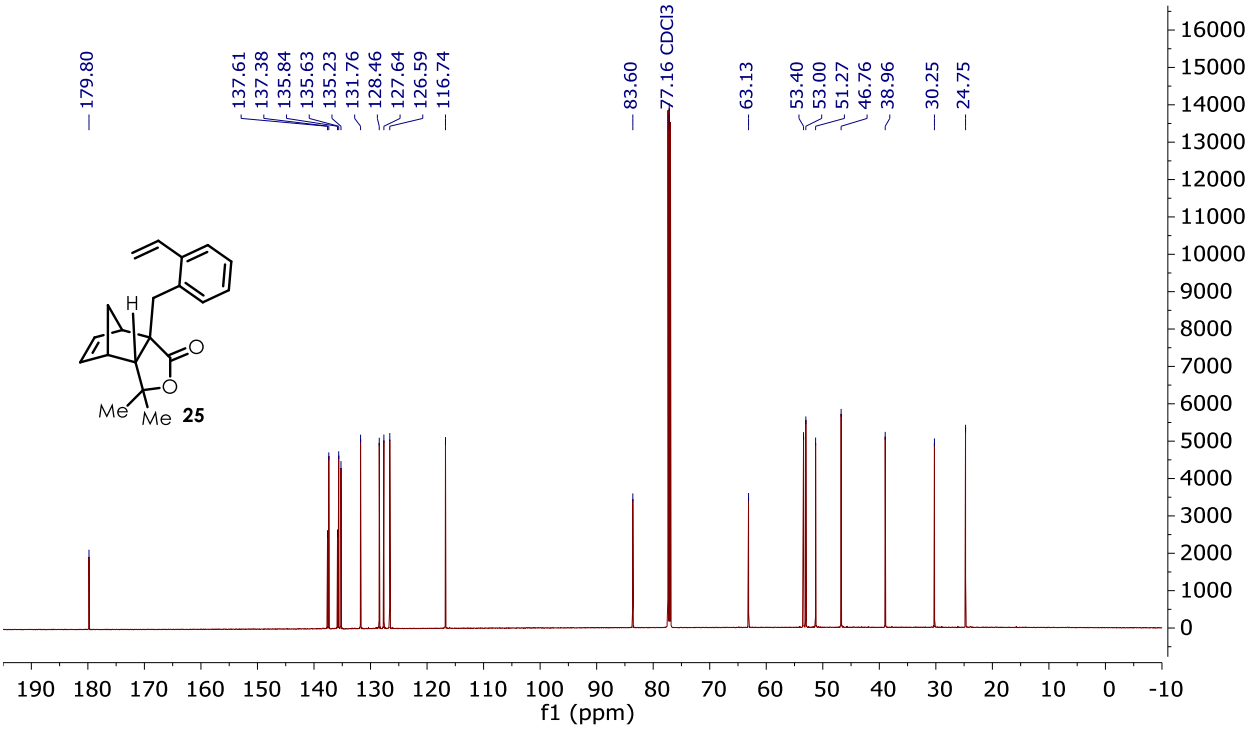


**Figure B.23** $^{13}$C NMR Spectrum of **25**

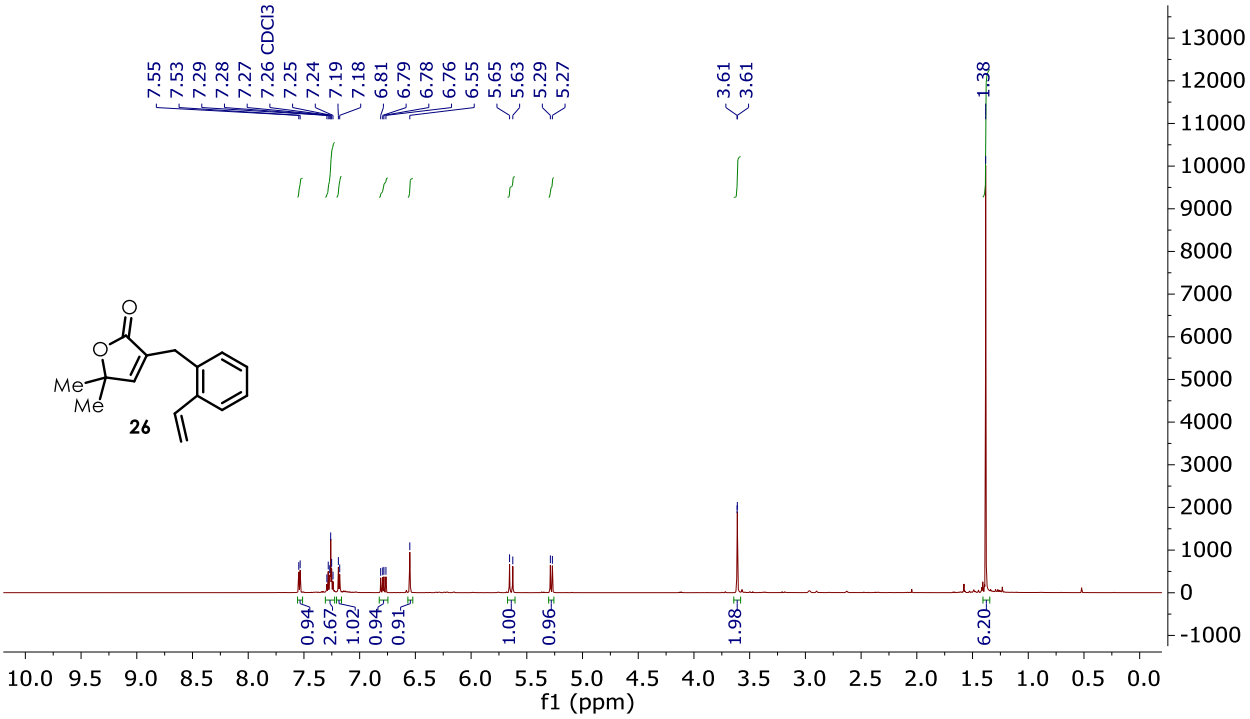


**Figure B.24** $^{1}$H NMR Spectrum of **26**

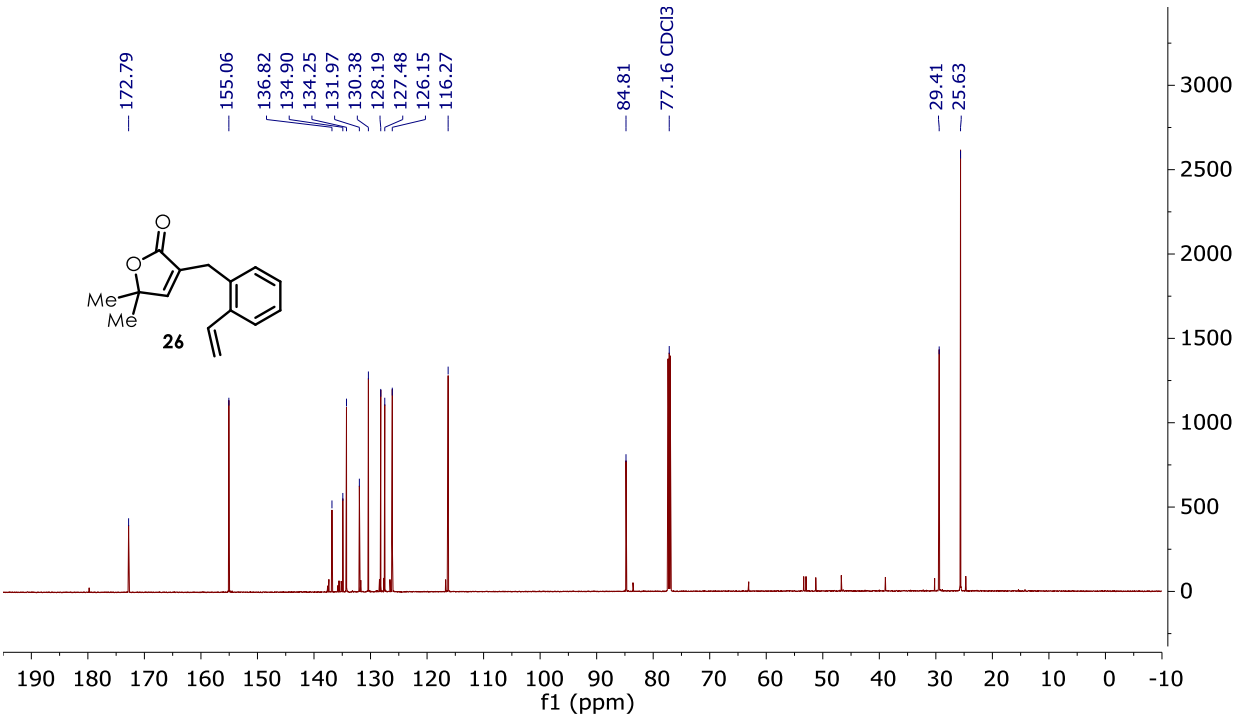


**Figure B.25** $^{13}$C NMR Spectrum of **26**

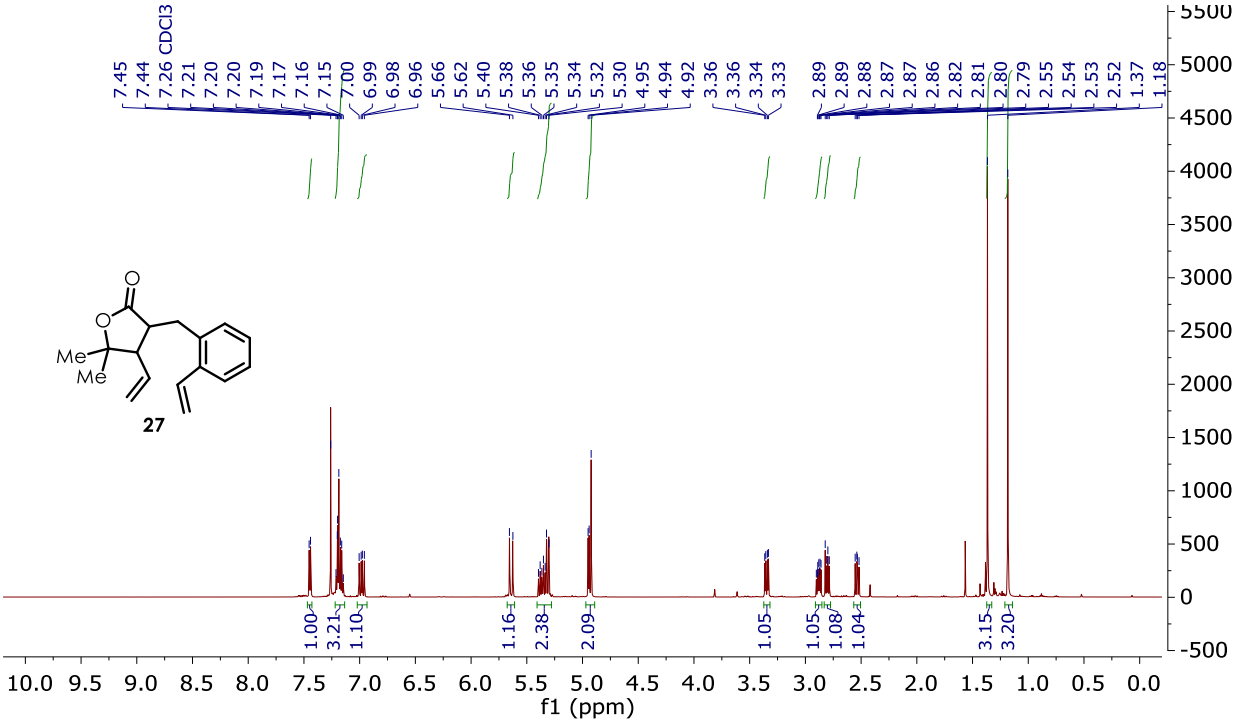


**Figure B.26** [1]H NMR Spectrum of **27**

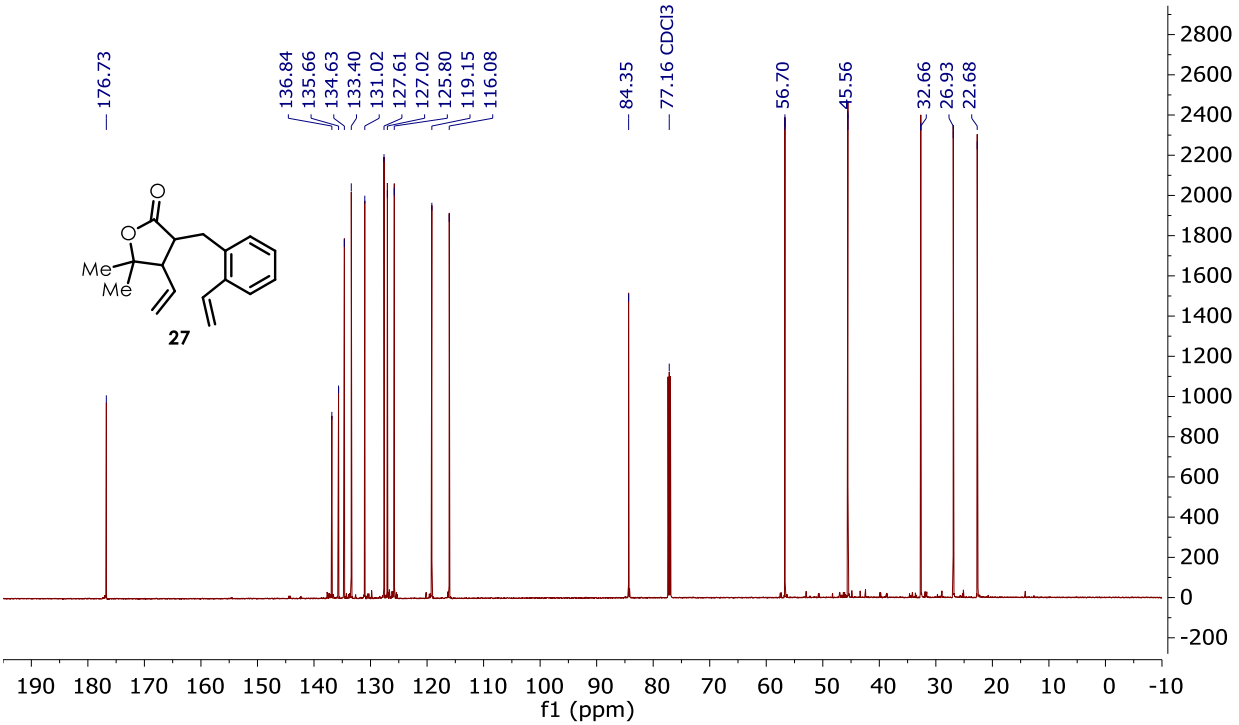


**Figure B.27** [13]C NMR Spectrum of **27**

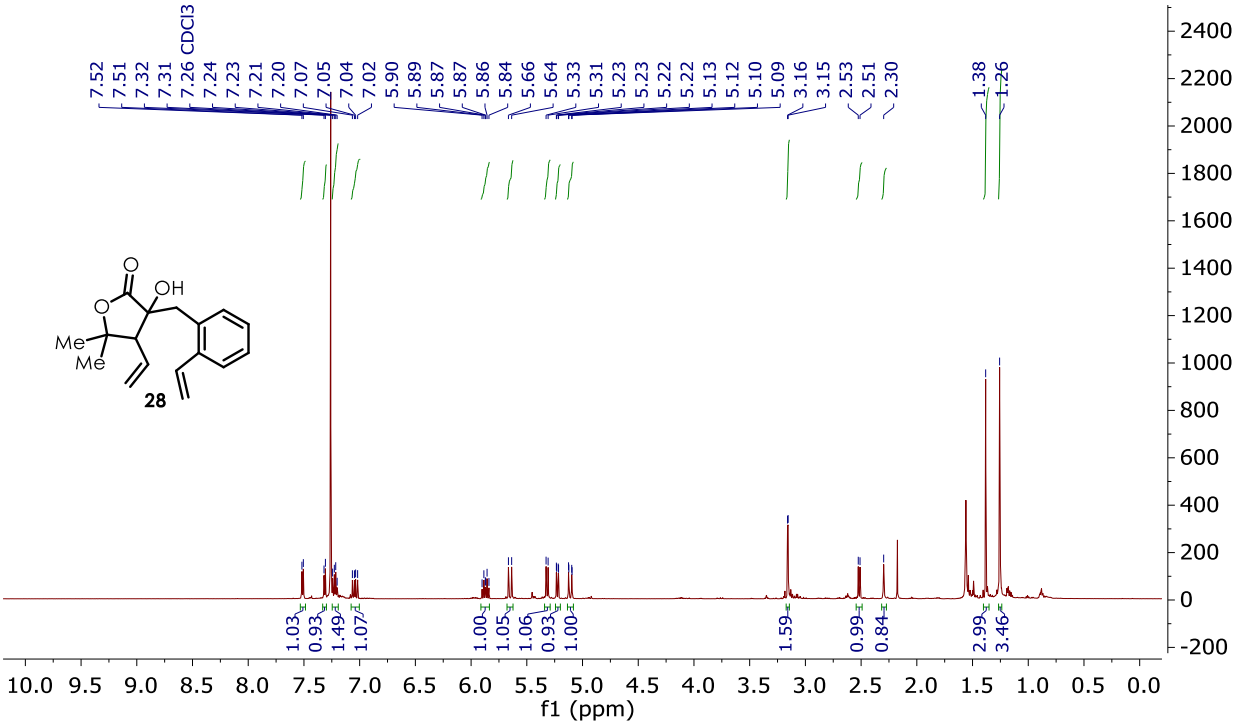


**Figure B.28** $^{1}$H NMR Spectrum of **28**

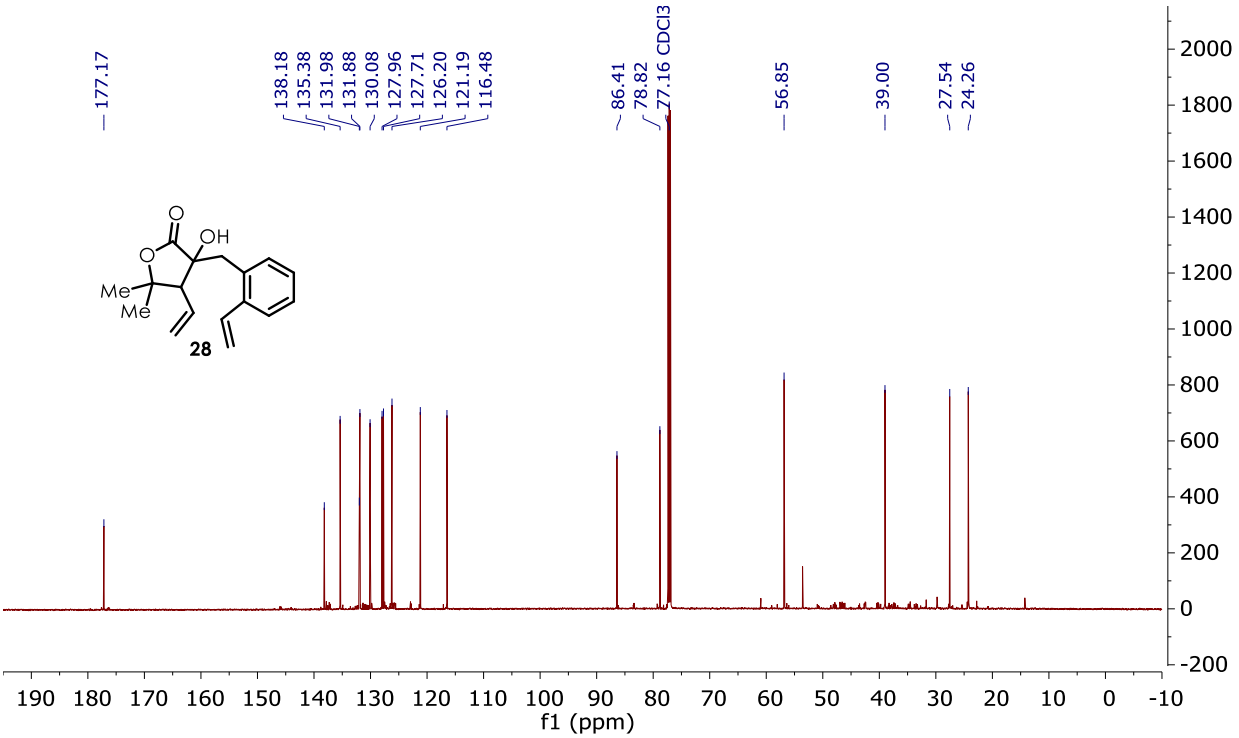


**Figure B.29** $^{13}$C NMR Spectrum of **28**

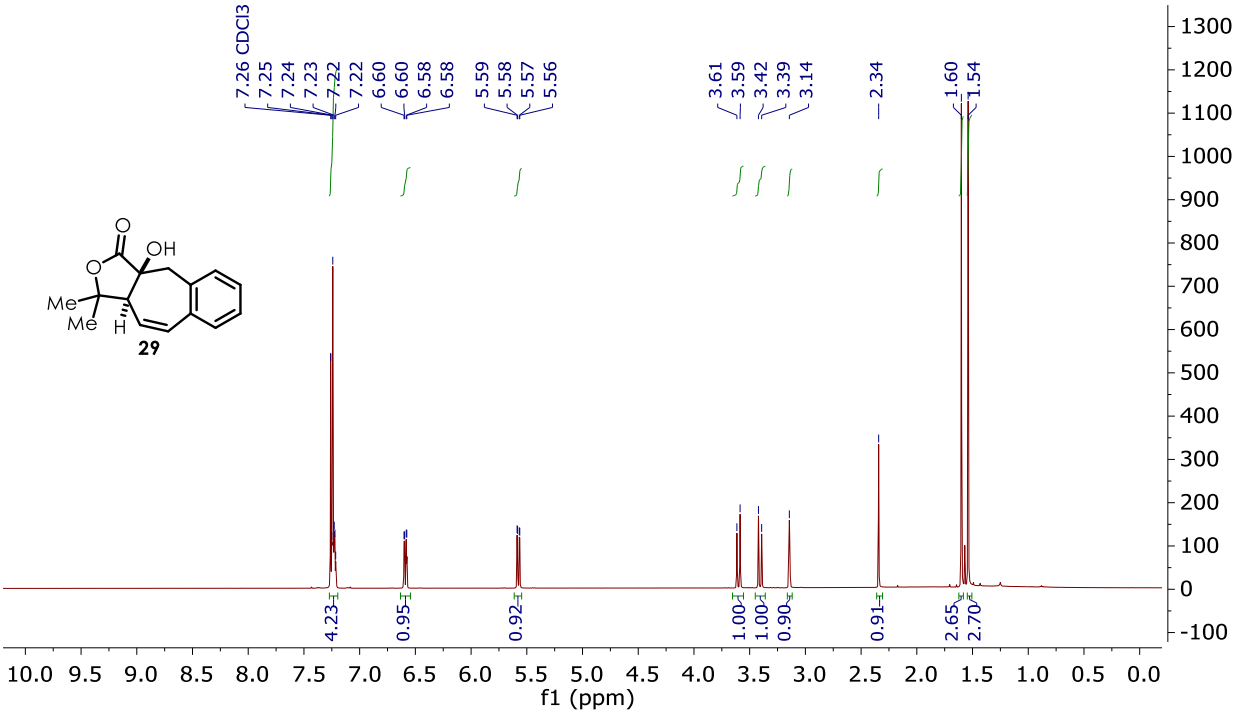


**Figure B.30** $^{1}$H NMR Spectrum of **29**

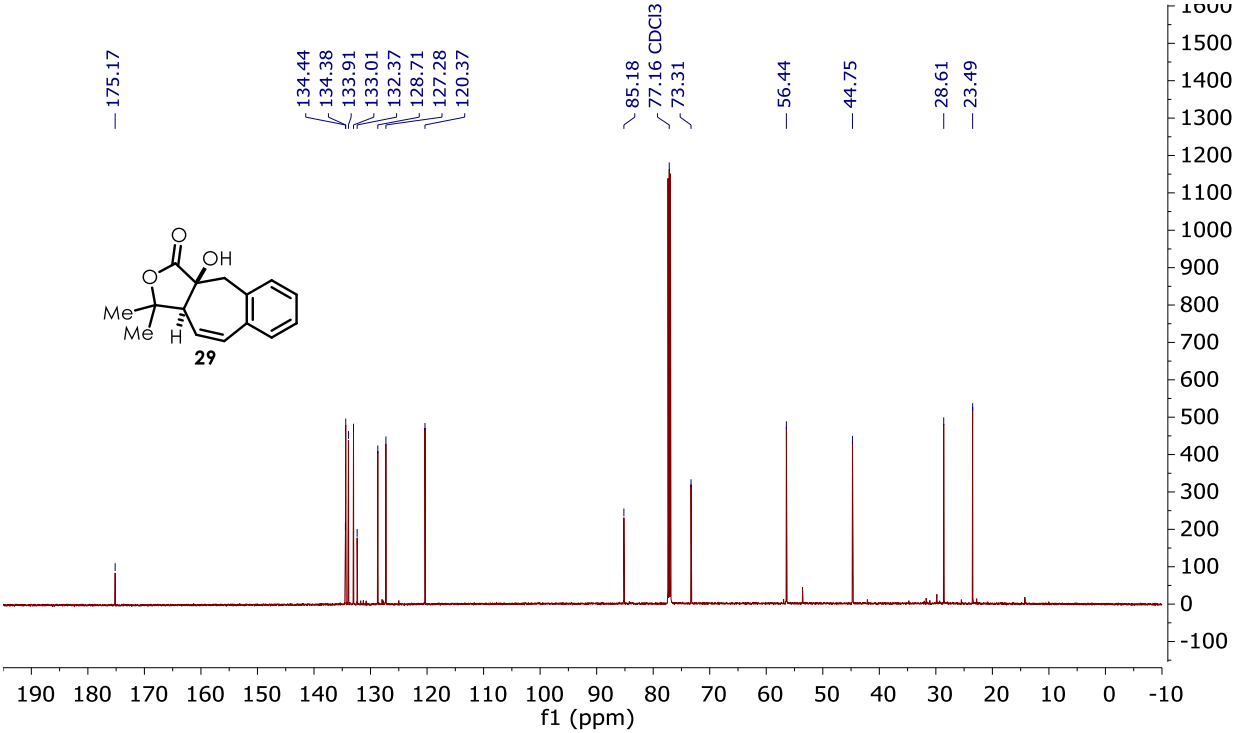


**Figure B.31** $^{13}$C NMR Spectrum of **29**

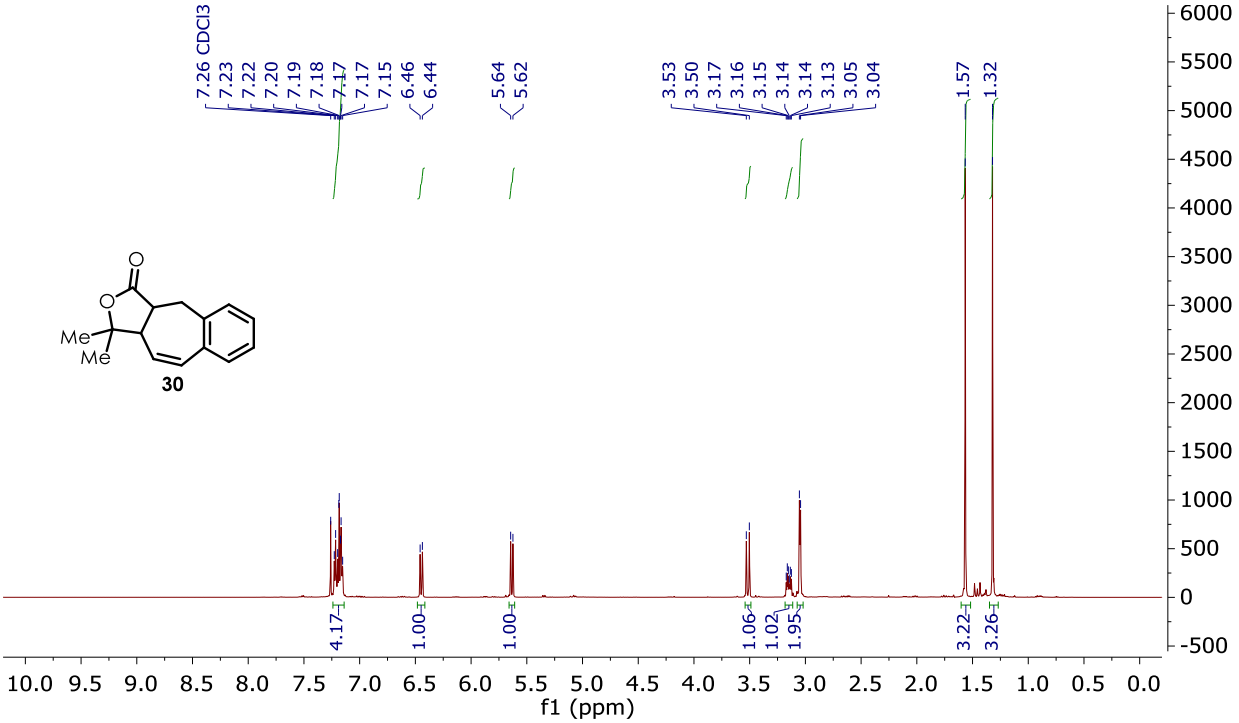


**Figure B.32** $^{1}$H NMR Spectrum of **30**

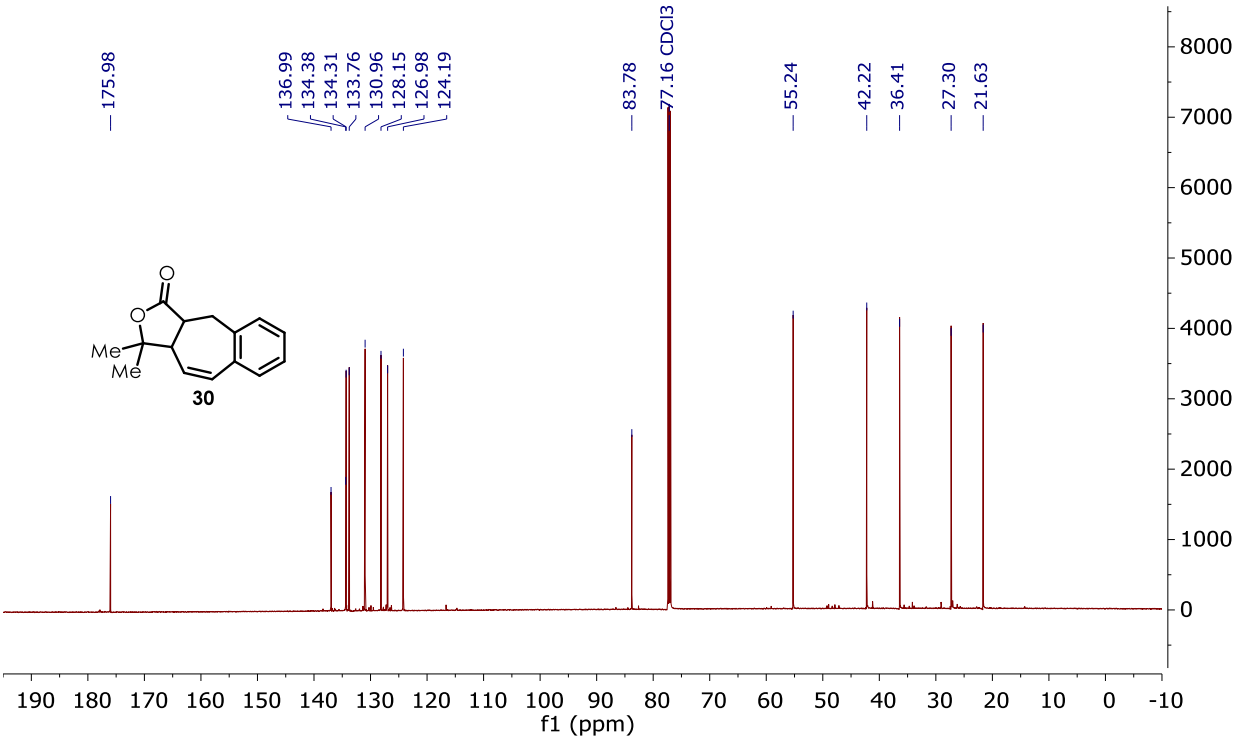


**Figure B.33** $^{13}$C NMR Spectrum of **30**

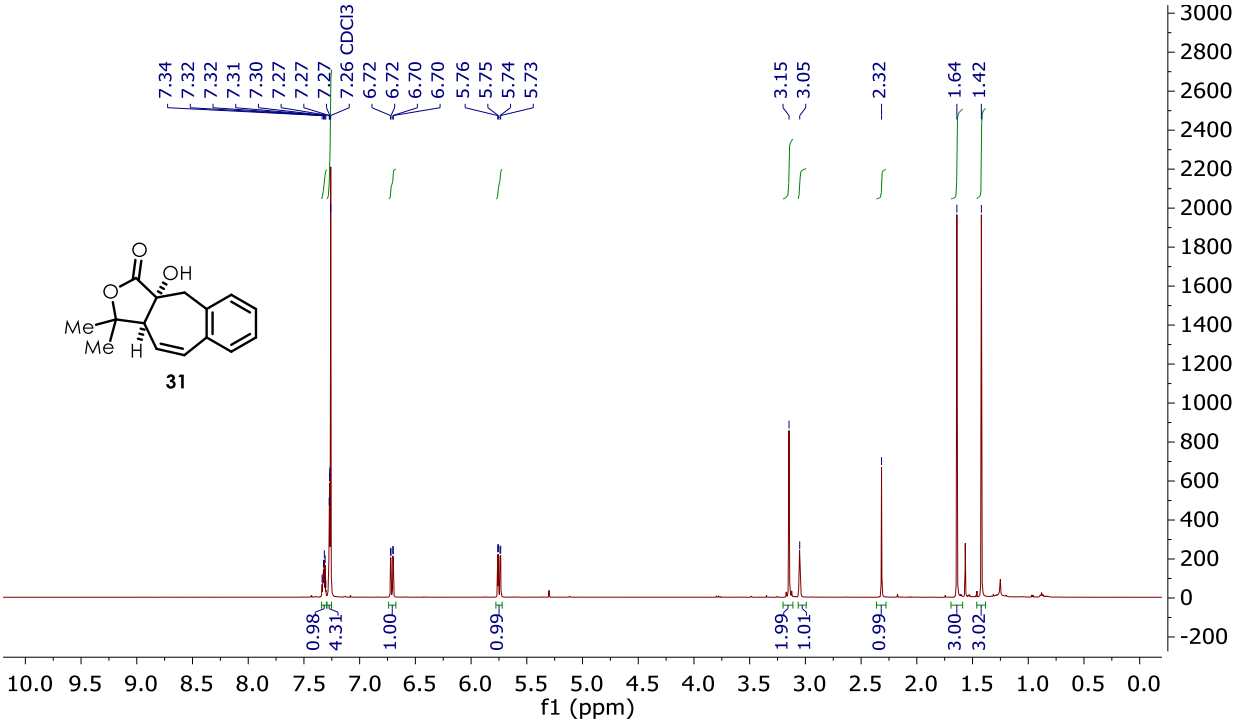


**Figure B.34** $^{1}$H NMR Spectrum of **31**

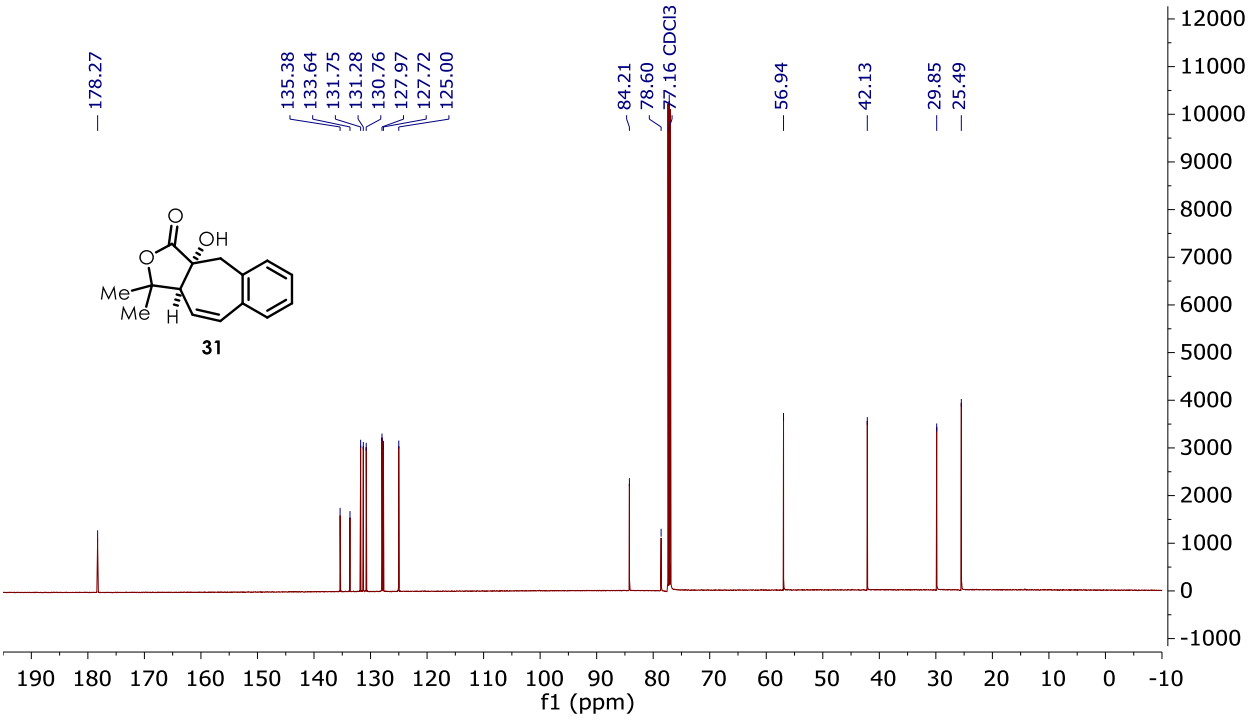


**Figure B.35** $^{13}$C NMR Spectrum of **31**

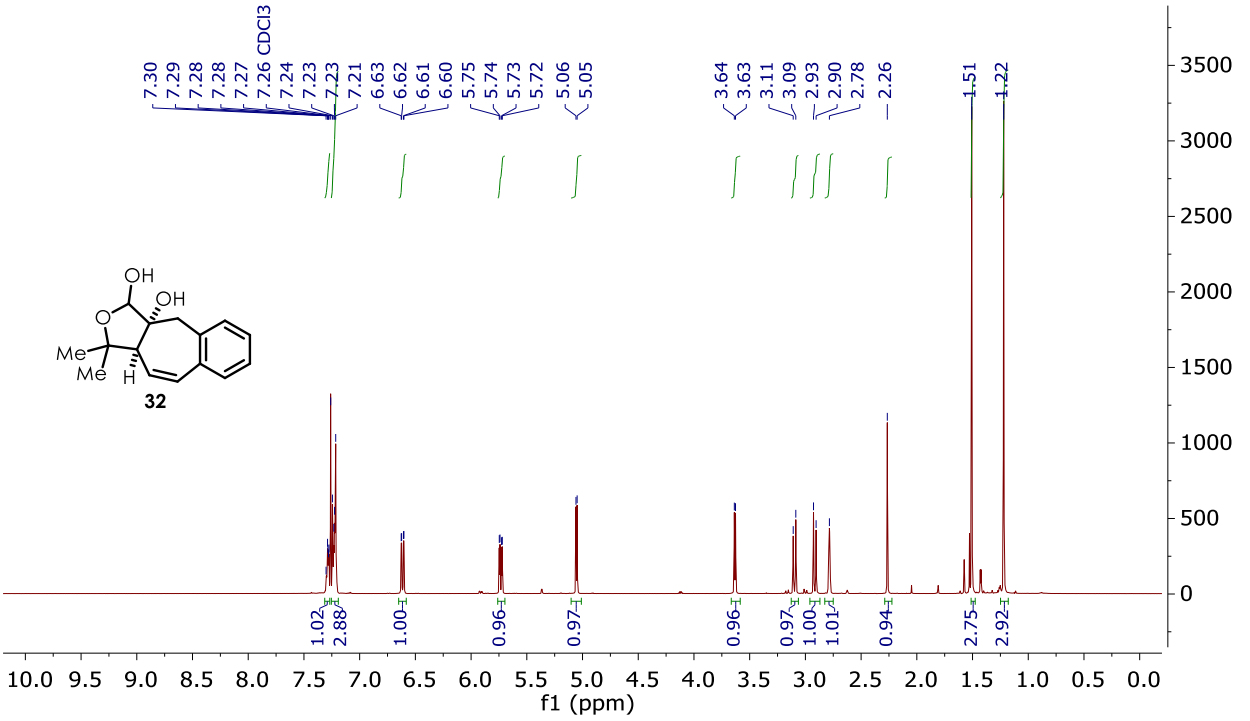


**Figure B.36** $^{1}$H NMR Spectrum of **32**

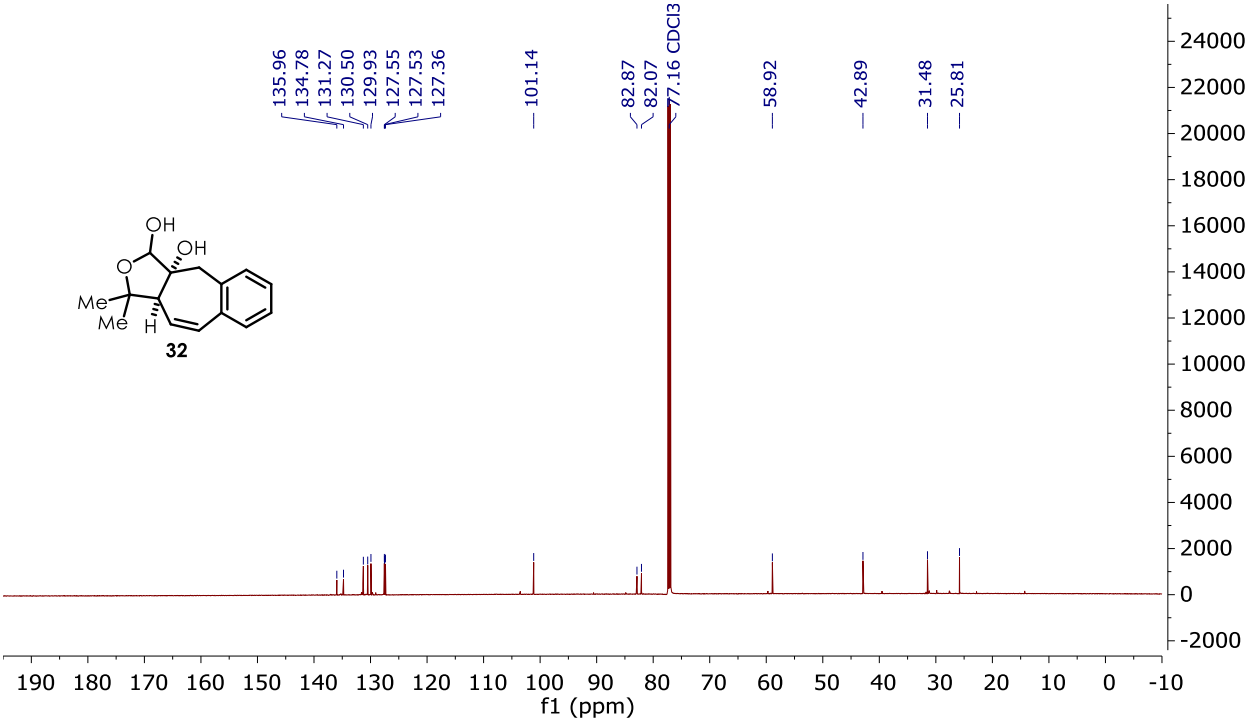


**Figure B.37** $^{13}$C NMR Spectrum of **32**

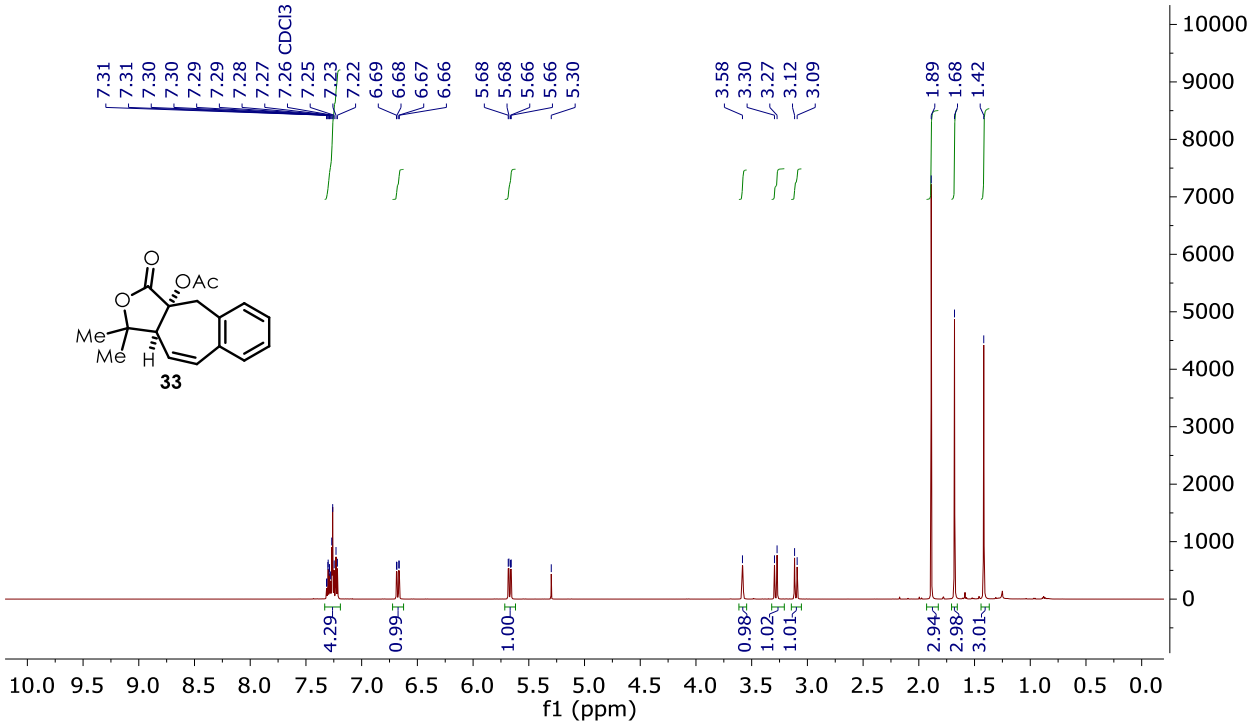


**Figure B.38** $^{1}$H NMR Spectrum of **33**

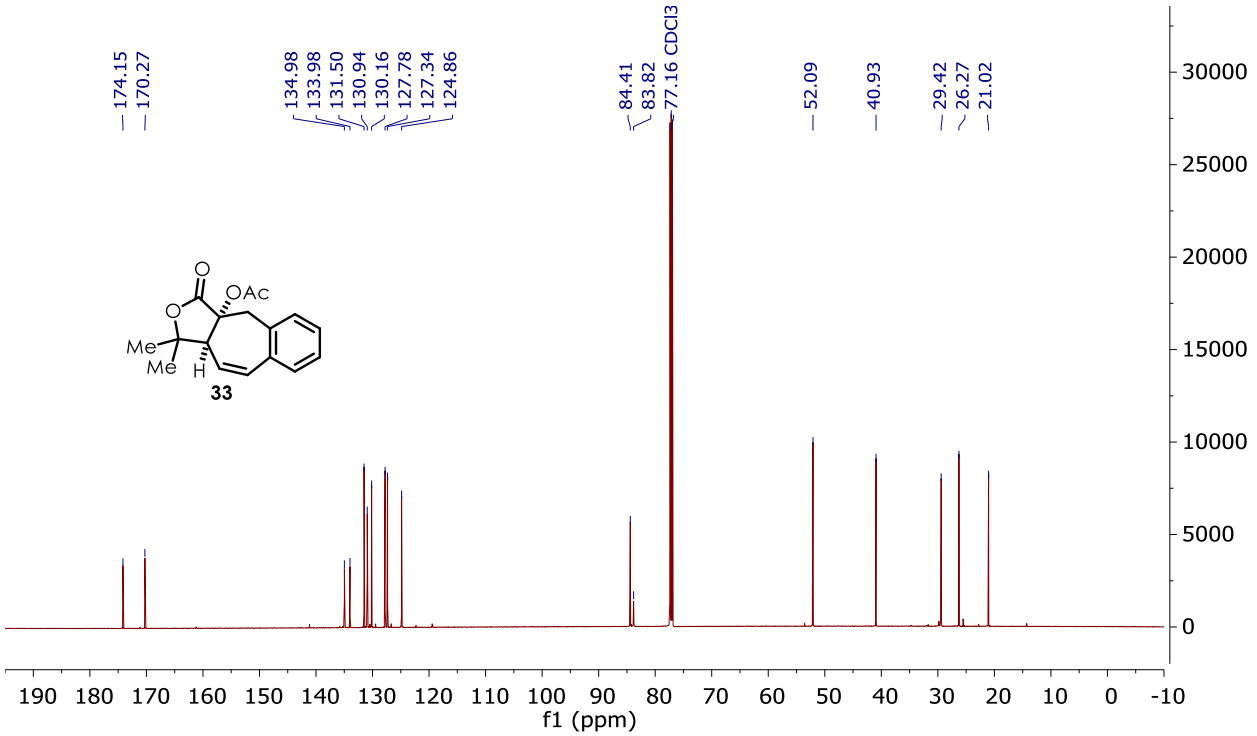


**Figure B.39** $^{13}$C NMR Spectrum of **33**

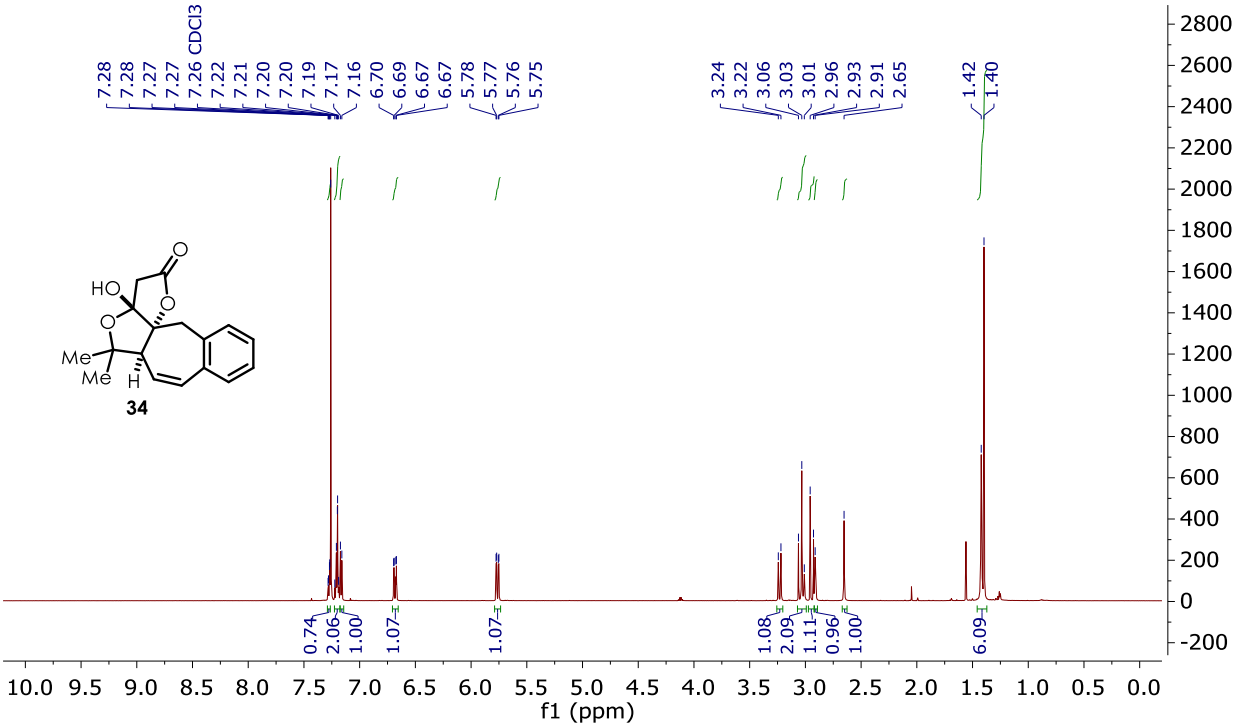


**Figure B.40** $^{1}$H NMR Spectrum of **34**

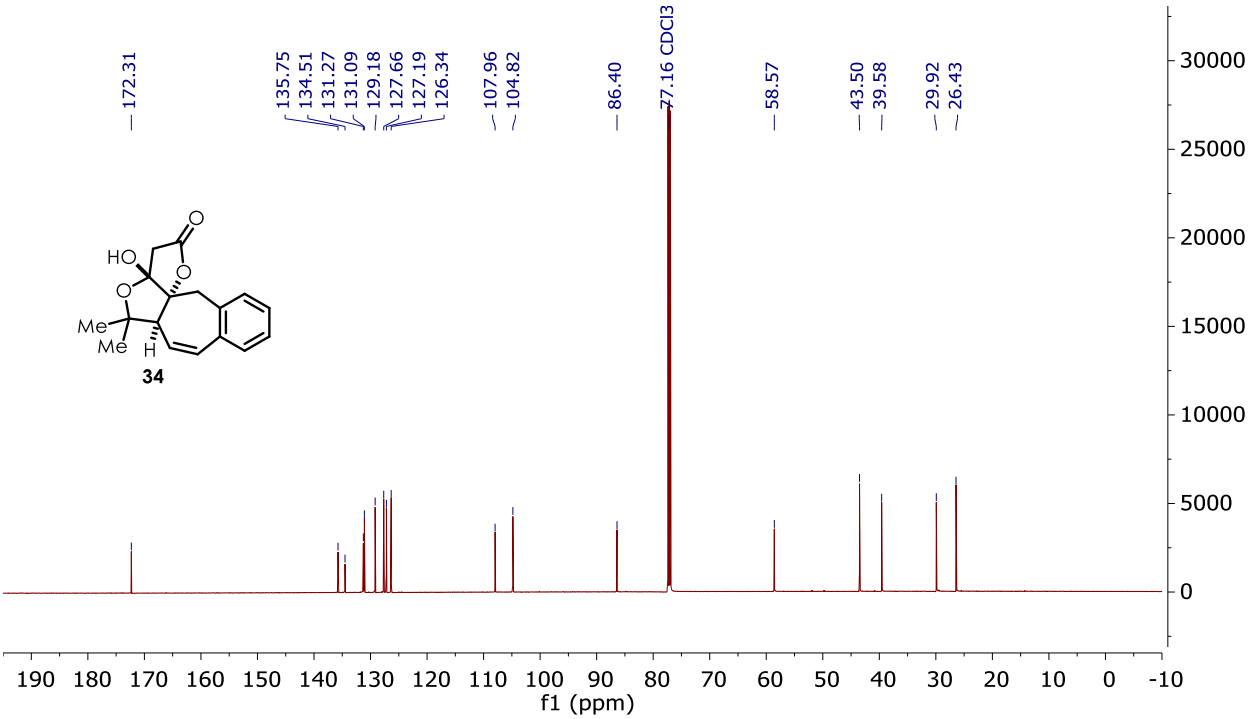


**Figure B.41** $^{13}$C NMR Spectrum of **34**

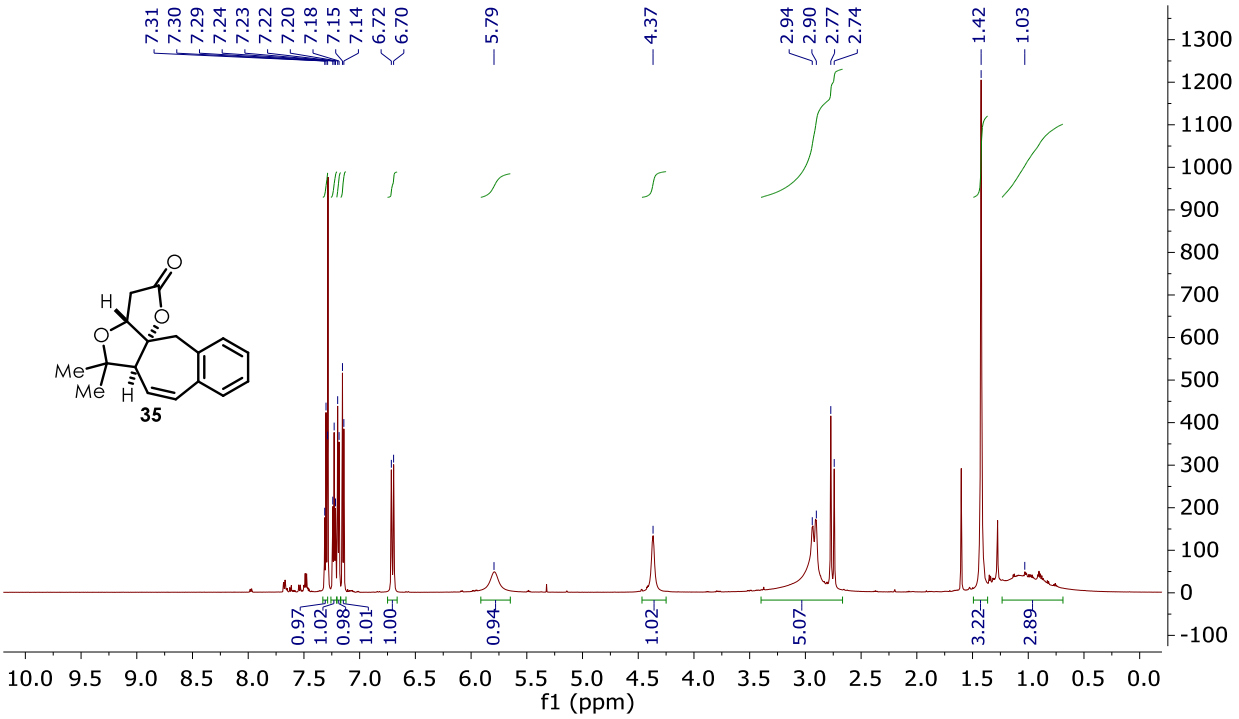


**Figure B.42** $^{1}$H NMR Spectrum ($CDCl_3$) of **35**

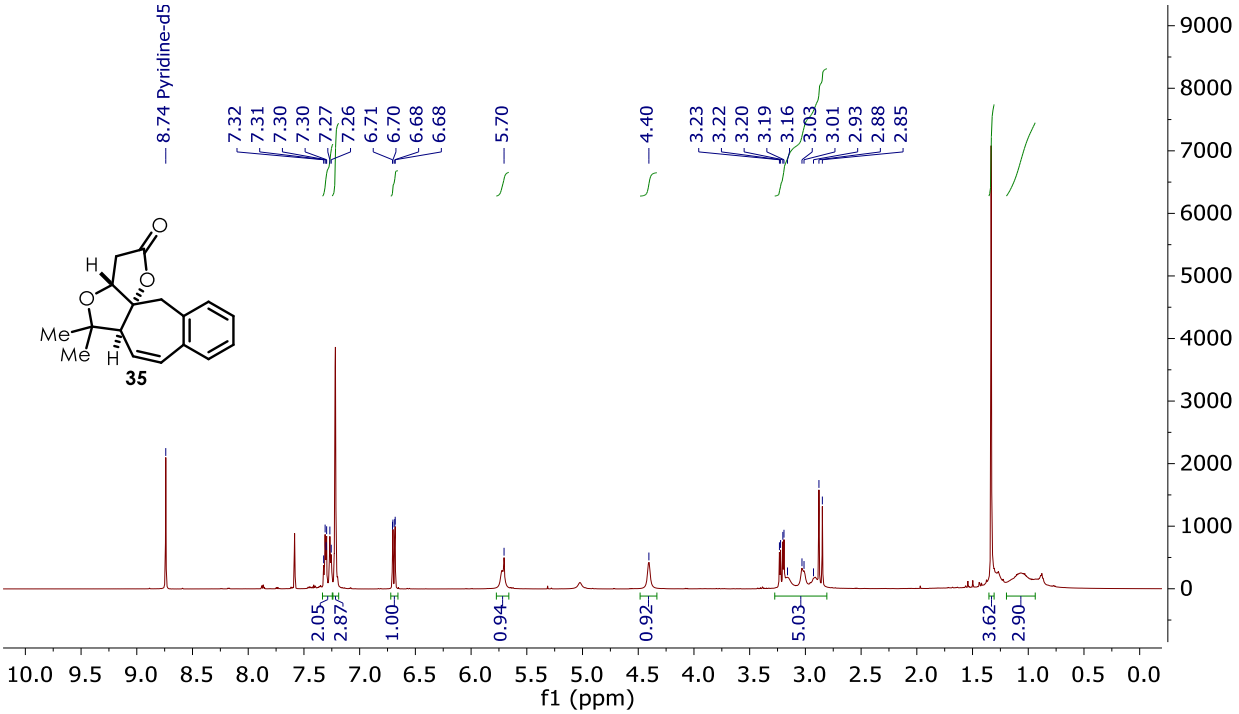


**Figure B.43** $^{1}$H NMR Spectrum (pyridine-$d_5$) of **35**

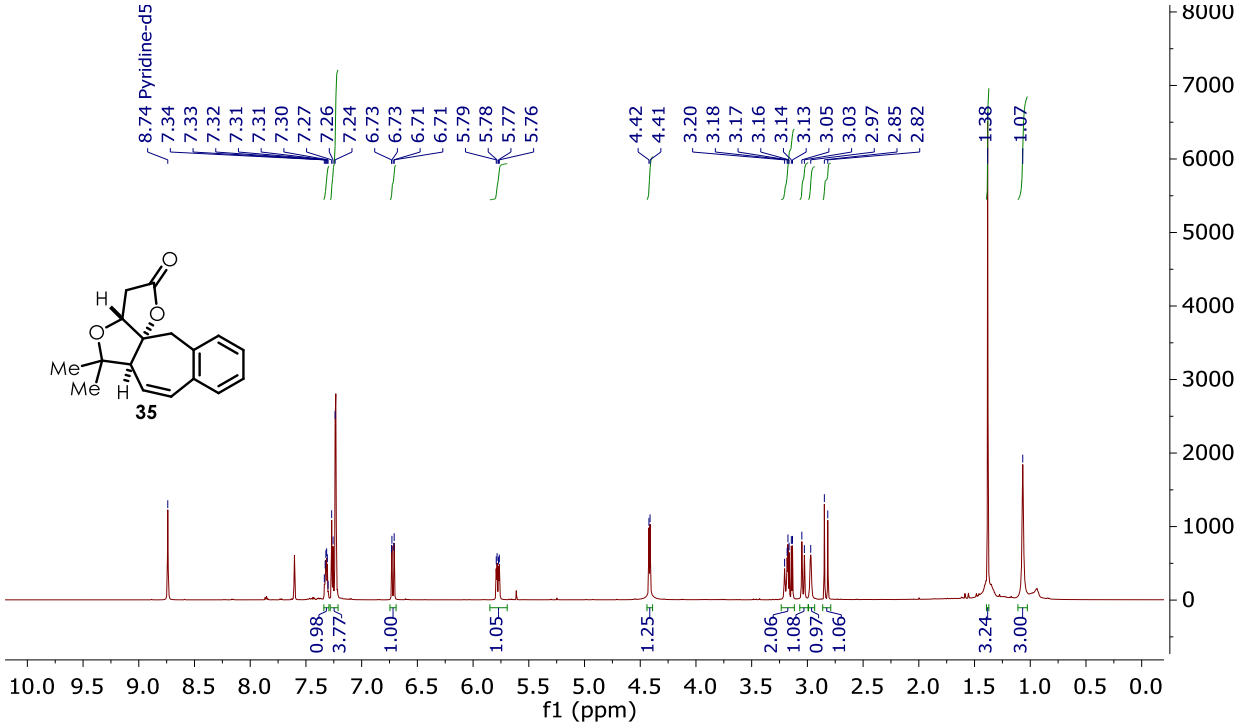


**Figure B.44** $^{1}$H NMR Spectrum (pyridine-$d_5$, 60 °C) of **35**

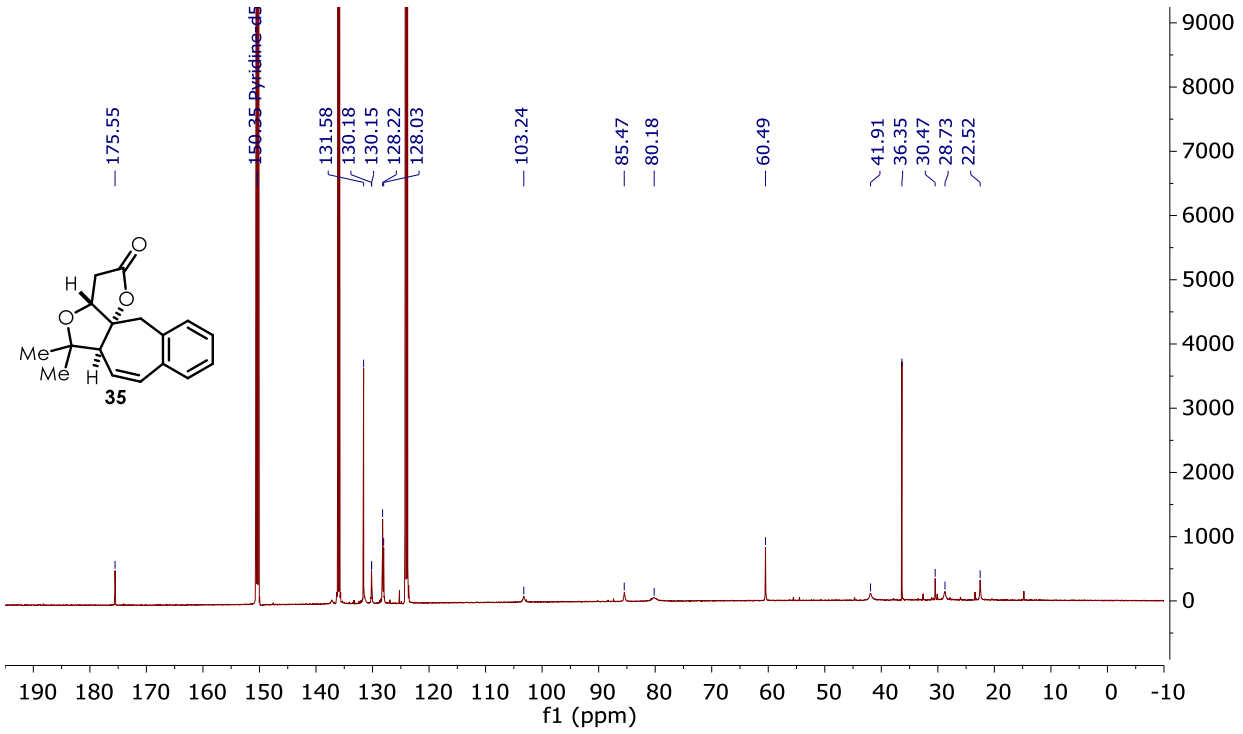


**Figure B.45** $^{13}$C NMR Spectrum (pyridine-$d_5$) of **35**

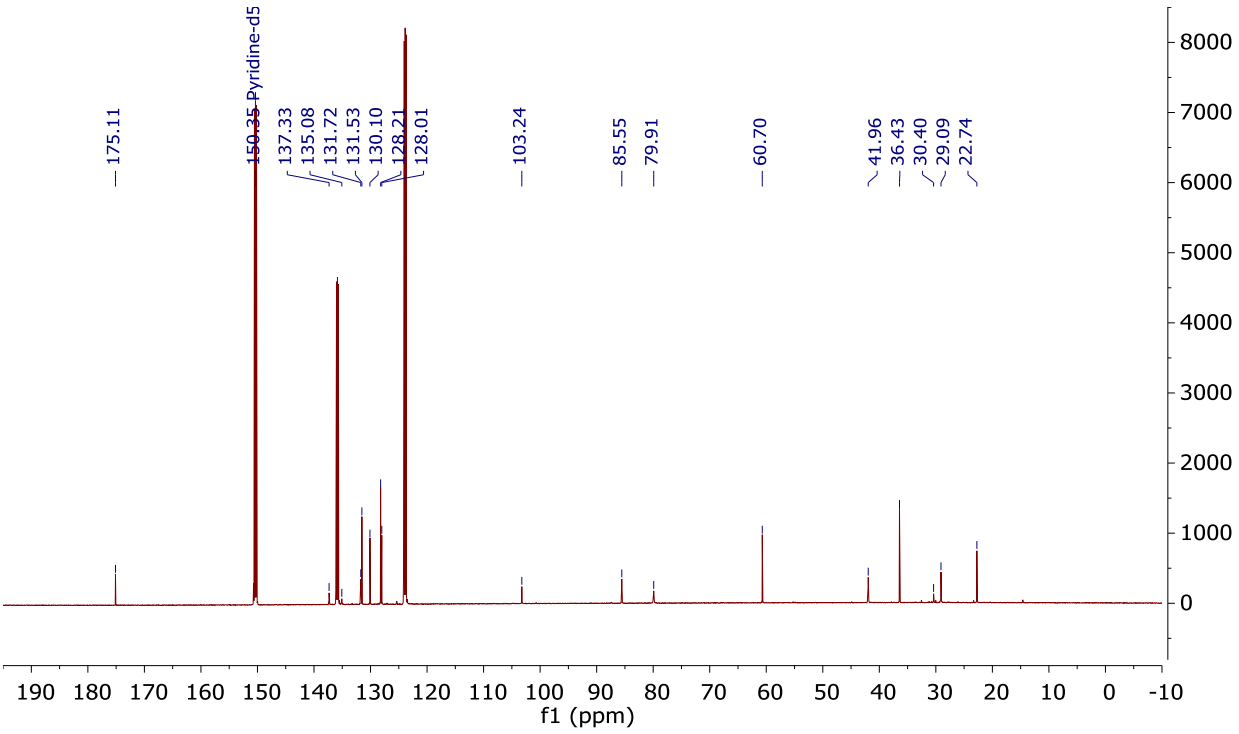


**Figure B.46** $^{13}$C NMR Spectrum (pyridine-$d_5$, 60 °C) of **35**

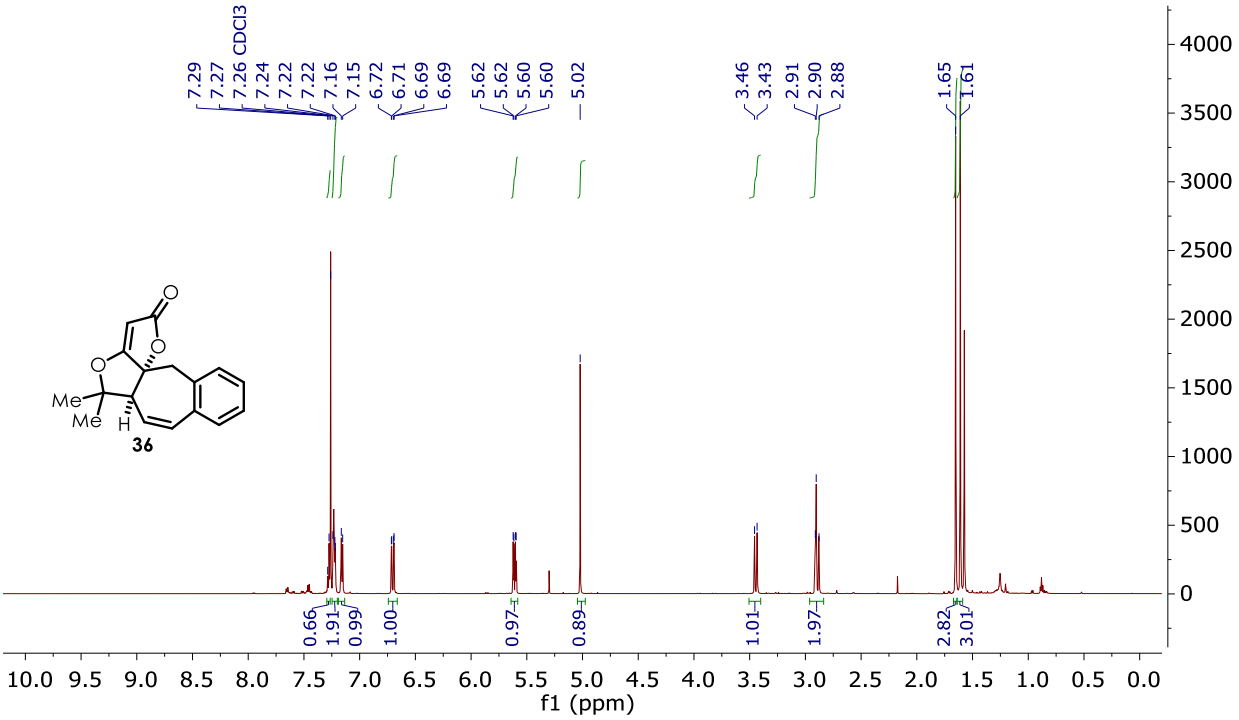


**Figure B.47** $^{1}$H NMR Spectrum of **36**

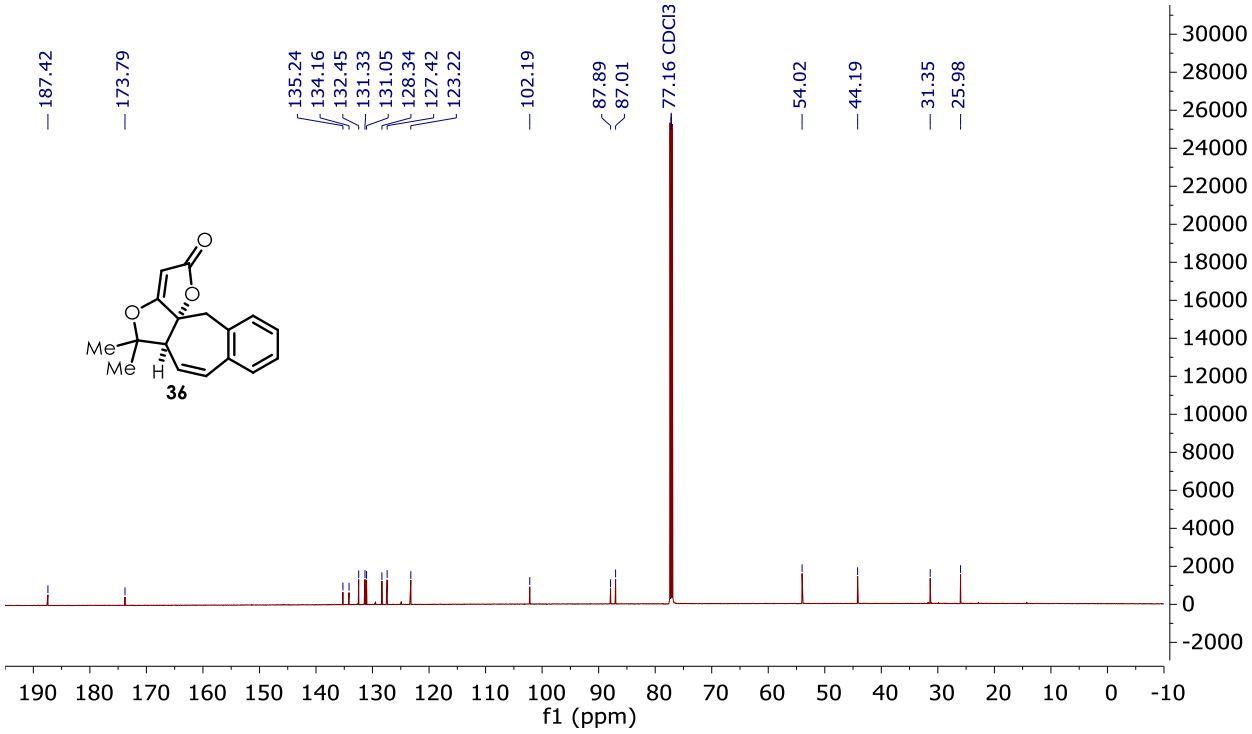


**Figure B.48** $^{13}$C NMR Spectrum of **36**

### B.3.2 Crystallographic Information

**Table B.1** Crystal Data for **29**

| | | |
|---|---|---|
| Empirical formula | C15 H16 O3 | |
| Formula weight | 244.28 | |
| Crystal color, shape, size | colorless block fragment, 0.355 x 0.241 x 0.130 mm$^3$ | |
| Temperature | 100 K | |
| Wavelength | 1.54178 Å | |
| Crystal system, space group | Monoclinic, $P2_1/c$ | |
| Unit cell dimensions | a = 9.2174(11) Å | α = 90°. |
| | b = 14.5768(16) Å | β = 111.790(7)°. |
| | c = 10.2658(11) Å | γ = 90°. |
| Volume | 1280.8(3) Å$^3$ | |
| Z | 4 | |
| Density (calculated) | 1.267 Mg/m$^3$ | |
| Absorption coefficient | 0.709 mm$^{-1}$ | |
| F(000) | 520 | |
| | | |
| Data collection | | |
| Diffractometer | Bruker Apex Kappa Duo, Bruker | |
| Theta range for data collection | 5.55 to 66.62°. | |
| Index ranges | -9<=h<=10, -17<=k<=17, -11<=l<=12 | |
| Reflections collected | 8237 | |
| Independent reflections | 2208 [R(int) = 0.0425] | |
| Observed Reflections | 1809 | |
| Completeness to theta = 66.613° | 97.7 % | |
| | | |
| Solution and Refinement | | |
| Absorption correction | Numerical from crystal shape | |
| Max. and min. transmission | 0.913 and 0.787 | |
| Solution | olex2.solve | |
| Refinement method | Full-matrix least-squares on F$^2$ | |
| Weighting scheme | $w = [\sigma^2 Fo^2 + (0.0553P)^2 + 0.2887P]$, where $P = (Fo^2 + 2Fc^2)/3$ | |
| Data / restraints / parameters | 2208 / 0 / 169 | |
| Goodness-of-fit on F$^2$ | 1.073 | |
| Final R indices [I > 2\σ(I)] | R1 = 0.0424, wR2 = 0.1058 | |
| R indices (all data) | R1 = 0.0528, wR2 = 0.1113 | |
| Largest diff. peak and hole | 0.200 and -0.229 e.Å$^{-3}$ | |

**Table B.2** Crystal Data for **31**

| | | |
|---|---|---|
| Empirical formula | C15 H16 O3 | |
| Formula weight | 244.28 | |
| Crystal color, shape, size | colorless block fragment, 0.225 x 0.176 x 0.066 | |
| $mm^3$ | | |
| Temperature | 100 K | |
| Wavelength | 1.54178 Å | |
| Crystal system, space group | Orthorhombic, Pbca | |
| Unit cell dimensions | a = 6.1481(4) Å | α = 90°. |
| | b = 14.3278(9) Å | β = 90°. |
| | c = 27.0063(16) Å | γ = 90°. |
| Volume | 2379.0(3) $Å^3$ | |
| Z | 8 | |
| Density (calculated) | 1.364 $Mg/m^3$ | |
| Absorption coefficient | 0.764 $mm^{-1}$ | |
| F(000) | 1040 | |

| | |
|---|---|
| Data collection | |
| Diffractometer | Bruker Apex Kappa Duo, Bruker |
| Theta range for data collection | 3.27 to 66.63°. |
| Index ranges | -7<=h<=7, -17<=k<=17, -30<=l<=32 |
| Reflections collected | 16710 |
| Independent reflections | 2102 [R(int) = 0.0345] |
| Observed Reflections | 1934 |
| Completeness to theta = 66.620° | 99.8 % |

| | |
|---|---|
| Solution and Refinement | |
| Absorption correction | Numerical from crystal shape |
| Max. and min. transmission | 0.951 and 0.847 |
| Solution | olex2.solve |
| Refinement method | Full-matrix least-squares on $F^2$ |
| Weighting scheme | $w = [\sigma^2 Fo^2 + (0.0377P)^2 + 1.2361P]$, where |
| | $P = (Fo^2 + 2FC^2)/3$ |
| Data / restraints / parameters | 2102 / 0 / 169 |
| Goodness-of-fit on $F^2$ | 1.079 |
| Final R indices [I > 2\σ(I)] | R1 = 0.0339, wR2 = 0.0824 |
| R indices (all data) | R1 = 0.0367, wR2 = 0.0844 |
| Largest diff. peak and hole | 0.291 and -0.236 $e.Å^{-3}$ |

**Table B.3** Crystal Data for **35**

| | | |
|---|---|---|
| Empirical formula | C17 H18 O3 | |
| Formula weight | 270.33 | |
| Crystal color, shape, size | colorless block fragment, 0.400 x 0.400 x 0.400 | |
| $mm^3$ | | |
| Temperature | 150 K | |
| Wavelength | 1.54178 Å | |
| Crystal system, space group | Orthorhombic, Pbca | |
| Unit cell dimensions | a = 14.5037(3) Å | α = 90°. |
| | b = 9.3162(2) Å | β = 90°. |
| | c = 20.2982(4) Å | γ = 90°. |
| Volume | 2742.68(10) $Å^3$ | |
| Z | 8 | |
| Density (calculated) | 1.309 $Mg/m^3$ | |
| Absorption coefficient | 0.715 $mm^{-1}$ | |
| F(000) | 1152 | |

| | |
|---|---|
| Data collection | |
| Diffractometer | Bruker Apex Kappa Duo, Bruker |
| Theta range for data collection | 4.356 to 72.343°. |
| Index ranges | -17<=h<=17, -11<=k<=11, -25<=l<=24 |
| Reflections collected | 22492 |
| Independent reflections | 2712 [R(int) = 0.020] |
| Observed Reflections | 2693 |
| Completeness to theta = 72.343° | 99.9 % |

| | |
|---|---|
| Solution and Refinement | |
| Absorption correction | Semi-empirical from equivalents |
| Max. and min. transmission | 0.75 and 0.75 |
| Solution | Charge-Flipping methods |
| Refinement method | Full-matrix least-squares on $F^2$ |
| Weighting scheme | $w = [\sigma^2 Fo^2 + AP^2 + BP]^{-1}$, with |
| | $P = (Fo^2 + 2\,Fc^2)/3$, A = 0.052, B = 1.290 |
| Data / restraints / parameters | 2702 / 0 / 235 |
| Goodness-of-fit on $F^2$ | 1.0313 |
| Final R indices [I > 2\σ(I)] | R1 = 0.0389, wR2 = 0.0955 |
| R indices (all data) | R1 = 0.0389, wR2 = 0.0955 |
| Largest diff. peak and hole | 0.31 and -0.25 $e.Å^{-3}$ |

## APPENDIX C: EXPERIMENTAL DETAILS AND CHARACTERIZATION OF KEY INTERMEDIATES

### C.1 General Information

Reactions were run under nitrogen and anhydrous conditions unless otherwise stated. Commercially available reagents were purchased from Sigma-Aldrich, Acros, Alfa Aesar, Oakwood Chemical, VWR, or Fisher Scientific and purified using reported methods as needed.[118] Solvents were dried by passing through activated alumina prior to use; the exceptions to this include DIPA, which was distilled from KOH, and THF, which was distilled from LAH.

Reactions were monitored by TLC using silica plates from VWR, and UV light or $KMnO_4$ stain as a method of visualization. Flash chromatography was conducted with 40-63 μm (230-400 mesh) silica from Silicycle.

Compounds where characterized primarily by NMR spectroscopy using Bruker 400 MHz or 600 MHz spectrometers and $CDCl_3$ as the solvent.

### C.2 Experimental Details

#### C.2.1 Attempting the Organic Photoredox Cascade

**Scheme C.1** Synthesis of **1-3**

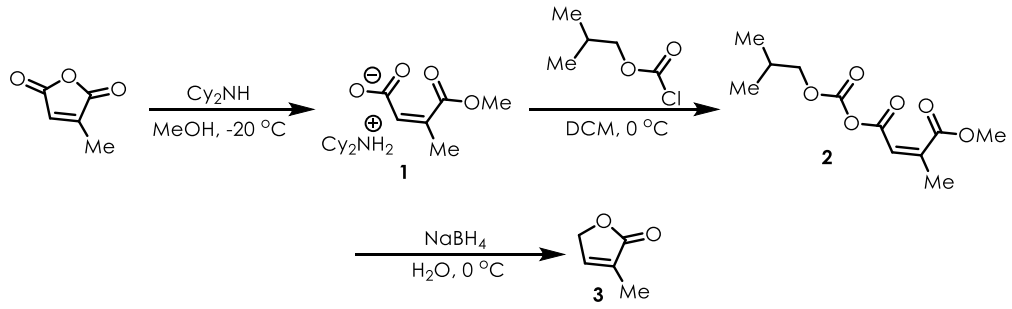


**Synthesis of 1** To a flame-dried flask containing methanol (180 mL) at -20 °C was slowly added citraconic anhydride (25.0 g, 223 mmol, 1 equiv) via an addition funnel. After stirring for 45 min, dicyclohexylamine (49.0 mL, 245 mmol, 1.1 equiv) was added dropwise via a separate

addition funnel. The cooling bath was removed and the solution stirred for an additional 2 hr at room temperature before concentration *in vacuo*. The resultant off-white solid was suspended in ethyl acetate (156 mL) and stirred vigorously for 1 hr before it was filtered off and washed with additional ethyl acetate (62.3 g, 86%).

**Synthesis of 2** Isobutyl chloroformate (27.3 mL, 211 mmol, 1.1 equiv) was added dropwise to a solution of **1** (62.3 g, 191 mmol, 1 equiv) in DCM (144 mL) cooled to 0 $^{o}$C. The contents were allowed to stir for 3 hr and gradually warm to room temperature, during which time a thick slurry formed; the contents were stored in the freezer overnight and the following day THF (182 mL) was added and the flask returned to the freezer for an additional hour before the solids present were filtered off and washed with additional THF while keeping the filtrate at 0 $^{o}$C. The filtrate was used directly in the next reaction.

**Synthesis of 3** $NaBH_4$ (14.5 g, 382 mmol, 2 equiv) as a solution in water (29 mL) was added to the cooled filtrate containing **2** (approx. 191 mmol). This addition must be done very slowly, as there is a brief induction period before hydrogen gas begins to form. Once all the $NaBH_4$ was added, the mixture was stirred for an additional 2 hr. The contents were filtered, concentrated, suspended in $Et_2O$, and filtered again. The filtrate was dried over $MgSO_4$, filtered, and concentrated again to a pale-yellow oil. Distillation afforded a colorless oil (14.2 g, 76% over 2 steps). $^{1}$H NMR (400 MHz, Chloroform-*d*) δ 7.13 (q, *J* = 1.6 Hz, 1H), 4.75 (p, *J* = 2.1 Hz, 2H), 1.93 (q, *J* = 2.1 Hz, 3H).

**Scheme C.2** Synthesis of **4-5**

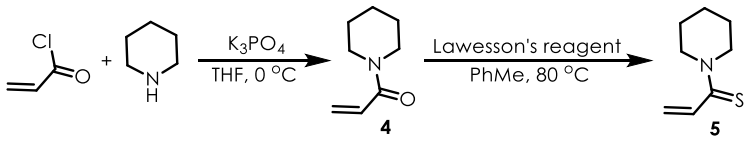


**Synthesis of 4** Acryloyl chloride (3.26 mL, 40.0 mmol, 1 equiv) was added to a suspension of $K_3PO_4$ (10.6 g, 50.0 mmol, 1.25 equiv) in THF (80 mL) cooled to 0 °C. After the addition of piperidine (4.00 mL, 40.0 mmol, 1 equiv) to this mixture, the contents were stirred for 1 hr before they were poured into water and extracted with EtOAc. The combined organic layers were washed with 2 N HCl, water, brine, and dried over $MgSO_4$. Filtration and concentration afforded a yellow oil (3.51 g, 63%). $^1$H NMR (400 MHz, Chloroform-*d*) δ 6.57 (dd, *J* = 16.8, 10.6 Hz, 1H), 6.23 (d, *J* = 16.8 Hz, 1H), 5.64 (d, *J* = 12.6 Hz, 1H), 3.61 (d, *J* = 5.2 Hz, 2H), 3.49 (d, *J* = 5.2 Hz, 2H), 1.65 (d, *J* = 17.6 Hz, 2H), 1.60 – 1.47 (m, 4H).

**Synthesis of 5** Lawesson's reagent (1.60 g, 3.95 mmol, 0.5 equiv) was added to a solution of **4** (978 μL, 7.18 mmol, 1 equiv) in PhMe (24 mL). The contents were heated to 80 °C for 3 hr, then cooled to RT, concentrated, and purified by chromatography with 20% EtOAc/hexanes to obtain a yellow oil (155 mg, 14%). $^1$H NMR (400 MHz, Chloroform-*d*) δ 6.70 (dd, *J* = 16.8, 10.9 Hz, 1H), 6.00 (dd, *J* = 16.8, 1.5 Hz, 1H), 5.50 (dd, *J* = 10.9, 1.5 Hz, 1H), 4.26 (s, 3H), 3.79 – 3.66 (m, 2H), 1.79 – 1.65 (m, 4H).

**Scheme C.3** Synthesis of **6-8**

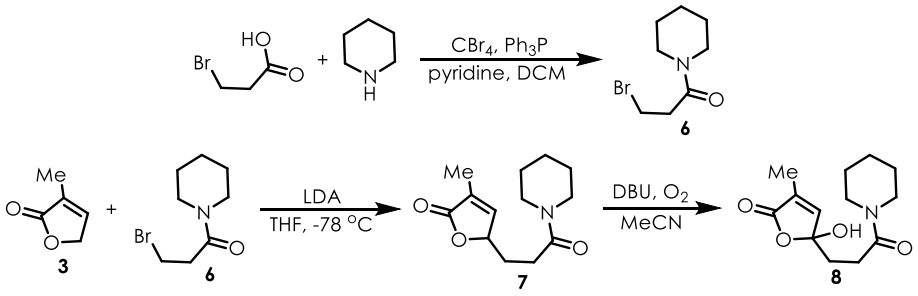

**Synthesis of 6** Combined 3-bromopropanoic acid (4.59 g, 30.0 mmol, 1 equiv), $CBr_4$ (10.9 g, 33.0 mmol, 1.1 equiv), and DCM (75 mL) in a flask then added pyridine (2.67 mL, 33 mmol, 1.1 equiv) followed by piperidine (2.96 mL, 30.0 mmol, 1 equiv). Contents were cooled to 0 °C before adding $Ph_3P$ (8.66 g, 30.0 mmol, 1 equiv) in 5 portions over 5 min. After 10 min, the reaction was concentrated and purified by chromatography with 80% $Et_2O$/hexanes to obtain a light-yellow oil (3.49 g, 53%). $^1$H NMR (600 MHz, Chloroform-*d*) δ 3.65 (t, *J* = 7.3 Hz, 2H), 3.59 – 3.52 (m, 2H), 3.42 – 3.34 (m, 2H), 2.90 (t, *J* = 7.3 Hz, 2H), 1.64 (q, *J* = 6.2, 5.8 Hz, 2H), 1.56 (dp, *J* = 17.1, 5.7 Hz, 4H).

**Synthesis of 7** Prepared a solution of LDA at -78 °C using DIPA (779 μL, 5.56 mmol, 1.2 equiv), *n*-BuLi (2.5 M, 2.0 mL, 5.1 mmol, 1.1 equiv) and THF (8 mL). Added a solution of **3** (402 μL, 4.63 mmol, 1 equiv) in THF (2 mL) to the LDA and let stir for 30 min before adding a solution of **6** (1.22 g, 5.56 mmol, 1.2 equiv) in THF (2 mL). The cooling bath was removed and the contents stirred for 16 hr at RT. The mixture was quenched with sat. aq. $NH_4Cl$, extracted with EtOAc, and the combined organic layers were washed with brine and dried over $Na_2SO_4$, filtered, then concentrated. Purification of the residue by chromatography with EtOAc as the eluent gave a colorless oil (278 mg, 25%). $^1$H NMR (600 MHz, Chloroform-*d*) δ 7.07 (s, 1H), 5.01 (ddd, *J* = 7.1, 3.3, 1.7 Hz, 1H), 3.54 (tq, *J* = 13.1, 6.6, 5.2 Hz, 2H), 3.38 (t, *J* = 5.5 Hz, 2H), 2.57 – 2.48 (m, 1H), 2.48 – 2.39 (m, 1H), 2.27 (dtd, *J* = 14.9, 7.5, 3.5 Hz, 1H), 1.91 (t, *J* = 1.6 Hz, 3H), 1.73 (td, *J* = 14.5, 6.4 Hz, 1H), 1.64 (q, *J* = 5.8 Hz, 2H), 1.58 – 1.49 (m, 4H).

**Synthesis of 8** Sparged a solution of **7** (278 mg, 1.17 mmol, 1 equiv) and DBU (212 μL, 1.41 mmol, 1.2 equiv) in MeCN (23 mL) with $O_2$ for 4 hr. Contents were concentrated and the residue purified by chromatography with EtOAc to obtain a colorless oil (70 mg, 24%). $^1$H NMR (600 MHz, Chloroform-*d*) δ 10.25 (s, 1H), 6.92 (s, 1H), 3.55 (t, *J* = 5.5 Hz, 2H), 3.40 (t, *J* = 5.5 Hz,

2H), 2.63 – 2.52 (m, 1H), 2.47 – 2.40 (m, 1H), 2.34 (hept, *J* = 7.6, 7.2 Hz, 2H), 1.95 (d, *J* = 1.6 Hz, 3H), 1.65 (p, *J* = 5.6 Hz, 2H), 1.55 (dq, *J* = 16.2, 5.6 Hz, 4H).

**Scheme C.4** Synthesis of **9**

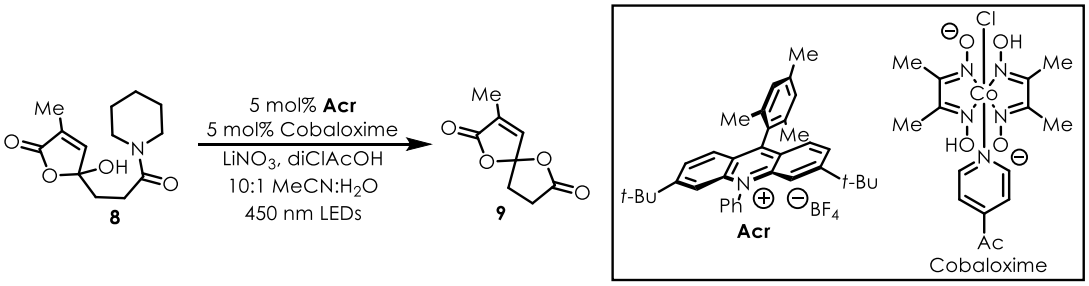


**Synthesis of 9** Added **8** (25.3 mg, 100 μmol, 1 equiv), acridinium ion (2.8 mg, 5.0 μmol, 5 mol%), cobaloxime (2.2 mg, 5.0 μmol, 5 mol%), a solution of dichloroacetic acid in MeCN (5.0 μM, 1.0 mL, 5.0 μmol, 5 mol%) and an aq. solution of $LiNO_3$ (2.0 M, 100 μL, 200 μmol, 2 equiv) to a 2-dram vial. The solution was sparged with argon for 15 min then irradiated with 450 nm LEDs for 24 hr. The aqueous layer was then extracted with DCM and the combined organic layers were washed with $NaHCO_3$ then concentrated. Crude residue was analyzed by NMR without purification. $^1$H NMR (400 MHz, Chloroform-*d*) δ 6.85 (d, *J* = 1.6 Hz, 1H), 2.94 (ddd, *J* = 17.7, 11.0, 9.3 Hz, 1H), 2.68 (ddd, *J* = 17.7, 9.0, 2.0 Hz, 1H), 2.59 – 2.39 (m, 2H), 2.00 (d, *J* = 1.6 Hz, 3H).

### C.2.2 Attempt at a PRCC

**Scheme C.5** Synthesis of **10-11**

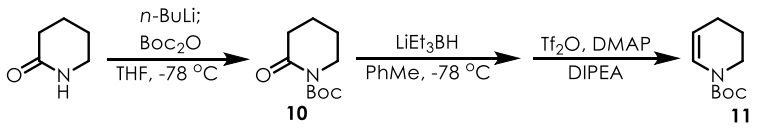


**Synthesis of 10** *n*-BuLi (2.5 M, 3.9 mL, 9.8 mmol, 0.97 equiv) was added to a solution of δ-valerolactam (1.00 g, 10.1 mmol, 1 equiv) in THF (124 mL) cooled to -78 °C. Let mixture stir for 10 min before adding $Boc_2O$ (3.50 mL, 15.1 mmol, 1.5 equiv). After 1 hr, the reaction was

quenched with sat. aq. $NH_4Cl$ and the aqueous layer was extracted with EtOAc. The combined organic layers were washed with brine, dried over $MgSO_4$, filtered, and then concentrated. The obtained residue was taken up in DCM (33 mL) and stirred with imidazole (409 mg, 6.00 mmol, 0.6 equiv) and for 45 min to destroy excess $Boc_2O$. The mixture was then washed with 2 N HCl, water, and brine, then dried over $MgSO_4$. Filtration and concentration gave a light-yellow oil (1.64 g, 82%). $^1$H NMR (600 MHz, Chloroform-*d*) δ 3.67 (t, *J* = 5.7 Hz, 2H), 2.53 (t, *J* = 6.4 Hz, 2H), 1.84 (d, *J* = 6.5 Hz, 4H), 1.54 (s, 9H).

**Synthesis of 11** $LiEt_3BH$ (1.0 M, 5.5 mL, 5.5 mmol, 1.1 equiv) was added to a solution of **10** (1.00 g, 5.02 mmol, 1 equiv) in PhMe (10 mL) cooled to -78 °C. After stirring for 40 min, DMAP (6.1 mg, 50 μmol, 10 mol%), DIPEA (5.00 mL, 28.6 mmol, 5.7 equiv) and trifluoroacetic anhydride (849 μL, 6.02, 1.2 equiv) were added to the solution. Contents were stirred for another 16 hr, then quenched with 2 N HCl. The aqueous layer was extracted with EtOAc, and the combined organic layers were washed with brine and dried over $MgSO_4$. Filtration and concentration gave a crude oil that was purified by chromatography with 0 → 10% EtOAc/hexanes to give a yellow oil (511 mg, 56%). $^1$H NMR (400 MHz, Chloroform-*d*) δ 6.71 (d, *J* = 8.3 Hz, 1H), 4.79 (d, *J* = 8.2 Hz, 1H), 3.55 (d, *J* = 5.3 Hz, 2H), 2.02 (d, *J* = 5.8 Hz, 2H), 1.85 – 1.73 (m, 2H), 1.48 (s, 9H).

**Scheme C.6** Synthesis of **12-15**

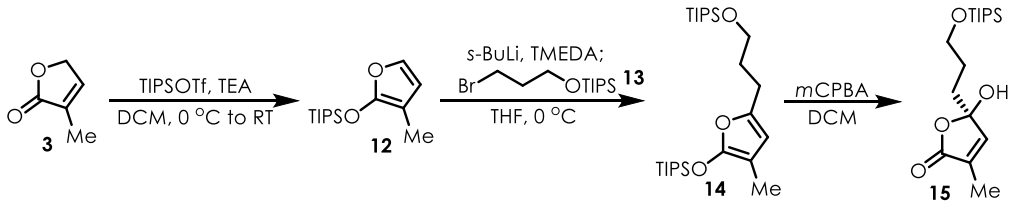


**Synthesis of 12** Added TIPSOTf (8.29 mL, 30.6 mmol, 1 equiv) to a solution of **3** (2.65 mL, 30.6 mmol, 1 equiv) and TEA (5.10 mL, 36.7 mmol, 1.1 equiv) in DCM (60 mL) at 0 °C. After

stirring for 60 min at 0 °C and 30 min at RT, the contents were diluted with pentanes and washed with pH 7 aq. phosphate buffer, 0.5 M aq. $CuSO_4$, and brine, then dried over $Na_2SO_4$. Filtration and concentration gave a colorless liquid (7.66 g, 98%). $^1$H NMR (400 MHz, Chloroform-*d*) δ 6.73 (d, *J* = 2.1 Hz, 1H), 6.10 (d, *J* = 2.1 Hz, 1H), 1.84 (s, 3H), 1.24 (dq, *J* = 14.0, 7.4, 6.9 Hz, 3H), 1.09 (d, *J* = 7.3 Hz, 18H).

**Synthesis of 13** Combined 3-bromo-1-propanol (2.19 mL, 25.0 mmol, 1 equiv), imidazole (1.70 g, 25.0 mmol, 1 equiv) and TIPSCl (5.30 mL, 25.0 mmol, 1 equiv) in DCM (50 mL) and let the mixture stir for 16 hr at RT before quenching it with water. The aqueous layer was extracted with DCM and the combined organic layers were washed with brine and dried over $MgSO_4$. Filtration and concentration gave a colorless oil (6.92 g, 94%). $^1$H NMR (600 MHz, Chloroform-*d*) δ 3.81 (t, *J* = 5.7 Hz, 2H), 3.56 (t, *J* = 6.5 Hz, 2H), 2.05 (p, *J* = 6.1 Hz, 2H), 1.06 (d, *J* = 6.2 Hz, 21H).

**Synthesis of 14** *s*-BuLi (1.4 M, 5.1 mL, 7.1 mmol, 1 equiv) was added to a solution of **12** (1.10 mL, 3.93 mmol, 1 equiv) and TMEDA (1.10 mL, 7.07 mmol, 1.8 equiv) in THF (20 mL) cooled to 0 °C. After stirring for 2 hr, **13** (1.28 g, 4.32 mmol, 1.1 equiv) was added and the mixture was stirred for another 16 hr at RT before it was quenched with 2:1 water:sat. aq. $NaHCO_3$. The aqueous layers were extracted with $Et_2O$ and the combined organic layers were washed with 0.5 M aq. $CuSO_4$ and brine, then dried over $MgSO_4$. Filtration and concentration gave an orange oil (1.00 g, 54%). $^1$H NMR (600 MHz, Chloroform-*d*) δ 5.68 (s, 1H), 3.82 (t, *J* = 5.7 Hz, 1H), 3.69 (t, *J* = 6.3 Hz, 2H), 3.56 (t, *J* = 6.5 Hz, 1H), 2.53 (t, *J* = 7.5 Hz, 2H), 2.06 (p, *J* = 6.1 Hz, 1H), 1.79 (s, 3H), 1.28 – 1.17 (m, 6H), 1.12 – 1.00 (m, 36H).

**Synthesis of 15** *m*CPBA (260 mg, 1.07 mmol, 1 equiv) was added to a solution of **14** (500 mg, 1.07 mmol, 1 equiv) in DCM (11 mL). After stirring for 1 hr, the solution was quenched with sat. aq. $Na_2S_2O_3$ and stirred for 10 min. The aqueous layer was extracted with DCM, then the

combined organic layers were washed with sat. aq. $NaHCO_3$ and brine, then dried over $Na_2SO_4$. Filtration and concentration gave a crude oil that was purified by chromatography with 10% $Et_2O$/hexanes to obtain a colorless oil (154 mg, 44%). $^1$H NMR (400 MHz, Chloroform-*d*) δ 6.20 – 6.11 (m, 1H), 3.82 (t, *J* = 5.7 Hz, 1H), 3.69 (t, *J* = 6.2 Hz, 2H), 3.55 (t, *J* = 6.5 Hz, 1H), 2.60 (t, *J* = 7.4 Hz, 2H), 2.09 – 2.04 (m, 1H), 2.04 – 1.98 (m, 3H), 1.84 (p, *J* = 6.8 Hz, 2H), 1.36 (td, *J* = 15.4, 14.9, 7.8 Hz, 6H), 1.15 – 0.99 (m, 36H).

### C.2.3 Application of α-Amino Alkylation

**Scheme C.7** Synthesis of **16-17**

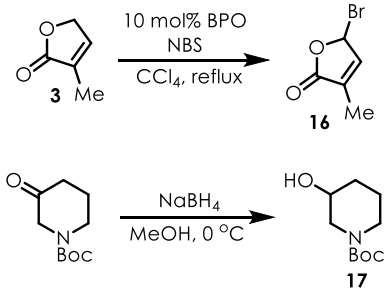


**Synthesis of 16** Combined **3** (1.35 g, 13.8 mmol, 1 equiv), BPO (333 mg, 1.38 mmol, 10 mol%), NBS (2.57 g, 14.4 mmol, 1.05 equiv) and $CCl_4$ (60 mL), then heated the solution to reflux for 1 hr. After cooling to RT, solids were filtered off and the filtrate was washed with sat. aq. $Na_2S_2O_3$, water, and brine, then dried over $MgSO_4$. Filtration and concentration gave a yellow oil. Used without purification.

**Synthesis of 17** $NaBH_4$ (190 mg, 5.02 mmol, 1 equiv) was added to a solution of *N*-Boc-3-piperidine (1.00 g, 5.02 mmol, 1 equiv) in MeOH (20 mL) cooled to 0 °C. After stirring for 16 hr, the contents were quenched with sat. aq. $NH_4Cl$ and extracted with EtOAc. The combined organic layers were washed with brine, dried over $Na_2SO_4$, filtered, and concentrated to a colorless oil (979 mg, 97%). $^1$H NMR (400 MHz, Chloroform-*d*) δ 3.73 (d, *J* = 10.3 Hz, 2H),

3.52 (s, 1H), 3.10 (dt, *J* = 22.1, 9.9 Hz, 2H), 1.88 (s, 1H), 1.76 (d, *J* = 19.3 Hz, 1H), 1.45 (s, 11H).

## REFERENCES


(1) The Beginnings of Organic Photochemistry - Roth - 1989 - Angewandte Chemie International Edition in English - Wiley Online Library https://onlinelibrary.wiley.com/doi/abs/10.1002/anie.198911931 (accessed May 9, 2019).

(2) Nicholls, T. P.; Leonori, D.; Bissember, A. C. Applications of Visible Light Photoredox Catalysis to the Synthesis of Natural Products and Related Compounds. *Nat. Prod. Rep.* **2016**, *33* (11), 1248–1254. https://doi.org/10.1039/C6NP00070C.

(3) McAtee, R. C.; McClain, E. J.; Stephenson, C. R. J. Illuminating Photoredox Catalysis. *Trends Chem.* **2019**, *1* (1), 111–125. https://doi.org/10.1016/j.trechm.2019.01.008.

(4) Shaw, M. H.; Twilton, J.; MacMillan, D. W. C. Photoredox Catalysis in Organic Chemistry. *J. Org. Chem.* **2016**, *81* (16), 6898–6926. https://doi.org/10.1021/acs.joc.6b01449.

(5) Koike, T.; Akita, M. Visible-Light Radical Reaction Designed by Ru- and Ir-Based Photoredox Catalysis. *Inorg. Chem. Front.* **2014**, *1* (8), 562–576. https://doi.org/10.1039/C4QI00053F.

(6) Prier, C. K.; Rankic, D. A.; MacMillan, D. W. C. Visible Light Photoredox Catalysis with Transition Metal Complexes: Applications in Organic Synthesis. *Chem. Rev.* **2013**, *113* (7), 5322–5363. https://doi.org/10.1021/cr300503r.

(7) Romero, N. A.; Nicewicz, D. A. Organic Photoredox Catalysis. *Chem. Rev.* **2016**, *116* (17), 10075–10166. https://doi.org/10.1021/acs.chemrev.6b00057.

(8) Roth, H. G.; Romero, N. A.; Nicewicz, D. A. Experimental and Calculated Electrochemical Potentials of Common Organic Molecules for Applications to Single-Electron Redox Chemistry. *Synlett* **2016**, *27* (5), 714–723. https://doi.org/10.1055/s-0035-1561297.

(9) Fukuzumi, S.; Kotani, H.; Ohkubo, K.; Ogo, S.; Tkachenko, N. V.; Lemmetyinen, H. Electron-Transfer State of 9-Mesityl-10-Methylacridinium Ion with a Much Longer Lifetime and Higher Energy Than That of the Natural Photosynthetic Reaction Center. *J. Am. Chem. Soc.* **2004**, *126* (6), 1600–1601. https://doi.org/10.1021/ja038656q.

(10) Wilger, D. J.; Grandjean, J.-M. M.; Lammert, T. R.; Nicewicz, D. A. The Direct Anti-Markovnikov Addition of Mineral Acids to Styrenes. *Nat. Chem.* **2014**, *6* (8), 720–726. https://doi.org/10.1038/nchem.2000.

(11) Romero, N. A.; Margrey, K. A.; Tay, N. E.; Nicewicz, D. A. Site-Selective Arene C-H Amination via Photoredox Catalysis. *Science* **2015**, *349* (6254), 1326–1330. https://doi.org/10.1126/science.aac9895.

(12) Griffin, J. D.; Zeller, M. A.; Nicewicz, D. A. Hydrodecarboxylation of Carboxylic and Malonic Acid Derivatives via Organic Photoredox Catalysis: Substrate Scope and Mechanistic Insight. *J. Am. Chem. Soc.* **2015**, *137* (35), 11340–11348. https://doi.org/10.1021/jacs.5b07770.

(13) Riener, M.; Nicewicz, D. A. Synthesis of Cyclobutane Lignans via an Organic Single Electron Oxidant–Electron Relay System. *Chem. Sci.* **2013**, *4* (6), 2625–2629. https://doi.org/10.1039/C3SC50643F.

(14) McManus, J. B.; Onuska, N. P. R.; Nicewicz, D. A. Generation and Alkylation of α-Carbamyl Radicals via Organic Photoredox Catalysis. *J. Am. Chem. Soc.* **2018**, *140* (29), 9056–9060. https://doi.org/10.1021/jacs.8b04890.

(15) Joshi-Pangu, A.; Lévesque, F.; Roth, H. G.; Oliver, S. F.; Campeau, L.-C.; Nicewicz, D.; DiRocco, D. A. Acridinium-Based Photocatalysts: A Sustainable Option in Photoredox Catalysis. *J. Org. Chem.* **2016**, *81* (16), 7244–7249. https://doi.org/10.1021/acs.joc.6b01240.

(16) White, A. R.; Wang, L.; Nicewicz, D. A. Synthesis and Characterization of Acridinium Dyes for Photoredox Catalysis. *Synlett* **2019**, *30* (07), 827–832. https://doi.org/10.1055/s-0037-1611744.

(17) Grandjean, J.-M. M.; Nicewicz, D. A. Synthesis of Highly Substituted Tetrahydrofurans by Catalytic Polar-Radical-Crossover Cycloadditions of Alkenes and Alkenols. *Angew. Chem. Int. Ed.* **2013**, *52* (14), 3967–3971. https://doi.org/10.1002/anie.201210111.

(18) Nguyen, T. M.; Manohar, N.; Nicewicz, D. A. Anti-Markovnikov Hydroamination of Alkenes Catalyzed by a Two-Component Organic Photoredox System: Direct Access to Phenethylamine Derivatives. *Angew. Chem. Int. Ed.* **2014**, *53* (24), 6198–6201. https://doi.org/10.1002/anie.201402443.

(19) Gesmundo, N. J.; Grandjean, J.-M. M.; Nicewicz, D. A. Amide and Amine Nucleophiles in Polar Radical Crossover Cycloadditions: Synthesis of γ-Lactams and Pyrrolidines. *Org. Lett.* **2015**, *17* (5), 1316–1319. https://doi.org/10.1021/acs.orglett.5b00316.

(20) Zeller, M. A.; Riener, M.; Nicewicz, D. A. Butyrolactone Synthesis via Polar Radical Crossover Cycloaddition Reactions: Diastereoselective Syntheses of Methylenolactocin and Protolichesterinic Acid. *Org. Lett.* **2014**, *16* (18), 4810–4813. https://doi.org/10.1021/ol5022993.

(21) Cavanaugh, C. L.; Nicewicz, D. A. Synthesis of α-Benzyloxyamino-γ-Butyrolactones via a Polar Radical Crossover Cycloaddition Reaction. *Org. Lett.* **2015**, *17* (24), 6082–6085. https://doi.org/10.1021/acs.orglett.5b03113.

(22) Xuan, J.; Xia, X.-D.; Zeng, T.-T.; Feng, Z.-J.; Chen, J.-R.; Lu, L.-Q.; Xiao, W.-J. Visible-Light-Induced Formal [3+2] Cycloaddition for Pyrrole Synthesis under Metal-Free Conditions. *Angew. Chem. Int. Ed.* **2014**, *53* (22), 5653–5656. https://doi.org/10.1002/anie.201400602.

(23) Roth, B. D.; Blankley, C. J.; Chucholowski, A. W.; Ferguson, E.; Hoefle, M. L.; Ortwine, D. F.; Newton, R. S.; Sekerke, C. S.; Sliskovic, D. R.; Wilson, M. Inhibitors of Cholesterol Biosynthesis. 3. Tetrahydro-4-Hydroxy-6-[2-(1H-Pyrrol-1-Yl)Ethyl]-2H-Pyran 2-One Inhibitors of HMG-CoA Reductase. 2. Effects of Introducing Substituents at Positions Three and Four of the Pyrrole Nucleus. *J. Med. Chem.* **1991**, *34* (1), 357–366. https://doi.org/10.1021/jm00105a056.

(24) Arias-Rotondo, D. M.; McCusker, J. K. The Photophysics of Photoredox Catalysis: A Roadmap for Catalyst Design. *Chem. Soc. Rev.* **2016**, *45* (21), 5803–5820. https://doi.org/10.1039/C6CS00526H.

(25) Mabbott, G. A. An Introduction to Cyclic Voltammetry. *J. Chem. Educ.* **1983**, *60* (9), 697. https://doi.org/10.1021/ed060p697.

(26) Andrieux, C. P.; Hapiot, P.; Pinson, J.; Saveant, J. M. Determination of Formal Potentials of Chemically Unstable Redox Couples by Second-Harmonic Alternating Current Voltammetry and Cyclic Voltammetry. Application to the Oxidation of Thiophenoxide Ions. *J. Am. Chem. Soc.* **1993**, *115* (17), 7783–7788. https://doi.org/10.1021/ja00070a026.

(27) Connelly, N. G.; Geiger, W. E. Chemical Redox Agents for Organometallic Chemistry. *Chem. Rev.* **1996**, *96* (2), 877–910. https://doi.org/10.1021/cr940053x.

(28) Luo, P.; Feinberg, A. M.; Guirado, G.; Farid, S.; Dinnocenzo, J. P. Accurate Oxidation Potentials of 40 Benzene and Biphenyl Derivatives with Heteroatom Substituents. *J. Org. Chem.* **2014**, *79* (19), 9297–9304. https://doi.org/10.1021/jo501761c.

(29) Xu, H.-C.; Moeller, K. D. Intramolecular Anodic Olefin Coupling Reactions: Use of the Reaction Rate To Control Substrate/Product Selectivity. *Angew. Chem. Int. Ed.* **2010**, *49* (43), 8004–8007. https://doi.org/10.1002/anie.201003924.

(30) Pavlishchuk, V. V.; Addison, A. W. Conversion Constants for Redox Potentials Measured versus Different Reference Electrodes in Acetonitrile Solutions at 25°C. *Inorganica Chim. Acta* **2000**, *298* (1), 97–102. https://doi.org/10.1016/S0020-1693(99)00407-7.

(31) Thomas, K. R. J.; Tharmaraj, P.; Chandrasekhar, V.; Bryan, C. D.; Cordes, A. W. Synthesis, Spectroscopy, and Electrochemistry of Ternary Copper(II) Complexes with 2,2-Diphenyl-4,4,6,6-Tetrakis(3,5-Dimethylpyrazolyl)Cyclotriphosphazene and Nitrogenous Bases. X-Ray Structures of N3P3Ph2(3,5-Me2Pz)4.Cntdot.Cu(ClO4)2.Cntdot.2H2O and N3P3Ph2(3,5-Me2Pz)4.Cntdot.Cu(ClO4)2.Cntdot.2ImH. *Inorg. Chem.* **1994**, *33* (24), 5382–5390. https://doi.org/10.1021/ic00102a008.

(32) Isse, A. A.; Gennaro, A. Absolute Potential of the Standard Hydrogen Electrode and the Problem of Interconversion of Potentials in Different Solvents. *J. Phys. Chem. B* **2010**, *114* (23), 7894–7899. https://doi.org/10.1021/jp100402x.

(33) Lee, C.; Yang, W.; Parr, R. G. Development of the Colle-Salvetti Correlation-Energy Formula into a Functional of the Electron Density. *Phys. Rev. B* **1988**, *37* (2), 785–789. https://doi.org/10.1103/PhysRevB.37.785.

(34) Becke, A. D. Density-functional Thermochemistry. III. The Role of Exact Exchange. *J. Chem. Phys.* **1993**, *98* (7), 5648–5652. https://doi.org/10.1063/1.464913.

(35) Zhao, Y.; Truhlar, D. G. The M06 Suite of Density Functionals for Main Group Thermochemistry, Thermochemical Kinetics, Noncovalent Interactions, Excited States, and Transition Elements: Two New Functionals and Systematic Testing of Four M06-Class Functionals and 12 Other Functionals. *Theor. Chem. Acc.* **2008**, *120* (1), 215–241. https://doi.org/10.1007/s00214-007-0310-x.

(36) McLean, A. D.; Chandler, G. S. Contracted Gaussian Basis Sets for Molecular Calculations. I. Second Row Atoms, Z=11–18. *J. Chem. Phys.* **1980**, *72* (10), 5639–5648. https://doi.org/10.1063/1.438980.

(37) Krishnan, R.; Binkley, J. S.; Seeger, R.; Pople, J. A. Self-consistent Molecular Orbital Methods. XX. A Basis Set for Correlated Wave Functions. *J. Chem. Phys.* **1980**, *72* (1), 650–654. https://doi.org/10.1063/1.438955.

(38) Cossi, M.; Rega, N.; Scalmani, G.; Barone, V. Energies, Structures, and Electronic Properties of Molecules in Solution with the C-PCM Solvation Model. *J. Comput. Chem.* **2003**, *24* (6), 669–681. https://doi.org/10.1002/jcc.10189.

(39) Barone, V.; Cossi, M. Quantum Calculation of Molecular Energies and Energy Gradients in Solution by a Conductor Solvent Model. *J. Phys. Chem. A* **1998**, *102* (11), 1995–2001. https://doi.org/10.1021/jp9716997.

(40) Gaussian 09 Citation | Gaussian.com https://gaussian.com/g09citation/ (accessed May 24, 2019).

(41) Nicewicz, D. A.; MacMillan, D. W. C. Merging Photoredox Catalysis with Organocatalysis: The Direct Asymmetric Alkylation of Aldehydes. *Science* **2008**, *322* (5898), 77–80. https://doi.org/10.1126/science.1161976.

(42) Chu, L.; Ohta, C.; Zuo, Z.; MacMillan, D. W. C. Carboxylic Acids as A Traceless Activation Group for Conjugate Additions: A Three-Step Synthesis of (±)-Pregabalin. *J. Am. Chem. Soc.* **2014**, *136* (31), 10886–10889. https://doi.org/10.1021/ja505964r.

(43) Li, R.-T.; Li, S.-H.; Zhao, Q.-S.; Lin, Z.-W.; Sun, H.-D.; Lu, Y.; Wang, C.; Zheng, Q.-T. Lancifodilactone A, a Novel Bisnortriterpenoid from Schisandra Lancifolia. *Tetrahedron Lett.* **2003**, *44* (17), 3531–3534. https://doi.org/10.1016/S0040-4039(03)00681-6.

(44) Li, R.-T.; Han, Q.-B.; Zheng, Y.-T.; Wang, R.-R.; Yang, L.-M.; Lu, Y.; Sang, S.-Q.; Zheng, Q.-T.; Zhao, Q.-S.; Sun, H.-D. Structure and Anti-HIV Activity of Micrandilactones B and C, New Nortriterpenoids Possessing a Unique Skeleton from Schisandra Micrantha. *Chem. Commun.* **2005**, No. 23, 2936–2938. https://doi.org/10.1039/B501932J.

(45) Xiao, W.-L.; Yang, L.-M.; Gong, N.-B.; Wu, L.; Wang, R.-R.; Pu, J.-X.; Li, X.-L.; Huang, S.-X.; Zheng, Y.-T.; Li, R.-T.; et al. Rubriflordilactones A and B, Two Novel Bisnortriterpenoids from Schisandra Rubriflora and Their Biological Activities. *Org. Lett.* **2006**, *8* (5), 991–994. https://doi.org/10.1021/ol060062f.

(46) Goh, S. S.; Chaubet, G.; Gockel, B.; Cordonnier, M.-C. A.; Baars, H.; Phillips, A. W.; Anderson, E. A. Total Synthesis of (+)-Rubriflordilactone A. *Angew. Chem. Int. Ed.* **2015**, *54* (43), 12618–12621. https://doi.org/10.1002/anie.201506366.

(47) Li, J.; Yang, P.; Yao, M.; Deng, J.; Li, A. Total Synthesis of Rubriflordilactone A. *J. Am. Chem. Soc.* **2014**, *136* (47), 16477–16480. https://doi.org/10.1021/ja5092563.

(48) Yang, P.; Yao, M.; Li, J.; Li, Y.; Li, A. Total Synthesis of Rubriflordilactone B. *Angew. Chem. Int. Ed.* **2016**, *55* (24), 6964–6968. https://doi.org/10.1002/anie.201601915.

(49) Chaubet, G.; Goh, S. S.; Mohammad, M.; Gockel, B.; Cordonnier, M.-C. A.; Baars, H.; Phillips, A. W.; Anderson, E. A. Total Synthesis of the Schisandraceae Nortriterpenoid Rubriflordilactone A. *Chem. – Eur. J.* **2017**, *23* (56), 14080–14089. https://doi.org/10.1002/chem.201703229.

(50) Wang, Y.; Li, Z.; Lv, L.; Xie, Z. Synthetic Study of Rubriflordilactone B: Highly Stereoselective Construction of the C-5-Epi ABCDE Ring System. *Org. Lett.* **2016**, *18* (4), 792–795. https://doi.org/10.1021/acs.orglett.6b00057.

(51) Peng, Y.; Duan, S.-M.; Wang, Y.-W. Concise Synthesis of the DEFG Ring System in Rubriflordilactone B. *Tetrahedron Lett.* **2015**, *56* (30), 4509–4511. https://doi.org/10.1016/j.tetlet.2015.05.117.

(52) Grimblat, N.; Kaufman, T. S.; Sarotti, A. M. Computational Chemistry Driven Solution to Rubriflordilactone B. *Org. Lett.* **2016**, *18* (24), 6420–6423. https://doi.org/10.1021/acs.orglett.6b03318.

(53) Zhang, Y.-D.; Tang, Y.-F.; Luo, T.-P.; Shen, J.; Chen, J.-H.; Yang, Z. Application of RCM Reaction in the Construction of ABC Ring of Micrandilactone A. *Org. Lett.* **2006**, *8* (1), 107–110. https://doi.org/10.1021/ol052630h.

(54) Chola, J.; Masesane, I. B. Stereoselective Synthesis of 3,4,5,6-Tetrahydroxycyclohexyl β-Amino Acid Derivatives. *Tetrahedron Lett.* **2008**, *49* (39), 5680–5682. https://doi.org/10.1016/j.tetlet.2008.07.094.

(55) Canonne, P.; Akssira, M.; Lemay, G. A Facile and General Route to 4-Substituted-2 Butenolides. *Tetrahedron Lett.* **1981**, *22* (28), 2611–2614. https://doi.org/10.1016/S0040-4039(01)92950-8.

(56) Janecki, T.; Ku, A.; Krawczyk, H.; Baszczyk, E. A New, General Approach to Substituted 3-Diethoxyphosphoryl-2,5-Dihydro-2-Furanones. *Synlett* **2000**, *2000* (5), 611–614. https://doi.org/10.1055/s-2000-6597.

(57) Janecki, T.; Baszczyk, E. A Convenient Synthesis of 3-Alkylidenetetrahydro-2-Furanones from 3-Diethoxyphosphoryl-2,5-Dihydro-2-Furanones. *Synthesis* **2001**, *2001* (3), 403–408. https://doi.org/10.1055/s-2001-11432.

(58) Blay, G.; Cardona, L.; Pedro, J. R.; Sanz-Marco, A. Enantioselective Zinc-Mediated Conjugate Addition of Terminal Alkynes to Enones. *Chem. – Eur. J.* **2012**, *18* (41), 12966–12969. https://doi.org/10.1002/chem.201201765.

(59) Cox, N.; Dang, H.; Whittaker, A. M.; Lalic, G. NHC–Copper Hydrides as Chemoselective Reducing Agents: Catalytic Reduction of Alkynes, Alkyl Triflates, and Alkyl Halides. *Tetrahedron* **2014**, *70* (27), 4219–4231. https://doi.org/10.1016/j.tet.2014.04.004.

(60) Canonne, P.; Akssira, M.; Lemay, G. Alkylation Des Lactones Tricycliques Pontees. Application a La Synthese Des Butenolides Trisubstitues En 2 et 4. *Tetrahedron Lett.* **1983**, *24* (18), 1929–1932. https://doi.org/10.1016/S0040-4039(00)81808-0.

(61) Canonne, P.; Akssira, M.; Fytas, G. Etude de l'action Des Alkylmagnesiens Primaires et Arylmagnesiens Sur Les Anhydrides Tricycliques Pontes. *Tetrahedron* **1984**, *40* (10), 1809–1815. https://doi.org/10.1016/S0040-4020(01)91134-2.

(62) Reed, T. H. and J. W. *The Way of Synthesis : Evolution of Design and Methods for Natural Products*; Weinheim : Wiley-VCH ; Chichester : John Wiley [distributor], c2007., 2007.

(63) Chen, B.-C.; Zhou, P.; Davis, F. A.; Ciganek, E. A-Hydroxylation of Enolates and Silyl Enol Ethers. In *Organic Reactions*; American Cancer Society, 2004; pp 1–356. https://doi.org/10.1002/0471264180.or062.01.

(64) Davis, F. A. Recent Applications of N-Sulfonyloxaziridines (Davis Oxaziridines) in Organic Synthesis. *Tetrahedron* **2018**, *74* (26), 3198–3214. https://doi.org/10.1016/j.tet.2018.02.029.

(65) Vedejs, E. Method for Direct Hydroxylation of Enolates. Transition Metal Peroxide Reactions. *J. Am. Chem. Soc.* **1974**, *96* (18), 5944–5946. https://doi.org/10.1021/ja00825a047.

(66) Anderson, J. C.; Smith, S. C. Oxodiperoxymolybdenum(Pyridine)-1,3-Dimethyl-3,4,5,6-Tetrahydro-2(1H)-Pyrimidinone (MoO5. Py . DMPU): A Safer Alternative to MoOPH for the α-Hydroxylation of Carbonyl Compounds. *Synlett* **1990**, *1990* (02), 107–108. https://doi.org/10.1055/s-1990-21003.

(67) Popsavin, V.; Grabež, S.; Popsavin, M.; Krstić, I.; Kojić, V.; Bogdanović, G.; Divjaković, V. Wittig Reaction with Partially Protected Sugar Lactol Derivatives. Preparation of Highly Cytotoxic Goniofufurone Analogues. *Tetrahedron Lett.* **2004**, *45* (51), 9409–9413. https://doi.org/10.1016/j.tetlet.2004.10.122.

(68) Popsavin, V.; Benedeković, G.; Srećo, B.; Popsavin, M.; Francuz, J.; Kojić, V.; Bogdanović, G. Divergent Synthesis of Cytotoxic Styryl Lactones from D-Xylose. The First Total Synthesis of (+)-Crassalactone C. *Org. Lett.* **2007**, *9* (21), 4235–4238. https://doi.org/10.1021/ol701734s.

(69) Gesmundo, N. J. The Development of Complexity Generating Organic Photoredox Transformations and the Application of These Transformations in Complex Molecule Synthesis. Ph.D., The University of North Carolina at Chapel Hill: United States -- North Carolina, 2015.

(70) Singer, R. A.; Carreira, E. M. Catalytic, Enantioselective Dienolate Additions to Aldehydes: Preparation of Optically Active Acetoacetate Aldol Adducts. *J. Am. Chem. Soc.* **1995**, *117* (49), 12360–12361. https://doi.org/10.1021/ja00154a049.

(71) Singer, R. A.; Brock, J. R.; Carreira, E. M. Synthesis of a Tridentate Ligand for Use in TiIV-Catalyzed Acetate Aldol Addition Reactions. *Helv. Chim. Acta* **2003**, *86* (4), 1040–1044. https://doi.org/10.1002/hlca.200390092.

(72) Yamaoka, M.; Nakazaki, A.; Kobayashi, S. Rate Enhancement by Water in a $TiCl_4$-Mediated Stereoselective Vinylogous Mukaiyama Aldol Reaction. *Tetrahedron Lett.* **2010**, *51* (2), 287–289. https://doi.org/10.1016/j.tetlet.2009.10.140.

(73) Valois Escamilla, I.; Rangel Ramos, L. F.; Sánchez Escalera, J.; Álvarez Hernández, A. Studies on the Deprotection of Triisopropylsilylarylacetylene Derivatives. *J. Mex. Chem. Soc.* **2011**, *55* (3), 133–136.

(74) Donohoe, T. J.; Winship, P. C. M.; Pilgrim, B. S.; Walter, D. S.; Callens, C. K. A. A Novel Oxidative Cyclisation onto Vinyl Silanes. *Chem. Commun.* **2010**, *46* (39), 7310–7312. https://doi.org/10.1039/C0CC01342K.

(75) Adam, W.; Saha-Möller, C. R.; Schmid, K. S. Synthesis of 4,6-Dideoxyfuranoses through the Regioselective and Diastereoselective Oxyfunctionalization of a Dimethylphenylsilyl-Substituted Chiral Homoallylic Alcohol. *J. Org. Chem.* **2001**, *66* (22), 7365–7371. https://doi.org/10.1021/jo010549w.

(76) Li, Y.; Chen, Z.-X.; Xiao, Q.; Ye, Q.-D.; Sun, T.-W.; Meng, F.-K.; Ren, W.-W.; You, L.; Xu, L.-M.; Wang, Y.-F.; et al. Diastereoselective Total Synthesis of (±)-Schindilactone A, Part 2: Construction of the Fully Functionalized CDEFGH Ring System. *Chem. – Asian J.* **2012**, *7* (10), 2334–2340. https://doi.org/10.1002/asia.201200364.

(77) Krishna, P. R.; Kunde, R.; Nomula, R.; Ramakrishna, K. V. S. Total Synthesis of Proposed Structure of Xylogiblactone B by Chiron Approach. *Tetrahedron Lett.* **2014**, *55* (38), 5244–5246. https://doi.org/10.1016/j.tetlet.2014.07.121.

(78) Menger, F. M.; Chow, J. F.; Kaiserman, H.; Vasquez, P. C. Directionality of Proton Transfer in Solution. Three Systems of Known Angularity. *J. Am. Chem. Soc.* **1983**, *105* (15), 4996–5002. https://doi.org/10.1021/ja00353a024.

(79) Liu, W.; Buck, M.; Chen, N.; Shang, M.; Taylor, N. J.; Asoud, J.; Wu, X.; Hasinoff, B. B.; Dmitrienko, G. I. Total Synthesis of Isoprekinamycin: Structural Evidence for Enhanced Diazonium Ion Character and Growth Inhibitory Activity toward Cancer Cells. *Org. Lett.* **2007**, *9* (15), 2915–2918. https://doi.org/10.1021/ol0712374.

(80) Hofsløkken, N. U.; Skattebøl, L.; Johansson, F.; Bertilsson, S. K.; Andersson, P. G.; Møller, J.; Senning, A.; Yao, X.-K.; Wang, H.-G.; Tuchagues, J.-P.; et al. Convenient Method for the Ortho-Formylation of Phenols. *Acta Chem. Scand.* **1999**, *53*, 258–262. https://doi.org/10.3891/acta.chem.scand.53-0258.

(81) Velder, J.; Robert, T.; Weidner, I.; Neudörfl, J.-M.; Lex, J.; Schmalz, H.-G. Modular Synthesis of Chiral Phosphine-Phosphite-Ligands from Phenolic Precursors: A New Approach to Bidentate Chelate Ligands Exploiting a P□O to P□C Migration Rearrangement. *Adv. Synth. Catal.* **2008**, *350* (9), 1309–1315. https://doi.org/10.1002/adsc.200800146.

(82) Bordwell, F. G.; Drucker, G. E. Acidities of Indene and Phenyl-, Diphenyl-, and Triphenylindenes. *J. Org. Chem.* **1980**, *45* (16), 3325–3328. https://doi.org/10.1021/jo01304a037.

(83) Tobisu, M.; Chatani, N. Cross-Couplings Using Aryl Ethers via C–O Bond Activation Enabled by Nickel Catalysts. *Acc. Chem. Res.* **2015**, *48* (6), 1717–1726. https://doi.org/10.1021/acs.accounts.5b00051.

(84) Rosen, B. M.; Quasdorf, K. W.; Wilson, D. A.; Zhang, N.; Resmerita, A.-M.; Garg, N. K.; Percec, V. Nickel-Catalyzed Cross-Couplings Involving Carbon−Oxygen Bonds. *Chem. Rev.* **2011**, *111* (3), 1346–1416. https://doi.org/10.1021/cr100259t.

(85) Igarashi, T.; Haito, A.; Chatani, N.; Tobisu, M. Nickel-Catalyzed Reductive Cleavage of Carbon–Oxygen Bonds in Anisole Derivatives Using Diisopropylaminoborane. *ACS Catal.* **2018**, *8* (8), 7475–7483. https://doi.org/10.1021/acscatal.8b02009.

(86) Natte, K.; Dumrath, A.; Neumann, H.; Beller, M. Palladium-Catalyzed Carbonylations of Aryl Bromides Using Paraformaldehyde: Synthesis of Aldehydes and Esters. *Angew. Chem. Int. Ed.* **2014**, *53* (38), 10090–10094. https://doi.org/10.1002/anie.201404833.

(87) Jiang, X.; Wang, J.-M.; Zhang, Y.; Chen, Z.; Zhu, Y.-M.; Ji, S.-J. Palladium-Catalyzed Formylation of Aryl Halides with Tert-Butyl Isocyanide. *Org. Lett.* **2014**, *16* (13), 3492–3495. https://doi.org/10.1021/ol5014262.

(88) Wang, Y.; Zhang, Y.; Li, Z.; Yang, Z.; Xie, Z. A Highly Efficient Synthesis of the DEFG-Ring System of Rubriflordilactone B. *Org. Chem. Front.* **2016**, *4* (1), 47–51. https://doi.org/10.1039/C6QO00241B.

(89) Hashimoto, Y.; Abe, R.; Morita, N.; Tamura, O. Inverse-Electron-Demand Diels–Alder Reactions of α,β-Unsaturated Hydrazones with 3-Methoxycarbonyl α-Pyrones. *Org. Biomol. Chem.* **2018**, *16* (46), 8913–8916. https://doi.org/10.1039/C8OB02132E.

(90) Schotten, T.; Janowski, F.; Schmidt, A.; Hinrichsen, K.; Ammenn, J. Synthesis of 2,3-Disubstituted 5,6,7,8-Tetrahydronaphthyls and Related Structures via Diels-Alder Reaction. *Synthesis* **2003**, *2003* (13), 2027–2032. https://doi.org/10.1055/s-2003-41449.

(91) Schrock, R. R.; Hoveyda, A. H. Molybdenum and Tungsten Imido Alkylidene Complexes as Efficient Olefin-Metathesis Catalysts. *Angew. Chem. Int. Ed.* **2003**, *42* (38), 4592–4633. https://doi.org/10.1002/anie.200300576.

(92) Khatri, B. B.; Sieburth, S. McN. Enyne-2-Pyrone [4 + 4]-Photocycloaddition: Sesquiterpene Synthesis and a Low-Temperature Cope Rearrangement. *Org. Lett.* **2015**, *17* (17), 4360–4363. https://doi.org/10.1021/acs.orglett.5b02207.

(93) Domingo, L. R.; Pérez-Prieto, J. Exploring Two-State Reaction Pathways in the Photodimerization of Cyclohexadiene. *ChemPhysChem* **2006**, *7* (3), 614–618. https://doi.org/10.1002/cphc.200500431.

(94) Gan, P.; Smith, M. W.; Braffman, N. R.; Snyder, S. A. Pyrone Diels–Alder Routes to Indolines and Hydroindolines: Syntheses of Gracilamine, Mesembrine, and Δ7-Mesembrenone. *Angew. Chem. Int. Ed.* **2016**, *55* (11), 3625–3630. https://doi.org/10.1002/anie.201510520.

(95) Jurkauskas, V.; Sadighi, J. P.; Buchwald, S. L. Conjugate Reduction of α,β-Unsaturated Carbonyl Compounds Catalyzed by a Copper Carbene Complex. *Org. Lett.* **2003**, *5* (14), 2417–2420. https://doi.org/10.1021/ol034560p.

(96) Posner, G. H.; Hutchings, R. H.; Woodard, B. T. Regiocontrolled and Stereocontrolled Diels-Alder Cycloadditions of 2-Pyrones and Unactivated, Unbranched 1-Alkenes. *Synlett* **1997**, *1997* (Sup. I), 432–434. https://doi.org/10.1055/s-1997-6126.

(97) Morse, P. D.; Nguyen, T. M.; Cruz, C. L.; Nicewicz, D. A. Enantioselective Counter-Anions in Photoredox Catalysis: The Asymmetric Cation Radical Diels-Alder Reaction. *Tetrahedron* **2018**, *74* (26), 3266–3272. https://doi.org/10.1016/j.tet.2018.03.052.

(98) Pilli, R. A.; Oliveira, M. da C. F. de. Recent Progress in the Chemistry of the Stemona Alkaloids. *Nat. Prod. Rep.* **2000**, *17* (1), 117–127. https://doi.org/10.1039/A902437I.

(99) Greger, H. Structural Relationships, Distribution and Biological Activities of Stemona Alkaloids. *Planta Med.* **2006**, *72* (02), 99–113. https://doi.org/10.1055/s-2005-916258.

(100) Mungkornasawakul, P.; Pyne, S. G.; Willis, A. C.; Jatisatienr, A.; Phuthsuk, D.; Lie, W. 6-Hydroxy-5,6-Seco-Stemocurtisine: A Novel Seco-Stemocurtisine-Type Alkaloid. *Phytochem. Lett.* **2013**, *6* (4), 602–605. https://doi.org/10.1016/j.phytol.2013.07.016.

(101) Mungkornasawakul, P.; Pyne, S. G.; Jatisatienr, A.; Supyen, D.; Lie, W.; Ung, A. T.; Skelton, B. W.; White, A. H. Stemocurtisine, the First Pyrido[1,2-a]Azapine Stemona Alkaloid. *J. Nat. Prod.* **2003**, *66* (7), 980–982. https://doi.org/10.1021/np020612s.

(102) Mungkornasawakul, P.; Pyne, S. G.; Jatisatienr, A.; Supyen, D.; Jatisatienr, C.; Lie, W.; Ung, A. T.; Skelton, B. W.; White, A. H. Phytochemical and Larvicidal Studies on Stemona Curtisii: Structure of a New Pyrido[1,2-a]Azepine Stemona Alkaloid. *J. Nat. Prod.* **2004**, *67* (4), 675–677. https://doi.org/10.1021/np034066u.

(103) Shengule, S. R.; Willis, A. C.; Pyne, S. G. Model Support Studies toward the Total Synthesis of the Stemona Alkaloid Stemocurtisine. *Tetrahedron* **2013**, *69* (37), 8042–8050. https://doi.org/10.1016/j.tet.2013.06.099.

(104) Diastereoselective Synthesis of the A-B-C Tricyclic Ring Structure of Stemocurtisine - Dau - 2015 - European Journal of Organic Chemistry - Wiley Online Library https://onlinelibrary-wiley-com.libproxy.lib.unc.edu/doi/full/10.1002/ejoc.201501080 (accessed Jun 23, 2019).

(105) Schrauzer, G. N.; Parshall, G. W.; Wonchoba, E. R. Bis(Dimethylglyoximato)Cobalt Complexes: ("Cobaloximes"). In *Inorganic Syntheses*; John Wiley & Sons, Ltd, 2007; pp 61–70. https://doi.org/10.1002/9780470132425.ch12.

(106) West, J. G.; Huang, D.; Sorensen, E. J. Acceptorless Dehydrogenation of Small Molecules through Cooperative Base Metal Catalysis. *Nat. Commun.* **2015**, *6*, 10093. https://doi.org/10.1038/ncomms10093.

(107) Dempsey, J. L.; Brunschwig, B. S.; Winkler, J. R.; Gray, H. B. Hydrogen Evolution Catalyzed by Cobaloximes. *Acc. Chem. Res.* **2009**, *42* (12), 1995–2004. https://doi.org/10.1021/ar900253e.

(108) Perkowski, A. J.; Nicewicz, D. A. Direct Catalytic Anti-Markovnikov Addition of Carboxylic Acids to Alkenes. *J. Am. Chem. Soc.* **2013**, *135* (28), 10334–10337. https://doi.org/10.1021/ja4057294.

(109) Peruzzi, M. T.; Mei, Q. Q.; Lee, S. J.; Gagné, M. R. Chemoselective Amide Reductions by Heteroleptic Fluoroaryl Boron Lewis Acids. *Chem. Commun.* **2018**, *54* (46), 5855–5858. https://doi.org/10.1039/C8CC01863D.

(110) Velázquez, F.; Olivo, H. F. Synthesis of Bicyclic γ-Ylidenetetronates. *Org. Lett.* **2002**, *4* (19), 3175–3178. https://doi.org/10.1021/ol026325x.

(111) Asaoka, M.; Yanagida, N.; Sugimura, N.; Takei, H. The Reaction of 2-(Trialkylsiloxy)Furans with Lead(IV) Acetate. The Synthesis of Dl-Pyrenophorin. *Bull. Chem. Soc. Jpn.* **1980**, *53* (4), 1061–1064. https://doi.org/10.1246/bcsj.53.1061.

(112) Yin, L.; Takada, H.; Lin, S.; Kumagai, N.; Shibasaki, M. Direct Catalytic Asymmetric Vinylogous Conjugate Addition of Unsaturated Butyrolactones to α,β-Unsaturated Thioamides. *Angew. Chem. Int. Ed.* **2014**, *53* (21), 5327–5331. https://doi.org/10.1002/anie.201402332.

(113) Boukouvalas, J.; Jean, M.-A. Streamlined Biomimetic Synthesis of Paracaseolide A via Aerobic Oxidation of a 2-Silyloxyfuran. *Tetrahedron Lett.* **2014**, *55* (30), 4248–4250. https://doi.org/10.1016/j.tetlet.2014.05.054.

(114) Praly, J.-P.; Kharraf, Z. E.; Corringer, P.-J.; Brard, L.; Descotes, G. Orthoesterification de Sucres C-1 Gem Dihalogenes. *Tetrahedron* **1990**, *46* (1), 65–75. https://doi.org/10.1016/S0040-4020(01)97584-2.

(115) Takeo, K. Silver Trifluoromethanesulfonate-Promoted Koenigs-Knorr Reaction of Methyl 4,6-O-Benzylidene-β-d-Glucopyranoside with 2,3,4,6-Tetra-O-Acetyl-α-d-Glucopyranosyl Bromide. *Carbohydr. Res.* **1980**, *87* (1), 147–152. https://doi.org/10.1016/S0008-6215(00)85199-X.

(116) Toda, F.; Tanaka, K.; Leung, C. W.; Meetsma, A.; Feringa, B. L. Preparation of Optically Active 5-Alkoxyfuran-2(5H)-Ones and 5-Methoxydihydrofuran-2(3H)-One by Chiral Inclusion Complexation. *J. Chem. Soc. Chem. Commun.* **1994**, No. 20, 2371–2372. https://doi.org/10.1039/C39940002371.

(117) Feringa, B. L.; de, L. B.; Jansen, J. F. G. A.; de, J. J. C.; Lubben, M.; Faber, W.; Schudde, E. P. New Approaches in Asymmetric Synthesis Using γ-Alkoxybutenolides. *Pure Appl. Chem.* **2009**, *64* (12), 1865–1871. https://doi.org/10.1351/pac199264121865.

(118) Purification of Laboratory Chemicals - 5th Edition https://www.elsevier.com/books/purification-of-laboratory-chemicals/armarego/978-0-7506-7571-0 (accessed Jun 21, 2019).